DEVELOPMENT OF NONLINEAR FINITE DIFFERENCE MODEL FOR CHLORIDE DIFFUSION IN CONCRETE

by

Alkailani Omer

Submitted in partial fulfillment of the requirements
for the degree of Doctoral of Philosophy

at

Dalhousie University
Halifax, Nova Scotia
June 2016

DEDICATION

I dedicate my humble effort and work in this thesis to the soul of my sweet heart and beloved daughter Mabrouka who passed away while I was working on this research back in May 27 2012. I also dedicate this thesis to the spirit of my younger brother Khalifa Omer who passed away on Nov. 26 2011. Their pure love and memories are in my heart and have always been a source of strength for me during the journey of this work. Rest in peace.

TABLE OF CONTENTS

LIST OF TABLES

LIST OF FIGURES

ABSTRACT

Owing to problems associated with chloride-induced corrosion, the reliable prediction of chloride ingress into concrete is one of the key elements of the durability design and redesign of concrete structures exposed to chloride environments. In this thesis, a nonlinear chloride penetration model based on the finite difference approach is developed that aims to predict chloride content at the reinforcement level after a certain period of exposure. The chloride ingress into concrete is modeled using a modified Fick's second law of diffusion, where the chloride binding is dealt with as a separate term in the model, allowing the nonlinear binding to be accounted for in the modeling process. Two finite difference models for both simplified and modified Fick's second law equations are derived and used to model chloride ingress into concrete. The influence of time and temperature on the effective chloride diffusion coefficient is accounted for in the model. The chloride parameters, which describe the predicted chloride profiles, are obtained by fitting to the experimental chloride profiles of acid-soluble chlorides the predicted chloride profiles resulting from the nonlinear model. Chloride parameters are obtained for three binding cases: no binding, linear binding, and nonlinear binding. The results of the nonlinear model are then compared to those of the error function solution and Life-365. A parametric study is also conducted to examine the sensitivity of the predicted service life against changes in the values of key parameters of interest used in the model.

In addition, the influence of the curing temperature on the chloride diffusion coefficient and age parameter (value of m) is experimentally investigated, and the influence of chloride binding on concrete porosity and pore volume at different exposure conditions is explored. Water-soluble and acid-soluble chloride profiles obtained at different exposure periods and temperatures are obtained and investigated. The error function solution and linear finite difference model are used to evaluate the chloride parameters of both types of chloride profiles and the results are compared and discussed. The results reveal that both the diffusion coefficient and the value of m are temperature-dependent. Furthermore, binding is found to have a significant influence on concrete porosity and pore volume, especially at 22.4^{o} C or lower. The diffusion coefficients of water-soluble chloride are higher than those of acid-soluble chloride, although a slight difference is observed in the value of m for both types. Elevated temperature is also found to significantly influence the value of m, based on the results of acid-soluble chloride profiles.

The results of the nonlinear model show that binding strongly affects the value of the effective diffusion coefficient, while the nonlinear binding relation results in the lowest value of the effective diffusion. Binding is also found to have a strong influence on the shape of free, bound, and total chloride profiles. The predicted service life notably increases when nonlinear binding is considered and drops drastically if binding is ignored. The linear binding relation still provides a reasonable estimation of service life, but on the conservative side compared to the nonlinear relation. The sensitivity results show that the value of m, temperature, and concrete cover have the greatest influences on the predicted service life with respect to the base case concrete mixture used in this study. The main contributions of this thesis are determining the effective diffusion coefficient using the total chloride profiles, and modeling nonlinear binding with the time and temperature dependencies of the effective diffusion coefficient.

LIST OF ABBREVIATIONS AND SYMBOLS USED

ACI	American Concrete Institute
AFm	Calcium aluminate Monosulfate hydrate
AFt	Calcium aluminate trisulfate hydrate (ettringite)
ASTM	American Society for Testing and Materials
C	Total chloride concentration or content
C_t	Total chloride concentration or content
C_b	Bound chloride
C_{bm}	Bound chloride by concrete material
C_f	Free chloride concentration or content
$C_{f,1}$	Free chloride concentration in cell 1
$C_{f,2}$	Free chloride concentration in cell 2
C_e	Free chloride concentration at equilibrium
C_i	Initial free chloride concentration of host solution
C_s	Chloride surface concentration
C_{se}	Free chloride concentration at surface
CSH	Calcium silicate hydrates
CTH	Chalmers Tekniska Högskola (Common name for rapid migration test)
C_{up}	Chloride content in the upstream cell
C/S	Calcium/Silica ratio
D	Chloride diffusion coefficient
Da	Apparent chloride diffusion coefficient
D_a^*	Apparent chloride diffusion coefficient (in nonlinear model)
D_{a28}	Instantaneous apparent diffusion coefficient at concrete age of 28 days
D_{AVG}	Average chloride diffusion coefficient
D_{e28}	Instantaneous effective diffusion coefficient at concrete age of 28 days
D_{nssm}	Non-steady state chloride migration coefficient
D_{ref}	Chloride diffusion coefficient at reference time and temperature
D(t)	Chloride diffusion coefficient at time t and
E_a	Activation energy of cementitious system

erf	Error function
erfc	Complementary error function
F	Faraday's constant
FA	Fly ash
i	Particular slice of concrete
J	Chloride flux
L	Thickness of the specimen
L.F.D.M	Linear finite difference model
m	Age parameter or age factor or reduction coefficient
m_{avg}	Age parameter as determined based on the average time method
m_e	Age parameter in the nonlinear model
m_{eff}	Age parameter as determined from the effective time method
m_{tot}	Age parameter as determined from the total time method
n	Time step
N.L.F.D.M	Nonlinear finite difference model
OPC	Ordinary Portland cement
PC	Portland cement
pH	Concrete alkalinity
P_{sol}	Porosity term or the amount of evaporable water
R	Gas constant
RCPT	Rapid chloride penetration test
SF	Silica fume
SG	Slag cement
X	Variable distance from concrete surface
X_d	Average chloride penetration depth
T	Time-dependent diffusion coefficient in error function solution
T	Temperature
T_{ref}	Reference temperature
t	Exposure time
t_{28}	Concrete age at 28 days
t_1	Concrete age at the start of exposure

t_2	Concrete age at the end of exposure
t_{avg}	Average time
t_{tot}	Total time (time at the end of exposure)
t_{eff}	Effective time
t_{ex}	Exposure time
t_{ref}	Reference time
U	Potential difference between both ends of the specimen
W_d	Mass of dry sample
w/c	Water to cement ratio
w/cm	Water to cementitious material ratio
w/b	Water to binder ratio
Å	Pore radius unit
α	Linear binding coefficient, linear binding capacity
α	Nonlinear binding coefficient
β	Nonlinear binding coefficient
δ	Specimen thickness
Δt	Time step
Δx	Concrete slice thickness (total depth divided by number of slices)
u_i^n	Chloride concentration at time n and slice i
ω_e	Evaporable water content in concrete

ACKNOWLEDGEMENT

Immeasurable appreciation and sincere gratitude for the help and support are extended to the following people who in one way or another have contributed in making this research possible.

First, I would like to acknowledge and thank the valuable advice, suggestions and provisions provided by my supervisor Dr. John Newhook and co-supervisor Dr. Christopher Barnes. Without their support, guidance and encouragement this work would not have been accomplished. Special thanks to Dr. Dean Forgeron for fruitful discussion and helpful comments on concrete porosity and microstructure. Thanks to Dr. George Jarjoura for his valuable discussion and contribution.

I would like to thank Dr. Guy Kember for helping with some of the mathematical derivation and coding process presented in this thesis. I thank him for his patience and friendship.

Special thanks to W. S. Langley Concrete and Materials Technology Ltd, for providing the concrete material tested in this project

Special thanks to Libyan- North American Scholarship Program and NSREC for their financial support. This thesis would not have been possible without their financial contribution and support.

I would like to thank and acknowledge the support and the assistance I got all the way from our wonderful laboratory stuff: Blair Nickerson, Brine Kennedy and Jesse Keane.

I wish to thank all my colleagues and friends for their support

Most of all, I am grateful and wish special thanks to my wonderful wife Salma and my lovely and gorgeous children Mohamed, Salem and Khaleda for their patience and endless support throughout my study period and time. I would like to express my deepest gratitude to my Family backhome in Libya for their generous support, encouragement, and wishes during the hard and difficult times of my research and work.

1 INTRODUCTION

1.1 General

Chloride transport in concrete has drawn significant attention due to the problem of chloride-induced corrosion in reinforced concrete structures, which has caused enormous economic loss worldwide. In developed countries, it is estimated that about 40% of the total resources of the construction industry are being applied to the repair and maintenance of existing structures, and 60% to new installations[1]. In Western Europe, approximately 50% of total national wealth is spent on infrastructure, and 50% of the expenditures in the construction industry are spent on the repair, maintenance and remediation of existing reinforced concrete structures. A large portion of this expenditure is related to the corrosion of the reinforcement [2]. In the United States, 134,000 reinforced concrete bridges (23% of the total) require immediate repair and 226,000 (39% of the total) are deficient. In the majority of these cases, corrosion of the reinforcing steel is the main cause of damage, and total repair costs are estimated at USD $100 billion[3]. Thus, to reduce such enormous expenditures, the service life of the structures should be predictable with respect to durability, future repair and maintenance, etc. If the future maintenance of a structure is easily predicted, the cost for repair, maintenance and remediation can be optimized.

The corrosion of the reinforcement in moderate concrete structures exposed to marine or de-icing salts is generally attributed to the ingress of chloride ions from the surrounding environment into concrete. Chloride ions from marine environments or de-icing salts have the ability to penetrate deeply into the concrete cover to the level of the reinforcement. When chlorides exceed a certain amount at the reinforcement, which is called a threshold or critical chloride content, C_{crit}, reinforcement corrosion is initiated. Despite the complicated transport mechanisms of chloride ions in concrete, diffusion and convection are considered to be the major transport processes in most cases.

Diffusion is the movement of a substance under a gradient of concentration, or, more strictly speaking, the chemical potential from a high concentration to a low one.

Convection is the movement of ions under the action of water or moisture gradient. Diffusion takes place in saturated concrete, whereas convection, which is sometimes referred to as capillary adsorption, occurs when the concrete is partially dry or unsaturated. Both mechanisms are believed to act simultaneously in concrete. However, in modern concrete, in particular in high performance concrete (which is typically used in the construction of marine applications and highway bridge deck projects exposed to chlorides), convection is limited to dry surfaces only and diffusion is often considered as the dominant process of chloride transport in the concrete.

Chloride prediction models are often used to predict the time to corrosion initiation caused by chloride ingress into concrete. Among potentially applicable models, those based on Fick's second law are commonly used for this purpose. Fick's second law-based models rely on observations of responses measured in concrete exposed to laboratory or field conditions. Experimental or field data are used to derive and quantify chloride parameters such as chloride diffusion coefficients and surface concentrations by curve-fitting of achieved chloride profiles. Although other methods and experimental test procedures have been developed over the past decades to measure chloride diffusion coefficients [4], Fick's second law-based models are often simple and, since observations are used to quantify them, do not require any intensive validation before being applied for predictions [5].

In current practice, the error function solution and Life-365 are the Fick's second law-based models most commonly used by engineers in the field to predict the service life of reinforced concrete structures for design or redesign purposes. The error function solution often uses acid-soluble chloride profiles that are obtained either from new concrete exposed to lab conditions or from existing concrete exposed to field conditions to project the chloride parameters required to carry out service life predictions. Life-365 uses a concrete mix design to estimate the chloride parameters, and a finite difference approach to predict the service life. It also takes into account the influence of certain material and environmental factors, such as time and temperature, on the chloride diffusion coefficient.

Despite intensive efforts in the past to improve Fick's second law-based models for predicting chloride ingress into concrete, there remain several limitations concerning their applications in predicting service life. A few assumptions involved in the current practice of Fick's second law-based models have been proven to be erroneous or invalid [5,6]. This has raised some doubts and serious concerns about the accuracy of these models in providing proper estimations for the service life of structures. Both the error function solution and Life-365 are derived based on the assumption that chloride binding in concrete is linear and that the apparent chloride diffusion coefficient is constant with depth. This assumption has been proven invalid.

Many researchers and numerous studies have shown that chloride binding in concrete is not linear but instead concentration-dependent and controlled by the level of free chloride concentration in the pore solution[7]. The linear binding assumption is made solely to simplify the solution of Fick's second law of diffusion in modeling and predicting chloride ingress into concrete. Fick's second law uses linear assumption in its solution and is often referred to as 'simplified Fick's second law'. When binding is assumed linear, the apparent diffusion coefficient becomes independent of the chloride concentration in concrete pores. This has made it mathematically easy to derive an analytical solution, such as that of the error function solution, to model the diffusion process in concrete, and facilitates the derivation of the numerical finite difference solution of Fick's second law, such as that used in Life-365. Furthermore, the error function solution assumes a constant diffusion coefficient and constant surface concentration during exposure, which has also proven to be inaccurate and very conservative.

Another important parameter found to have a great influence on Fick's second law-based models is the age parameter, also known as the reduction coefficient or value of m. This parameter has to date received scant attention in the published literature. The age parameter has been used in Fick's second law-based models to account for the reduction of the chloride diffusion coefficient over time as a result of the ongoing hydration of the concrete. Its value is often kept constant in prediction models and is believed to be

influenced only by the concrete mix proportions, in particular the level of supplementary cementitions materials incorporated in concrete. Different methods have been used to determine the value of this parameter, with each yielding a different value. It has been reported that the predicted service life is greatly influenced by the estimate value of m [8], a parameter that is often obtained based on the data measured from acid-soluble chloride profiles. However, sometimes water-soluble chloride profiles are used to describe chloride ingress into concrete. No data is available in the literature concerning the value of m when water-soluble chlorides are used instead. This is a notable gap in the current literature and current knowledge, which must be addressed.

In addition, limited knowledge is available in the literature on the effect of binding on concrete microstructure and porosity [9]. To the author's knowledge, no detailed study yet exists that investigates the influence of binding products such as Friedel's salt on the porosity and pore size distribution of concrete. Furthermore, very little has been done regarding the effect of temperature level on chloride binding [10,11]. This is a notable gap in the knowledge, since most concrete structures have temperature conditions far removed from those of laboratory conditions (around 20^{o} C), where most tests are performed. This can be a limiting factor for predictions of chloride penetration in structures. The influence of binding and temperature on the pore structure of concrete could also influence the value of m, which, in turn, will impact service life predictions.

1.2 Research Objective

The main objective of this research work is to improve the accuracy of chloride models based on Fick's second law of diffusion by including the nonlinearity behavior of chloride binding in concrete and taking into account the time-dependent effective diffusion coefficient and the influence of exposure temperature in the modeling process. Additionally, in order to gain more knowledge about the influence of binding on the transport properties of concrete, the shape of predicted chloride profiles, and ultimately service life estimations, the influence of other binding types (such as linear binding) and when no binding is assumed at all will be considered in the developed model. This research work is also aimed at improving knowledge about the influence of binding

products on concrete porosity and pore structures at different exposure and temperature conditions as well as on the value of m. Finally, this research highlights the use of improved finite difference models over the traditional error function solution in obtaining the chloride parameters used to estimate and predict service life.

An intensive experimental program was carried out in this thesis to provide the database required to achieve the outlined objectives. Water-soluble and acid-soluble chloride profiles were obtained from the bulk diffusion test at three different exposure times and temperatures. A rapid migration test was also performed to evaluate the influence of the amount of curing on the migration diffusion coefficient and the age parameter values. The binding parameters of the cementitious system for both linear and nonlinear isotherms were obtained through the equilibrium test. Additional experiments were performed to investigate the influence of binding and temperature on the pore size distribution and porosity of the high performance concrete. A mercury intrusion porosimetry (MIP) test was carried out to examine the influence of binding products on concrete porosity and pore size distribution at different exposure conditions. Additional tests, including compressive strength and porosity tests, were also conducted. All testing procedures were performed using high performance concrete samples from the same mix.

The study presented in this thesis has been limited to a fully saturated high performance concrete made with ternary blended cement and treated under different temperature conditions up to age 208 days. The chloride profiles used to obtain the chloride parameters under these conditions have been projected from concrete samples exposed to a high chloride concentration as per the bulk diffusion test (ASTM C1556).

2 BACKGROUND

This chapter presents a background on the general causes of deterioration of reinforced concrete exposed to a saline environment. The focus is on corrosion as the main cause of structural distress, as well as the definitions of service life with respect to corrosion, and chloride sources and their penetration mechanisms into concrete material. The background also covers an overview of the diffusion theory and the use of Fick's second law in modeling chloride ingress into concrete. Factors influencing chloride ingress into concrete along with common test procedures and methods used to evaluate and quantify chloride transport parameters are included.

Section 2.1 outlines the deterioration of reinforced concrete structures exposed to a chloride environment, with a focus on the corrosion of reinforcement as the major cause of structural distress and deterioration. The general definition of the service life of reinforced concrete structures with respect to the corrosion of reinforcements is outlined in section 2.2. Because chloride attacks are considered as the main cause for the corrosion initiation of reinforcement, an overview of chloride ion penetration, its transport mechanisms, the chloride diffusion theory, and the factors affecting chloride ion ingress into concrete are outlined and presented in section 2.3. Finally, the common experimental methods and procedures used to quantify concrete transport parameters are presented in section 2.4.

2.1 Deterioration of Reinforced Concrete Structure in Saline Environments

Reinforced concrete structures such as bridge decks, parking structures and marine structures are experiencing durability issues during their service life. Of specific concern are those structures exposed to harsh and severe environments such as marine and deicing salt applications. The structures are often designed to be durable, are expected to last for a long period of time (e.g., 75 to 100 years), and are anticipated to require a minimum level of maintenance and repair during their service life. However, premature deterioration of these structures has been observed and reported.

In many cases, the corrosion of reinforcement is reported as the main cause of the deterioration of reinforced concrete and structure durability[12]. As an example, a survey of collapsed buildings in England showed that, from 1974 to 1978, the immediate cause of failure of at least eight concrete structures was corrosion of the reinforcing steel [1]. Most of these structures were 12 to 40 years old at the time of collapse, although one was only 2 years old. Due to the importance of corrosion and its complications in reinforced concrete structures, a general background on the corrosion of concrete reinforcement is provided in the following subsections.

2.1.1 Initiation and Mechanisms of Reinforced Concrete Corrosion

The corrosion of reinforcements in concrete material is initiated as soon as the protective layer that develops on the surface of the steel rebar is broken down. The protective layer develops as a result of the concrete's high alkalinity. The pore solution of the concrete, which presents pH values ranging from 13 to approximately 14 due to the presence of Na^+, K^+, OH^- and Ca^{2+}, serves as an electrolyte. The high alkalinity causes the reinforcing steel embedded in concrete to develop a passive oxide layer (Fe_3O_4 – $Fe_2O_3\gamma$) with a 10^{-3} to 10^{-1} μm thickness, which maintains the underlying metal in a thermodynamically stable state [13].

Concrete is a permeable material. As such, it allows aggressive agents such as chloride ions (Cl^-) and carbon dioxides (CO_2) to penetrate into the level of reinforcement, causing the depassivation of the protective layer. Once the protective layer is destroyed and oxygen and moisture are present, corrosion is initiated and begins to propagate. The propagation process depends on the availability of oxygen and moisture within the concrete cover in the vicinity of the reinforcement. A common corrosion model for reinforced concrete structures, as proposed by Tuutti [14], is shown in Figure 2.1. According to Tuutti's model, the corrosion process can be divided into two periods or stages: the initiation period and the propagation period.

The initiation period refers to the time it takes for aggressive ions to penetrate the concrete to the level of the reinforcement in order to destroy (depassivate) the protective film and initiate corrosion.

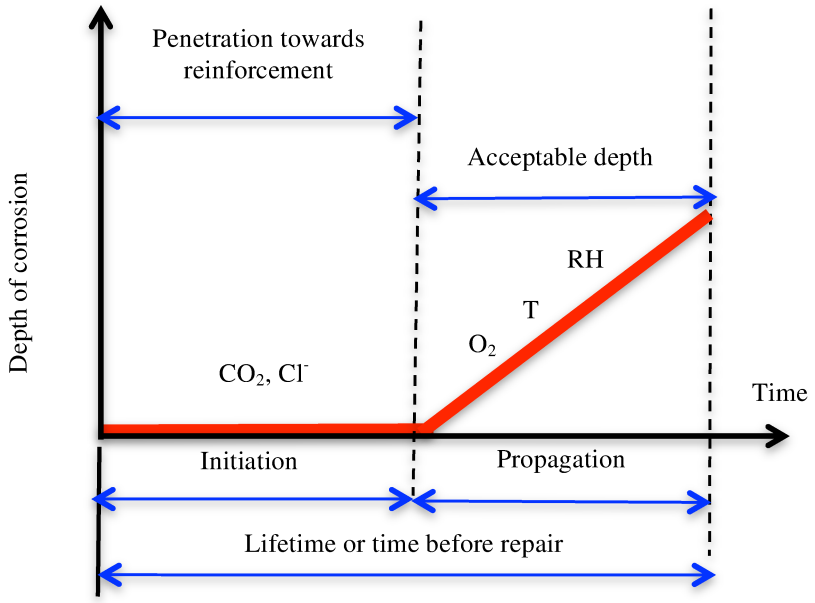

Figure 2.1 Various stages of corrosion [14]

The propagation period is associated with rust production and concrete volume increase. This stage starts at the time of initial corrosion and ends at the critical time at which corrosion would produce cracking and spalling of the concrete cover. The severity of this period depends on the availability of the oxygen and water in the area surrounding the reinforcing steel. The propagation phase corresponds to the development of the following reactions, which take place at the reinforcing steel surface:

$Fe \rightarrow Fe^{2+} + 2e^-$ (Anodic Reactions)

$Fe^{2+} \rightarrow Fe^{3+} + e^-$

$O_2 + 2H_2O + 4e^- \rightarrow 4OH^-$ (Cathodic Reaction)

$xFe^{++} + yO_2 + H_2O \rightarrow Fe_3O_4, Fe_2O_3, Fe(OH)_3, Fe(OH)_3.3H_2O$ (rust)

As a result of heterogeneities in the steel surface and due to the heterogeneous nature of concrete, one region of the steel rebar will act as an anode and another region as a

cathode, as shown in Figure (2.2). On the anodic locations, iron atoms lose electrons (oxidation) and flow as ferrous ions (Fe^{2+}) into the adjacent concrete. This reaction is known as the anodic reaction. The opposite reaction is the cathodic reaction, which takes place at the cathodic sites where the electrons flow through the steel to the cathodic locations and combine with oxygen and water to form hydroxyl ions (OH^-).

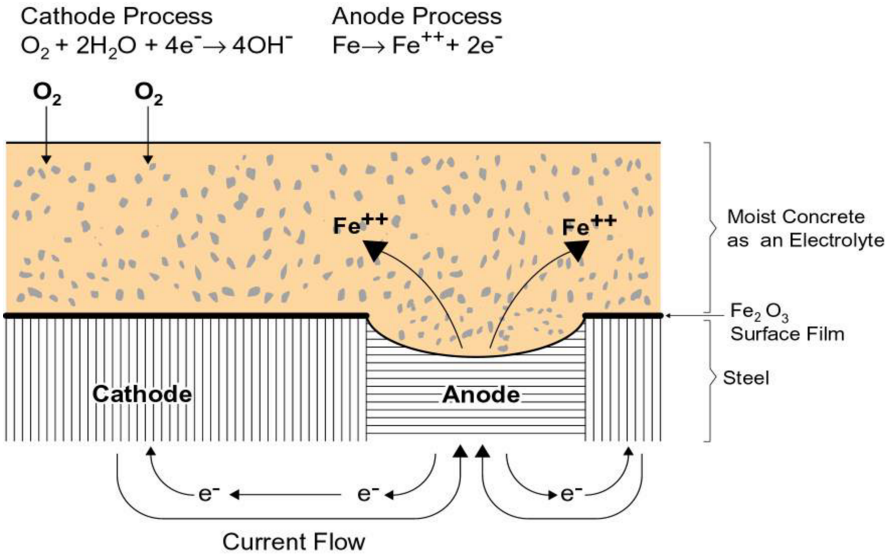

Figure 2.2 Schematic illustration of the corrosion of reinforcements in concrete [1]

Electrical neutrality is maintained when the ferrous ions migrate through the pores of the concrete to the cathode, where they combine with the hydroxyl ions to generate iron oxide, which is rust [15]. The volume occupied by the rust products is much greater than that occupied by the original reinforcing steel rebar. The volumes occupied by the different rust products in unit mass of concrete are shown in Table 2.1. As a result of increased volume in the vicinity of the reinforcements, expansive stresses are created on the surrounding concrete, which ultimately leads to cracking and spalling of the concrete cover.

Table 2.1 Various sizes of corrosion products [13]

Corrosion product	**Color**	**Volume in cm^3**
Fe_2O_4	Black	2.1
$Fe(OH)_2$	White	3.8
$Fe(OH)_3$	Brown	4.2
$Fe(OH)_3,3H_2O$	Yellow	6.4

2.1.2 Causes of Steel Corrosion

There are two main causes for the depassivation of the protective oxide layer in reinforced concrete structures: carbonation, and the ingress of chloride ions exceeding a certain amount or value, which is called the "threshold" or critical concentration. Carbonation often takes place in dry and high permeable concrete and induces a generalized corrosion. Chloride ions are more aggressive because they have the ability to penetrate deeply to the level of reinforcement. They attack the reinforcement and induce pitting or localized corrosion. A brief description for each of these causes and their role in the depassivation of the protective film is provided in the following subsections [12].

2.1.2.1 Carbonation

Carbonation is a process in which carbon dioxide in the atmosphere reacts with the hydration products of concrete, mainly the calcium and alkaline hydroxides. It starts at the surface and penetrates slowly to the interior concrete cover. The reactions that take place in the concrete as a result of carbonation are shown below [13]:

$CO_2 + Ca(OH)_2 \rightarrow CaCO_3 + H_2O$
$CO_2 + 2KOH \rightarrow K_2CO_3 + H_2O$
$CO_2 + 2NaOH \rightarrow Na_2CO_3 + H_2O$

In addition to the above reactions, other cement hydrates are also decomposed and hydrate silica, alumina, and ferric oxide being produced [92]. For instance, by a secondary reaction with pozzolanic silica, the carbonation of the C-S-H is also possible. When the carbonation front reaches the reinforcement and the pH of the concrete drops to approximately 8, the protected dioxide layer is depassivated or destroyed [16]. Figure 2.3 illustrates the mechanism of corrosion that results from carbonation.

Carbonation by diffusion is a very lengthy process and is controlled by a number of parameters [14]. These include the amount of material to carbonate, the concentration and diffusion coefficient of CO_2, and the relative humidity of the concrete cover. However,

carbonation can be very harmful for cracked concrete. The cracks allow easy penetration of carbon dioxide into the concrete cover and can lead to rapid carbonation. The diffusion of carbon dioxide follows air-filled pores. Corrosion due to carbonation is a relatively low probability and is generally associated with lower quality concrete and reduced cover. Therefore, in modern and fully saturated concrete with high quality, carbonation is not a major concern and is rarely responsible for the corrosion initiation of reinforced concrete structures.

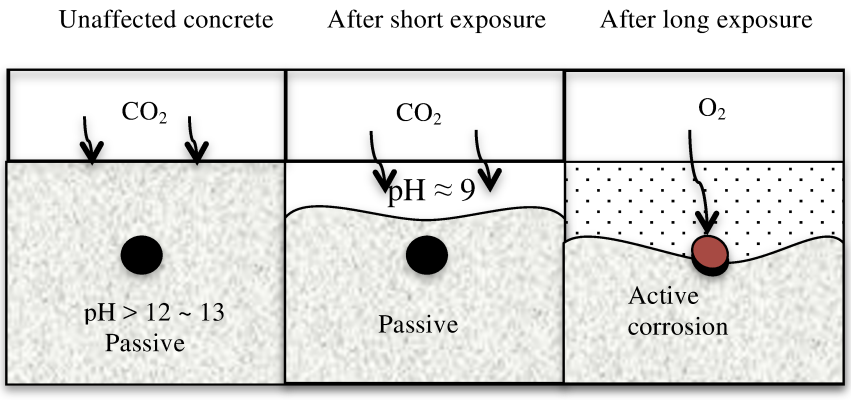

Figure 2.3 Corrosion process by carbonation [13]

2.1.2.2 Chloride Ingress

A common cause of reinforcement corrosion in reinforced concrete structures is the ingress of external chloride ions through a concrete cover. Unlike carbonation, chlorides have the ability to penetrate deeply into the saturated uncracked concrete cover, driven by the force of a concentration gradient of diffusion. When they reach the level of the reinforcement, they initiate corrosion. The specific role of chloride ions in the mechanisms of corrosion and chemical reactions that take place at the steel surface as a result of accumulated chloride ions are not clear. However, the depassivation of the steel protective layer by chloride can be seen as a function of the net balance between two competing processes: stability of OH^- ions, and disruption of the protective film by chloride ions [16]. In the electrochemical corrosion reactions, it is assumed that the chloride ions are not consumed but instead form only intermediate corrosion products,

such as $FeCl_2$. Subsequently, hydrolysis liberates the chloride ions again, and hydrogen is released [17]. This reaction can be expressed as follows:

$FeCl_2 + 2H_2O \rightarrow Fe(OH)2 + 2H^+ + 2Cl^-$

On an electrochemical level, there is also an exchange of electrons taking place:

$Fe + 2H^+ + Cl^{2-} \rightarrow Fe^{2+} + Cl^{2-} + H_2$

Note that the chloride atom does not enter into reaction itself. These reactions reduce the pH at anodic sites and increase the (OH^-) ions formation, which may increase the pH at cathodic sites. Therefore, the conditions become more favorable for corrosion and high corrosion rates may be generated. Chloride ions are often produce pitting corrosion. The depassivation of the protective layer by chloride ions and chloride-induced pitting corrosion process is illustrated in Figure 2.4. For chloride ions to break down the passivity of steel, they need to exceed a certain concentration, called the chloride threshold concentration. This threshold was found to be a function of the concrete pH (i.e., the OH^- concentration). According to Hausman [18], the threshold Cl^- ion concentration is about 0.6 times the OH^- ion concentration.

As a matter of practice, most of the standards and code specifications do not address the Cl^-/OH^- ratio but rather refer only to the total content of chloride in concrete, specified by weight of concrete, weight of binder, or weight of chloride per volume of concrete. While most data on chloride ingress are often presented by concrete weight, the chloride threshold level is most commonly expressed as a percentage weight of the binder content. To convert values of chloride levels from percentage weight of concrete to percentage weight of binder, researchers use a multiplier equal to the ratio of concrete density to binder content [19]. On the basis of binder weight, the threshold chloride concentration values vary but are typically in the range of 0.35 to 0.8 %. These threshold values can be approximated to about 0.05 to 0.1% by weight of concrete, which is about 1.2 to 2.4 kg/m^3 chloride per volume of concrete.

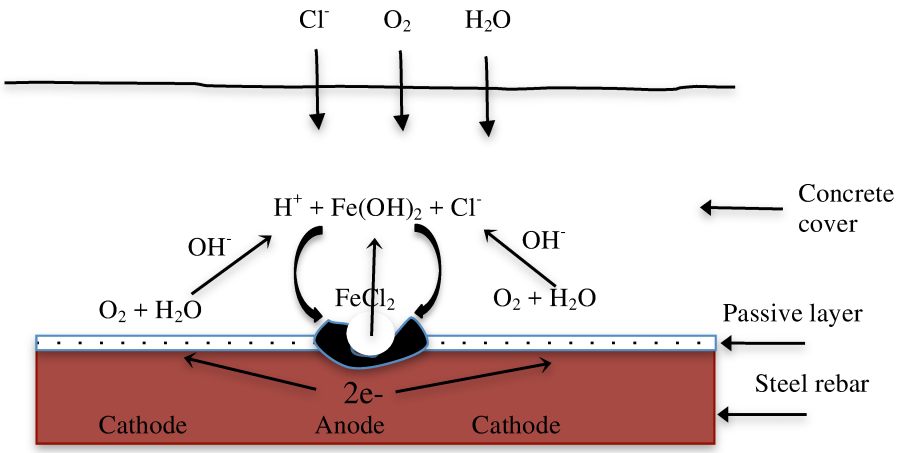

Figure 2.4 Depassivation of protective layer by chloride-induced pitting corrosion process [17]

In North America it has become common practice to limit the chloride threshold to 0.4% by weight of cement, indicating that this is a reasonable value to use for design purposes. Further details on the critical chloride content in reinforced concrete are discussed by Angest et al. [20].

2.1.2.3 Deterioration of Reinforced Concrete Structure Due to Corrosion

The deterioration of concrete due to corrosion is a progressive process. Corrosion by-products occupy a much larger volume than the original reinforcing steel, as indicated in Table 2.1. This increase in volume results in increased pressure on the reinforcing steel and concrete interface, which leads to cracking or delamination of the concrete cover. The process of corrosion is somewhat self-accelerating, since once cracking and spalling begin, the chemical and physical effectiveness of the cover is impaired, and higher corrosion rates may be expected. Structural distress may eventually result owing to the loss of cross-sectional areas of the reinforcement or the loss of bond from continued spalling. This process is schematically shown in Figure 2.5.

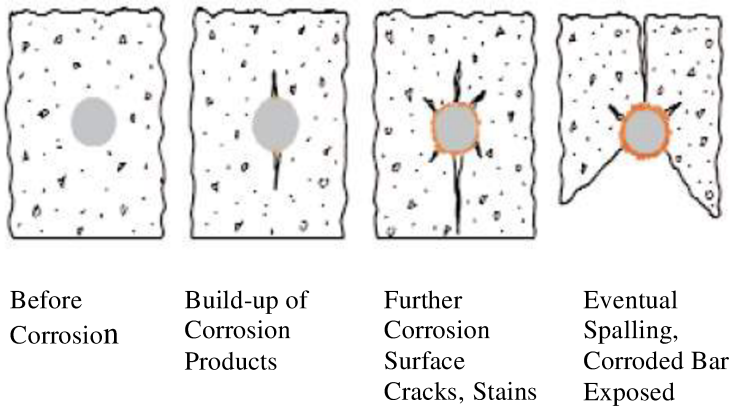

Figure 2.5 Influence of corroded rebar on surrounding concrete [21]

The corrosion damage is usually observed first as rust stains and minute cracking over the concrete surface. Frequently, the cracks run in straight lines parallel to the underlying reinforcement, as shown in Figure 2.6. If repair steps are not taken at this early stage, the corrosion of the steel will proceed further, causing severe damage through delamination and spalling of the concrete cover. This can lead to safety hazards and in extreme cases, a loss of structural integrity. A photo of this type of damage is shown in Figure 2.6

Figure 2.6 Heavy delamination and corrosion damage in reinforced concrete structures exposed to marine environments [21]

2.2 Service Life of Reinforced Concrete Structures

In terms of corrosion, the service life of concrete structures is defined as the time during which the performance of the structure is fulfilled. However, structure lifetime is usually described in terms of initiation and propagation of corrosion, as presented in Tuutti's model [14]. The technical criteria for the service life can be summarized as follows:

- Initiation of corrosion
- Visibility of corrosion products on concrete surface
- Cracking and spalling of concrete cover due to corrosion
- Reduction in the bearing capacity of the structure as a result of steel cross-section loss

Additional important factors reported by Fidjestol [22] regarding the determination of the structure service life include:

- Aesthetics
- Public opinion
- Public safety

From the above criteria, it can be seen that limiting the structural service life to be identical with the initiation period stage would be a conservative approach. However, it would have the advantage of reducing rehabilitation costs compared with those accrued during the propagation period. The damage that might have occurred usually requires less expensive work repair, which will significantly reduce expenditures. Furthermore, from the structural aspect, reinforced concrete structures such as marine structures, bridge decks and parking structures are exposed to dynamic loads and need to be ductile; corroded reinforcement may not be able to satisfy this criterion. Structural designers often provide excess reinforcement, so an acceptable degree of corrosion might be more appropriate to determine the structure lifetime.

The above factors might need to be balanced in order to determine the time at which the repair and maintenance should be applied. In this regard, Karlsson [23] suggested that a probabilistic approach might be useful in determining the time at which the repair might

be needed. This is based on the fact that all reinforced concrete structures in a particular instance will not start to corrode at the same time. Therefore, the most appropriate and convenient approach to define the structure service life is the time by which a certain level of corrosion (say, 5% of the inspected zone) has started to corrode.

As can be noted from the above definitions, no agreement has yet been reached on a specific term of the structure service life. After the initiation period, a structure might serve for many years. This will include the propagation period in the service life terminology. Even after severe corrosion has taken place, which could involve cracking and spalling of the concrete cover and the loss of the cross-section area of the reinforcement, the load-carrying capacity of the structure might well satisfy technical requirements. The service life may be reached despite satisfactory structural capacity due to aesthetics, safety, and/or public opinion. In this research, the structure service life is limited to the initiation period of corrosion.

2.3 Chloride Ingress into Concrete

Chloride ions represent one of the most aggressive and hazardous attacks on reinforced concrete structures during their service life[12,24]. Therefor, understanding its fundamental mechanisms and transport in concrete is crucial. The following sections provide some fundamental information on the source of chlorides in concrete, the transport mechanisms of chlorides, diffusion theory and the use of Fick's laws in modeling chloride into concrete, and factors influencing chloride ingress into concrete.

2.3.1 Sources of Chlorides in Concrete

Chloride ions may exist in concrete either as a result of an internal source (e.g., by using contaminated ingredients and certain chemical admixtures) or as a result of penetration from external sources in the surrounding environment (e.g., seawater, de-icing salts or industrial processes). Today, many concrete codes and practices prohibit the use of any chemical admixtures containing chloride ions such as calcium chloride accelerators. The American Concrete Institute (ACI) Publication 222R-01, for instance, limits the amount

of chloride in concrete for new construction to 0.06%, 0.08% and 0.15% by weight of cement for prestressed steel, wet conditions and non-prestressed dry conditions, respectively. In modern reinforced concrete applications, the external sources such as seawater and deicing salts are often the major chloride sources [24].

2.3.1.1 Seawater

Seawater, which is one of the main sources of chloride ions, makes up 70% of the surface of the earth. Not surprisingly, a large number of reinforced concrete structures are exposed to seawater either directly or indirectly (e.g., winds can carry seawater spray for a few miles inland from the coast). Seawater is fairly uniform in terms of chemical composition, which is characterized by the presence of soluble salts. The ionic concentrations of sodium (Na^+) and chloride (Cl^-) are the highest, typically 11,000 and 20,000 mg/l, respectively [12]. Three zones of exposure are recognized for reinforced concrete structures exposed to seawater: submerged zone, splash zone (tidal) and atmosphere zone. Each zone has its own unique exposure condition, which determines the type involved in the chloride transport mechanism[24].

2.3.1.2 Deicing Salts

Deicing salts are considered as the major source of chloride ions that attack reinforced concrete structures in cold climate regions. Deicing salts are frequently used in cold climate regions during winter periods to remove ice from concrete pavement and traffic areas such as roads, bridge decks, sidewalks, and parking decks. They become essential materials for winter roadway maintenance operations. In the United States alone, the amount of deicing salts used per year was estimated to be 15 to 20 million tons, and Canada used another 4 to 5 million tons [25]. The use of road salt for deicing is cost-effective but causes damages to concrete and is often responsible for the corrosion initiation of reinforcements. This has become a serious problem and major concern for reinforced concrete structures such as concrete pavement and bridge decks. When de-icing salt is used to remove snow and ice from the roads, concrete structures are exposed

to melt water with very high chloride concentration. Other structures such as parking garages may be exposed to chloride solutions transported from the roads by vehicles.

2.3.2 Chloride Transport Mechanisms

The ingress of chloride ions into concrete takes place through pore spaces in the cement paste matrix or micro-cracks that may exist within the concrete cover. A variety of physical and chemical mechanisms may govern the chloride transport process in concrete, depending on chloride concentration, exposure conditions, ambient temperature, concrete porosity, pore structure, and the degree of saturation of the concrete cover. According to Poulsen and Mejlbro [24], the transport mechanisms of chlorides in concrete usually take place in the form of diffusion, permeation, convection (capillary section) or migration. These mechanisms may act simultaneously or in sequence, or one of them may serve as the exclusive transport mechanism. How they act depends on the exposure conditions as well as the moisture content of the concrete cover. A brief description of each of these mechanisms is given below.

2.3.2.1 Diffusion

Diffusion is the movement of a substance under a gradient of concentration from a high concentration zone to a low one. In order for chloride ions to move in a pore system, a certain level of moisture must be available. In fully saturated concrete, diffusion is the dominant transport mechanism for chloride ions in pore solution. The diffusion process into concrete is governed by Fick's first and second laws as will be discussed later in this chapter. As a mechanism, diffusion is a relatively slow process because it takes long time for chloride ions to travel under the concentration gradient and reach the level of reinforcement.

2.3.2.2 Permeation

Permeation is a process in which chloride transport is driven by differences in hydraulic pressure in various zones. Chlorides move into zones of lower hydraulic pressure. As a transport mechanism for chloride ions, permeation may occur in instances where one face

of a structure is exposed to high hydraulic pressure (such as marine structures in harbors and tunnels) or when the seepage of solution takes place through retaining structures [17].

2.3.2.3 Convection (Capillary Section)

Similar to permeation, the ingress of chloride is driven by a moisture gradient, where chlorides move with water towards zones with less moisture content due to the capillary suction action of the pore solution. Convection takes place when the concrete is partially saturated or dry. In real-life conditions, concrete surfaces usually undergo wetting and drying cycles. When water encounters a dry surface, it will be drawn into the pore structure through capillary channels. Since the depth of the drying surface is typically small, the convection process cannot by itself bring chloride ions to the reinforcement level, unless the concrete is of extremely poor quality or the cover thickness is shallow. Convection mechanism is considered as a rapid transport process.

2.3.2.4 Migration

Migration is the movement of charged substance (i.e., chlorides) under the action of an electrical field [26]. The migration of chloride ions may occur in concrete when it is exposed to a stray current, such as in subway tunnels. Chlorides migrate from soil to concrete under electrical potential and cause pitting corrosion. The speed of the migration process depends on the magnitude of the applied electrical field but is in general considered a rapid transport process. Based on the migration theory, the derived chloride coefficient is often known as the chloride migration coefficient.

Of the mechanisms, diffusion and convection are the predominant transport mechanisms of chloride ions in concrete structures such as bridge decks and marine application exposed to splash and atmosphere zones. The level of moisture content in the capillary pores of concrete microstructure determines which mechanism is dominant. When the capillary pores are relatively dry, convection dominates, but if the capillary pores are fully saturated, diffusion dominates. These two transport mechanisms usually act

simultaneously, and the dominant transport mechanism varies with the porosity of the concrete, the moisture content, and the exposure conditions.

The focus of this research is on the modeling of chloride ingress into saturated concrete where the chloride transport is controlled only by diffusion process. Accordingly, the fundamental principles of diffusion theory and its application in modeling and predicting chloride penetration into concrete are presented herein.

2.3.3 Diffusion Theory and Derivation of Fick's Second Laws

Diffusion is the predominant transport mechanism of chloride ions in saturated concrete. It is therefore important to understand the principle and background of diffusion theory and how it was applied to concrete. The diffusion theory was first introduced by Adolph Eugen Fick (1829-1901), who proposed the mathematical models on which the theory of diffusion is mainly based [24]. His mathematical theory was valid for diffusion as well as for heat movement. He proposed and developed two laws, known as Fick's first and second laws. However, the application of Fick's laws on chloride diffusion in concrete came many years later, with work by Collepardi et al. (1970, 1972) [5].

2.3.3.1 Fick's First Law

Fick's first law is presented in Eq. (2.1). The law suggests that the transport of chloride ions through a unit area of concrete per a unit of time (the flux J) is proportional to the concentration gradient of the chloride ions.

$$J = -D_{eff} \cdot \frac{\partial C_f}{\partial x} \quad \text{..... Eq. (2.1)}$$

where:

J : the flux of free chloride ions ($kg/m^2.s$)

D_{eff} : the diffusion coefficient, (m^2/s)

C_f : the concentration of free chloride ions, (kg/m^3 of solution)

X : a position variable, (m)

The negative sign in Eq. (2.1) shows that the chloride ions move in a direction opposite to that of increasing chloride concentration. The chloride effective diffusion coefficient, D_{eff}, is assumed to be constant and is usually referred to as D_{Fl} in the published literature. It should be noted that D_{eff} is the effective chloride diffusion coefficient when the free chloride concentration, C_f, is expressed in kg/m^3 of pore solution. However, if C_f is expressed in kg/m^3 of material, D_{eff} needs to be multiplied by a porosity term [27].

2.3.3.2 Fick's Second Law

In practice terms, Fick's first law presented in Eq. (2.1) is only useful where there is no change in chloride concentration with time after the steady-state conditions have been reached. In real conditions, chloride concentration is not constant but changes with time. This is called a non-steady state of diffusion. The non-steady state of chloride diffusion in concrete can be explained graphically, as shown in Figure 2.8 [24]. When chloride ions diffuse into concrete, a change in the chloride concentration, C, takes place at any time t along every point x of the concrete depth.

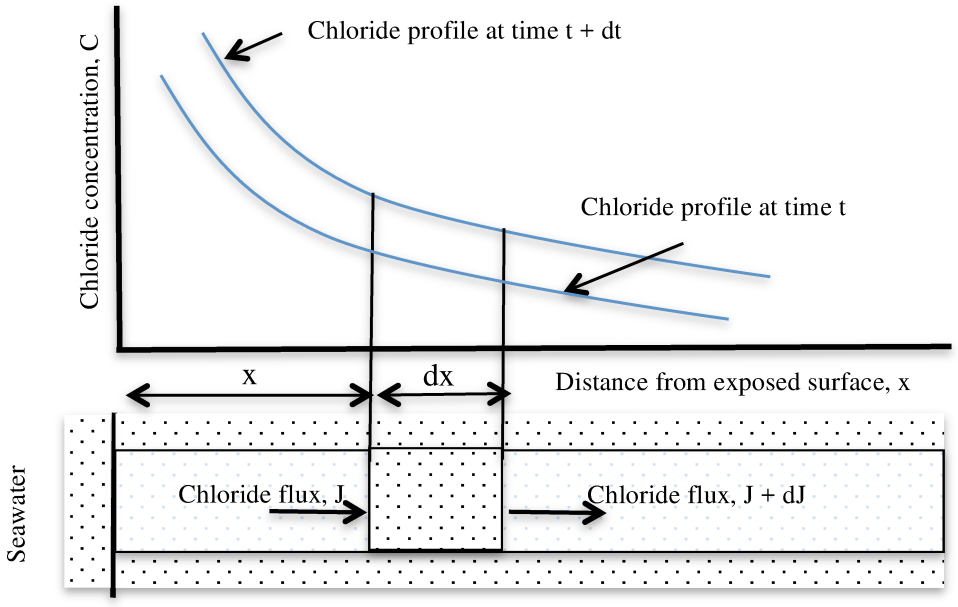

Figure 2.7 Chang e of chloride concentration, as described by Fick's second law [24]

According to Poulsen and Mejlbro [24], the relevant Fick's second law can be derived by considering an element (infinitesimal concrete slice) parallel to the chloride diffusion into a semi-infinite volume of concrete. If the element cross-section is taken as dA = 1, then the element volume dV between the two consecutive sections at a distance of dx will be equal to dx and the amount of total chloride per unit time dt = 1 which diffuses into this volume dV will be equal to the flux J, as can be seen in Figure 2.7. Similarly, the amount of chloride which diffuses out from the volume dV is equal to the flux at the abscissa x + dx. Hence, the flux J changes along the x-axis into the concrete by dJ/dx per unit length of x-axis. Therefore, the increases in chloride in volume dV at time dt = 1 become:

$$\frac{\partial C}{\partial t}dx = J - \left(J + \frac{\partial J}{\partial x}dx\right) = -\frac{\partial J}{\partial x}dx \qquad \text{Eq. (2.2)}$$

or:

$$\frac{\partial C}{\partial t} = -\frac{\partial J}{\partial x} \qquad \text{Eq. (2.3)}$$

Equation (2.3) represents Fick's second law of diffusion, which is also called a mass balance equation. Here, it pertains to the chloride amount in a unit volume of concrete, since it describes how the change in chloride content per unit time of an infinitesimal volume is equal to the difference in chloride flux to and from the infinitesimal volume per unit length. Fick's second law simply says that the change in chloride concentration per unit time is equal to the change of flux per unit length.

By applying Eq (2.1) in Eq (2.3), the mass balance equation Eq (2.3) becomes:

$$\frac{\partial C}{\partial t} = \frac{\partial}{\partial x}\left(D_{eff}\frac{\partial C_f}{\partial x}\right) \qquad \text{Eq. (2.4)}$$

Equation (2.4) is also known as Fick's second law of diffusion. The Fick's second law as applied in concrete requires that the chloride concentration on the both sides of the

equation need to be the same. This is due to the influence of binding in concrete. Chloride binding will be discussed in details in Chapter 3. If the binding is assumed to be linear or constant and the chloride concentration on the both sides of Eq. (2.4) are equal, the Fick's second low in its simplified form is written as shown in Eq. (2.5)

$$\frac{\partial C}{\partial t} = D\frac{\partial^2 C}{\partial x^2} \quad \text{.....Eq. (2.5)}$$

Where D is the diffusion coefficient (m^2/s). If the C in Eq. (2.5) represents total chloride concentration in concrete, also known as acid-soluble chloride, then the $D = D_a$ where, D_a is called the apparent diffusion coefficient. Equation (2.5) is the well-known Fick's second law form that has been widely used in chloride models to predict chloride ingress into reinforced concrete structures.

Under the assumptions of homogenous concrete, constant diffusion coefficient and surface chloride concentration, linear chloride binding, and one-dimensional diffusion in semi-infinite space, the traditional error function solution to Fick's second law, which has been widely used in modeling chloride ingress into concrete, is as shown in Eq. (2.6) [6,28]:

$$C(x, t) = C_s \left[1 - \text{erf}\left(\frac{x}{2\sqrt{D.t}}\right)\right] \quad \text{.....Eq. (2.6)}$$

When initial chloride content, C_i, is presented, Eq. (2.6) becomes:

$$C(x, t) = C_s - (C_s - C_i)\,\text{erf}\left(\frac{x}{2\sqrt{D.t}}\right) \quad \text{.....Eq. (2.7)}$$

where C(x,t) is the chloride concentration at x depth (m) and time t (sec), C_s is the surface chloride concentration (% mass of concrete), C_i is the initial chloride content (% mass of concrete), erf is the error function. Equation (2.6) represents the simplest and most well-known error function solution used by researchers and engineers in the field to model

chloride ingress into concrete and to predict the service life of reinforced concrete structures exposed to marine or de-icing salts environments. The historical development of the error function as well as its limitations and drawbacks in modeling chloride ingress into concrete are presented and discussed in Chapter 4. Another solution to Fick's second law is the use of numerical finite difference approach. A typical example of a chloride model that uses the finite difference solution is Life-365. The finite difference approach in solving Fick's second law is detailed in Chapter 5.

2.3.4 Factors Affecting Chloride Ingress into Concrete

Chloride ingress into concrete is a complex process that is dependent on an interaction of many factors. Some of these factors are related to the concrete mix design, proportion and construction, while others are related to the construction and surrounding environmental exposure conditions. Factors related to concrete mix design may include cement type and content, water-to-binder ratio, and the use of supplementary cementitious materials. Poor placement, inadequate consolidation and cover thickness, and improper curing regime are construction factors that could significantly impair the quality of a concrete mix design and thus facilitate the ingress of chloride ions deep inside the concrete. Factors that are related to the environmental conditions may include exposure temperature, chloride type and intensity, and environmental exposure conditions (marine or de-icing).

Because of the practical importance of these factors, a separate discussion of each of these factors is provided in the following subsections.

2.3.4.1 Factors Related to Concrete Material

Chloride ingress into concrete is a function of concrete porosity, number, size distribution and interconnectivity of pore structures of the cement paste. The pore structure characteristics of the concrete are controlled by a number of factors, including cement type and content, water-to-binder (w/b) ratio, use of supplementary cementitious materials (SCMs) and curing/maturity.

2.3.4.1.1 Portland Cement Type and Content

The influence of Portland cement type and content on the chloride ingress of the concrete has been studied extensively. Previous studies have shown that the chemical compositions of cement, in particular its alumina content, play a significant role in controlling the chloride penetration into concrete [29-33]. The key role of cement type influencing chloride penetrability into concrete is mainly related to its ability to bind chloride ions and prevent them from moving to the reinforcement level [34]. The influence of cement type on binding is discussed in greater detail in Chapter 3.

2.3.4.1.2 Water-to-Binder Ratio (w/b)

Water-to-binder ratio (w/b) plays an important role in controlling the porosity and permeability of concrete material and thus has a direct influence on its chloride transport properties. The connectivity of the pore system depends on the amount of original mixing-water-filled space and the degree to which it has been filled with hydration products. Generally speaking, a high w/b ratio leads to high concrete porosity, and vice-versa. A higher w/b ratio leads to higher porosity because the excess water in the cement paste matrix that escapes from the mass during the hydration process forms a continuous porous pore system [35]. When the w/b ratio is high and the degree of hydration is low, the binder paste will have a high capillary porosity and will contain a relatively large and well-connected pore structure. This will lead to high permeability and ease the transport of chlorides in the pore structure system. Binder type and content, degree of hydration and curing conditions are some factors that contribute to the porosity and permeability of concrete [36].

With regard to chloride diffusivity, previous research and studies have shown that chloride diffusion coefficients are strongly influenced by the w/b ratio of concrete [37-41]. Page et al. [40] tested concrete with a w/b ratio ranging from 0.4 to 0.6, and found that the effective diffusion coefficient is significantly influenced by the w/b ratio. Their data showed that the chloride diffusion coefficient of concrete with a w/b ratio of 0.4 was about 6 times lower than that of concrete made with a 0.6 w/b ratio (with the other

parameters being equal). Additional recent studies reported similar conclusions [39,42,43] Song et al. [39] investigated concrete containing 60% slag cement with w/b ratio ranging between 0.3 and 0.4. They concluded that both the apparent chloride diffusion coefficient and surface chloride concentration were significantly influenced by the water-to-binder ratio. Both parameters decreased as the w/b increased.

The water-to-binder ratio has also been found to influence the age parameter (m-value) that stands for reduction in diffusion coefficient over time. Several studies have shown that the age factor of the time-dependent diffusion coefficient is a function of the w/b ratio, with the value of m found to increase as the w/b ratio decreases [24,44]. This is very important, as the value of m has considerable implications in assessing and predicting the service life of reinforced concrete structures in chloride environments.

2.3.4.1.3 Supplementary Cementitious Materials and Blended Cement

Supplementary cementitious materials (SCMs), also known as mineral admixtures, such as fly ash, silica fume and ground granulated blast-furnace slag have a positive effect on the chloride diffusivity of concrete due to their physical properties and chemical compositions [36]. The addition of SCMs has two main benefits with regard to chloride penetration. First, they enhance concrete resistance to the ingress of chloride ions by physically altering and refining the pore structure, which reduces porosity and chloride permeability. The second beneficial effect is that both fly ash and slag have been found to increase the binding capacity of the concrete, which reduces the amount of free chlorides in the pore solution [45]. Some SCMs also have significant impact on the value of m.

Numerous studies confirmed that the incorporation of SCMs in concrete significantly reduces its porosity and permeability, which thus increase the ability of concrete to resist the ingress and the movement of aggressive substances such as chloride ions and carbon dioxide [46-53]. The incorporation of SCMs in concrete improves the microstructure of the concrete by subdividing and refining the capillary pores, reducing the connectivity of the pore structure, and densifying the porous paste-aggregate interfacial transition zone. This is because the reactive silica presented in some SCMs such as fly ash and silica fume

reacts with the lime (calcium hydroxide) formed from the first reaction of Portland cement with water during the hydration and converts it to secondary calcium silicate hydrate (C-S-H) gel. As a result of the consumption of the calcium hydroxide by the pozzolanic reaction, the concrete microstructure is densified and the pore structure is refined. Good correlations were found between the chloride diffusion coefficient and the total pore volume of the blended cement pastes tested by Hossain [54].

SCMs can influence the diffusivity of concrete in several ways. While silica fume results in a fast reduction in the chloride diffusion coefficient due to its extreme fineness and high surface area, its effect is limited to the early age of concrete. Fly ash and slag contribute to the reduction in the chloride diffusivity at later ages. The influence of fly ash and slag is related to the pozzolanic reaction and slow hydration rate, which take place over time. For this reason, concrete made with ternary blended cement is characterized by its improved diffusivity at early ages due to the influence of silica fumes, but at later ages due to the influence of fly ash or slag [46,54,55]. The diffusion coefficients of blended ternary cement concrete have been found to be much lower than that of concrete made with normal Portland cement when other parameters are equal [46].

Daube and Bakker [56] have shown that when slag cement content is at least 60% by mass of the cementitious materials, the chloride diffusion coefficient of the concrete is at least ten times smaller than that of concrete made from Portland cement only. More recently, Hossain et al. [57] found that the addition of Ultra-fine fly ash improved the chloride penetration resistance of concrete, and that the partial replacement of Portland cement by silica fume has even more pronounced benefits.

Blended cement is known to improve chloride resistance at later ages and its use is often associated with high reduction in the diffusion coefficient value. The reduction in the diffusion coefficient is often measured by means of the age parameter. The age parameter for blended ternary cement concrete has been reported in the range of 0.3 to 0.7, depending on the replacement levels of fly ash or slag [58], whereas the typical value of the age parameter for Portland cement concrete is in the range of 0.2 to 0.25 [46]. The

reduction of the diffusivity over time is related to the evolution of the porosity as a result of the ongoing hydration and pozzolanic reactions of fly ash or slag cement. Figure 2.8 shows the effect of fly ash and slag cement on the value of chloride diffusion coefficient.

In general, the addition of SCMs to concrete is considered an effective measure to mitigate chloride-induced corrosion of steel rebar in concrete. The role of SCMs with regard to binding is discussed in detail in Chapter 3.

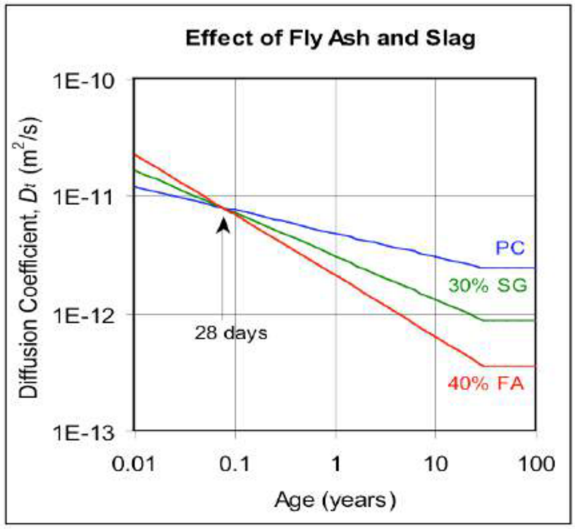

Figure 2.8 Influence of fly ash and slag cement on chloride diffusion coefficients, Life-365

2.3.4.2 Factors Related to Construction Practices

Despite the fact that modern reinforced concrete structures like bridge decks, parking garages and marine applications are typically constructed using blended cement concrete with relatively low permeability, some of these structures have shown premature deterioration and have required early repairs and maintenance. Corrosion of embedded steel reinforcement is generally the major cause of the deterioration in these structures, as stated earlier in this chapter. However, corrosion does not initiate until there are sufficient chloride ions at the surface of the reinforcing steel, and this accumulation should not occur fast as long as the concrete possesses low permeability. Therefore, a

reasonable explanation for the premature deterioration of reinforced concrete structures exposed to chloride environments is poor construction practices.

Construction factors such as improper casting, bad placement, inadequate consolidation techniques and cover thickness, and poor curing regimes can lead to surface cracking, poor compaction, and high concrete porosity and permeability. These outcomes can reduce concrete's resistance to the ingress of aggressive agents. The effects of construction factors on the permeability and durability of concrete structures are discussed in detail in the next sections.

2.3.4.2.1 Improper Vibration and Consolidation

The vibration and consolidation techniques used to facilitate the placement and casting of conventional concrete can, when performed improperly, adversely affect its mechanical properties and its ability to resist the ingress of chloride ions. Improper vibration and consolidation can lead to inhomogeneous distribution of solids, liquids and air in concrete. For instance, over-vibration can cause bleeding and segregation, whereas under-vibration can result in honeycombing and excessive entrapped air-voids (bug-holes).

Over-vibration can lead to excessive bleeding, where the relatively heavy solid constituents in freshly cast concrete tend to settle. This results in an upward displacement of part of the free water in the form of bleeding. Rising bleed water causes variations in the w/b ratio between the upper and lower portions of a cast section, which affects the in-situ porosity and mechanical properties of concrete [59]. The effect of bleeding on concrete durability can be dramatic when fine desiccated bleed water channels, pathways and voids are formed within the concrete matrix, increasing its permeability. This is especially harmful because most of these pathways have a capillary nature that enables the absorption of deleterious agents (chlorides, moisture, oxygen, etc.) into the concrete cover, which accelerates the deterioration of the reinforcement [60].

Segregation, on the other hand, which is usually coupled with bleeding, can also form as a result of over-vibration. Segregation is the tendency for coarse aggregate to separate

from the sand-cement mortar. This results in part of the mixture having too little coarse aggregate and the remainder having too much. The lack of coarse aggregate can lead to high potential of shrinkage cracking, which substantially facilitates the ingress of aggressive agents and thus the deterioration of steel reinforcement. Moreover, the lack of fines can lead to voids and gaps within the concrete, which can significantly impair the permeability and durability of the structure.

The most serious defects resulting from under-vibration is honeycombing, which occurs in stiff concrete mixtures that are not sufficiently vibrated. The lack of vibration results in a mortar that does not fill the spaces and gaps between the coarse aggregate particles, as shown in Figure 2.9. Honeycombing is generally caused by using improper or faulty vibrators, improper placement procedures, and poor vibration procedures. Honeycombs can extend deep into a concrete structure. This will result in further deterioration of the concrete structures because moisture and chlorides can easily work their ways through the honeycombed areas to the reinforcement level.

Figure 2.9 Influence of poor compaction and vibration on concrete matrix made with blended cement

Bug-holes are surface voids that result from the migration of entrapped air to the fresh concrete-form interface. Perhaps the most influential cause of bug-holes is improper

vibration. Consolidation, usually through vibration, sets the air and water bubbles into motion. An improper amount of vibration sends both entrapped air and excess water to the free surface of the concrete, either vertically winding through the matrix or laterally to the form wall. Although these surface voids are primarily considered an aesthetic problem for exposed structural concrete, they could impair the durability of the concrete surface by reducing the time of penetration of destructive agents to the reinforcement.

2.3.4.2.2 Inadequate Concrete Cover Thickness and Properties

The time to corrosion onset in reinforced concrete structures and the rate at which the corrosion reactions will take place strongly depend on the cover thickness and the details of its properties. Reinforced concrete structures exposed to severe environmental conditions such as marine and de-icing salt environments require a 50 to 75 mm cover thickness, as specified by many concrete codes and practices. This cover thickness is necessary to provide sufficient protection to the reinforcement against aggressive ions such as chloride ions. The goal is to ensure adequate durability. However, in practice, providing a consistence cover thickness over the reinforcement is difficult and in many cases not achievable. Variations in slab cover thickness during construction are a common problem in structures such as bridge decks, parking garages and marine structures. Cover thickness is a key parameter in the service life of models, so its quality and thickness are crucial. Premature deterioration of numerous reinforced concrete structures is probably due to a lack of proper concrete cover thickness [61], which then requires corrective action involving costly repairs.

2.3.4.2.3 Poor Curing Regime

Another important factor that can adversely affect the durability of concrete is an initial poor curing regime. Curing in the field is perhaps one of the most critical factors in the concrete construction process. Sufficient curing is essential if the concrete is to perform its intended function over the life of the structure. Poor curing practices can also adversely affect concrete hardened properties of the cover thickness and increase its porosity and permeability. The two key parameters for estimating the service life of a

concrete structure are the chloride diffusion coefficient and the age parameter. These can be significantly affected by poor curing [62]. Poor curing also leads to high diffusion coefficient values and low age parameter values, both of which promote high ingress of chloride ions into concrete, from which premature deterioration can be expected to ensue.

Another potentially detrimental effect associated with poor curing is plastic shrinkage cracking. Plastic shrinkage cracking occurs within the first few hours after the concrete has been placed and before it gains significant strength. Plastic shrinkage occurs when the rate of water loss due to evaporation exceeds the rate at which the bleed water rises up to the surface of the concrete. This leads to volume changes and results in a build-up of tensile tresses in the surface layer of concrete. When the shrinkage tensile stresses caused by plastic shrinkage exceed the tensile strength of the fresh concrete that is only beginning to develop, cracking occurs [63]. Typically, plastic shrinkage cracks are parallel and are spaced from 0.3 m and 1 m apart. The crack depth generally ranges from 25 to 50 mm [1].

Plastic shrinkage cracks can become critical weak points for the penetration of aggressive substances, in particular chloride ions. This penetration leads to the acceleration of the corrosion process and other detrimental forms of concrete deterioration such as spalling and delamination of the concrete cover. Consequently, the performance, serviceability, and durability of concrete structures are significantly reduced.

It is interesting to note that construction factors are rarely considered in the existing service life models. This may be due to the difficulties associated with modeling such factors, given their wide variety and intricacy. Existing service life models estimate the design life of concrete structures based on chloride parameters derived from the mix design proportions and data available on the environmental conditions of the location in which the structure is intended to be built. They often assume that the concrete is ideally constructed and free of any defects. These models generally ignore the fact that the concrete quality of the mix design could be unfavorably affected during the construction process due to any number of construction factors. As a result, in many cases, the

designed service life does not, in reality, reflect the actual service life of the built structure.

For a proper estimation of the structure's service life and to include the potential influence of construction factors in concrete hardened properties, the values of chloride parameters such as chloride diffusion coefficient and age factor should be derived from a concrete that has already been placed and cured. A mix design whose properties could significantly be altered by such factors will not necessarily provide a realistic service life estimate.

2.3.4.3 Factors Related to Exposure Conditions and Chloride

2.3.4.3.1 Exposure Time Dependency

Chloride ingress into concrete is time-dependent. Field observations and careful studies have shown that both the chloride diffusion coefficient and surface chloride concentration are strongly dependent on the period of exposure of concrete to a chloride environment [62,64-69]. Costa and Appleton [69] examined 54 concrete panels made with three different concrete mixes that were exposed to various marine environmental zones for three to five years. Their study concluded that both the chloride diffusion coefficient and the surface chloride concentration were time-dependent. This is because of the ongoing hydration of the cement matrix and binding effects, both of which alter the porosity and pore volume distribution of the concrete microstructure. As result, the rate at which chloride ions penetrate into concrete is changing over time.

The general trend is that the chloride diffusion coefficients decrease with time and the surface chloride concentrations increase with the time in the first few years of exposure [38]. However, the magnitude of the decrease in diffusion coefficients and increase in the surface concentration with time are functions of numerous factors, including binder content and type, curing, concrete maturity, and local environmental exposure conditions [70-72]. The effect of time on chloride diffusion coefficients has been extensively studied and well documented [6,46,58,62,73]. Moreover, surface chloride concentration varies

with the length of the exposure time and chloride concentration in the environment [74], and thus it is difficult to experimentally determine the surface concentration. For practical means, it should be determined either from examining old reinforced concrete structures or from concrete specimens placed in field exposure conditions.

2.3.4.3.2 Exposure Temperature

Exposure temperature has a great impact on chloride diffusivity, concrete microstructure and its binding capacity and corrosion rate [75]. Temperature can change chloride diffusion by altering the rate of chloride ions diffusing through the pore system of concrete and by altering the rate at which cement paste hydrates [58]. An increasing temperature can reduce chloride binding by releasing bound chlorides into the pore solution [10]. Therefore, it can be expected that when concrete is exposed to chloride at different exposure temperatures, changes in the rate of chloride ingress will occur. From the thermodynamic principles, an increase in temperature will lead directly to an increase in ionic diffusivity [75]. As is the case with exposure time effect, the influence of temperature on chloride ingress will be strongly dependent on the type and content of the concrete binder. Previous research and studies have suggested that the influence of temperature on chloride diffusivity obeys Arrhenius' Equation [76]. Therefore, in many chloride prediction models (in particular those based on Fick's second law), the influence of temperature on chloride diffusivity has been modeled using this equation. The influence of exposure temperature on chloride diffusion in concrete is often studied based on laboratory experiments. Examining chloride profiles from concrete exposed to hot and cold environmental conditions would yield a better understanding and more realistic results.

2.3.4.3.3 Chloride Concentration in Different Exposure Environments

The ingress of chloride into concrete depends on the intensity of chlorides in the surrounding environment. The chloride concentration in the surrounding environment varies with the exposure conditions of that environment. For instance, reinforced concrete structures in marine environments have exposure conditions different from that of

concrete exposed to de-icing salts agents. Consequently, the chloride aggressiveness will vary between the two types of environments.

Three zones are identified for reinforced concrete structures in marine environments: submerged zone, tidal or splash zone, and atmosphere zone. Each zone has its own chloride exposure characteristics [24]. Concrete structures in submerged zones will be constantly exposed to chloride, whereas concrete in tidal zones will be exposed to wetting and drying, and heating and drying cycles. The tidal zone is considered the most severe exposure condition. This is because the deterioration of concrete within this zone is not limited to the corrosion of the reinforcement by chloride ingress but also to other types of deterioration such as freezing and thawing attacks, thermo-cracking, leaching of calcium hydroxide, and so on. The atmosphere zone is a semi-wet zone where airborne chloride, as a result of wind and wave action, is considered the main source of chloride ions.

Chloride concentrations resulting from the use of de-icing salts for road bridges and equivalent concrete structures are prominent in winter but less significant in summer, when the surface chlorides are often washed out by rain. The main difference between concrete structures exposed to marine environments and those exposed to roadway de-icing salts is that while the marine exposure is continuous and quasi-homogeneous in time, the exposure to the de-icing salts is discontinuous and highly concentrated in the winter.

2.4 Common Methods and Test Procedures For Chloride Diffusion Parameters

A variety of techniques and test methods have been developed over the past decades to determine the chloride diffusion parameters, mainly diffusion coefficients. In many cases, the diffusion coefficient is used as a single indicator of the concrete's ability to resist the penetration of chloride ions [77]. However, the value of the diffusion coefficient is often influenced by the test conditions and techniques involved in its determination. The common test methods used to quantify the diffusion coefficient are the bulk diffusion test and rapid migration test. Diffusion tests are time-consuming and require a minimum testing period of 35 days. However, rapid migration test procedures are short-term tests

and usually only require 24 hours of testing. Examples of chloride diffusion tests include the bulk diffusion test (ASTM C1556) and Nordtest (NT BUILD 443). An example of rapid migrations tests is the Rapid Migration test, Nordtest (NT BUILD 492), also known as CTH test. Others tests that are widely used to evaluate concrete resistance to chloride ion penetrability include the Rapid Chloride Permeability Test (ASTM C1202), resistivity test methods, and pressure penetration techniques [4,78,79]. However, these methods do not provide any quantification for the diffusion parameters. Table 2.2 summarizes theses test procedures along with their features and durations.

Table 2.2 Summary of common chloride test methods

Test	**Method**	**Considers chloride ion movement**	**At a constant temperature**	**Approximation of testing period**
Long- term	Salt ponding (AASHTO T259)	Yes	Yes	90 days after curing and conditioning
	Bulk diffusion (ASTM & Nordtest)	Yes	Yes	≥ 35 days after curing and conditioning
Short-term	Rapid migration test (CTH)	Yes	No	24 hours after curing and conditioning
	Pressure penetration	Yes	Yes	Depends on pressure and concrete type
Others	RCPT (T277)	No	Yes	6 hours after curing and conditioning
	Resistivity	No	Yes	30 minute
	Sorptivity	No	Yes	One week
	Gas diffusion	No	Yes	2 – 3 hours

2.4.1 Chloride Diffusion Coefficients as Determined from Different Test Procedures

Chloride diffusion coefficients are critical parameters in chloride and service life prediction models of concrete structures. These coefficients can either be determined from natural diffusion experiments or from accelerated migration as outlined above. In terms of chloride concentration, two types of chloride coefficients exist: effective chloride coefficients and apparent chloride coefficients. The effective chloride diffusion/migration coefficient is determined from steady-state diffusion/migration tests, whereas the apparent diffusion/migration coefficient is determined from non-steady-state diffusion/migration tests. The steady-state chloride coefficient describes only the movement of free chloride in pore solution after the steady-state condition is established or when binding is completed. The non-steady-state chloride coefficient describes the movement of the total chloride content in concrete, with the assumption that the binding capacity is constant or linearly changes with concentration.

2.4.1.1 Effective Chloride Diffusion/Migration Coefficient (Steady-state Coefficient)

The effective chloride diffusion coefficient, D_{eff} or D_{F1}, can be determined from the steady-state diffusion cell test method or the steady-state migration test method. In the diffusion cell test, a thin slice of the material is placed between two cell chambers. One cell contains chloride solutions with known initial concentrations $C_{f,1}$ (mol/m^3), while the other cell, called a "downstream cell", collects chlorides passing through the specimen. The chloride concentration in the downstream cell, $C_{f,2}$ (mol/m^3), is kept close to zero by replacing the solution. By analyzing the chloride concentration in the downstream cell on a regular basis, the chloride flow through the specimen is measured. The steady-state flow, J (m^2.s), is reached once the flow becomes constant with time. The D_{eff} is then calculated from Equation (2.8) [28]:

$$D_{eff} = \frac{J.\delta}{(C_{f,1} - C_{f,2})} \quad \text{..... Eq. (2.8)}$$

where δ is the thickness of the specimen (m). The test period takes from few days to weeks, depending on the thickness of the specimen and quality or type of concrete.

The second test method, which has been frequently used by researchers in determining the effective chloride diffusion, is the steady-state migration test [75,80]. In this test, a saturated concrete specimen is placed between two compartments containing two different solutions. The upstream compartment contains sodium chloride solution saturated with sodium hydroxide and potassium hydroxide, whereas the downstream compartment contains sodium hydroxide and potassium hydroxide only. The sodium and potassium hydroxides are added to avoid the leaching of alkalis during the migration test, which could affect the test results (leaching of alkalis could change the pH which will influence the binding capacity of the concrete). An electrical potential of fixed magnitude (usually 4 V/cm) is applied across the specimen to accelerate the movement chloride ions through the concrete specimen. As for the diffusion cell test, the chloride concentration in the downstream cell is analyzed regularly and when the flow becomes constant after the steady state is reached, the effective migration coefficient is determined form Eq. (2.9) [79]:

$$D_{eff} = \frac{J}{C_{up}} \frac{RTL}{FU} \quad \text{.....Eq. (2.9)}$$

where J is the effective flux (mol/(m^2.s)), F is Faraday's constant, R is the gas constant, T is the absolute temperature (K), U is the potential difference between both ends of the specimen (V), L is the thickness of the specimen (m) and Cup is the chloride content in the upstream cell (mol/m^3). The test is time-consuming due to the low applied voltage. It takes from 15 days to two months for the steady state to be reached [79].

The effective chloride diffusion coefficients are more often used in the multi-ionic species model [78,79].

2.4.1.2 Apparent Chloride Diffusion/Migration Coefficient (Non-steady-state Coefficient)

The chloride diffusion coefficient, as determined from the bulk diffusion test, is called the apparent diffusion coefficient, D_a. The apparent diffusion coefficient is a chloride transport parameter often calculated from acid-soluble chloride profile data obtained from saturated concrete specimens exposed to chloride solution with a certain concentration for a specific period of time. The apparent diffusion coefficient is commonly used in Fick's second law of diffusion and chloride models to predict chloride ingress into concrete. In ASTM C1556 test method, the apparent diffusion coefficient along with the surface chloride concentration are determined by fitting the error function solution, i.e., Eq. (2.7) to the measured acid-soluble profile data by means of a nonlinear regression analysis using the method of least squares.

Some researchers use the water-soluble chloride profile data to obtain what is called water-soluble diffusivity or "effective" chloride diffusion coefficient based on water-soluble analysis [81-83]. The water-soluble chloride content of concrete powder is often determined as specified in ASTM C1218 standard test method. Limited data are available in the published literature concerns the use of water-soluble data in estimating the time to corrosion initiation. This is a noticeable gap found in the literature review. Many studies assume that the water-soluble chlorides can be used to represent free chlorides in the pore solution [83]. This assumption may not accurate, as the chloride concentration measured by water extraction process (in addition to the free chlorides) could also include loosely adsorbed chlorides (i.e., chlorides physically bound to the surface of C-S-H gel), which are soluble in water.

The apparent diffusion coefficient can also be determined from the rapid migration tests (non-steady state migration test). In this case it is called non-steady state migration coefficient, D_{nssm}, to differentiate it from the one obtained from bulk diffusion tests. A common method to determine the D_{nssm} is known as NT BUILD 492, initially developed by Luping and Nilsson [84]. The test consists of a migration cell set-up with a 50 mm thick, 100 mm diameter preconditioned concrete specimen cut from the center of a cast

cylinder. The bottom side of the specimen is subjected to a 10% sodium chloride (NaCl) solution and the upper surface is subjected to a 0.3 M sodium hydroxide (NaOH) solution. A voltage potential of 30 V is applied to the specimen, as shown in Figure 2.10. The voltage potential drives the chloride ions (in the 10% NaCl solution) to migrate into the specimen.

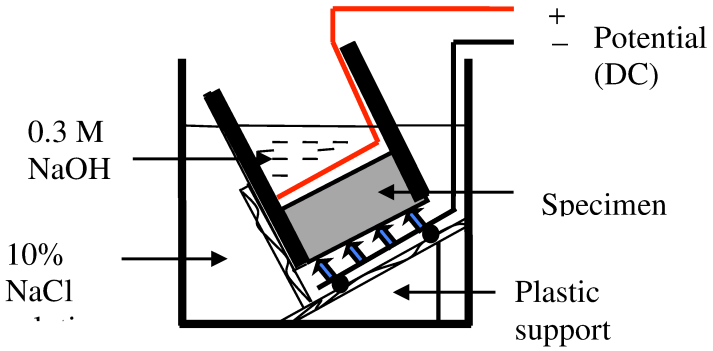

Figure 2.10 Chloride migration cell set-up

After a specified duration (24 hours), the specimen is removed and axially split. The depth of chloride penetration is determined in one-half of the specimen utilizing a colorimetric technique in which a silver nitrate solution is used as the colorimetric indicator, as specified in the test procedure. When silver nitrate solution is sprayed on concrete containing chloride ions, a chemical reaction occurs. The chlorides bond with the silver to produce silver chloride, which is a white substance. In the absence of chlorides, the silver bonds instead with the hydroxides present in concrete, creating a brownish color. To measure the penetration depth accurately, seven depth readings are obtained at intervals of 10 mm, and the average depth is calculated. The average depth of chloride penetration can then be used to determine a chloride ion diffusion coefficient, which is calculated using Eq. (2.10):

$$D_{nssm} = \frac{0.0239(173 + T)L}{(U - 2)t}\left(X_d 0.0238\sqrt{\frac{(173 + T)LX_d}{U - 2}}\right) \quad \text{.....Eq. (2.10)}$$

where D_{nssm} is the migrarion coefficient, m^2/s; U is the applied potential, V; T is the average value of the initial and final temperature in 0.3 N NaOH solution, in ºC; L is the thickness of the specimen, in mm; X_d is the average value of the penetration depths, in mm; and t is the test duration, in hours.

Despite the fact that the bulk diffusion test simulates the real chloride penetration mechanism in fully saturated concrete, it requires a long immersion period of at least 35 to 90 days. This long period affects the diffusion coefficient because the concrete pore structure is evolving with time as a result of the hydration process and binding. Therefore, the assumption used in the derivation of the error function solution to Fick's second law as presented in Eq. (2.7) (namely, that the diffusion coefficient remains constant during the testing period) is not representative of the actual test conditions. This is one of the criticisms for the use of bulk diffusion test as specified by ASTM C1556 test method [85].

The non-steady-state chloride migration coefficient as determined by the non-steady state migration test can be assumed as an instantaneous apparent diffusion coefficient due to the shortness of the testing period. Unlike diffusion tests where the period of exposure is long, which allows for the effects of binding and hydration process to take place, thus, influence the obtained value of the diffusion coefficient. In the migration test the binding and the hydration effect will be very limited as there is not sufficient time for them to take place.

3 CHLORIDE BINDING IN CONCRETE

This chapter provides an overview of chloride binding in concrete exposed to chloride environments. The chloride binding mechanism is discussed in section 3.1. The beneficial effect of binding to reinforcement is highlighted in section 3.2, followed in section 3.3 by a discussion of some factors influencing the binding process. A brief discussion of binding capacity is provided in section 3.4. Chloride isotherms and binding capacity are discussed in section 3.5. Modeling of binding cases is highlighted in section 3.6. Finally, a summary of test methods used to evaluate chloride binding is provided in section 3.7.

3.1 Chloride Binding Mechanism

When chloride ions are introduced into concrete (whether externally transported from the surrounding environment or internally introduced during the mixing process), some of the ions will interact with cement-hydration products or, in the case of admixed chlorides, with as yet unhydrated cement compounds and the rest will continue as dissolved ions in the pore solution [86]. The interaction process between chloride ions and cement hydrated or unhydrated products is called binding. Despite the lack of clarity of the binding mechanism in concrete, it is believed that physical adsorptions and chemical reactions are involved in the chloride binding process [87,88]. The calcium silicates (C_2S and C_3S) in the cement and their hydration products such as calcium hydroxide ($Ca[OH]_2$) and calcium silicate hydroxide (CSH) gel are reported to be responsible for the physical binding [7,88,89]. Additionally, the aluminate content of cement (i.e., C_3A and C_4FA) and hydrated products such as monosulfate are thought to be responsible for the chemical binding [29,78,86]. Calcium chloro-aluminate ($3CaO\_ Al_2O_3\_ CaCl_2\_ 10H_2O$), known as Friedel's salt, is commonly thought to be a major product of chemical binding.

No general agreement exists in the literature as to which process plays the key role in the binding process of concrete. Luping [7] suggested that the large surface area of hydrate gel supplies plenty of sites for physical binding. Therefore, his study concluded that physical adsorption plays the major role in chloride binding. Others believe that Friedel's salt, the main product of chemical binding, is the major product of chloride binding

[29,87,88]. Many researchers reported that the alumina content of cement is crucial for controlling the chemical binding of chloride ions in concrete [34,86,90,91]. Zibara [34] treated pure C_3A, C_4AF, C_3S and C_2S with chloride solutions and found that C_3A plays the most important role in the chloride binding capacity of cement. This was further confirmed by Florea and Brouwers [88].

3.1.1 Friedel's Salt

Friedel's salt is the common name of the chlorinated lamellar double hydroxide of composition $3CaO\_ Al_2O_3\_ CaCl_2\_ 10H_2O$ [12]. This compound was mentioned for the first time by Friedel in 1897. It results from chemical reactions that take place within the concrete matrix between the intruded chloride ions and the aluminate components such as mono aluminate ferrite (AFm) and sulfate ettringite (AFt). According to Suryavanshi et al. [32], Friedel's salt, in the presence of sodium chloride (NaCl), forms by two separate mechanisms: an adsorption mechanism, and an anion-exchange mechanism. In the adsorption mechanism, Friedel's salt forms due to the adsorption of the bulk chloride ions present in the pore solution into the interlayers of the principal layers, $[Ca_2(Al,Fe)(OH)_6.2H_2O^+]$, of the (AFm) structure, to balance the charge. In the anion-exchange mechanism, a fraction of the chloride ions bind with the AFm hydrates (C_4AH13 and its derivatives) to form Friedel's salt by an anion-exchange with the OH^- ions present in the interlayers of the principal layer, $[Ca_2Al(OH\text{-})_6.nH_2O]^+$.

As a result of Friedel's salt formation by the adsorption mechanism, an amount of Na^+ ions equivalent to the adsorbed chloride ions are removed from the pore solution to maintain the ionic charge neutrality. The Na^+ ions removed from the pore solution bind with the calcium silicate hydrate (CSH) gel lattice to balance the charge arising due to the replacement of Si_4^+ ions by Al_3^+ and $Fe3^+$ ions. In contrast, the Friedel's salt formation by the anion-exchange mechanism involves the release of OH ions from the AFm hydrates into the pore solution, thereby increasing the pH of the pore solution. A similar chain of reactions takes place to convert the sulfate ettringite hydrate to Friedel's salt [91].

3.1.2 Morphology of Friedel's Salt

According to Talero and Trusilewicz [9], Friedel's salt tends to form large crystals with distinctive hexagonal-prism plates. The morphology and size usually vary from non-descriptive to stacks of large plates, depend on the source of origin, and are affected by the available space and temperature. In a concrete matrix, there are two routes from which Friedel's salt can originate: the tricalcium aluminate (C_3A) phase in Portland cement, and the reactive alumina (Al_2O_3) of pozzolans. Friedel's salt originating from pozzolans occupies a larger volume because it forms at a faster rate than that originating from Portland cement only. However, the size of the crystals formed from the reactive alumina origin is relatively smaller than that formed from C_3A. Friedel's salt crystals originating from reactive alumina are in the range of 2.6 to 13.7 μm, whereas those originating from C_3A are in the range of 5.6 to 22.1 μm. It was also found that, for blended cements, when both C_3A and Al_2O_3 are present in the same chloride medium, miscellaneous morphological Friedel's salt crystal is formed.

The latter case is considered as the most favorable combination of morphological Friedel's salt crystals. The formation of Friedel's salt (molar volume = 296.69 cm^3, which is often of the same magnitude as calcium aluminate hydrates from OPC) within the microstructure of the concrete may greatly reduce concrete porosity by intensifying and filling the spaces of the capillary pores between the hydration products, thus hindering the access of new chloride ions, particularly in the skin layer. The particle size of a Friedel's salt crystal, as reported earlier, is the same as that of the capillary pores in which the diffusion and the flow of the ions takes place. However, formed Friedel's salt compounds can become soluble under some future circumstances (e.g., temperature elevation, reduction in the concentration of the free chlorides in pore solution, etc.) and be detrimental to reinforcement. In this state, it may dissolve in the pore solution, leaving the pores unfilled and releasing chloride ions so as to replenish those removed from the pore solution by transport to the surface of the steel [92].

3.2 Beneficial Effect of Chloride Binding to Reinforcement

Chloride binding is generally thought to be beneficial to reinforcement. Neville [92] and Arya et al. [33] reported that cement paste is capable of binding between 28% to 75% of the total penetrated chloride into concrete, depending on factors such as cement type, water-to-cement ratio, chloride concentration, temperature, etc. The beneficial effect of chloride binding in concrete is due to bonded chloride ions not contributing to the initiation of corrosion, as they are removed from the pore solution. Some researchers [93,94] believe that only free chloride ions in a pore solution have the ability to reach the level of reinforcement and initiate corrosion. Yuan et al. [86] and Martin-Perez et al. [95] summarized the beneficial effects of binding as follows. First, the concentration of free chloride in the vicinity of the reinforcement (threshold) is reduced as a result of a binding mechanism. Secondly, the removal of chlorides from the diffusion flux will slow the rate at which the chloride ions approach the level of the steel. Thirdly, the formation of solid compounds (Friedel's salt) could alter the microstructure and the porosity of concrete, which may slow the ingress of chlorides.

By assuming that bound chlorides are entirely removed from the pore solution and induce no threat for corrosion initiation, it would suggest that only free chloride concentrations should be considered. However, other studies indicated that bound chlorides, under some circumstances, might be dissolved and released in the pore solution, thus increasing the risk of corrosion initiation [29,90,96,97]. This suggests that, for design purposes, the total chloride content might be a more appropriate indicator of the corrosion risk of reinforced concrete structures.

3.3 Factors Affecting Chloride Binding

Chloride binding in concrete is a complicated process influenced by several factors. These factors, as summarized by Yuan et al. [86], include Portland cement composition, chloride concentration, supplementary cementitious materials, hydroxyl ion concentration, temperature, carbonation, electrical field, etc. The influence of these factors on chloride binding is discussed in detail in the following subsections.

3.3.1 Portland Cement Composition

The content of the four major cement mineral constituent compounds (i.e., C_3A, C_4AF, C_3S, and C_2S) and their resultant hydration products (i.e., monosulfate, $Ca(OH)_2$, and C-S-H gel) were found to play a major role in the binding process. The aluminate content of the Portland cement and their hydration products control the chemical binding, and the calcium silicates and their hydration products control physical binding. Numerous studies have concluded that chloride binding increases as the tri-calcium aluminate or C_3A content of the Portland cement increases [29,31-33,98,99]. Arya et al. [100] tested ordinary Portland cement and sulfate-resistant Portland cement in a 20 g/l NaCl solution and found that the ordinary cement bound considerably more chloride than the sulfate-resistant cement. This was attributed to the high C_3A content of the ordinary Portland cement. Racheeduzzafar et al. [101] found a substantial reduction in water-soluble chloride content for concrete mixtures with high C_3A content. All of these test results point to higher C_3A content results in the higher chloride binding capacity of the tested concrete. The formation of Friedel's salt and its analogues as a result of the chemical reaction between the aluminate minerals in cement and chloride ions was confirmed in all of these studies.

The other important cement compound that has also been found to have an influence on chloride binding is calcium silicate content (C_2S and C_3S). CSH gel, which is the main hydration product of Portland cement, controls the physical binding of chloride [7,88]. It has been reported that the higher the content of C_3S and C_2S in the cement, the more chloride ions will be bound or adhere to the surface of the CSH gel, and the higher the physical binding will be [102]. Luping and Nilsson [7] found that the chloride binding capacity of OPC concrete is strongly dependent on the CSH content in the concrete, regardless of the water–cement ratio and the addition of aggregate. According to Ramachandran [103], chlorides can either be present in a chemisorbed layer on the hydrated calcium silicates, penetrate into the CSH interlayer spaces, or be intimately bound in the CSH lattice. The capacity of the CSH was also found to be dependent on the C/S ratio. Beaudoin et al [102] suggested that lower C/S ratios result in lower binding capacities.

3.3.2 Supplementary Cementitious Materials

Supplementary Cementitious Materials (SCMs), such as silica fume, slag and fly ash, are widely used in the construction of reinforced concrete structures. Their use has shown a significant impact on the ability of concrete to resist the ingress of chloride ions in concrete, as explained in Chapter 2. Because these materials have different chemical compositions and vary in their physical properties, they will influence the binding capacity of the concrete in various ways. The influence of SCMs such as silica fume, fly ash and slag cement on chloride binding is briefly discussed below.

3.3.2.1 Silica Fume

Previous research and studies showed that the partial replacement of Portland cement with silica fume decreased the binding capacity of the concrete [29,96,104]. The replacement of cement with silica fume up to certain level was found to increase the physical binding due to the increase in the specific surface area of the CSH phase as a result of the inclusion of the silica fume. However, the amount of Friedel's salt for concrete containing silica fume was found to be very small, especially at high silica fume replacement levels [105]. Nilsson et al. [96] suggested that silica fume could influence binding capacity in the following ways: 1) reduce the pH of the pore solution; 2) reduce the C_3A amount, which would then reduce the chemical binding; and 3) increase the amount of CSH gel, which should increase the physical binding. It has also been reported that the effect of silica fume on the binding capacity is influenced by the calcium-to-silica ratio (C/S) [29]. A lower C/S ratio leads to a lower binding capacity. In general, the beneficial influence of silica fume in delaying the ingress of chloride ions into concrete is attributed to its physical properties and high surface area in refining the pore structures and increasing its tortuosity.

3.3.2.2 Fly Ash

Various research and studies have shown that the addition of fly ash as partial replacement of Portland cement in concrete has a positive impact on chloride binding

[29,33,37,92,106,107]. Both the physical binding and the chemical binding are increased by an increase in the fly ash replacement ratios. This is attributed to the pozzolanic reactivity of the fly ash as well as the high alumina content which both increase the amount of bound chlorides. Dhir et al. [52] tested concrete with different fly ash replacement quantities up to 50% and found that the cement paste with a higher percentage of fly ash revealed a higher chloride binding capacity. Others have reported similar observations [105]. It is believed that the high alumina content, which is responsible for the formation of the Friedel's salt is the main cause for its good binding characteristics. However, it is well known that the fly ash may vary considerably depending on the source and burning process of coal, which may lead to different binding characteristics.

3.3.2.3 Slag Cement

Many studies have reported that partial replacement of cement with slag increases the binding capacity of the concrete when exposed to a chloride environment [29,53,92,105]. Ishida et al [105] concluded that when the cement is replaced with ground granulated blast furnace slag at levels up to 40%, the amount of the formed Friedel's salt rises as the replacement ratio of the slag increased. It was suggested that the high binding capacity of slag cement is attributed to its high alumina content, resulting in the formation of Friedel's salt. However, some researchers found that the binding capacity of cement pastes containing slag cement is dependent on the level of sulfate ions present in slag cement [108,109]. Xu [109] found that when the sulfate ions in slag cement are increased to the same level as cement paste, the higher binding capacity disappeared. He thus ascribed the higher binding capacity of slag to the dilution effects of sulfate ions.

3.3.3 Temperature

There is no general agreement found in the literature on the influence of elevated temperature on chloride binding mechanisms. Some researchers have suggested that elevated temperature reduces binding and thus could be detrimental to reinforcement [10,34,78,110]. Roberts [111] and Larson [10] concluded that the amount of bound

chloride decreases as temperature increases. Zibara [34] found that increased temperature resulted in a decreased binding, particularly at chloride concentrations ranging from 0.1 mole/l to 1 mole/l. However, other researchers have reported the opposite, that a higher temperature results in slightly more chloride binding, and that the higher the chloride concentration, the larger the difference will be [87]. Luping [78] suggested that increased temperature reduces chloride binding by liberating both physically and chemically bound chlorides into the pore solution. For physical binding, elevated temperature increases the thermal vibration of bound chlorides, leading to more unbound chlorides in the pore solution. Although an increase in temperature accelerates the rate of reaction of chemically bound chlorides, it may also enhance the solubility of the binding products (Friedel's salt), resulting in a high chloride concentration in the pore solution. Therefore, chloride-binding properties of concrete could vary with exposure temperatures. Nguyen et al. [112] concluded that elevated temperatures up to 35^{o} C have no effect on the amount of bound chlorides and binding kinetics. Very recently, Dousti [113] investigated the influence of temperatures ranging from -4^{o} C to 70^{o} C on chloride binding and the amount of formed Freidel's salt. He found that the intensity of Friedel's salt decreased with increases in temperature, and that the greatest bound chloride content was exhibited at 22^{o} C, followed by - 4^{o}, 3^{o}, 35^{o}, and 70^{o} C.

3.3.4 Carbonation

As mentioned earlier, carbonation is one of the main causes of corrosion initiation in reinforced concrete structures. Carbonation could also contribute to the deterioration of reinforced concrete structures by liberating bound chlorides in the pore solution. As carbonation changes the nature of hydration products, it should be expected that it would have a great influence on the ability of concrete to bond chloride ions. Zibara [34] found that the binding capacity of three different pre-carbonated cement pastes immersed in chloride solutions with different concentrations was almost zero. Xiao-mei et al. [114] examined the pore solution of cement mortar and hardened cement made with chloride contaminated mixing water. They found that, with complete carbonation, dissolved chloride increased by a factor between 2 and 12, and bond chloride decreased by 27% to 54%.

When concrete is carbonated, the hydration products are converted to $CaCO_3$ and the pH of the system drops to about 9 or less. Carbonation influences both physical and chemical binding. For physical binding, the decomposition of CSH and the reduction in total porosity may provide fewer sites for ion exchange reactions and physical binding [86]. For chemical binding, the solubility of Friedel's salt was found to increase with the degree of atmospheric carbonation of the concrete [32,115]. As a result, the presence of carbonation would increase the risk of reinforcement corrosion in concrete.

3.3.5 Hydroxyl Ion Concentration (pH)

A number of studies have suggested that the hydroxyl concentration in the surrounding environment would have a significant effect on chloride binding [116-118]. The general tendency is that the binding capacity of cement paste decreases as the concentration of hydroxyl increases, and vice versa. Tritthart [118] tested cement pastes in chloride solutions with different pH values and observed that chloride binding increased as the pH of the host solution decreased. This finding was linked to the competition that exists between hydroxyl ions (OH^-) and chloride ions (Cl^-) in the pore solution for adsorption sites on the surface of the hydration products of the cement paste. Roberts [111] indicated that the solubility of Friedel's salt increases with increased pH of the chloride solution, thus releasing chlorides to the pore solution and reducing the amount of chemically bound chlorides.

3.3.6 Chloride Concentration

The chloride binding capacity is largely affected by the amount and concentration of chloride ions entering the concrete. Therefore, chloride concentration in the surrounding environment is one of the most important factors affecting chloride binding. Several studies have confirmed that a higher chloride binding capacity results when the chloride concentration in the pore solution is high [119,120]. For given cement, a maximum binding capacity exists for chloride ions [86]. Under this condition, the higher the chloride concentration in the pore solution, the more chlorides will have chance to access

the binding sites. This will result in higher chloride binding.

Despite the fact that chloride binding has been extensively studied in past decades, there is a general lack of knowledge on the influence of binding products on the concrete porosity. The consequence of binding on concrete porosity and the capillary pore system, which influences the diffusivity, has received relatively little attention in the published literature. Both chemical and physical binding could alter the concrete pore structure, Omer et al (2015). Moreover, chemical binding could influence the structure of the capillary pores, which greatly contribute to the diffusivity of the concrete. However, the effect of physically bound chlorides on the porosity, which takes place as a result of the adsorption process on the surface of the CSH layer, will be limited to the gel pores only. The gel pores are unlikely to contribute to the diffusivity, as these are micropores with characteristic radii of only 0.5 to 2 nm, compared to capillary pores, which are mesopores with average radii ranging from 5 to 50 nm [121]. Furthermore, approximately 70% of the binding capacity of the cement paste was found to be due to the formation of Friedel's salt, whereas less than 30% was contributed to the C-S-H phase [1,88].

3.4 Chloride Binding Capacity

Binding capacity is defined as the ability of concrete material to bind chloride ions when the ion concentration changes:

$$\text{Binding capacity} = \frac{\partial C_b}{\partial C_f} \quad \text{..... Eq. (3.1)}$$

As stated earlier, binding affects the time it takes for corrosion initiation to begin, due to its influence on the chloride transport mechanism. Generally speaking, a higher chloride binding capacity is desirable because it slows down the rate of corrosion initiation and thus improves the durability of reinforced concrete structures in saline environments. Over the years, numerous studies and investigations have suggested that the binding capacity of concrete is directly influenced by a wide range of factors, such as the type and

content of the binder, the chloride concentration in the pore solution, the instability of the local pH, the water-to-binder ratio (w/b), and ambient temperatures.

3.5 Chloride Binding Isotherms

In chloride prediction models, binding is usually modeled by means of binding isotherms [29,78,79,95]. Binding isotherms describe the relationship between free and bound chlorides in concrete at a given temperature over a range of chloride concentrations. They are unique to each cementitious system, as they are influenced by the contents of alumina and CSH components. Four types of isotherm relationships have been reported in the literature to describe binding in concrete: linear isotherm, Langmuir isotherm, Freundlich isotherm, and Brunauer, Emmett, Teller (BET) binding isotherm [122]. Previous studies have shown that service life prediction models are significantly influenced by the type of binding isotherm used to describe chloride binding in concrete [86,95]. A brief discussion of each type of binding isotherm is given in the following subsections.

3.5.1 Linear Binding Isotherm

Several researchers have suggested that the relationship between free and total chlorides in concrete exposed to field conditions has a linear trend [31,81]. Tuutti [14] analyzed the pore solution that had been pressed out of various mortar specimens conditioned in various climates. His experimental results indicated that a linear relationship does exist between free and bond chlorides. This relationship was modeled as shown in Eq. (3.2):

$$C_b = \alpha * C_f \quad \text{Eq. (3.2)}$$

where C_b is the concentration of bound chlorides, α is a constant, and C_f is the concentration of free chlorides. According to Yuan et al. [86], however, Tuutti's relationship is valid only when the free chloride concentration is 20 g/l or lower. Some studies suggested that the linear relationship of chloride binding oversimplifies the binding process and is valid only for low free chloride concentrations [7,95]. It overestimates the amount of bound chlorides at high free chloride concentrations, and

underestimates the amount of bound chlorides at low free chloride concentrations, as shown in Figure 3.1[95].

3.5.2 Langmuir Binding Isotherm

It has been found that, in most cases, the relationships between free and bound chlorides are non-linear [7,123-125]. The Langmuir isotherm is derived from physical chemistry based on assumptions that binding takes place as a result of a monolayer adsorption. Pereira and Hegedus [125] applied the Langmuir adsorption model to account for the chloride binding isotherm in concrete, as shown in Eq. (3.3):

$$C_b = \alpha * C_f / (1 + \beta C_f) \quad \text{Eq. (3.3)}$$

where α and β are binding constants.

Since then, several researchers have employed the Langmuir binding isotherm to describe the non-linear behavior between bound and free chlorides in concrete [7,95]. According to Luping and Nilsson [7], the Langmuir isotherm better describes the binding behavior when the concentration of free chloride in pore solution does not exceed 0.1 mole/l. One reason for this is that the monolayer adsorption occurs only at low chloride concentration and becomes very complex at higher chloride concentrations. Luping and Nilsson [7] concluded that the binding isotherm is described well by the Freundlich isotherm.

3.5.3 Freundlich Binding Isotherm

Similar to the Langmuir isotherm, the non-linear binding isotherm can also be expressed by the Freundlich binding isotherm. Luping and Nilsson [7] reported that the Langmuir relationship diverges from the experimental data when free chloride concentrations exceed 0.05 mole/l. They also found that the Freundlich relationship fits their data very well when the free chloride concentrations range from 0.1 mole/l to 1 mole/l. This range covers the two most important magnitude orders of free chloride concentration in seawater (0.6 mole/l). The Freundlich binding isotherm equation is shown in Eq. (3.4):

$$C_b = \alpha * C_f^{\beta} \quad \text{.....Eq. (3.4)}$$

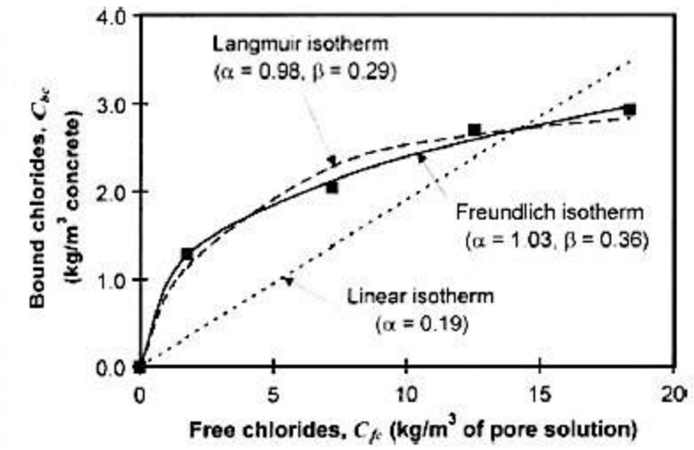

Figure 3.1 Chloride binding isotherm relationships [95]

The difference between the Langmuir and Freundlich binding isotherms is insignificant. Nevertheless, the Freundlich isotherm was found to better describe the binding process of chloride ions at high concentrations, as shown in Figure 3.1.

3.5.4 Brunauer, Emmett, Teller (BET) Binding Isotherm

Xu [126] modified the BET equation to describe the relationship between bound and free chlorides. It was found that BET corresponds with experimental data very well for free chlorides less than 1 mol/l [78]. BET has been used by several researchers to model chloride binding isotherm in concrete. It should be noted that BET was originally applied to gas adsorption and modified by Xu [126] to describe the chloride binding isotherm. The BET equation is shown in Eq. (3.4):

$$\frac{C_b}{C_{bm}} = \frac{\alpha \frac{C}{C_s}\left[1-(1-\beta)\left(1-\beta\frac{C}{C_s}\right)^2\right]}{\beta\left(1-\beta\frac{C}{C_s}\right)\left(1-\beta\frac{C}{C_s}+\alpha\frac{C}{C_s}\left(1-\beta\frac{C}{C_s}+\frac{C}{C_s}\right)\right)} \quad \text{..... Eq. (3.5)}$$

where C_s is the free chloride concentration in the saturated solution and C_{bm} is the monolayer adsorption capacity of bond chlorides. The constant α relates to the difference between the adsorption energy at the first layer and those at the second or higher layers. The constant β relates to the difference between the adsorption energy at the second layer and those at the third or higher layers.

It is clear from the literature review that the Freundlich relationship and BET equation describe the binding isotherm very well when free chloride concentration is in the range of 0.1 - 1 mole/l or higher. Due to the complexity of the BET relationship, the non-linear binding isotherm is often described either by Langmuir or Freundlich isotherms.

3.6 Experimental Determination of Binding Isotherm

Different experimental methods have been reported in the literature to determine the chloride binding isotherms [7,86]. Some of the more common approaches are the equilibrium method, the pore solution expression method, the diffusion cell method, and the migration cell method. In addition to these methods, some researchers used water-soluble and acid-soluble chloride measurements to account for free and total chloride contents [86]. A brief description of each of these methods is provided in the following sections.

3.6.1 Equilibrium Method

This is the most straightforward and widely used test method for determining binding isotherms. The method was first used by Blunk et al. [119] and Byfors [37], and later developed by Luping and Nilsson [7]. The method involves storing a crushed particle or ground powder sample in a known concentration of chloride solution for a certain period of time until equilibrium is reached. At the equilibrium stage, the chloride concentration in the storage solution is measured as a free chloride concentration. The amount of bound chlorides is calculated from the difference between the concentration of the initial solution and the concentration of the solution. The time it takes to reach equilibrium depends on the type of concrete and the size of the crushed particles.

Luping and Nilsson [7] tested concrete made with ordinary Portland and used crushed particles in sizes ranging from 0.25 to 2 mm. They reported that the equilibrium state was reached within 14 days of immersion in the chloride solution. After reaching equilibrium, the inside solution is pipetted to determine the chloride concentration by a titration process using 0.01 M AgNO3. By immersing the particles in a series of solutions, the complete binding isotherm can be obtained. The bound chlorides are calculated using Eq. (3.6).

$$C_b = \frac{35.453V(C_i - C_e)}{W_d} \quad \text{.....Eq. (3.6)}$$

where C_b is a bound chloride given in mg/g of the sample, V is the volume of the solution (ml), C_i is the initial chloride concentration of the solution (mole/l), C_e is the chloride concentration of the solution at equilibrium (mole/l), and W_d is the mass of the dry sample (g).

3.6.2 Pore Solution Expression Technique

In this method, the concrete sample is pressed by applying very high pressure to extrude the pore solution. The extruded solution is then collected and chemically analyzed to determine its free chloride content [86]. This method is inconvenient, as special equipment is required for extruding the pore solution out of the sample. Moreover, it might not be applicable for concrete made with low w/c ratios, as it is very difficult to obtain a sufficient quantity of pore solution that can be reasonably analyzed. Furthermore, the method has been criticized for its accuracy and reproducibility [78]. The loosely bonded chlorides may be released as a result of the very high pressure, which would increase the concentration of the free chloride in the pore solution.

3.6.3 Diffusion Cell Method

As proposed by Glass et al. [127], the diffusion cell that is employed to determine the effective diffusion coefficient can be used to obtain the binding isotherm. After steady state is reached, the sample is removed from the cell and ground to powder. An acid-soluble solution is then used to determine the total chloride content by titration. The free chloride is obtained by assuming that the concentration gradient is linear under steady state diffusion conditions. It has been found that the chloride binding obtained using this method is similar to that obtained by other methods. However, this method is time-consuming and not easy to perform.

3.6.4 Migration Test Method

Chloride isotherms can also be obtained using the migration test. A few researchers have used the migration test to calculate chloride binding [128,129]. Andrade [128] obtained chloride isotherms by applying the steady state migration test on a series of concrete samples. One point on the binding isotherm can be determined from each migration test, after which a full binding isotherm can then be obtained. Castellote et al. [129] used the non-steady state migration test to determine chloride concentration profiles and then fitted them to the BET isotherm to model chloride binding. Their results were compared to those obtained from the natural diffusion test. They concluded that for chloride concentrations higher than 1 mole/l, both the migration and diffusion tests yield similar amounts of combined chlorides. Truc et al. [79] obtained chloride binding isotherm from steady state migration tests, where one chloride binding point is determined from each test. By changing the chloride concentration in the upstream cell for each test, several chloride binding points can then be obtained. The disadvantage of using migration tests in determining chloride binding is that the application of the electrical field, which shortens the time to reach equilibrium, could have an influence on the binding mechanism. Ollivier et al. [130] assumed that the electrical field has no influence on chloride binding.

The equilibrium method as developed by Luping and Nilsson [7] was selected in this research to determine the binding isotherm and binding capacity of the concrete investigated in this research.

4 CHLORIDE PREDICTION MODELS IN CONCRETE: AN OVERVIEW

Numerous chloride models have been developed to predict and analyze chloride ingress into concrete in order to improve concrete performance and to facilitate future repair-planning strategies. The existing chloride models can be broadly divided into two types: those based on Fick's 2nd law, and those based on multi-ionic species [5]. The focus of this research is on the use of Fick's second law in modeling chloride ingress into concrete. However, a brief review of multi-ionic species models is provided in section 4.1. An overview of Fick's second law-based models is given in section 4.2. The error function solution to Fick's second law is discussed in section 4.3. The review of the error function solution includes its original use and assumptions, an introduction of time-dependent diffusion coefficients, and the determination of age factor (value of m). Some limitations and drawbacks associated with the use of the error function solutions in modeling chloride ingress into concrete are also highlighted. A brief review of the finite approach is provided in section 4.4, followed by a review of the Life–365 model presented in section 4.5.

4.1 Multi-ionic Species-Based Models

These models were developed based on the principle that chloride ions are charged ions and thus interact with other ions in the pore solution and with the hydrated cement matrix. The models describe the physical and chemical processes that take place in concrete as a result of the penetration of chloride ions. In addition to chloride ions, the multi-ionic species models take into consideration the effect of other ionic species presented in the pore solution on the movement of chlorides into concrete. The models solve the mass balance equations for the ionic species by separately describing the flux of ions, and the interaction between ions in the pore solution and solid phases in the cement matrix. These models are often complex, and since they are not directly derived from measurements, extensive validations against measured data are necessary before they can be applied to practical predictions. The chloride movement in multi-ionic species models is often described by two different flux equations [5]:

- Fick's 1st law, and

- Nernst-Plank equation.

The Nernst Plank equation is an equation used to describe the movement of ionic species in a pore solution under the action of the gradient of electrochemical potential [26]. Examples of multi-ionic species models include ClinConc [78], Percolation [131], MsDiff [79] and STADIUM [132]. A brief description of these models is given in the following sections.

4.1.1 ClinConc Model

Luping [78] developed the ClinConc model to estimate chloride ingress into concrete. In ClinConc, the flux is described by Fick's first law, and the chloride concentration profiles are obtained by solving a mass-balance equation. The chloride binding is described by Freundlich isotherm, and the effects of pH and temperature on chloride penetration are also considered. The model is solved using a finite difference method. The influence of other species present in the pore solution is not considered, except for the effect of hydroxide ions. The chloride diffusion coefficient is determined using the non-steady state migration test, as described in NT Build 492. The effect of time on the chloride diffusion coefficient is limited to the first six months, after which the D_{nssm} value was assumed to be constant.

4.1.2 Percolation Theory-Based Model

Masi et al. [131] developed a chloride transport model where the flux of different ionic species is predicted using Nernst-Plank's equation. The equations are solved numerically with a finite difference method. The model makes it possible to simulate the transport of several species with or without superimposed currents when assuming the electro-neutrality of the pore solution. The effective diffusion coefficients in the model were determined by means of the percolation concepts, where the microstructure of the solid is described by using a network representation of pore space called Bethe lattice. The chloride binding is implemented by means of the Langmuir adsorption isotherm.

4.1.3 MsDiff Model

The MsDiff model was developed by Truc [79]. It simultaneously predicts the flux of several different ionic species (Cl^-, Na^+, K^+, HO^-) in saturated concrete using Nernst-Plank's equation. The binding influence is considered in MsDiff with the Freundlich isotherm. The interaction between different ions in the pore solution is determined based on the electro-neutrality assumption. The chloride diffusion coefficient is determined with a test procedure, called the LMDC test, and the model is solved with a finite difference approach. The influence of temperature on the chloride diffusion coefficient is not considered in the model.

4.1.4 STADIUM Model

STADIUM is the most recent multi-ionic species model. It uses an advanced finite-element approach to physically describe and analyze almost all of the interaction processes involved in the concrete system as a result of chloride ingress [132]. The model is based on a multi-ionic approach that considers eight ionic species of the pore solution and their chemical interactions with the cementitious paste. The ionic species that are considered in the model include OH^-, Na^+, K^+, SO_4^-, Ca^{2+}, $Al(OH)_4^-$, Mg^{2+}, and Cl^-. The flux of different ions is predicted using the extended Nernst-Plank equation. The electrical coupling between different ions is described with a Poisson equation, while the water flow in unsaturated concrete is described with Richard's equation. A homogenization technique is used to describe ion diffusion in cement-based materials. Several functions describe the influence of temperature, water movement, hydration and chemical interaction on the diffusion coefficient and are implemented in the model. The binding effect is modeled by means of a chemical equilibrium and ion exchange mechanisms instead of using binding isotherms. The physical binding, which plays an important role in the binding phenomenon, is not considered in the model. Further details on this model can be found in Henchi et al. [132].

Although multi-ionic species models make it possible to accurately predict how different species are transported into concrete material and how changes take place as a result of

chloride ingress, the models are complex and require enormous amount of input data. This data is not easy to obtain and is not always available for engineers in the field. Furthermore, the computation of these models is time-consuming, and powerful computers are needed to run the models in a timely manner. Given these consideration, and despite their accuracy, many researchers and field engineers believe that multi-ionic species models remain research tools not meant for practical use except in well-defined cases. This thesis is considering the modeling of chloride ingress into concrete based on Fick's second law approach, which is relatively simple, less expensive and more practical for predicting the time to corrosion initiation. Therefore, the multi-ionic species will not be discussed further, and the discussion in the rest of this chapter will be limited to Fick's second law models.

4.2 Models Based on Fick's Second Law

In general, Fick's second law chloride models result in prediction models that consider only chloride ions and do not account for the effect of other ionic species present in the pore solution. It is assumed that the ions are neutral particles and do not interact with other ions in the pore solution. Some researchers believe that this simplest model cannot provide a correct analysis for prediction of chloride ingress in concrete [79]. It should be noted that while the multi-ionic models intend to model the actual physical and chemical processes involved in the chloride ingress into concrete, Fick's second law models aim to describe the results of the physical and chemical processes of this transport (i.e., chloride profiles). Furthermore, Fick's second law models are user-friendly and are still widely used by engineers for predicting the service life of reinforced concrete structures with regard to reinforcement corrosion. Examples of Fick's second law-based models are the error function solutions and Life -365.

4.3 Error Function Solution Models

Over the past several decades, various error function solution models have been developed for modeling chloride ingress into concrete [62,133-135]. The simplest and the most straightforward form of the error function solution is that by Collepardi et al. [135].

This was also marked as the first attempt to use Fick's second law of diffusion in modeling chloride ingress into concrete [5]. In the early 1970s, Collepardi et al. [135] used the error function solution given in Eq. (2.6) to fit experimental chloride profiles, relating concentration with depth over time. From that relation, the chloride diffusion coefficient and surface chloride concentration are obtained. Then, in the late 1980s, some researchers realized that the chloride ingress in many laboratory specimens and field exposure concrete did not advance as suggested by Collepardi's model. Collected data from laboratory measurements and field exposure indicated that the apparent diffusion coefficient resulting from fitting the error function solution to the measured chloride profiles is far from being constant during exposure, as assumed by the model, but instead decreases with time, as shown in Figure 4.1 [73,134,136]. From then on, the chloride diffusion coefficient became known as time-dependent chloride diffusion, $D_a(t)$.

The chloride diffusion coefficient typically decreases as time elapses. This effect is attributed mainly to the ongoing hydration process, which alters and refines the capillary pore structure of concrete [73,137]. There is also a potential influence of binding contributing to this phenomenon [138]. The effect of time on diffusion coefficients can be significant if the concrete contains supplementary cementitious materials such as fly ash or slag [46].

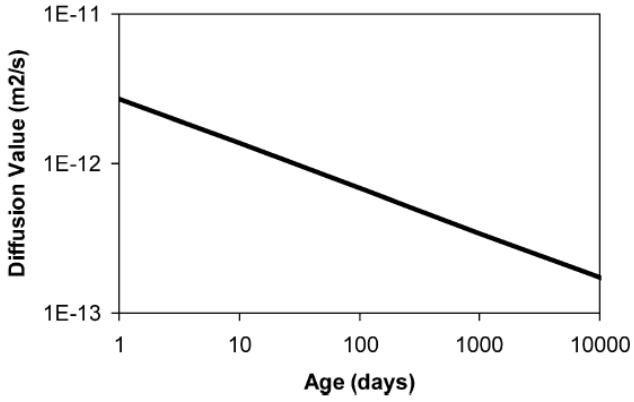

Figure 4.1 Typical change in diffusion coefficient with time

The decline of the chloride diffusion coefficient with time was ignored in Collepardi's

model, causing the chloride concentration profiles predicted by the model to deviate from the experimental and field exposure data.

4.3.1 Time-dependent Diffusion Coefficient

Takewaka and Matsumoto [73] were probably the first to notice the time-dependency of the chloride diffusion coefficient. They suggested an empirical relationship for describing the reduction in the diffusion coefficient with time. A commonly used empirical model for time-dependency, which was originally proposed based on Takewaka and Matsumoto's work and later proved by Frederiksen et al. [133], is given in Eq. (4.1):

$$D(t) = D_{ref}\left(\frac{t_{ref}}{t}\right)^{m} \quad \text{.....Eq. (4.1)}$$

Where D(t) is the diffusion coefficient at time t and D_{ref} and t_{ref} are the diffusion coefficient and time at reference time, respectively, t_{ref} is usually taken at 28 days in North America. The m is the age factor, also known as reduction coefficient, which stands for the reduction of chloride diffusion coefficient with time. The D_{ref} and m-value are merely looked upon as parameters that can be quantified from exposure data [5]. The two parameters are determined from the bulk diffusion values measured by fitting the error function solution to a series of chloride profiles taken at different concrete ages and exposure periods.

4.3.2 Error Function Solution with Time-dependent Diffusion Coefficient

Mangat and Molloy [62] were the first to introduce the time-dependent diffusion coefficient in the error function solution. They proposed the error function solution with time-dependent diffusion coefficients, given by Eq. (4.2)

$$C(x,t)=C_s\left[1\text{-}\mathrm{erf}\left(\frac{x}{2\sqrt{T}}\right)\right] \quad \text{..... Eq.(4.2)}$$

where:

$$T = \int_0^t D(t)dt = \frac{D_{ref}}{1\text{-}m} t^{1-m} \quad \text{.....Eq. (4.3)}$$

Recently Luping and Gulikers [6] showed that the time-dependent diffusion coefficient as used by Mangat and Molly in the error function solution lacks a mathematical accuracy because incorrect time integration was used for the time-dependent diffusion coefficient. According to Luping and Gulikers, time integration should start from the age of the concrete at the time of exposure and ended at the age of the concrete at the end of exposure (i.e. the age of concrete before exposure + the exposure period) and not from age 0 to the end of exposure. Accordingly, Luping and Gulikers provided a corrected mathematical expression for the time-dependent diffusion coefficient where the time was integrated over the period of exposure, starting from the age of the concrete at the first exposure, t_1, and ending at the age of the concrete at final exposure (t_1+t_{ex}), as shown in Eq. (4.4):

$$T = \int_{t_1}^{t_{1+t_{ex}}} D(t)dt = \frac{D_{ref}(t_{ref})^m}{1\text{-}m}.[(t_{ex}+t_1)^{1-m}-(t_1)^{1-m}] \quad \text{.....Eq. (4.4)}$$

By rearranging items:

$$T = \frac{D_{ref}}{1\text{-}m}.\left[\left(1+\frac{t_1}{t_{ex}}\right)^{1-m} - \left(\frac{t_1}{t_{ex}}\right)^{1-m}\right].\left(\frac{t_{ref}}{t_{ex}}\right)^m .t_{ex} \quad \text{.....Eq. (4.5)}$$

Luping and Gulikers [6] stated that Equation (4.5) is the correct mathematical expression that should be used in the error function solution to account for the time-dependent chloride diffusion coefficient.

It should be noted that Fick's second law shown in Eq. (2.5) is representing the equation for diffusion when the diffusion coefficient is taken to be constant. However, in a case where the diffusion coefficient is not constant, Fick's second law of diffusion from a mathematical point of view becomes:

$$\frac{\partial C}{\partial t} = D(t)\frac{\partial^2 C}{\partial x^2} \quad \text{.....Eq. (4.6)}$$

and by writing:

$$dT = D(t)\,dt \quad \text{.....Eq. (4.7)}$$

$$T = \int_{t_1}^{t_1+t_{ex}} D(t)dt \quad \text{.....Eq. (4.8)}$$

Eq. (4.17) can be reduced to:

$$\frac{\partial C}{\partial T} = \frac{\partial^2 C}{\partial x^2} \quad \text{.....Eq. (4.9)}$$

Equation (4.9) presents the correct Fick's second law form for a time-dependent diffusion coefficient that returns the solution presented in Eq. (4.2). It should thus be clear that when the diffusion coefficient is taken to be constant, Fick's second law and Eq. (2.5), and the error function solution shown in Eq. (2.6), should be used. When the diffusion coefficient is a function of time, the Fick's second law shown in Eq. (4.9) and the error function solution shown in Eq. (4.2) along with Eq. (4.5) should be used.

4.3.3 Determination of Age Parameter (m-value)

In order to implement the error function solution presented in Eq. (4.2), both D_{ref} and m need to be determined. The determination of theses parameters requires multiple chloride profiles from the same concrete and same exposure conditions but at various times or ages. The traditional experimental way to determine these parameters is to use Eq. (4.1). The apparent diffusion coefficients, which are obtained from using the simplified version of error function solution following the Collepardi's approach, are plotted with time on log-log scale. The log D_a is on y-axis and the log t on x-axis. Linear regression analysis of the data is then used to determine D_{ref} and m. The slope of the regression line is equal to

m and the intercept of the represents line with the y-axis determines the diffusion coefficient at day one [8,62].

It has been found that the value of m is greatly influenced by the maturity time, which is used as a time basis [8]. There are three methods used in the literature to determine m, as pointed out by Nokken et al. [8]. The three methods use different techniques to present time, generating three m values. The first method assumes that the apparent diffusion coefficient as projected form the bulk diffusion coefficient occurs at the end of the exposure period. Therefore, this method uses the time at the end of exposure, total time t_{tot}., (i.e., the age of the specimen at the end of the exposure) as the time basis and the value of m generated using this method is marked as m_{tot}. The second technique assumes that the apparent diffusion coefficient occurs at the average time of the specimen age, t_{avg}., (the age of the specimen at the beginning of exposure plus the age of the specimen at the end of exposure divided by 2) as the time basis. The value of m obtained from this technique is marked as m_{avg}., The third technique uses the effective time, t_{eff}., as proposed by Stanish and Thomas [85] and the value of m based on this technique is marked as m_{eff}. The proposed equation for effective time as by [85] is shown in Eq. (4.10):

$$t_{eff} = \begin{cases} \left[\dfrac{(1-m)(t_2-t_1)}{t_2^{\,1-m}-t_1^{\,1-m}}\right]^{1/m} & m \neq 0.1 \\ \dfrac{t_2-t_1}{\ln\left(\dfrac{t_2}{t_1}\right)} & m = 1 \end{cases} \quad \text{..... Eq. (4.10)}$$

where t_1 is the age of the sample at the beginning of exposure and t_2 is the age of sample at the end of exposure.

Nokken et al. [8] investigated the effect of the three methods mentioned above on the value of m. Their results are graphically represented in Figure 4.2. As can be seen, the obtained value of m is highly dependent on the used method.

The accurate determination of the age parameter, m, is crucial for service life modeling. If the effect of this parameter is not properly considered, significant bias can be introduced when predicting the service life of reinforced concrete structures. A brief review of the current knowledge along with some published m values for different concrete mixtures is provided. The previous research has shown that the value of m with respect to concrete is highly dependent on factors such as concrete mix design and proportions, environment, and exposure conditions [133].

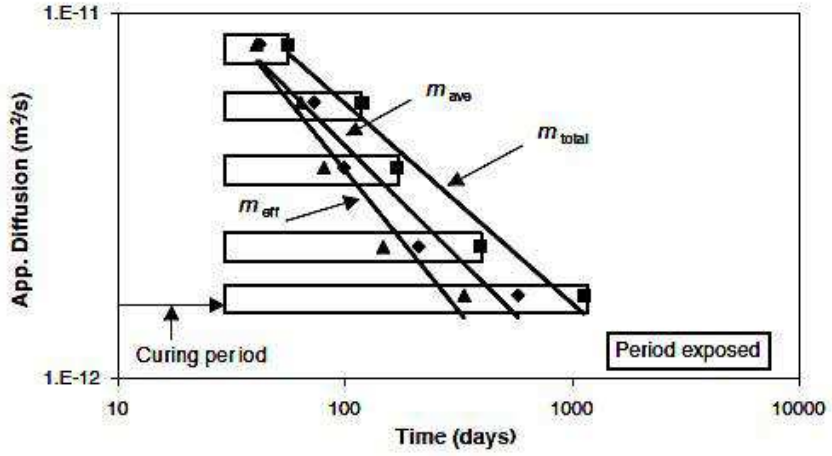

Figure 4.2 Comparison of the calculate value of m based on three different methods, Nokken et al. [8]

A few relationships aimed at estimating the value of m based on mix design and proportions have been reported in the published literature [24,44,62]. These relationships are derived from intensive research and data analysis of different concrete types in various environments and exposure conditions and presented below in chronological order as found in the published literature.

Mangat and Molloy [62] proposed the relationship shown in Eq. (4.11), which is a function of the w/c ratio of the concrete.

$$m = 2.5 \left(\frac{W}{C}\right) - 0.6 \quad \text{.....Eq. (4.11)}$$

Equation (4.11) suggests that the value of m is a function only of the w/c ratio. It indicates that the value of m increases as the w/c ratio increases. This is in contrast with the findings of other researchers, who suggested that the value of m increases with decreases in the w/c ratio [44]. Mangat and Molloy derived their equation for m based on the results of various concrete mixtures made with different cement compositions and types. The resulting values of m for the various concrete mixtures conducted in their study ranged from 0.44 for Portland cement concrete with a 0.4 w/c ratio to 1.34 for concrete made with a 0.58 w/c ratio containing 25% fly ash as partial replacement. Although the authors reported that the value of m is a function of several factors such as the use of SCMs and curing conditions, their proposed relationship does not reflect the influence of these factors in direct way. According to Luping and Gulikers [6], the values of m reported by Mangat and Molloy are inordinately large and thus cannot be correct. The reason was that the values of m were obtained based on inappropriate values of time-dependent diffusion coefficients. They used an incorrect time integration, which led to their calculating large values for the instantaneousness of the chloride diffusion coefficient.

The second development for the value of m came from Tang and Sørensen [44], who proposed the power relationship shown in Eq. (4.12) to estimate the value of m:

$$m = 0.152 \left(\frac{w}{c}\right)^{-0.6} \quad \text{.....Eq. (4.12)}$$

Equation (4.12) was derived from a regression analysis of the data for Portland cement presented in [139]. In contrast to Eq. (4.11) proposed by Mangat and Molloy [62], Eq. (4.12) suggests that the value of m increases as the w/c ratio of concrete decreases. Although Eq. (4.12) was derived based on the data of normal Portland cement concrete, it has also been used by several researchers to calculate the value of m for blended cement concretes [44].

Poulsen and Mejlbro [24] reported an empirical relationship, shown in Eq. (4.13), for estimating the value of m for blended cement concrete exposed to marine environments. The relationship was originally proposed by Frederiksen et al. [133].

$$m = k_{\alpha}\left(1\text{-}1.5\left(\frac{w}{PC+FA+7SF}\right)\right) \quad \text{Eq. (4.13)}$$

Where k_{α} is a parameter accounting for exposure conditions, it is equal to 1.0 for concrete exposed to marine atmosphere exposure conditions, 0.6 for submerged concrete, and 0.1 for concrete in the splash zone. This formula was used in the LIGHTCON model to estimate the service life of concrete structures exposed to marine environments [24]. Equation (4.13) suggests that the value of m is a function of the w/c ratio as well as the content and type of the supplementary cementitious materials, and is strongly dependent on the type of marine exposure.

The Life-365 model uses the formulation shown in Eq. (4.14) to estimate the value of m, which is purely dependent on the amount of fly ash and slag used in the concrete mix.

$$m = 0.26+0.4\left(\frac{\%FA}{50}+\frac{\%SG}{70}\right) \quad \text{Eq. (4.14)}$$

Equation (4.14) is used in Life-365 model to estimate the value of m for concrete mixes with maximum replacement levels of 50% and 70% for fly ash and slag, respectively. When fly ash and slag in the concrete mix are incorporated at their upper limits, a maximum value of m equal to 0.66 will result. The new Life-365 model uses m = 0.26 for concrete without fly ash and slag, and increases linearly to m = 0.66 as the fly ash and slag increase to 50% and 70%, respectively, Life-365. The model assumes that the silica fume addition has no effect on the value of m.

Equation (4.14) is illustrated graphically in Figure 4.3. As can be seen, the value of m increases with an increase in fly ash or slag replacement levels in concrete. Eq. (4.14) does not consider the influence of the w/c ratio or the influence of exposure conditions on

the value of m and assumes that m is solely dependent on the amount of fly ash or slag used in the concrete mix.

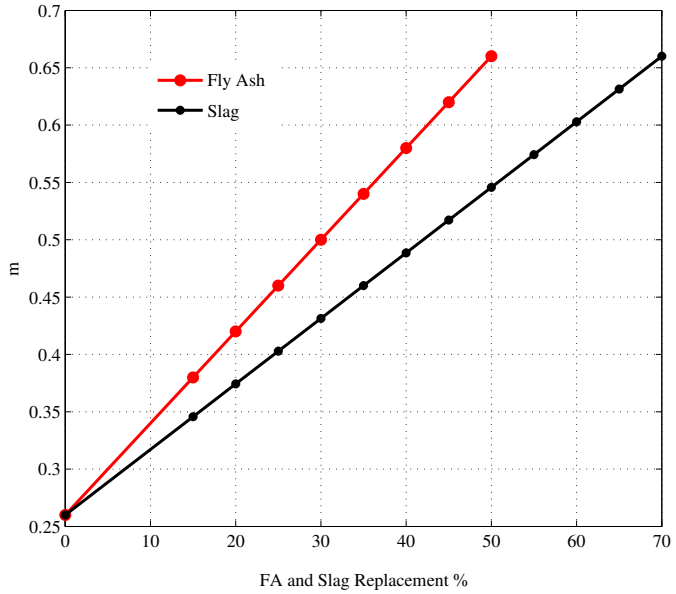

Figure 4.3 Influence of fly ash and slag contents on the value of m as per Life-365 relationship

Bamforth [140] conducted a comprehensive analysis of published data for a range of concrete mix types. He suggested that design values of m should be based on the type of cement used in the concrete, such that m = 0.264 for ordinary Portland cement concrete, m = 0.699 for concrete containing fly ash, and m = 0.621 for slag concrete. These values are very close to those used in Life-365. However, Bamforth did not specify for which replacement levels of fly ash or slag these values should be used. The general practice is that low values in range of 0.2 – 0.3 are common for normal Portland concrete, and higher values in range of 0.5 – 0.7 could be used for concrete containing high replacement levels of fly ash and slag [141].

For the purpose of administration, the values of m over the range of w/c ratios as calculated based on Mangat and Molloy [62], Tang and Sørensen [44], and Poulsen and Mejlbro [24] are plotted in Figure 4.4. As can be seen in Figure 4.4, the relationship

proposed by Tang and Sørensen correlates very well with that presented by Poulsen and Mejlbro for the marine submerged zone of exposure. Both relationships show that the value of m increases as the w/c ratio decreases. However, the relationship proposed by Mangat and Molloy gives a trend that is totally in disagreement with the trend given by the other two relationships. As mentioned earlier, some mathematical errors are involved in the derivation of their formula, which have led to these results. It can also be noted that the type of marine exposure has a significant influence on the value of m, as suggested by the Poulsen and Mejlbro formula. From this it can be understood that the value of m is not unique only for each cementitious system but also for each exposure condition or zone.

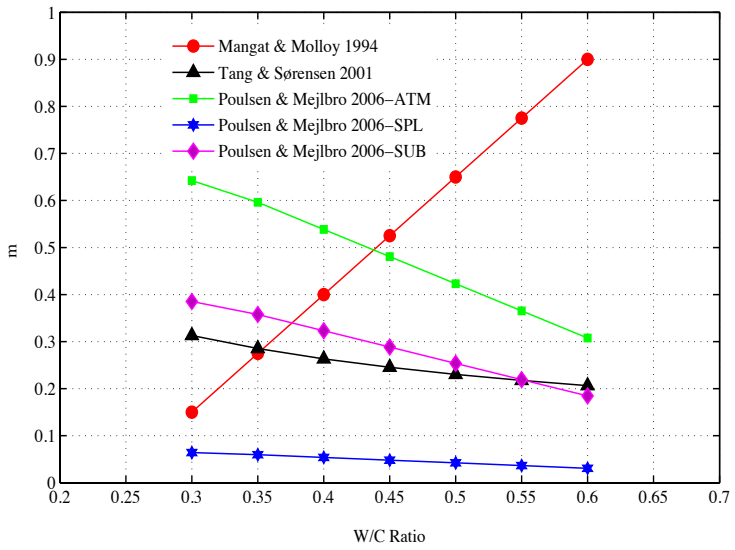

Figure 4.4 Influence of w/c ration on value of m for various relationships

It must be noted that the published values of m mentioned above were derived based on the acid soluble chloride content (i.e., total chloride content). In other words, the published values of m primarily concern the influence of time on the apparent chloride diffusion coefficients, D_a, as they are often projected based on acid soluble chloride measurements. No data made available in the literature concerned the values of m for the water-soluble measurements.

From the above literature review, the following can be pointed out:

- Disparities do exist in the literature concerning the selection of an appropriate value of m for a particular concrete type.
- The determination of the value of m based on diffusion coefficients obtained from the use of the error function solution is questionable, as there are different approaches used to calculate m, and each yields different results.
- It is clear that the value of m is influenced by a number of factors, including w/c ratio, cement type and content, and quantity, type of replacement SCMs used, and exposure conditions. However, some of these factors are also a function of curing and exposure temperatures, this will lead to that curing and exposure temperatures could have a great influence on the value of m. No data available in the literature concerns such influences on the value of m.
- Binding can alter the pore microstructure of concrete, which in turn could potentially influence the value of m.
- No published values of m found in the literature in the case where water-soluble chloride instead of acid-soluble is used to estimate the service life?

Despite of the some published values of m for different concrete mixtures and types, values of m have yet to be well established. Further research to properly quantify this parameter would help to improve the accuracy of service life estimations. Some of the above concerns with regard to the value of m for high performance concrete mix design will be investigated and addressed in this research.

4.3.4 Error Function Solution: Limitations and Drawbacks

Despite the simplicity of the use of analytical solutions to Fick's second law of diffusion (i.e., the error function solution in modeling chloride ingress into concrete), this approach is, for the most part, restricted to simple modeling. It does not allow for other important factors influencing chloride penetration into concrete to take place in the modeling process. The limitations and drawbacks associated with the use of the error function solution can be summarized as follows:

- The fit of the error function solution, Eq. (2.7), to the chloride profile determines a single diffusion value. This diffusion value is the average of the changing diffusion coefficient, D_a, over the testing exposure period, Maage et al. [134] and Stanish and Thomas[85].
- Three methods exist to calculate the m-value based on the sample age used as a reference age for D_{AVG} value. As reported previously by Nokken et al. [8], the value of m is highly dependent on the method used.
- When the diffusion coefficient, D_a, as projected from the bulk diffusion test is used to estimate the service life, inherent in that assumption is that the conditions in service are identical to the conditions during testing. For example, the age at which the concrete is first exposed to chloride ions is identical, the surface concentration is constant throughout the life of the structure, and the surface concentration is identical in both cases. If this is not the case, then the diffusion coefficients projected from the test results are invalid, as was argued by Stanish and Thomas [85].
- When the error function solution is derived it was assumed that the apparent diffusion coefficient and the chloride binding capacity are constant and do not change with concentration (i.e., linear binding).
- The error function solution ignores the influence of temperature on the diffusion value, which as been found to be significant.

From the above observations, it is clear that the use error function solution for making long-term service life predictions is strongly challenged.

4.4 Fick's Second Law and Finite Difference Approach

Another way to solve Fick's second law is to apply a numerical analysis. A common numerical method for approximating solutions of partial differential equations such as Fick's second law is to employ a finite difference approach. The finite difference method involves generating a grid in space and time where the solution needs to be approximated. This is usually done by discretizing the space into i discrete slices with equal intervals Δx and a time of interest into n equally spaced intervals of Δt, where i and n are integers. The

space and time region is covered by a grid of sides Δx and Δt. Finite difference schemes can then be obtained by applying Taylor's series in the time direction and space direction. By substituting the derivatives in the partial differential equation of Fick's second law with finite difference schemes, the system become a linear system of algebraic equations, which can be solved numerically with the help of a computer program such as MATLAB. The advantage of using a numerical solution is that it is more practical and allows the inclusion of the time-dependent diffusion coefficient and varying environmental parameters in a straightforward manner. An example of a chloride model that uses this approach is the Life-365 model. The finite difference approach is discussed in more detail in Chapter 5. In the following section, an overview of a common chloride model useing finite different approach is given.

4.5 Life-365 Model

Life-365 is a computer program that predicts the service life and life cycle cost of reinforced concrete structures exposed to chloride environments. The software is available free of charge on the Internet, and uses the linear version of Fick's second law presented in Eq. (2.5) to predict chloride ingress into concrete for service life design purposes. The service life in the model is defined by both the initiation period and propagation period of corrosion.

Life-365 software contains built-in models for one-dimensional (1-D) walls and bridge decks, two-dimensional (2-D) columns, and circular columns. The model uses the Crank-Nicolson finite difference approach as a solution for Fick's second law of diffusion, where future chloride concentrations in the concrete are estimated based on the current chloride concentration for the given boundary conditions. The model estimates the instantaneous diffusion coefficient at age of 28, D_{28}, from the mix design proportions. The influence of time on the instantaneous diffusion coefficient is taken into account by Eq. (4.1). The value of m is estimated by Eq. (4.12). In addition, the influence of temperature on the instantaneous diffusion coefficient is included in the model using an Arrhenius equation, as shown in Eq. (4.15):

$$D(T)=D_{ref}.\exp\left[\frac{E_a}{R}.\left(\frac{1}{T_{ref}}-\frac{1}{T}\right)\right] \quad \text{Eq.(4.15)}$$

where D(T) is the diffusion coefficient (m^2/s) at time t (sec) and temperature T (K), D_{ref} is the instantaneous diffusion coefficient (m^2/s) at time t_{ref}, E_a is the activation energy of the diffusion process (J/mol), R is the gas constant, and T is the absolute temperature (K). The software allows the user to input a temperature profile relevant to the location in terms of monthly average temperatures.

For the surface chloride concentration, Life-365 uses buildup linear function, and starts from a constant initial maximum concentration, with increases to that maximum from time zero. The last version of the software also includes ASTM C1556 module for estimating the maximum surface using the experimental data of the bulk diffusion test.

From the above consideration, it can be clearly seen that Life-365 has several advantages over the error function solution. The software uses the finite difference approach to model chloride ingress into concrete, which allows, in a straightforward manner, for the inclusion of time and temperature influences on the diffusion coefficient and surface concentration. There are a number of very useful papers cited in Lif-365 manual covers the validation of Life-365 with chloride profiles from concrete in the field.

As stated earlier, in the current practice in both the error function solution and Life-365, Fick's second law assumes linear binding and ignores the fact that the natural behavior of chloride binding in concrete is nonlinear, as outlined in Chapter 3. The inclusion of the nonlinearity of binding in the modeling process, along with time and temperature dependencies of a diffusion coefficient, is very important for proper and accurate predictions of service life. Furthermore, the accuracy of any model would depend on how accurately the key diffusion parameters are determined and whether or not some of the significant factors influencing chloride ingress into concrete are included. More work needs to be done in order to improve the current practice of Fick's second law chloride models and predictions in order to arrive at more accurate and reliable estimations of

service life. A proper estimation of service life will help owners to manage the cost and expenditures, and to develop more realistic and strategic plans for future repair and maintenance of their structures.

5 NONLINEAR CHLORIDE MODEL BASED ON FICK'S SECOND LAW OF DIFFUSION

This chapter provides a description of the nonlinear chloride model developed in this thesis based on Fick's second law of diffusion to overcome some of the limitations presented in the current practice, as outlined in the previous chapter. The nonlinear model is developed based on a modified Fick's second law of diffusion that includes a separate term for binding. The modified Fick's second law will allow the influence of binding to be considered explicitly in the model, unlike the commonly used simplified Fick's second law given by Eq. (2.5), where binding is implicitly included in the apparent diffusion coefficient and always assumed to be linear. Accordingly, a nonlinear numerical solution based on a finite difference approach is derived for the modified Fick's second law of diffusion to model chloride ingress into concrete. The chloride parameters used to model chloride ingress into concrete, which include the instantaneous effective diffusion coefficient, the value of m and the surface concentration, are derived from fitting the nonlinear finite difference model to the experimental acid-soluble chloride profiles. The influence of time and temperature is directly applied to the instantaneous effective diffusion coefficient, D_{e28}. This is very unique modeling approach and presents the main contribution of this thesis.

A linear numerical solution for the simplified Fick's second law, Eq. (2.5), is also derived. The purpose of the linear model is to evaluate chloride parameters obtained from acid-soluble chlorides to those obtained from water-soluble chlorides, and to study the influence of temperature on the value of m. Therefore, the numerical solution of the linear version of Fick's second law will be fitted to the experimental profiles of both acid-soluble and water-soluble chlorides obtained at different exposure conditions, and the results will be compared. The results of the linear numerical model will also be compared to that of the error function solution.

The modified Fick's second law equation, with a binding term added along with its derivation, is given in section 5.1. The modified Fick's second law will allow the

influence of different binding scenarios to be considered and accounted for during the modeling process. Three binding cases (no binding, linear binding and nonlinear binding) will be investigated in the nonlinear model. The modeling of binding cases is outlined in section 5.2. This will include the corresponding binding capacities and resulting apparent diffusion coefficients for the different binding relations considered in the nonlinear model. The modified Fick's second law is solved using the Crank-Nicolson finite difference method. A general description of the finite difference approach in solving partial differential equations such as those of diffusion is outlined in section 5.3. The derivation of the linear Crank-Nicolson finite difference solution is provided in section 5.3.1, followed by the derivation of the nonlinear solution in section 5.3.2.

A model describing the time and temperature dependencies of the diffusion coefficient is presented in section 5.5, a description of the nonlinear model is outlined in section 5.7, and a description of the linear model is provided in section 5.8. Units and conversions of chloride concentrations as used in the modeling process are presented in section 5.9. Chloride threshold values are briefly discussed and presented in section 5.10. The applied assumptions and limitations of the model are presented in section 5.11. Finally, the linear model validation is presented in section 5.12.

5.1 Modified Fick's Second Law of Diffusion

In order to model the influence of binding in concrete, Fick's second law as presented in Chapter 2 needs to be modified. In the published literature, several forms of Fick's second law with a separate binding term have been reported [27,95,142]. The difference between these forms is mainly related to the type of chloride and units used to describe chloride concentrations in Fick's second law. Three types of chloride concentrations exist in concrete: free chloride concentration, C_f, bound chloride concentration, C_b, and total chloride concentration, C_t. The free chlorides represent the concentration of free chloride ions in a pore solution and are often expressed as kg/m^3 of pore solution, kg/m^3 of concrete or as mole/l per solution. The bound chlorides represent the chloride ions captured by the concrete hydration products and are frequently expressed as kg/m^3 of

concrete. The total chloride concentration is the sum of the free and bond chlorides and is regularly expressed as kg/m^3 of concrete or % by weight of concrete.

In Fick's second law, either the movement of free chloride ions in a pore solution or the diffusion of the total chlorides can be used to describe the transport of chloride ions in concrete material. Consequently, Fick's second law may be written in terms of free chlorides or total chlorides [6]. The derivation of the modified Fick's second law with a separate binding term for free chloride concentration is considered in the developed model and provided herein.

It has been shown that the penetration of chlorides can be described by Fick's second law, as given by Eq. (2.4), where C is the total chloride concentration, expressed as kg/m^3 of concrete, and C_f is the free chloride concentration, expressed as kg/m^3 of solution. In order to use Eq. (2.4) equation to describe chloride penetration into concrete, both sides need to be written in the same chloride type and units. The chloride concentration given in Eq. (2.4) can be expressed either as kg/m^3 of concrete or as kg/m^3 of pore solution. To carry out this conversion, the relationship between the chloride concentrations units, as expressed in terms of material or pore solution, needs to be known. According to Nilsson et al. [27], the relationship between the free chloride concentrations as expressed in terms of kg/m^3 of solution and kg/m^3 of material is given by Eq. (5.1):

$$C_f\left(\frac{kg}{m^3}\text{of solution}\right) = \frac{C_f}{P_{sol}}\left(\frac{kg}{m^3}\text{ of material}\right) \quad \text{Eq. (5.1)}$$

where the term P_{sol} is the part of the concrete porosity in which the free chloride ions diffuse. This is can be taken as equal to the amount of evaporable water in capillary pores of a concrete microstructure system, ω_e, with the assumption that the capillary pores are totally filled with water.

Accordingly, Fick's first law, as presented in Eq. (2.1), can be written in terms of kg/m^3 of material, as shown in Eq. (5.2):

$$J = -D_e . \omega_e \frac{\partial C_f}{\partial x} \quad \text{.....Eq. (5.2)}$$

where D_e is the chloride effective diffusion coefficient (m^2/s) when the C_f is expressed in kg/m^3 of concrete material.

Thus, Fick's second law with all chloride concentrations as kg/m^3 of concrete can be given by Eq. (5.3):

$$\frac{\partial C_t}{\partial t} = \frac{\partial}{\partial x}\left(D_e . \omega_e \frac{\partial C_f}{\partial x}\right) \quad \text{.....Eq. (5.3)}$$

Notice that the chloride concentration is not the same on both sides of the equation. Equation (5.3) gives the change in total chloride with time as a function of the spatial gradient of the free chlorides [95]. To apply Eq. (5.3) to describe the movement of chloride ions into concrete, as mentioned earlier, the concentration on both sides needs to be the same either as total chloride or as free chloride concentrations. In order to write both sides in the same concentration, the relation between total and free chlorides needs to be identified. According to Nilsson et al. [27] and Martine-Perez et al. [95], the total bound and free chlorides are related by Eq. (5.4):

$C_t = C_b + \omega_e . C_f$ [all in kg/m^3 of concrete].....Eq. (5.4)

By applying mass conservation to Eq. (5.4) and substituting it in Eq. (5.3), the following results:

$$\frac{\partial C_t}{\partial t} = \frac{\partial C_b}{\partial t} + \omega_e \frac{\partial C_f}{\partial t} = \frac{\partial}{\partial x}\left(D_e . \omega_e \frac{\partial C_f}{\partial x}\right) \quad \text{.....Eq. (5.5)}$$

Furthermore, by rearranging terms, the following form of Fick's second law results:

$$\frac{\partial C_f}{\partial t} = \frac{\partial}{\partial x}\left(\frac{D_e}{\left[1 + \frac{1}{\omega_e}\frac{\partial C_b}{\partial C_f}\right]}\frac{\partial C_f}{\partial x}\right) \quad \text{.....Eq. (5.6)}$$

by writing:

$$D_a^* = \frac{D_e}{1 + \frac{1}{\omega_e}\frac{\partial C_b}{\partial C_f}} \quad \text{.....Eq. (5.7)}$$

Equation (5.6) can then be reduced to

$$\frac{\partial C_f}{\partial t} = \frac{\partial}{\partial x}\left(D_a^* \frac{\partial C_f}{\partial x}\right) \quad \text{.....Eq. (5.8)}$$

where D_a^* is the apparent diffusion coefficient (m^2/s) and $\partial C_b / \partial C_f$ is the binding capacity in terms of bound (kg/m^3 of concrete) and free chlorides (kg/m^3 of pore solution).

The binding capacity is a unique parameter for each cementitious material system and needs to be determined experimentally. Once the binding capacity of a specific cementitious system is established, the free chloride concentration can then be determined from Eq. (5.8). Consequently, the total chloride can be calculated using Eq. (5.4). It should be noted that the apparent diffusion coefficient, D_a^*, and the D_e are not the same, and are related by binding capacity and porosity terms.

In summary, the modified Fick's second law given in Eq. (5.8) allows binding to take place in the modeling process as a separate term. However, attention must be paid to the type of concentration used to describe chloride movement to avoid any confusion in the analysis and interpretation of results. By taking the natural influence of chloride binding into account, more accurate results can be achieved. However, the numerical solution of the modified Fick's second law becomes more complicated due to the dependency of the apparent diffusion coefficient on the free chloride concentration and binding capacity of the concrete, which changes with depth and concentration. For this reason, chloride binding in Fick's law is often assumed to be linear to avoid the complexity of such dependency. In the case of the linear binding assumption, the apparent diffusion coefficient is constant with depth and independent of the free chloride concentration in

the pore solution. Therefore, the numerical solution in such cases becomes relatively simple and straightforward.

5.2 Modeling of Binding Cases

In the following sections, the modeling of different binding scenarios and the corresponding binding capacities along with the resulting apparent diffusion coefficients as reported in the literature [95,143] are provided.

5.2.1 No Binding

When no binding is assumed, the following results:

Bound chlorides $C_b = 0$ ……...……Eq. (5.9)

Binding capacity: $\frac{\partial C_b}{\partial C_f} = 0$……..…….……..Eq. (5.10)

Apparent diffusion coefficient: $D_a^* = D_e$……..……Eq. (5.11)

5.2.2 Linear Binding

Where linear binding is assumed, the following results:

Bound chlorides: $C_b = \alpha C_f$ ……..…..…...…..Eq. (5.12)

Binding capacity: $\frac{\partial C_b}{\partial C_f} = \frac{\alpha}{\omega_e}$ ……...……..Eq. (5.13)

Apparent diffusion coefficient: $D_a^* = \frac{D_e}{1 + \frac{\alpha}{\omega_e}}$ ……..…….……...…Eq. (5.14)

Despite many researchers having reported that the relationship between bound and free chlorides is nonlinear, chloride binding is often modeled as linear for simplicity's sake. It can be noted that when the binding capacity is assumed to be constant, D_a^* in Eq. (5.14) becomes independent of the chloride concentration in the pore solution.

From an engineering standpoint, the nonlinearity of chloride binding is of significance. It

has been reported that the nonlinear nature of chloride binding has to be taken into account in any reliable prediction of the penetration of chlorides in concrete structures [144]. It should also have a strong influence on the predicted chloride profiles and service life estimations.

5.2.3 Non-linear Binding (Langmuir Isotherm)

Based on the Langmuir binding isotherm, the amount of bound chlorides, the corresponding binding capacity, and the resulting D_a^* will be given by:

Bound chloride: $C_b = \frac{\alpha C_f}{(1+\beta C_f)}$ ……..……. Eq. (5.15)

Binding capacity: $\frac{\partial C_b}{\partial C_f} = \frac{\alpha}{(1+\beta C_f)^2}$ ……..…….Eq. (5.16)

Apparent diffusion coefficient: $D_a^* = \frac{D_e}{1+\frac{\alpha}{\omega_e(1+\beta C_f)^2}}$ ……...……Eq. (5.17)

5.2.4 Nonlinear Binding (Freundlich Isotherm)

It is believed that the relationship between bound and free chlorides in concrete is best described by the Freundlich relationship [7,144]. The amount of bound chlorides, the corresponding binding capacity, and resulting apparent diffusion coefficient based on the Freundlich isotherm can be calculated from:

Bound chloride: $C_b = \alpha C_f^{\beta}$……...……Eq. (5.18)

Binding capacity: $\frac{\partial C_b}{\partial C_f} = \alpha\beta C_f^{\beta-1}$ ……..... Eq. (5.19)

Apparent diffusion coefficient: $D_a^* = \frac{D_e}{1+\frac{\alpha\beta C_f^{\beta-1}}{\omega_e}}$ ……..…...…..…Eq. (5.20)

The governing partial differential equation of the modified Fick's second law given by Eq. (5.8) is solved numerically using the Crank-Nicolson finite difference method. In the

following sections, both linear and nonlinear finite difference solutions for the simplified and modified Fick's second laws will be provided.

5.3 Finite Difference Approach to Fick's Second Law of Diffusion

Fick's second law, in all its forms, is a partial differential equation. Of the numerical approximation methods available for solving partial differential equations, those using a finite difference approach are more frequently used and more universally applicable than any others. A finite difference approach is approximate, in the sense that derivatives at a point are approximated by difference quotients over a small interval (i.e., $\partial c/\partial x$) is replaced by $(\Delta c/\Delta x)$ where Δx is small [145]. Finite difference methods generally provide adequate numerical solutions that are more simple and efficient. In these methods, the area of integration of the partial differential equation (in our case, the concrete slab thickness) is covered by a system of grids formed by two sets of equally spaced lines, one in the time direction, t (on the vertical axis), and the other in the space direction, x. The area of integration is bounded by known boundary and initial conditions. The approximate solution to the partial differential equation is found at the points of intersection, which are called grid points. This solution is obtained by approximating the partial differential equation over the integrated area by N number of algebraic equations involving the value of u (chloride concentration) at the N grid points.

5.4 Crank-Nicolson Solution for Simplified (Linear) Fick's Second Law of Diffusion

The derivatives of the partial differential equation of Fick's second law of diffusion given by Eq. (2.5) can be replaced by the Crank-Nicolson scheme, as shown in Equations (5.21) – (5.23). It is important to note that the differences in expressions are centered about some depth slice, i, in the space domain, but are centered between time slices, t and t+Δt at t+Δt/2 in the time domain.

The Crank-Nicolson approximation for the left-hand side derivative of Eq. (2.5) is:

$$\frac{\partial C_t}{\partial t} = \frac{u_i^{n+1} - u_i^n}{\Delta t} \quad \text{..... Eq. (5.21)}$$

and for the right-hand side derivative is:

$$\mathrm{D}\frac{\partial^2 C_t}{\partial x^2} = D\left(\frac{1}{2}\left\{\frac{u_{i+1}^{n+1} - 2u_i^{n+1} + u_{i-1}^{n+1}}{\Delta x^2} + \frac{u_{i+1}^{n} - 2u_i^{n} + u_{i-1}^{n}}{\Delta x^2}\right\}\right) \quad \text{.....Eq. (5.22)}$$

In Eq. (5.23), the derivative $(\partial^2 C_t/\partial x^2)$ is replaced by the mean of its finite difference representations on the $(n+1)^{th}$ and n^{th} time rows, as the Crank-Nicolson method suggests,

by taking $r = \frac{\mathrm{D}.\Delta \mathrm{t}}{\Delta \mathrm{x}^2}$ and rearranging terms:

$$-ru_{i+1}^{n+1} + (2 + 2r)u_i^{n+1} - ru_{i-1}^{n+1} = ru_{i+1}^{n} + (2 - 2r)u_i^{n} + ru_{i-1}^{n} \quad \text{... Eq. (5.23)}$$

As can be seen, the left-hand term in Eq. (5.23) represents three unknown values of u at the future time step of n+1 (i.e., future value of chloride concentration), and the right-hand term represents the three values of u, which are known at the current time level of n. Therefore, if there are N internal grid points along each time step row, then for n = 0 and i = 1, 2,…N, Eq. (5.12) will give N simultaneous equations for N unknown values along the first time step row expressed in terms of the known initial values and the boundary values at i = 0 and N+1. This follows that for n = 1, unknown values of u are expressed along the second time row in terms of those calculated from the first row, and so on [146]. This method is described as an implicit method, because the solution of a set of simultaneous equations is called for at each time step to solve for u.

Equation (5.23) can be written in terms of a matrix, as follows:

$$AU^{n+1} = BU^{n} \quad \text{.....Eq. (5.24)}$$

where A is the coefficient matrix for the $n+1^{th}$ time level and B is the coefficient matrix for the n^{th} time level. Equation (5.24) can be solved as shown in Eq. (5.25):

$U^{n+1}=A^{-1}b$……Eq. (5.25)

where $b = BU^n$. Inverting A and multiplying it with the product of B and the current chloride concentration profile at time n (i.e. U^n) will provide an estimate of the future chloride concentrations at time n+1 (i.e. U^{n+1}).

5.5 Crank-Nicolson Solution for Modified Fick's Second Law

The Crank-Nicolson solution for the modified Fick's second law given by Eq. (5.8) is slightly different from that given by Eq. (5.23). This is because the diffusion coefficient, in this case, is concentration-dependent and tends to change as the chloride concentration in the pore solution changes with depth. In this case, the diffusion value changes as the chloride ions penetrate. To include this change in the Crank-Nicolson finite difference formula, the right-hand side of Fick's second law needs to be approximated twice. The solution was first approximated at X_i by considering the two points X_{i-1} and X_{i+1} and then by considering the two mid-points $X_{i-1/2}$ and $X_{i+1/2}$, as shown in Figure 5.1. The Crack-Nicolson solution scheme is shown in Eq. (5.26) – Eq. (5.31).

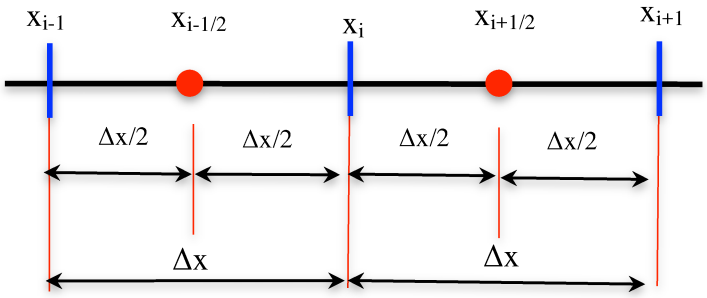

Figure 5.1 Grid system for nonlinear Crank-Nicolson solution

The left-hand side of Eq. (5.8) will be the same:

$$\frac{\partial C}{\partial t} = \frac{u_i^{n+1} - u_i^n}{\Delta t} \quad \text{……Eq.(5.26)}$$

For the right side, the first approximation will be for the first derivative ($\partial C/\partial x$) using the two points at x_{i-1} and x_{i+1}:

$$\frac{\partial}{\partial x}\left(D\frac{\partial C}{\partial x}\right) = \frac{\partial}{\partial x}\left(\frac{D[u_{i+1}^{n} - u_{i-1}^{n}]}{2\Delta x}\right) + \frac{\partial}{\partial x}\left(\frac{D[u_{i+1}^{n+1} - u_{i-1}^{n+1}]}{2\Delta x}\right) \text{……...……Eq. (5.27)}$$

Note that the distance between x_{i-1} and x_{i+1} is equal to 2Δx, as shown in Figure 5.3.

$$= \left[\frac{\left(\frac{\partial}{\partial x}[D(u_{i+1}^{n})] - \frac{\partial}{\partial x}[D(u_{i-1}^{n})]\right)}{2\Delta x}\right] +$$

$$\left[\frac{\left(\frac{\partial}{\partial x}[D(u_{i+1}^{n+1})] - \frac{\partial}{\partial x}[D(u_{i-1}^{n+1})]\right)}{2\Delta x}\right] \text{……...……Eq. (5.28)}$$

The second approximation will be for ($D\,\partial C/\partial x$) at $x_{i-1/2}$and $x_{i+1/2}$, where the distance between these two points is equal to Δx.

$$= \left[\frac{\left(\left[D_{i+\frac{1}{2}}(u_{i+1}^{n} - u_{i}^{n})\right]/\Delta x - \left[D_{i-\frac{1}{2}}(u_{i}^{n} - u_{i-1}^{n})\right]/\Delta x\right)}{2\Delta x^{2}}\right] +$$

$$\left[\frac{\left(\left[D_{i+\frac{1}{2}}(u_{i+1}^{n+1} - u_{i}^{n+1})\right]/\Delta x - \left[D_{i-\frac{1}{2}}(u_{i}^{n+1} - u_{i-1}^{n+1})\right]/\Delta x\right)}{2\Delta x^{2}}\right] \text{……...….. Eq. (5.29)}$$

Thus, the centered difference formula for the entire expression at x_i is:

$$\frac{u_i^{n+1} - u_i^{n}}{\Delta t} = \frac{1}{2\Delta x^{2}}\left[\left(D_{i+\frac{1}{2}}u_{i+1}^{n} - D_{i+\frac{1}{2}}u_{i}^{n} - D_{i-\frac{1}{2}}u_{i}^{n} + D_{i-\frac{1}{2}}u_{i-1}^{n}\right)\right] +$$

$$\frac{1}{2\Delta x^2}\left[\left(D_{i+\frac{1}{2}}u_{i+1}^{n+1} - D_{i+\frac{1}{2}}u_i^{n+1} - D_{i-\frac{1}{2}}u_i^{n+1} + D_{i-\frac{1}{2}}u_{i-1}^{n+1}\right)\right] \text{.....Eq. (5.30)}$$

The final expression of the complete solution for Fick's second law with nonlinear binding, as approximated by the Crank-Nicolson method, can be written as:

$$-r\,D_{i+\frac{1}{2}}u_{i+1}^{n+1} + \left(2 + r\left(D_{i+\frac{1}{2}} + D_{i-\frac{1}{2}}\right)\right)u_i^{n+1} - rD_{i-\frac{1}{2}}u_{i-1}^{n+1} \quad =$$

$$r\,D_{i+\frac{1}{2}}u_{i+1}^{n} + \left(2 - r\left(D_{i+\frac{1}{2}} + D_{i-\frac{1}{2}}\right)\right)u_i^{n} + rD_{i-\frac{1}{2}}u_{i-1}^{n} \text{..... Eq. (5.31)}$$

where $D = D_a^*$, and $r = \frac{\Delta t}{\Delta x^2}$

Similarly, Eq. (5.31) can be written in terms of a matrix. The future concentration can then be solved by:

$$U^{n+1} = A^{-1}.b \text{..... Eq. (5.32)}$$

where A is the coefficient matrix for the left side of Eq. (5.31), and b is the result of the right side of Eq. (5.31), a column vector equal to (BU^n).

The set of simultaneous linear algebra equations resulting from using the Crank-Nicolson approach in both cases to the two governing equations of Fick's second given by Eq. (2.5) and Eq. (5.8) can be solved in time steps up to the time where the specific chloride threshold is attained at the level of reinforcement.

The coding approach (in the space domain) for the above solution is illustrated in Figure 5.2. Notice that D_p and D_m are equal to $D_{i+1/2}$ and $D_{i-1/2}$ in Eq. (5.31), respectively. The D_p and D_m are the coefficients, which contain the binding portion in the process and are loaded in the matrices A and b along with the boundary conditions. A full MATLAB code for this model is provided in Appendix G.

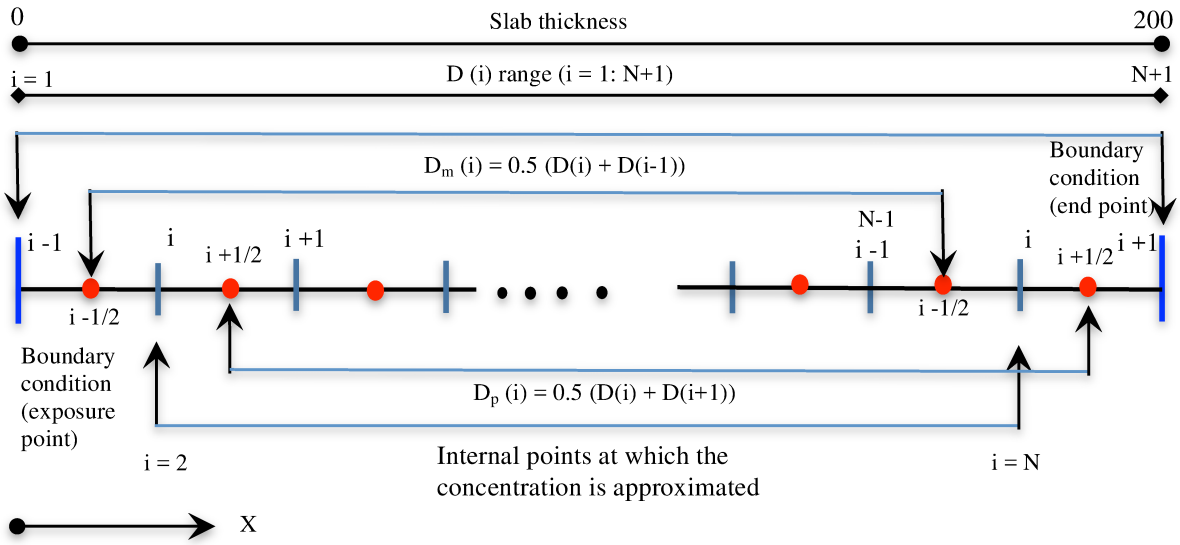

Figure 5.2 Coding approach for nonlinear Crank-Nicolson solution

5.6 Time and Temperature Dependencies of Diffusion Coefficient

As mentioned earlier, the diffusion coefficient is dependent on time and temperature, decreasing with time as the concrete ages, and increasing or decreasing as the temperature increases or decreases, respectively. The reduction in diffusion occurs as a result of ongoing hydration, where the capillary porosity of the pore system decreases and the tortuosity of the pore structures increases over time. Therefore, the influence of time and temperature needs to be taken into account when chloride ingress into concrete is modeled.

According to Luping and Gulikers [6], a more accurate representation of the diffusion coefficient is achieved when both the time dependence as described by Takewaka and Matsumoto [73] and the temperature dependence of the diffusion coefficient according to the Arrhenius equation are accounted for, as per Eq. (5.33)

$$D(t,T) = D_{28,\,T_{ref}} \left(\frac{t_{28}}{t}\right)^{m} .\exp\left[\frac{E_a}{R}.\left(\frac{1}{T_{ref}} - \frac{1}{T}\right)\right] \quad \text{.....Eq.(5.33)}$$

where $D_{28,T_{ref}}$ is the chloride diffusion coefficient at 28 days and reference temperature, E_a is the energy activation of the concrete (J/mol), R is the universal gas constant, (J/mol), T_{ref} is the reference temperature (K), and T is the exposed temperature (K).

The activation energy, E_a, for chloride transport in many models is taken to be equal to 35,000 J/mole. These include Life-365 and ClinConc. Some researches used the migration test to experimentally determine the value of E_a, and reported that for high performance concrete made with 0.30 w/b ratio, the activation energy was found to be equal to 32800 j/mole [143]. In this research a value of 33,500 J/mole was used for the E_a in modeling the influence of temperature on the diffusion coefficient.

Equation (5.33) is incorporated in the nonlinear model to account for the effects of exposure temperature and time on the effective instantaneous diffusion coefficient. Equation (5.33) is also used in the linear model to account for the influence of time and temperature on the apparent diffusion coefficient. The activation energy of the concrete tested in this thesis was determined experimentally.

5.7 Description of the Nonlinear Model

This model is developed to include nonlinear binding behavior in concrete. It also considers the influence of other binding types on the modeled chloride concentration profiles. Three binding isotherm scenarios were considered in this model: no binding, linear binding, and non-linear isotherms. A Freundlich binding isotherm is selected to model nonlinear binding behavior. The free chlorides are calculated from Eq. (5.8), the amount of bound chlorides for linear and linear binding relationships are calculated from Eq. (5.12) and Eq. (5.18), respectively, and total chloride content is calculated from Eq. (5.4). The influence of time and temperature on the diffusion coefficient is solved by Eq. (5.22). Note that the influence of time and temperature is applied to the effective instantaneous diffusion coefficient, D_e, which is taken in this model at a reference age of 28 days. Flow chart of the model structure is shown in Figure 5.3.

The initial and boundary conditions used in the model for numerical analysis:

For exposure time equal to zero, i.e., t = 0:

$C_f = C_i$ at $x > 0$

During exposure where $t > 0$:

$C_f = C_s$ at $x = 0$ and,

$C_f = C_i$ at x = slab thickness.

Note that the C_s here is equal to the chloride concentration of the solution in contact with the concrete surface (kg/m^3 of solution), and x is the slab thickness (mm).

5.7.1 Determination of Chloride Parameters for Nonlinear Model

The chloride parameters are mainly the effective instantaneous diffusion chloride coefficient at 28 days, D_{e28}, so the m value will be determined by fitting the nonlinear finite difference model to multiple experimental chloride profiles obtained at different times of exposure or concrete ages. The D_{e28} and m for the corresponding binding are selected as the values that give the best fit of the corresponding predicted profiles to the experimental chloride profiles at all concrete ages used. The total chloride concentration at the surface is calculated from Eq. (5.4) for each binding case and assumed to be constant for all chloride profiles used. The quality of the fit is determined by the sum of the mean squared errors between the model prediction and the experimental data at all concrete ages. The determination process of these parameters is very similar to that used by Thomas and Bamforth [70], except that the surface concentration will be calculated numerically based on the free chloride concentration at the surface and the amount of bound chloride resulting from the corresponding binding relation.

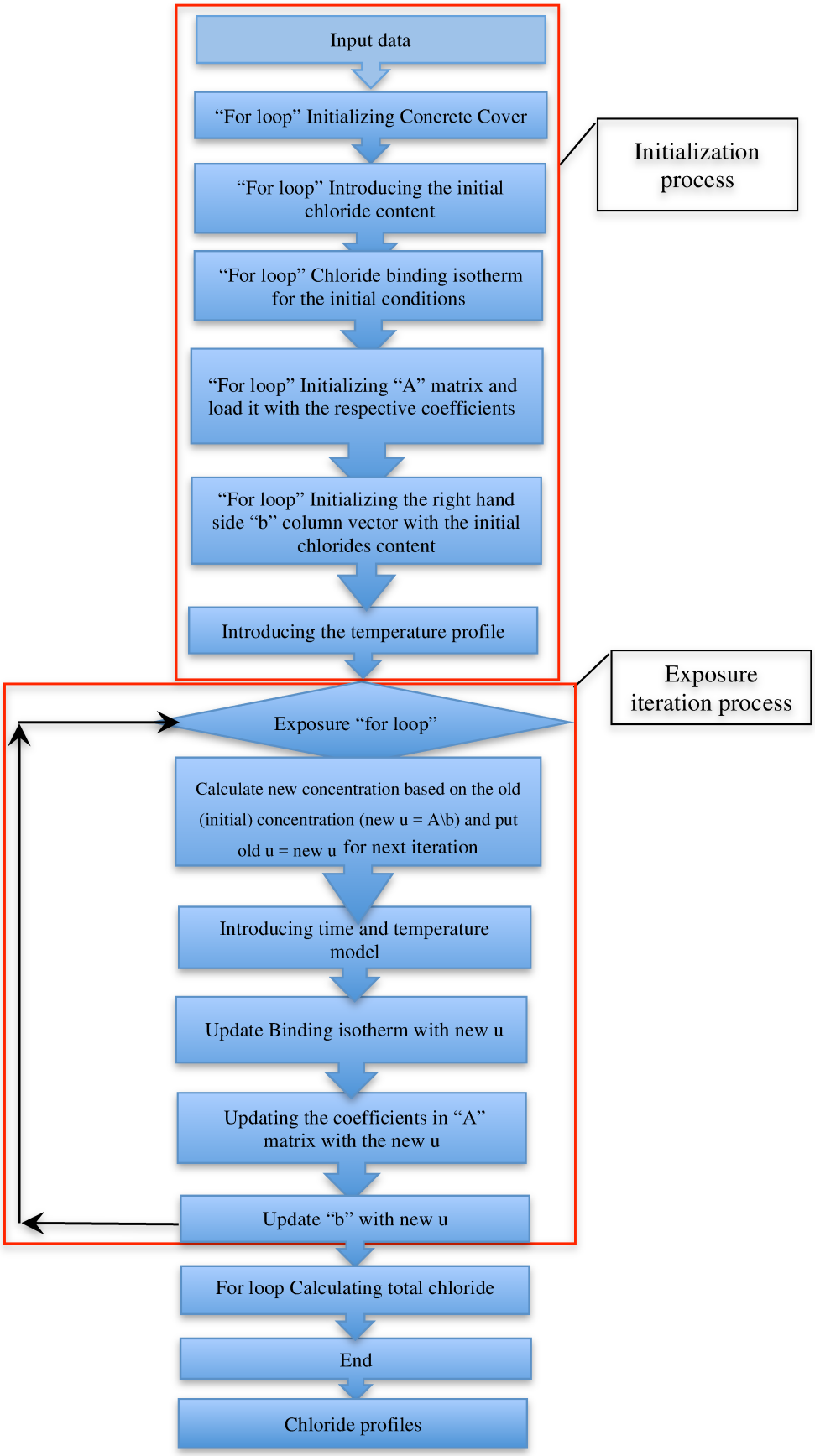

Figure 5.3 Algorithm structure of the nonlinear model

5.8 Description the Linear Model

The linear model uses Fick's second law, given by Eq. (2.5), as the case of current practice. Note that Eq. (2.5) describes the movement of total chlorides in concrete and is expressed as % by weight of concrete. The time and temperature influences on the apparent diffusion coefficient are taken into account by Eq. (5.33). Similar to the nonlinear model, the chloride parameters will be determined by fitting the numerical profiles to the experimental chloride profiles of acid-soluble and water-soluble obtained at different concrete ages. The surface concentration in this case will be taken as the average value of the surface concentrations that provide the best fit for individual chloride profiles. Complete MATLAB codes for the linear model are provided in Appendices E & F.

5.9 Chloride Units and Unit Conversions

The chloride concentrations, units, and unit conversions used in this thesis are listed below.

- Free chloride concentration: kg/m^3 of pore solution, kg/m^3 of concrete.
- Bound chlorides: kg/m^3 of concrete.
- Total (acid-soluble) chloride concentration: kg/m^3 of concrete and % by weight of concrete.
- Water-soluble chloride concentration: kg/m^3 of concrete and % by weight of concrete

Conversions:

- To convert chloride concentration from kg/m^3 of pore solution to kg/m^3 of concrete, a multiplier equal to the porosity term of the concrete is used.
- To convert chloride concentration from % by weight of concrete to kg/m^3 of concrete, a multiplier factor equal to the concrete density is used.

5.9.1 Units of Free and Bound Chlorides – Binding Isotherm

Special care should be taken for units of free and bound chlorides used in the determination of binding constants α and β. The values of these parameters are highly dependent on the units used for C_f and C_b. In this thesis, the C_f and C_b are measured in kg/m^3 of pore solution and kg/m^3 of concrete, respectively. In some cases, the C_b is expressed in mg/g of concrete sample or kg/kg of binder. The use of different units for C_b will result in different values of α and β for the same cementitious system.

5.10 Chloride Threshold (Critical Chloride Content)

The service life of any concrete structure exposed to a chloride environment is often defined as the time it takes for a sufficient amount of chloride to penetrate the concrete cover and accumulate in sufficient quantity, i.e., critical chloride content (C_{crit}), at the depth of the reinforcement to initiate corrosion. Therefore, the C_{crit} is one of the most decisive input parameters. Despite the considerable work done in the past decades for determining the value of C_{crit} responsible for corrosion initiation, no general agreement on a particular value of C_{crit} has been achieved. The values of C_{crit} reported in the literature are scattered over a wide range [20]. Thus, for design purposes, conservative values are often employed in chloride models as critical chloride concentrations.

In North America and Europe, the common practice is to limit the tolerable chloride content to 0.4% by weight of binder, which is approximately equivalent to 0.07% by weight of concrete, in concrete that contains 350 kg/m^3 of cement. These values are often expressed as the total chloride content (free and bound chlorides) relative to the weight of the binder or the weight of the concrete. Other values of C_{crit} have also been reported for free chloride concentration. The conservative C_{crit} value for free chloride concentration has been reported to be equal to 0.07% by weight of binder or cement, which is equivalent to 0.01% by weight of concrete and 0.045 mol/l in terms of free chloride concentration in the pore solution [20]. Life-365 uses 0.05% by weight of concrete as a critical chloride content value that is responsible for corrosion initiation. The values of C_{crit} for both acid-soluble and water-soluble chlorides along with the C_{crit} value for free

chloride concentrations are presented in Table 5.1.

Table 5.5.1 Design values for chloride threshold

Chloride threshold values (C_{crit})						
Acid-soluble			**Water-soluble**			***Free concentration**
% by weight of cement	% by weight of concrete	Kg/m^3 of concrete	% by weight of cement	% by weight of concrete	Kg/m^3 of concrete	% by weight of cement
0.4	0.05	1.15	0.15	0.02	0.45	0.09%

*Glass and Buenfeld [148]

These values were used in this research to estimate the time to corrosion initiation for both total and free chloride concentrations.

5.11 Assumptions and Limitations

The following assumptions and limitations are applied to the concrete and models used in this thesis:

1. The concrete is homogeneous and free of any gross cracking or defects.
2. The concrete is fully saturated and the movement of chloride ions in the concrete is described solely by the diffusion transport process.
3. One-dimensional diffusion into semi-infinite space.
4. The initial chloride content, C_i, if presented, is uniformly distributed at the time of the first chloride exposure.
5. Constant surface concentration.
6. In order to prevent the diffusion coefficient from decreasing indefinitely with time, the maturity (hydration) of concrete is assumed to cease at 25 years of exposure, beyond which time the value of the diffusion coefficient remains constant at the De (25 years) value.
7. The chloride transport parameters are obtained experimentally using the exposure conditions of the bulk diffusion test.

8. A constant value for a porosity term, P_{sol}, is used in the model when the movement of chloride ions is described by the free chloride concentrations of the pore solution. The constant value is used for the sake of simplicity, and the author understands that this might, to some extent, yield a conservative prediction of the service life.
9. Finally, chloride-induced corrosion is assumed to be the primary cause of reinforced concrete structure deterioration. It is acknowledged that there are many other causes of deterioration including alkali aggregate reaction, carbonation, sulfate attack, and freeze/thaw damage, which may also interact with chloride initiated corrosion and shorten the service life of the structure. However, these causes of deterioration are beyond the scope of modeling and investigation undertaken in this thesis.

5.12 Validation of Linear Model

Since the linear and nonlinear models use the experimental profiles to evaluate and obtain the chloride parameters, no significant validation is needed. However, the nonlinear model was validated against the linear models by comparing the results of the linear binding assumption in the nonlinear model to those of other linear models as will be seen in Chapter 8 of this thesis. In this section, the linear model was validated against the error function solution to ensure that mathematical errors in the finite difference models are kept at a minimum. To make the comparison, a particular set of linear model parameters needs to be kept constant. These parameters include the surface chloride concentration (1% by weight of concrete), the diffusion coefficient (2×10^{-12} m^2/s), and the temperature (22.4^o C). All data have been obtained at a specific time (t) equal to 5 years. The comparison of the test results is shown in Table 5.2. To shorten the table, only the estimate values at depths from 10 mm to 100 mm were illustrated. The continuous estimates of both models for the entire thickness of the slab are graphically illustrated in Figure 5.4.

As can be seen from both the table and graphical representations of the estimated data, the estimated values of the linear model are almost identical to the error function solution

estimates. The difference between the estimated values obtained from the two models is extremely small.

Table 5.2 Estimated chloride concentration values: linear finite difference model vs. error function solution

No.	Depth (mm)	Linear model % by weight of concrete	Error function model % by weight of concrete	Differences (errors)
1	0	1	1	0
12	10	0.690479675	0.690495983	1.6308E-05
3	20	0.425809255	0.425820416	1.11614E-05
4	30	0.232277575	0.232264377	1.31981E-05
5	40	0.111257464	0.111221162	3.63025E-05
6	50	0.046533597	0.046490745	4.28518E-05
7	60	0.016924195	0.016890053	3.41418E-05
8	70	0.005335778	0.005315344	2.04342E-05
9	80	0.001454871	0.001445258	9.61269E-06
10	90	0.000342482	0.000338841	3.64123E-06
11	100	6.95165E-05	6.83894E-05	1.1271E-06

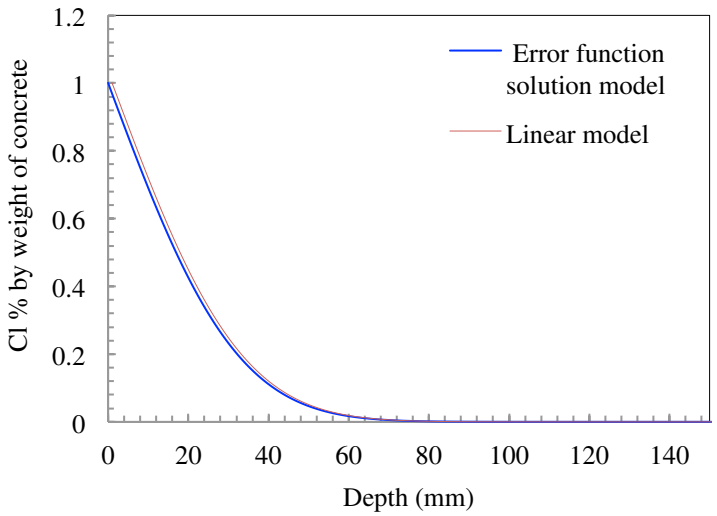

Figure 5.4 Developed model estimate chloride profile vs. error function solution chloride profile after 5 years of exposure

6 EXPERIMENTAL PROGRAM

A large experimental program was conducted to provide the database required to achieve the objectives of this thesis. Water-soluble and acid-soluble chloride profiles were obtained from the tested concrete samples using the bulk diffusion test at three different exposure times and temperatures. A rapid migration test was also performed to evaluate the influence of the amount of curing on the migration diffusion coefficient and the age parameter values. The binding parameters of the cementitious system for both linear and nonlinear isotherms were obtained through the equilibrium test. Additional experiments were performed to investigate the influence of binding and temperature on the pore size distribution and porosity of the high performance concrete. A Mercury Intrusion Porosimetry (MIP) test was carried out to examine the influence of binding products on concrete porosity and pore size distribution at different exposure conditions. Additional tests, including compressive strength and porosity tests, were also conducted. All testing procedures were performed using high performance concrete samples from the same mix.

6.1 Concrete Mix Design and Samples Preparations

A high performance concrete mixture typically used in Nova Scotia for highway bridge deck construction was evaluated to satisfy the research aims and objectives. The mix design and the preparations of the test samples are given in the following subsections.

6.1.1 Concrete Mix Design and Proportions

The concrete mix design and proportions are shown in Table 6.1. The concrete is made of ternary blended cement, commercially known as Lafarge Tercem 3000. The cement incorporated 5% silica fume and 25% ground granulated blast furnace slag as a partial replacement for Portland cement. The chemical composition and the physical properties of the blended cement are provided in Table 6.2.

Table 6.1 Concrete mix design and proportions

Lafarge Tercem (kg/m^3)	Water (kg/m^3)	W/C	Sand (kg/m^3)	20 mm Coarse Aggregate (kg/m3)	AEA (ml/m^3)	HRWR (ml/m^3)	Retarder (ml/m^3)
435	140	0.32	740	1060	1500	2500	1000

Table 6.2 Cement chemical and physical properties

Chemical analysis			Physical analysis		
Item	Spec. Limit	Test results	Item	Spec. Limit	Test results
SiO_2 (%)	-	27.2	Blaine fineness (m^2/kg)	-	568
Al_2O_3 (%)	-	6.4			
Fe_2O_3 (%)	-	1.81	Fineness, res. passing on 45 um	76 min	98.2
CaO (%)	-	51			
MgO (%)	5.0 max	4	Fineness, res. retained on 45 um	24 max	1.8
Sulphate as SO_3 (%)	3.0 max	4.18			

6.1.2 Casting and Preparation of Concrete Samples

A concrete ready-mix truck supplied the concrete to the lab site. As soon as the concrete was received, the slump and air content tests were performed, followed by the casting of the concrete cylinders. In total, 90 standard concrete cylinders measuring 100 mm in diameter and 200 mm in height, and 40 large cylinders measuring 150 in diameter and 300 mm in height, were cast and molded. A vibrated table was used to consolidate the cast cylinders. The cylinders were demolded after 24 hours and kept in the moisture room for standard curing up to age 28 days. A photo of the cast cylinders is shown in Figure 6.1. The small-size cylinders are used to test compressive strength, rapid migration, and equilibrium. The large cylinders are used to obtain smaller cylinders for the bulk diffusion and MIP tests.

Figure 6.1 Concrete cylinders tested in the project

After standard curing (age 28 days), three of the small-size cylinders were tested for compressive strength. The rest of the small standard cylinders were divided equally into three groups. Each group was subjected to continuing curing maintained at three different temperatures of 6.9^{o}, 22.4^{o} and 40^{o} C for three different periods of time: 56, 90 and 180 days. The large cylinders were centrally cored using a diamond core drill with a diameter of 100 mm, as shown in Figure 6.2. The first 25 mm from the top and the bottom surfaces were then cut, so only the internal concrete was tested for chloride diffusion. This was to eliminate any possible segregation, wall or finishing effects on the intruded chlorides. The cored cylinders were then cut and prepared for the bulk diffusion test, as per the ASTM C1556-11a standard.

Figure 6.2 Extracting of concrete cores from larger cylinders

6.2 Test Procedures and Specimens Preparations

6.2.1 Bulk Diffusion Test (ASTM C1556 - 11a)

The bulk diffusion test was conducted as per ASTM C1556-11a to obtain the chloride concentration profiles. All cored specimens were 100 mm in diameter and 75 mm in height and were side-coated (except for the exposed surfaces) using a thin continuous layer of waterproof sealant paste. The sealed specimens were saturated in a calcium hydroxide solution for 24 hours at 23 ± 2^{o} C prior to immersion in a chloride solution to avoid capillary suction of exposure chloride solution. The specimens were then immersed in a chloride solution with a concentration of 165g/l maintained at three different temperatures: 6.9^{o} C (considered a cold temperature), 22.4^{o} C (considered room temperature), and 40^{o} C (considered a hot temperature) for three periods of exposure: 56, 90 and 180 days. The purpose of subjecting the concrete specimens to different exposure temperatures after 28 days of standard curing was to simulate real conditions where concrete in the field is often subjected to standard curing up to age 28 days before it is exposed to the various temperature conditions. Table 6.3 summarizes the number of specimens tested for diffusion in this thesis to obtain chloride profiles at different exposure periods and temperature conditions.

Table 6.3 Number of concrete specimens for bulk diffusion test

Exposure period (days)	**Temperature condition (^{o} C)**					
	6.9		**22.4**		**40**	
	*A - S	*W -S	A - S	W -S	A - S	W -S
56	3	3	3	3	3	3
	3	3	3	3	3	3
	3	3	3	3	3	3
90	3	3	3	3	3	3
	3	3	3	3	3	3
	3	3	3	3	3	3
180	3	3	3	3	3	3
	3	3	3	3	3	3
	3	3	3	3	3	3
Total	54		54		54	

*A –S: Acid-soluble, *W – S: Water-soluble

After each specified exposure period, the test specimens were removed and prepared for the grinding process. The grinding was performed using the milling machine shown in

Figure 6.3. One of the exposed surfaces was ground off parallel to the exposed surface layer by layer, with each layer 1 mm thick. The powder from each 1 mm layer was collected and kept in a sealed bag, each with a weight ranging from 10 to 13 g. It was estimated that for the shorter period of immersion, the chloride would penetrate only a few millimeters inside the concrete. Therefore, only 10 layers were ground off for the specimens of 56 days of exposure. However, when the immersion period was extended to 90 and 180 days, 20 layers up to a depth of 20 mm from the exposed surface were obtained from the specimens.

Special arrangements were made around the specimen during the grinding process to collect the produced powders, as shown in Figure 6.3. The collected powders were then analyzed for acid-soluble and water-soluble chloride contents. The acid-soluble chloride concentration was obtained by analyzing the chloride content of the concrete layers in accordance with ASTM C1152/C1152M-04, and the water-soluble concentration was determined by analyzing the concrete powders, as per ASTM C1218/C1218M-99. To reduce the cost involved in performing the chloride analysis process, only the odd layers were analyzed for chloride content (e.g., 1, 3, 5…19) for specimens immersed in the chloride solution for 90 and 180 days.

Figure 6.3 Milling machine

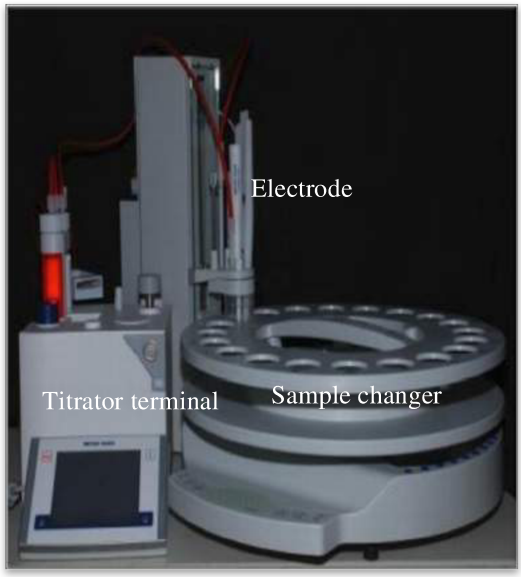

Figure 6.4 Titration equipment set-up

A METTLER TOLEDO T50 Titrator was used to titrate and analyze the water-soluble and acid-soluble chloride contents. The device set-up is shown in Figure 6.4. The system consists of a T50 M terminal with touchscreen (control unit) connected to a sample changer (Rondo 30). A silver ring sensor type DMi 141-SC was associated to the sample changer and mounted on the top of the sample beaker. It is used as an indicator electrode to determine the ion concentration of the sample solution. The sample changer was equipped with an automatic stirrer for dispensing solution during the titration process. The system could also be connected to a PC for easier control of the system. LabX light titration software was pre-installed on the PC for analyzing the data and controlling the titration process.

The titration methods for analyzing the chloride content of the acid-soluble and water-soluble measurements were pre-programed in the titrator. Once the representative samples of the extracted chloride solutions were prepared and placed in the sample changer, the titration method was called using either the associated PC or the titrator terminal to begin the tirtration process. Potentiometric titration was carried out using

standardized silver nitrate (0.05 $AgNO_3$) as a titrant. Once the titration process was completed, the results of the chloride content in each sample were recorded and saved in the library folder under the name of the specified method. Figure 6.5 shows the sample changer (Rondo 30) fully loaded with the sample beakers. The sample changer type used in this study could accommodate as many as 30 sample beakers.

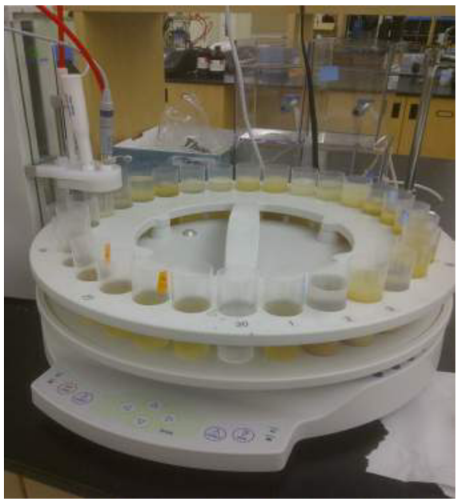

Figure 6.5 Samples changer fully load with the sample beakers

Once the chloride concentrations of all layers are determined, they were plotted against their corresponding depths to obtain the chloride profiles.

6.2.2 Rapid Migration Test

The rapid migration test (Non-steady-state migration test) was conducted following NT Build 492. The purpose of this test was to study the influence of curing temperature on the chloride migration parameters and to compare the migration test results to that of the diffusion test. The migration specimens were tested at age 28, 84, 118 and 208 days, which correspond to the curing periods of 28, 56, 90, and 180 days, respectively. Table 6.4 presents the number of concrete specimens evaluated for chloride penetration under the migration test.

Table 6.4 Concrete specimens test for chloride migration

Curing period	Concrete age	Curing temperature (°C)		
		**6.9	*22.4	**40
28	28	-	3	-
56	84	3	3	3
90	118	3	3	3
180	208	3	3	3
Total	-	9	12	9

*Standard curing, **Bath curing.

Prior to testing, the specimens were pre-conditioned in a vacuum treatment container for 18 ± 2 hours. A description of the specimens' preparation and test steps is as follows:

- The cast cylinders were removed from the curing moisture room at 28 days and prepared for cutting.
- Each cylinder was first cut into two halves (two lengths of 100 mm diameter x 100 mm) using a water-cooled diamond saw, and a 50 ± 2 mm thick slice was cut from one half. The end surface nearer to the first cut was the one to be exposed to the chloride solution (catholyte).
- After sawing, the specimens were washed to remove any burrs, and wiped off.
- The specimens were then transferred to the vacuum container for pre-treatment.
- In the vacuum container, the specimens were subjected to an air pressure of 5 kPa for 3 hours, as shown in Figure 6.6.
- After 3 hours, and with the vacuum pump still running, the vacuum container was filled with a saturated calcium hydroxide solution (lime water). The vacuum was maintained for an extra hour before allowing the air to enter the container. The specimens were kept in the solution for an additional 18 ± 2 hours. This was necessary to absorb any air within the voids in the concrete specimen.
- After the vacuum pre-treatment was conducted, each specimen was inserted into a 150 mm rubber sleeve and the sleeve secured around the specimen with two clamps.

The specimen age at the time of testing was selected to match the age of those tested for bulk diffusion at the end of each exposure period.

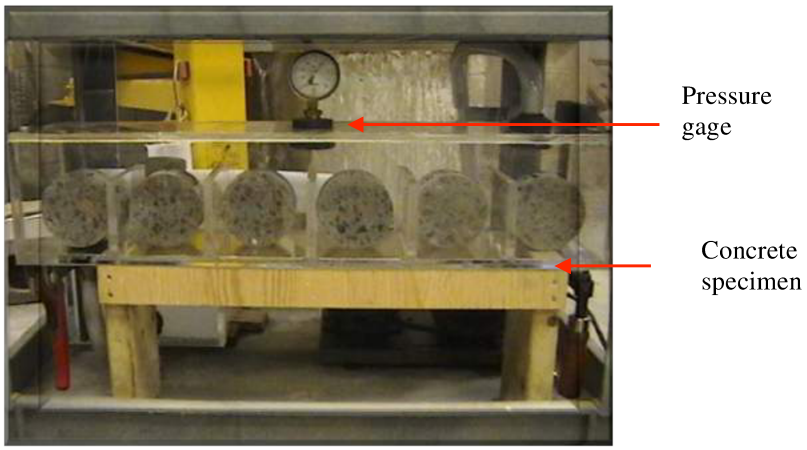

Figure 6.6 Pre-treatment of concrete specimen

After the specimens' preparation procedure, the following was performed on each specimen:

- The sleeve above the specimen was filled with 300 ml of 0.3 M sodium hydroxide solution (anolyte).
- The exposed end of the specimen was placed in a chloride solution that filled the chamber, as shown in Figure 4.12.
- A potential of 25 to 30 volts DC was applied across the specimens for the specified test duration (24 ± 0.5 hours).
- During testing, the temperature of the anolyte solution and the electrical current were monitored.

Due to the number of specimens that were required to be tested simultaneously, six test cells, as shown in Figure 6.7, were used and connected in parallel to test six specimens simultaneously. Following the test, the specimens were removed and washed with tap water, wiped off, and axially split into two halves. A silver nitrate solution was then sprayed on the freshly split section to identify the depth of the chloride penetration into

the specimens. The chloride penetration depth is identified by the white color of the silver chloride, and the depth of the chloride is determined using a slide caliper. Seven depths of chloride were taken from each specimen and the average depth was calculated. The depth of chloride penetration was then used to calculate the chloride coefficient.

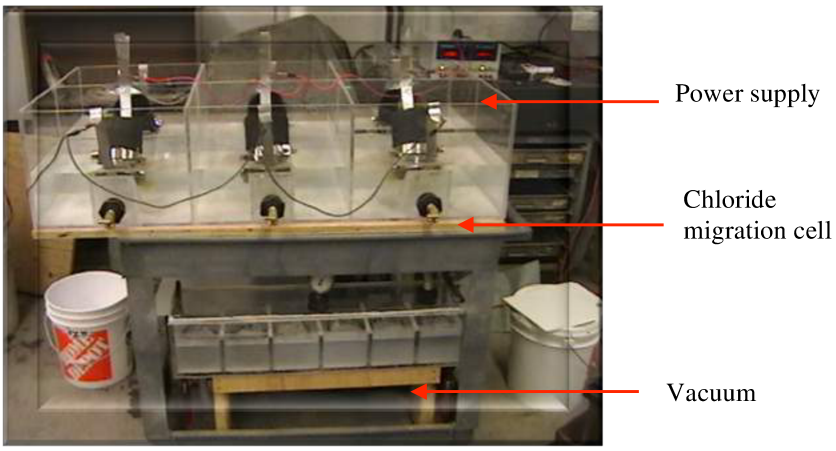

Figure 6.7 Migration test set-up

6.2.3 Chloride Binding Equilibrium Test

In this research, the chloride binding capacity and isotherms were determined according to the procedure developed by Luping and Nilsson[7]. This procedure is based on the concept of immersing crushed concrete specimens in a chloride solution until equilibrium is reached between the specimen pore solution and the external solution. It is then assumed that the chloride concentration in the pore solution (free chloride concentration) is equal to the chloride concentration in the external solution. The amount of bound chlorides is estimated from the decrease in the chloride concentration of the external solution at the equilibrium state. Crushed concrete samples were taken from standard cylinders cured up to 180 days at three different temperatures of 6.9^{o} C, 22.4^{o} C, and 40^{o} C. The crushed samples of the three concrete types were vacuum dried in a desiccator filled with silica gel at room temperature for a minimum period of 4 days to remove most of the water. The samples were then kept in the desiccator at a relative humidity of 11% (over a saturated LiC1 solution) for 21 days so that only a monolayer of water was

adsorbed. The crushed samples (approximately 20 to 25 g each) were then immersed in solutions of different chloride concentrations.

Five NaCl concentrations were used in this study: 0.1, 0.3, 0.5, 0.7 and 1 M. The containers containing the crushed samples and the chloride solutions were sealed (to prevent evaporation of the solution) and stored at 20° C until equilibrium was reached. At the end of the immersion period, the new chloride concentrations of the solutions were determined by means of potentiometric titration using a silver nitrate electrode. Luping and Nilsson[7] suggested that for normal concrete, 14 days of immersion were generally sufficient to achieve equilibrium between a solid and a solution. According to Thomas et al. [29] the time to reach equilibrium between the external solution and the pore solution is a function of both the w/cm ratio and the mix composition. The concrete samples tested in this study were 0.32 w/cm and required a stabilization period of about two months, after which equilibrium was reached for all the samples. The chloride concentrations of the concrete samples were determined after three months to ensure that constant chloride concentrations for all samples were obtained. Data clearly confirmed that the equilibrium had been achieved after a period of three months of exposure. When the equilibrium was reached between the external solution (host solution) and the pore solution of the concrete sample, the reduction in the chloride concentration of the host solution was attributed to the chlorides being bounded by the concrete hydration products. The bound chlorides content can then be calculated using Equation (6.1):

$$C_b = \frac{35.453V(C_i - C_e)}{W_d} \quad \text{.....Eq. (6.1)}$$

where C_b is bound chloride given in mg/g of sample, V is the volume of the solution (ml), C_i is the initial chloride concentration of the solution (mol/l), C_e is the chloride concentration of the solution at equilibrium (mol/ l), and W_d is the mass of the dry sample (g). Afterwards the bound chlorides plotted on the y-axis against the initial free chloride concentrations on the x-axis and the binding isotherm relationships were then established.

6.2.4 Mercury Intrusion Porosimetry (MIP) Test

The mercury intrusion porosimetry (MIP) test method was adopted in this research to evaluate the pore size distribution of the concrete samples investigated. It should be mentioned that, in the literature review, there are several test methods and techniques available to measure pore size distribution of concrete in addition to the MIP technique. These methods include conductometric phase transition porosimetry (CPTP), fluid displacement, helium pycnometer, capillary condensation and adsorption desorption isotherm, small angle X-ray scattering (SAXS), scanning electron microscope (SEM), nuclear magnetic resonance (NMR), AC impedance spectroscopy, and back-scattered electron images (BSE). However, MIP, which is capable of measuring a wide range of pore sizes from 1 nm to 200 μm, is the most popular technique as it is known that the resistance of concrete pore system to transport aggressive ions such as chloride ions is controlled by the pore entry radius rather than the true internal radius [18]

Nevertheless, the MIP approach does have some disadvantages, one of which is that the high applied pressure can break down the walls between pores, which may result in higher porosity of the tested concrete samples. Also, due to the dynamic hesitation of mercury in pore paths, the MIP approach is often used for very small samples sizes (e.g., less than 10 mm), such as paste or mortar with fine aggregates. Since concrete in practice contains aggregate pieces larger than 10 mm, it is rather difficult to take a representative sample for the application of MIP. However, for comparative study, MIP can give a very good indication of how the pore size distribution of the tested samples could be altered by binding products such as Friedel's salt.

The concrete samples were cut from the other exposed face of the concrete specimens subjected to bulk diffusion test under different temperature conditions. The selected side was cut into a number of slices 3 to 5 mm thick. The slices were then dried in an oven at $105^{o} \pm 5^{o}$ C for 72 hours to halt any further hydration, after which they were cooled to room temperature, crushed into small pieces of about 1 to 2 g as shown in Figure 6.7, and kept in sealed bags to avoid carbonation and moisture adsorption until tested. For the purpose of the study, the porosity and pore size distribution of both chloride-

contaminated samples and free chloride-contaminated samples (plain concrete) were determined using the MIP test. The chloride-contaminated samples were obtained from the first 12 mm of the exposed surface and the plain samples were cut from the middle of the cured cylinder (30 mm away from the exposed surface) for the three exposure periods.

Figure 6.8 Concrete specimens for MIP test

In addition, the pore size distribution of the plain concrete cured in a moisture room under normal conditions at age 28 days was determined. Due to technical problems with the MIP testing equipment, several samples were not tested as planned, including those subjected to 180 days of exposure, and some samples were damaged during the test. Table 6.5 summarizes the samples that were tested for 56 and 90 days.

Table 6.5 Concrete samples tested for MIP

Concrete age	**Sample type**	**Exposure temperature (^{o}C)**		
		6.9	**22.4**	**40**
28	Plain	-	4	-
84	Chloride	3	-	3
	Plain	4	-	4
118	Chloride	2	2	4
	Plain	2	1	4

The MIP test was carried out using a Quantachrome Poremater-33 instrument with a maximum pressure of 231 MPa, which is designed to measure pore volume to a minimum radius of 0.0030 micrometers (30 Angstrom) in diameter. This equipment is shown in Figure 6.8 and consists of a sample cell assembly, filling apparatus, and a high-pressure cell assembly. A trimmed-to-size (less than 10 mm diameter) concrete sample of approximately 1 g was assembled in the sample cell for low-pressure measurements. This sample cell was inserted in the vacuum jar of the filling apparatus and evacuated to at least 50 microns of mercury pressure. The test was then performed by applying pressure of up to 0.165 MPa to the sample cell and simultaneously measuring the volume of mercury intruded. Next, the sample was transferred to the high-pressure cavity assembly, where a gradually increasing capillary pressure was applied in the range of 0 to 228 MPa while the volume of mercury that intruded in the sample was measured. Withdrawal by reducing pressure to atmospheric pressure (0.10 MPa) and re-injection by raising pressure again to 231 MPa were applied. High-resolution pressure versus mercury saturation volume data were recorded for interpretation with the help of computer software linked to the system. Data from the low-pressure and high-pressure assemblies were combined and processed for plotting the capillary pressure curves and interpreting the pore-throat-size distribution.

Cylindrical pore geometry and a contact angle between the mercury and the pore wall, θ, of 130^{o} were assumed. The pore radius, r, at intruded pressure, P, was calculated using Washburn's equation: $P.r = -2\gamma cos\theta$, where γ = 480 erg/cm^2 (0.480 Nm^{-1}), the surface tension of mercury. The pore size distribution curves were then obtained by plotting the cumulative mercury intruded volume (cm^3/g – sample) on the y-axis against the pore radius (Angstrom, Å) on the x-axis. To obtain the average intruded volume of mercury at a particular radius, the intruded volumes of mercury for all samples tested under a given condition were obtained at that particular radius of the pore. This procedure was repeated at a large number of radii to generate the resulting average pore size distribution curve.

Figure 6.9 Quantachrome Poremaster - 33 apparatus (MIP) test

7 RESULTS AND DISCUSSION

In this chapter, the results of the experimental program are presented and discussed. The results of the rapid migration test are discussed in section 7.1, those of the mercury intrusion porosimetry (MIP) are discussed in section 7.2, and those of the equilibrium test and the establishment of binding isotherms are discussed in section 7.3. Bulk diffusion test results, which include water-soluble and acid-soluble chlorides, are presented in section 7.4. The determination of chloride parameters using the error function solution approach and linear finite difference model for both water-soluble and acid-soluble chlorides are discussed in detail in section 7.5.

The slump and the air content tests were conducted in accordance with ASTM C143/C143M-12 and ASTM C231/C231M-10 respectively. The concrete mixture was workable and had slump of 110 mm and air content of 8 %. The concrete had a compressive strength of 59 MPa at 28 days.

7.1 Migration Test Results

7.1.1 Chloride Penetration Depth

The rapid migration test was conducted to investigate the influence of curing conditions, mainly time and temperature, on the depth of chloride penetration and the resultant diffusion coefficient. The penetration depth of the chloride ions for concrete samples exposed to different sub-curing conditions after an initial standard curing of 28 days is shown in Figure 7.1. As can be seen, the penetration depth is clearly influenced by the curing conditions. The concrete samples tested after 28 days of standard curing exhibited the highest chloride penetration depth, while those subjected to subsequent curing at different curing temperatures exhibited lower penetration depth values. This indicates that a long curing time has beneficial effects on the concrete's durability and improves its resistance to the ingress of chloride ions. Likewise, the elevated curing temperature seems also to have a beneficial influence on the concrete's durability and resistance. Concrete samples treated under higher continuing curing temperatures result in lower chloride

penetration depths.

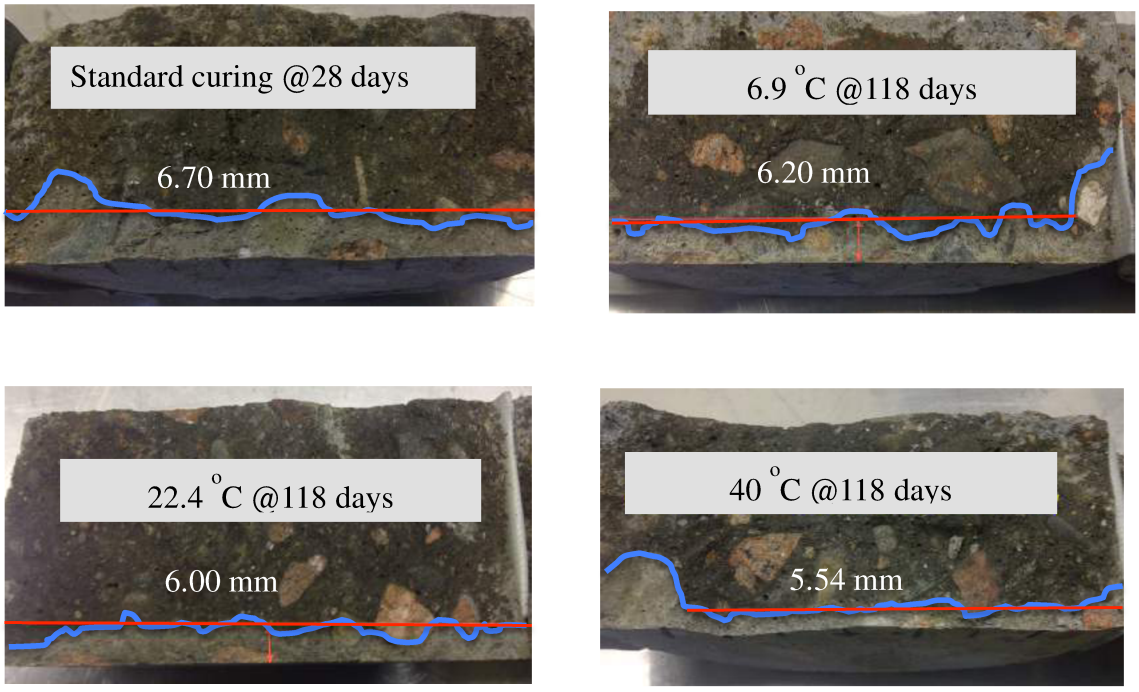

\

Figure 7.1 Chloride penetration depth for concrete samples exposed to different curing conditions

7.1.2 Chloride Migration Coefficients

Table 7.1 summarizes the averaged values of the D_{nssm}, as calculated based on the depth of chloride penetration using Eq. (2.10) for different curing conditions. These values are plotted against the corresponding concrete age in Figure 7.2. Full details of the test results are provided in Appendix A.

Table 7.1 Average D_{nssm} values at different curing conditions

Time (days)	Average D_{nssm} value (m^2/s)			
	21 °C	6.9 °C	22.4 °C	40 °C
28	2.59E-12	-	-	-
84	-	2.08E-12	1.42E-12	1.34E-12
118	-	1.88E-12	1.25E-12	1.14E-12
208	-	1.57E-12	1.01E-12	8.80E-13

The influence of the subsequent curing on the obtained migration coefficient, D_{nssm}, has

been found to be significant, in particular for 22.4° C and 40° C. The migration coefficients significantly decreased as the curing time and temperature increased. This reduction in the values of D_{nssm} is attributed to the ongoing hydration of the cementitious materials after age 28 days, in particular the slag cement. The elevated temperature is also known to accelerate the rate of cement hydration, which will reduce the time for the concrete to produce denser microstructure.

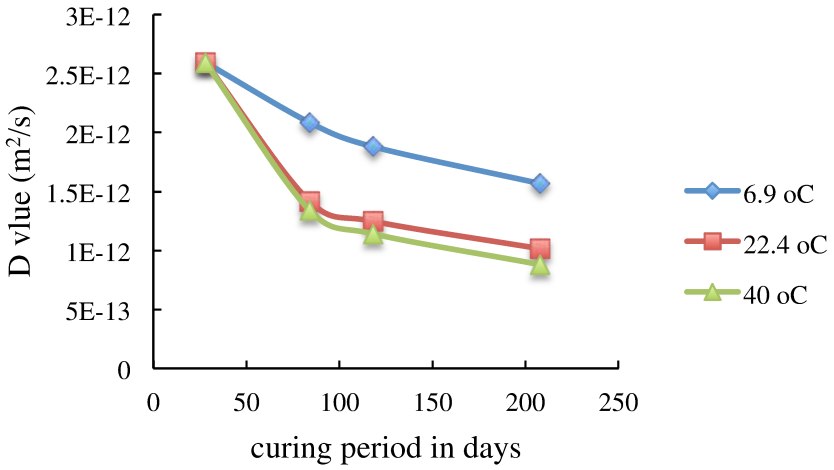

Figure 7.2 Reduction of the migration coefficient with time at different curing conditions

7.1.3 Determination of Migration Age Parameter

The values of the migration coefficients are plotted against the corresponding time on a log-log scale, as shown in Figure 7.3. By applying a linear regression to the experimental data of the migration coefficient values, the age parameter value, m, can be found from the slope of the regression line. The resulting values of m and D_{nssm} for all continuing curing conditions are listed in Table 7.2

Table 7.2 Average D_{nssm} and values of m for rapid migration test

Sample age (days)	Avg. D_{nssm} (6.9 °C)	m	Avg. D_{nssm} (22.4 °C)	m	Avg. D_{nssm} (40 °C)	m
28	2.59E-12	0.245	2.59E-12	0.475	2.59E-12	0.544
84	2.08E-12		1.42E-12		1.34E-12	
118	1.88E-12		1.25E-12		1.14E-12	
208	1.57E-12		1.01E-12		8.80E-13	

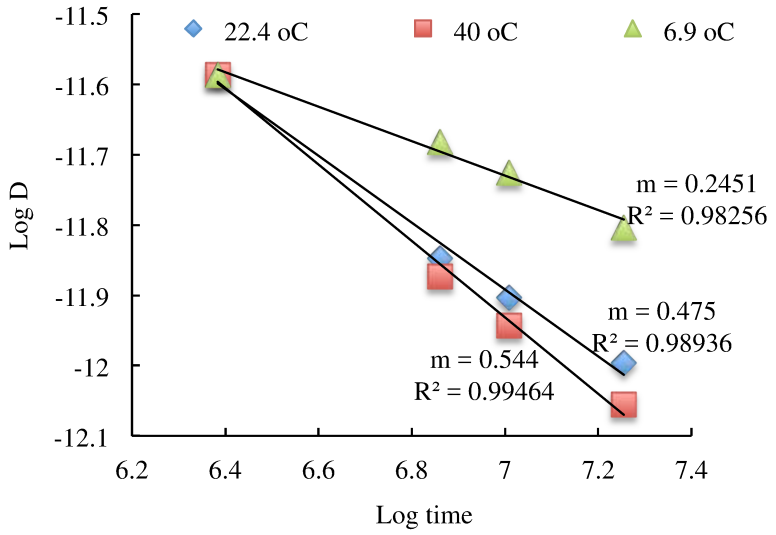

Figure 7.3 Linear relationship between log D_{nssm} and log t for different curing conditions

7.1.4 Discussion of Chloride Migration Test Results

As indicated previously, continuous curing at different temperatures has a significant influence on the migration transport properties of concrete. The 40^{o} C sub-curing condition resulted in the highest reduction in the value of D_{nssm}, whereas the 6.9^{o} C condition demonstrated the lowest reduction in the value of D_{nssm} over time. This could be attributed to the influence of high and low temperatures on the hydration rate of the cement. Higher curing temperatures help concrete to develop a dense microstructure at a rate that is much faster than that resulting from concrete exposed to low temperatures. Therefore, different concrete microstructures can result from different curing conditions. The magnitude of reduction in the value of D_{nssm} can also be noted from the values of m, where higher temperatures resulted in higher m values. Concrete with higher values of m has lower diffusivity and better quality. This implies the importance of the curing condition prior to chloride exposure.

The paramount importance of the m-value is evident in the modeling of the service life of a concrete structure. The current practice of chloride modeling into concrete assumes a constant value of m during the exposure time and does not take into account the possible

influence of the curing conditions on such factor, which might lead to errors in the estimated service life of the structure. Previous studies have shown that the modeled service life of a structure is highly sensitive to the used value of m and that this value is always assumed to be constant [8] However, the experimental results of this study have shown that the m-value is not constant but is instead a function of the curing conditions, in particular at early ages. The migration test results suggested that, for proper estimation of the service life, the used value of m should be linked to the type and period of curing prior to chloride exposure.

7.2 Mercury Intrusion Porosimetry (MIP) Test Results

The MIP test was carried out to determine the porosity and pore size distribution of both chloride-contaminated and plain concretes in order to highlight the effect of chloride binding on the capillary pore system under different exposure conditions. The test results are summarized in Table 7.3.

Table 7.3 Results of MIP test at different exposure conditions

Temperature (^oC)	Concrete age (days)	Exposure period (days)	Total intruded volume		Reduction in total intruded volume (%)	Total porosity (%)	
			Plain (cm^3/g)	Chloride (cm^3/g)		Plain	Chloride
Control	28	-	0.084	-	-	16.5	-
6.9^o	84	56	0.059	0.04	32	15.9	13.8
	118	90	0.042	0.027	36	12.9	10.9
22.4^o	84	56	-	-	-	-	-
	118	90	0.045	0.025	45	10.4	9.1
40^o	84	56	0.048	0.039	20	14.7	14.1
	118	90	0.047	0.046	2	15.1	15.6

7.2.1 Discussion of MIP Test Results

7.2.1.1 Porosity and Pore Size Distribution of Plain Concrete Cured at Different Conditions

As can be noted from Table 7.3, the total intruded volume of mercury for all plain samples beyond age 28 days decreased with increasing exposure periods at different rates,

depending on the exposure temperature. This could be due to ongoing hydration and pozzolanic reactions that take place within cement paste as time passes. The development of the hydration process refines the pore structures as more hydration products deposit into the capillary pores, reducing the volume of the capillary pore system and resulting in a lower penetrated volume of mercury. Recently, Das and Kondraivendhan [149] investigated the effect of curing time on concrete pore size distribution and concluded that pore size decreases with increases in curing ages.

Limited information is presently available in the published literature regarding the effect of temperature on pore size distribution in concrete [150]. The general trend, however, is that increased temperature accelerates the hydration process and pozzolanic reactions at early ages and refines the pore structure at a faster rate [92]. The effect of temperature on the pore volume of the concrete specimens is more pronounced after 56 days (84 days of age) than after 90 days (118 days of age) of exposure. As can be noted from Table 7.3, the intruded volume varies considerably between the specimens exposed to 6.9^{o} C and those exposed to 40^{o} C after age 84 days, although the difference in the intruded volume of all specimens after age 118 days is relatively smaller. This indicates that the influence of temperature on pore volume distribution is strong only at early ages and tends to be weaker at later ages.

The reduction in the total intruded volume for specimens exposed to 40^{o} C at age 84 days is much larger than that of specimens exposed to 6.9^{o} C at the same age; however, when the exposure time is prolonged to 118 days, the difference in the total intruded volume between the two concretes is relatively low. This difference could be attributed to the effect of temperature on the hydration rate and pozzolanic reactions of the cement paste at early ages. For specimens exposed to 40^{o} C, high temperature in the first 56 days of exposure accelerates the rate of hydration and the chemical reaction of the pozzolans, which leads to a quick reduction in the capillary pore volume, especially that of small pore sizes. In specimens exposed to 6.9^{o} C, the low temperature slows the rate of hydration and subsequent pozzolanic reactions, which causes the pore volume of the capillary pore system to decrease at slower rates. When the exposure time is prolonged to

90 days (i.e., 118 days of age), the influence of temperature on the development of the pore system is less pronounced and cold specimens exhibit a decreased pore volume. This is because the low temperature allows the concrete to effectively develop a dense microstructure with a less porous system [151]

The total porosity of the tested concrete is reduced as pore volume decreases with time. However, the samples exposed to 40^{o} C showed an opposite trend, in that their total porosity increased with an increase in the exposure period, although the intruded volume of the mercury slightly decreased. It can also be noted that the total porosity of concrete specimens exposed to low temperatures at age 118 days is considerably less than that of concrete specimens exposed to relatively higher temperature. This, again, could be attributed to the effect of temperature on pore size due to its effect on the hydration process of the cement paste.

Neville [92] reported that the increased temperature at early ages could result in poor physical structure (meaning, it is probably more porous), so that a portion of the small pores will always remain unfilled. Verbeck and Helmuth [151] suggested that the rapid rate of hydration at higher temperatures retards the subsequent hydration and produces a non-uniform distribution of the products of hydration within the paste. The reason for this is that, at high initial rates of hydration, there is insufficient time for the diffusion of the products of hydration away from the cement particle and for uniform precipitation in the interstitial space (as is the case at lower temperatures). As a result, a high concentration of the products of hydration is built up in the vicinity of the hydrating particles, slowing subsequent hydration and adversely affecting long-term durability. Bouikni et al. [152] tested concrete containing 50% and 65% slag replacement and found that its porosity increased as the curing time was prolonged. They suggested that there was insufficient lime produced from the first reaction to continue the second pozzolanic reaction with slag.

It should be kept in mind that only capillary porosity, not total porosity, can contribute to the diffusivity of cement paste [1] Hence, when pore sizes are reduced after a certain limit

($r \leq 0.01$ μm), they will not affect the diffusivity of the cement paste. Furthermore, only the large and well-connected pores will control the diffusivity of the concrete.

7.2.1.2 Binding Effect on Porosity and Pore Size Distribution Under Different Exposure Conditions

Figure 7.4 shows the average pore size distribution curve of plain specimens and the corresponding average pore size distribution curve of chloride contaminated specimens obtained after 56 days of exposure at 6.9° C. It demonstrates that while the pore volume of both concretes is the same for larger pore sizes (>1.8 μm), the chloride-contaminated concrete exhibited considerably lower pore volume at the smaller pore sizes (0.0027 – 1.8 μm). Binding products such as Friedel's salt could be responsible for changing the pore structure of small pores, especially those with pore radii of less than1.8 μm. The reduction in pore volume is increased as pore size decreases. The total intruded volume of the chloride-contaminated concrete is about 32% less than that of plain concrete. The reduction in pore volume as a result of binding has led to a considerable reduction in the porosity of the plain concrete, as indicated in Table 7.3.

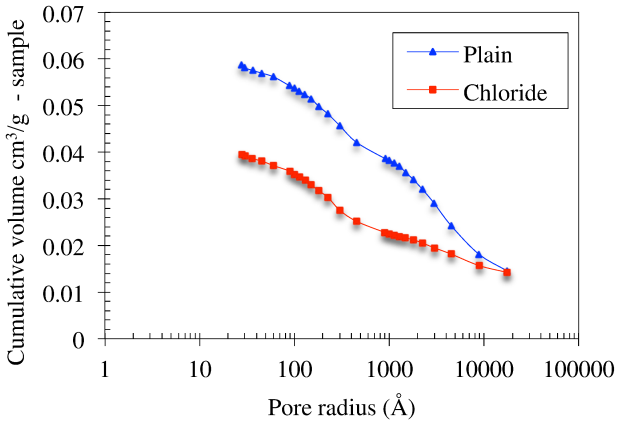

Figure 7.4 Effect of chloride binding on pore size distribution of concrete specimens exposed to 6.9° C after 56 days of exposure

The prolonged exposure period of 90 days resulted in further reductions in pore volume by 36%. As shown in Figure 7.5, additional decreases in all pore sizes were observed,

with the reduction in pore volume increasing as pore sizes decreased. This indicates that the binding, at cold temperature conditions, increases with time. All of the pores decreased in size after 90 days of exposure as a result of binding. Arya et al. [33] studied the binding in OPC with a w/c ratio of 0.5 chloride introduced during the mixing process. The samples were then cured for 28, 56, and 84 days. They found that the amount of bound chlorides increased with increasing curing time, although most of the binding happened prior to 28 days.

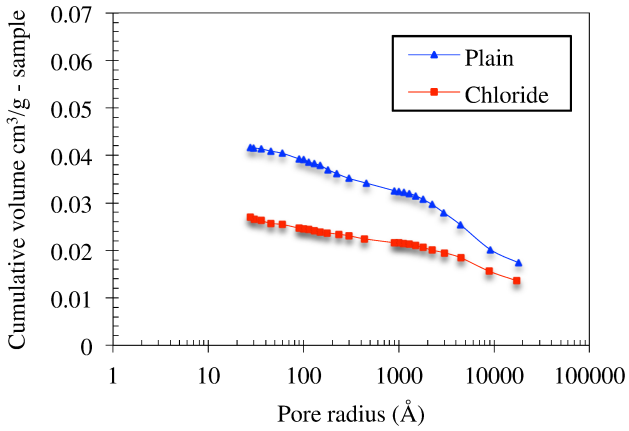

Figure 7.5 Effect of chloride binding on pore size distribution of concrete specimens exposed to 6.9° C after 90 days of exposure

Unfortunately, the data for room temperature conditions (22.4° C) after 56 days of exposure is not available and only the data of MIP test results after 90 days of exposure is presented. This has made it difficult to evaluate the effect of time on binding at room temperature conditions. As Figure 7.6 shows, the binding significantly reduced the pore volume of the concrete after 90 days of exposure.

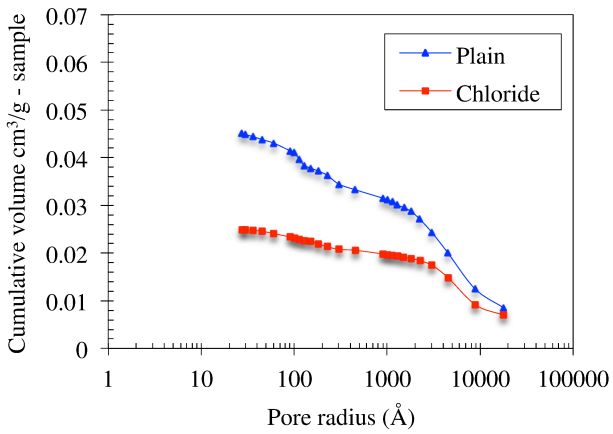

Figure 7.6 Effect of chloride binding on pore size distribution of concrete specimens exposed to 22.4° C after 90 days of exposure

The reduction in the pore volume due to binding was the highest among all tested specimens in this study. The volume of pore size as a result of binding is reduced by 45%, which is almost half that of plain concrete. In the literature review, it was reported that the highest binding amount occurs at a room temperature of about 22° C [11]. This was observed in the present study, although the presented data may not be sufficient to confirm this conclusion. The reduction in pore volume becomes significant for pores measuring 0.30 μm and smaller, as can be noted in Figure 7.6. However, substantial reduction in pore volume (from 0.45 to 0.25) due to binding was not noted in the overall porosity. The porosity of chloride-contaminated at room temperature was only 1.3% lower than that of plain concrete for the same exposure conditions.

Figure 7.7 shows the results of the average pore size distribution curves for both plain and chloride-contaminated specimens after 56 days of exposure at 40° C. It is clear that the binding effect at the elevated temperature is less compared to that of specimens treated at lower temperatures for the same period of exposure. At 40° C, the binding reduced the pore volume by 20%, whereas at 6.9° C, the pore volume after the first exposure period was reduced by 32%. This indicates that the effect of binding on pore volume at cold temperatures is more significant.

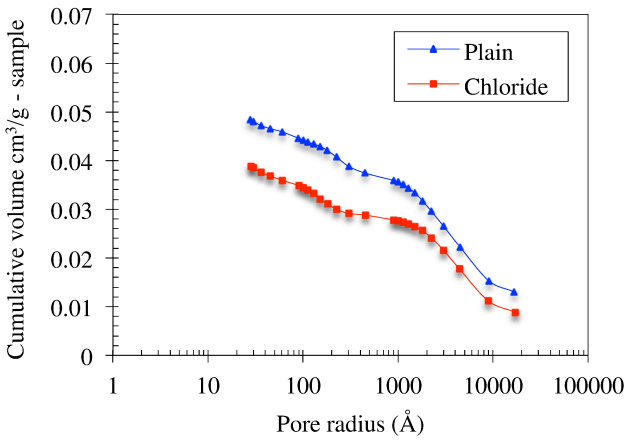

Figure 7.7 Effect of chloride binding on pore size distribution of concrete specimens exposed to 40° C after 56 days of exposure

Larsson [10] found that an increasing temperature reduces chloride binding and liberates bound chlorides into the pore solution. Hussain et al. [110] reported that the chloride content of the pore solution of cured cement paste increased drastically when the curing temperature increased from 20° to 70° C. This was attributed to the solubility of Friedel's salt due to increased temperature, which led to the release of chloride ions in the pore solution. Rapin et al. [153] reported that Friedel's salt presents a structural transition at 35° C, which is significantly different from that at normal temperature when sufficient curing time is provided. They suggested that Friedel's salt becomes unstable after 35° C and that its structure and volume drastically reduce. From this, it can be understood that binding is in fact a reversible process and that the released bound chlorides, due to the solubility of Friedel's salt as a result of increased temperature, could significantly increase the risk of corrosion initiation by increasing the concentration of free chlorides in the pore solution.

Prolonged exposure (up to 90 days) at 40° C appears to have an adverse effect on binding, as shown in Figure 7.8. The pore size distribution curve of the chloride-contaminated concrete is slightly higher than that of plain concrete, especially for pores larger than 1000 Å in radius. There is very small reduction in the pore volume (by only 2 %) as a result of binding for concrete exposed to 40° C for 90 days.

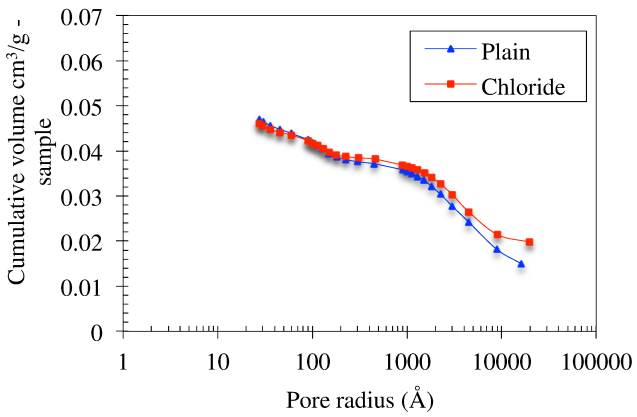

Figure 7.8 Effect of chloride binding on pore size distribution of concrete specimens exposed to 40° C after 90 days of exposure

This reduction however is observed only in the gel pores, which have a pore radius of less than 100 Å as indicated in Figure 7.8. It appears that the majority of Friedel's salt compounds, which were formed and filled the capillary pores when the concrete was exposed to the chloride solution for the first time at 56 days, dissolved or disappeared after the extended period of exposure, causing the volume of pores to increase. This, as explained earlier, could be attributed to the instability of Friedel's salt at relatively higher temperature conditions over extended periods of time, which indicates that even if binding has taken place at an elevated temperature, it would be just for a short period of time. At the beginning of the exposure, a reaction takes place between the intruded chlorides and the alumina content of the cement paste, leading to the formation of Friedel's salt. At this stage, the effect of binding on porosity and pore size distribution was recognized, as shown in Figure 7.7. However, once Friedel's salt has been formed, it becomes unstable due to the high exposed temperature and is perhaps partially or totally dissolved in the pore solution. Unfortunately, the pore solution was not analyzed in this study to confirm that this is indeed what has happened. The solubility of Friedel's salt could be responsible for the increased porosity of the specimens exposed to 40° C after 90 days of exposure, as indicated in Table 7.3.

The data presented in Figures 7.4 to 7.8 showed that, in general, the total intruded pore volume of chloride-contaminated specimens is less than that of plain concrete. Data

presented in Figure 7.8 shows almost no difference in the volume of the pore system of the two concretes, except at larger pores sizes of r ≥ 1000 Å. The changes in pore sizes probably arise from the chloride binding in the form of Friedel's salt, which is the main product of the chloride binding process. Therefore, it can be concluded that binding does, in fact, alter pore structure and reduce the pore volume of concrete to a significant extent, particularly at exposure temperatures of 22.4 ^{o} C or lower. This in line with the very recent findings by Doust [113] who found that the amount of Friedel's salt was the greatest at a temperature of 22^{o} C. Furthermore, higher exposure temperatures (≥ 40 ^{o} C) could have an adverse effect on the amount of bound chlorides and can be responsible for increased porosity at later ages.

7.3 Equilibrium Test Results

This test was carried out to investigate the binding behavior of the high performance concrete tested in this study. The results of this test are also needed to determine the binding isotherm parameters or coefficients required to run the nonlinear model developed in this thesis. These parameters are determined by fitting the binding isotherm relationships presented in Chapter 3 to the experimental data obtained from the equilibrium test. The results of the equilibrium test for the three concrete curing conditions are shown in Figure 7.9. In this figure, the calculated bound chlorides are plotted against the free chloride concentration at equilibrium.

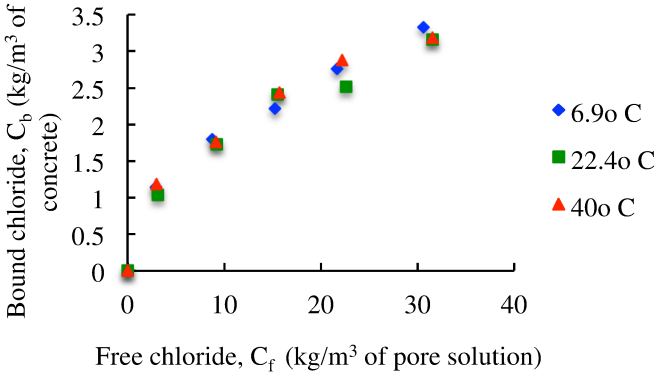

Figure 7.9 Bound chlorides versus free chlorides at equilibrium

Note that the amount of bound chlorides (C_b) is expressed as a unit mass per volume of concrete, while the free chloride concentration (C_f) is expressed per volume of solution. It should be mentioned that, in the published literature, different units have been used for bound and free chloride for the description of the binding isotherms. For instance, Luping and Nilsson [7] used mg Cl/g – gel for bound chloride and mol/l for the free chloride, Dousti [113] used mg Cl/g – sample for the bound chlorides and mol/l for the free chloride, and Martin-Perez et al. [95] used kg/kg binder for the bound chloride and kg/m^3 of pore solution for the free chloride. These units led to different values for the binding isotherm parameters, which makes it difficult to compare the results of different studies reported in the literature.

7.3.1 Influence of Free Chloride Concentration of the Exposure Solution

Figure 7.9 clearly demonstrates that the amount of bound chlorides increases as the free chloride concentration of the solution increases in a nonlinear trend. This confirms the concentration dependency and shows that the relationship between free and bound chlorides is non-linear in nature. This is in line with the findings of other investigations reported in the literature [7,87,95]. It has been generally recognized that the amount of bound chlorides tends to increase as the chloride concentration increases, regardless of the type of cementitious materials or the w/c ratio. The ability of concrete to bind more chlorides as the chloride concentration in the pore solution increases is limited by the number of chemical and physical sites available to bind chlorides.

7.3.2 Influence of Curing Temperature on the Amount of Bound Chlorides

As Figure 7.9 shows, the curing temperature has little influence on the amount of bound chlorides over the free chloride concentration range used in this test. The data slightly scatter at free chloride concentrations of 10 kg/m^3 of pore solution and higher. This indicates that the curing temperature prior to exposure to chlorides has little to no effect on chloride binding in the cementitious system. However, distinctions should be made between the influence of curing temperature prior to chloride exposure and the effect of

temperature during the exposure to the chloride once the concrete is placed in service. The above results were obtained by conducting the equilibrium test at a fixed temperature of 20^{o} C.

In the previous section of the MIP test, it was shown that the elevated temperature of the exposure solution (chloride solution) tends to have a significant influence on the amount of bound chlorides. Hussain and Rasheeduzzafar [110] found that an increase in temperature from 20^{o} C to 70^{o} C led to an increase in the chloride concentration of the pore solution. Panesar and Chidiac [154] conducted an equilibrium test for a series of cement pastes at different exposure temperatures ranging from -5^{o} to 22^{o} C, discovering that the binding capacity of the cement pastes was the highest for 22^{o} C and -3^{o} C cement pastes and relatively lower for 5^{o} C cement paste. This has led to different values of α and β for the tested cement pastes. More recently, Dousti [113] tested cement pastes containing different supplementary cementitious materials at -4^{o} C to 70^{o} C. His data show that the amount of bound chlorides decreased as the temperature is increased and that the room temperature of 22^{o} C resulted in the highest amount of free chlorides, regardless of the type of cement paste. These results imply that the highest chloride binding occurs at 22^{o} C irrespective of binder type, which has also been confirmed in this research.

7.3.3 Establishment of Binding Isotherm

The binding isotherm for the concrete tested in this thesis was established by fitting the linear and nonlinear binding isotherm relationships presented in Chapter 3 to the experimental data of the equilibrium test using the least squares method. Full description of the binding isotherms for concrete at 6.9^{o} C, 22.4^{o} C and 40^{o} C are illustrated in Figures 7.10a, 7.10b and 7.10c, respectively.

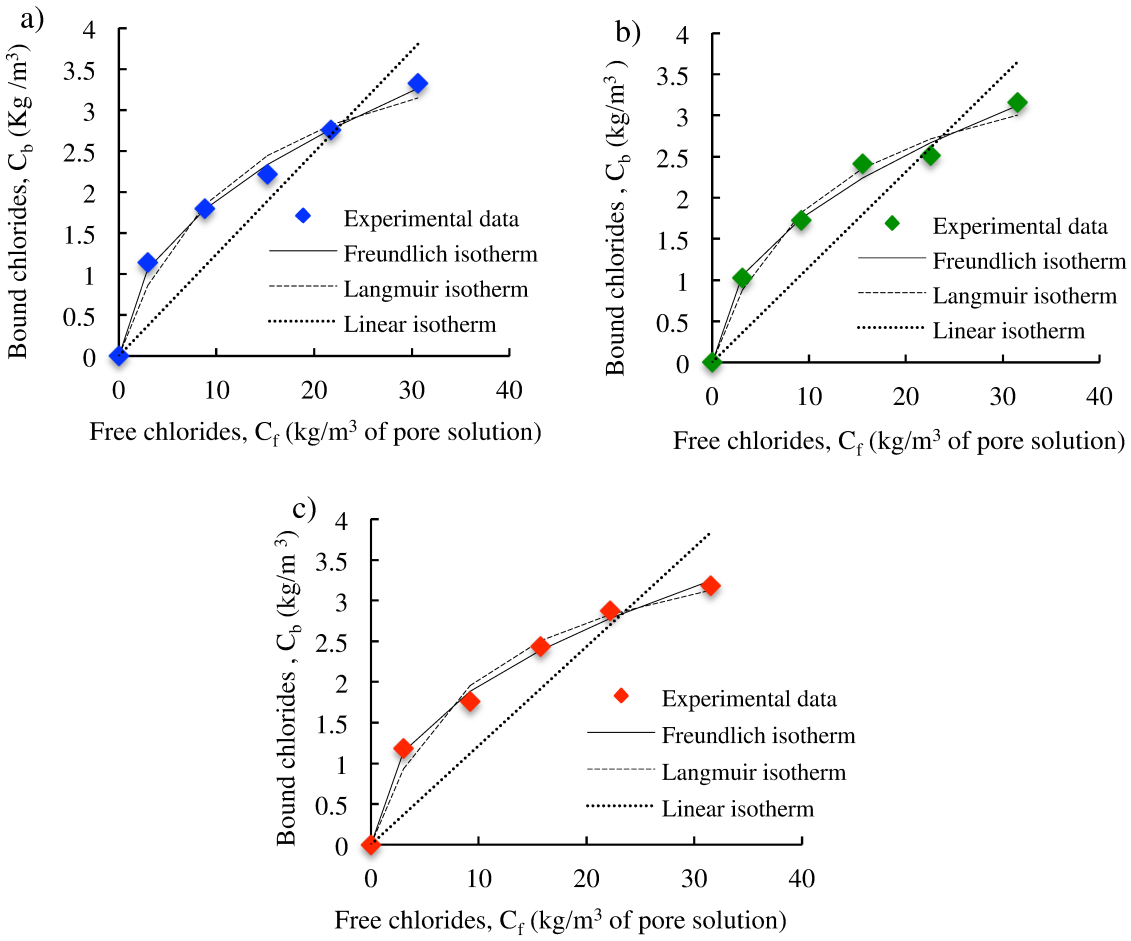

Figure 7.10 Chloride binding isotherm of concrete cured at: a) 6.9^o C, b) 22.4^o C and c) 40^o C

From the above figures, it is clear that the nonlinear binding isotherms (i.e., Frundlich and Lamgmuir) provide a much better fit to the experimental data than the linear binding isotherm. According to Tuutti [155] linear binding is only valid for very low free chloride concentration (< 20 g/l). Numerous researchers have reported that the linear assumption of binding is valid only for very low free chloride concentrations and that the chloride binding is, in nature, nonlinear for the range of free chloride concentrations expected in the exposure environments [7,156,157]. The shapes of the curves of nonlinear binding isotherms obtained in this study are very similar to those in previous studies [7,88,95,158-161].

Furthermore, the above figures clearly show that the linear binding relationship does not provide a good fit to the experimental data and tends to oversimplify the binding process, especially for high chloride concentrations (> 5 kg/m^3 of pore solution). The linear binding seems to be applicable only within a very limited range of chloride concentrations (< 10 kg/m^3 of pore solution). As can be seen, the linear binding isotherm underestimates the amount of bound chlorides for free chloride concentrations equal to or less than 20 kg/m^3 of pore solution, whereas it tends to overestimate the amount of bound chlorides at higher free chloride concentrations (>20 kg/m^3 of pore solution). Another important observation is that the margin of free chloride concentrations for which the linear fit is made could have a great influence on the quality of the linear fit. It can be predicted that the quality of the linear fit would become poorer if the limit of the free chloride concentration increased to higher values. This suggests that the binding capacity of the linear relation can be influenced if the limit of free chloride concentration in the pore solution is increased or decreased.

As expected, the nonlinear binding relationships gave a much better fit to the experimental data for the limit of free chloride concentrations considered in this test. Both the Freundlich and Langmuir relationships fit the experimental data very well, but the Freundlich relationship provides a slightly better fit than the Langmuir relationship. This tends to support the conclusions of Nilsson [27], Luping and Nilsson [7] and Martin-Perez et al. [95] that the Freundlich form gives a better indication of the binding behavior of chloride ions in the concrete cementitious system. According to Luping and Nilsson [7], the Langmuir isotherm describes the best the relationship between free and bound chlorides only when the level of chloride concentration in the pore solution is less than 1.773 kg/m^3. Previous work done by Martine-Perez et al. [95] showed that the margin of free chloride concentration in the pore solution has no impact on the fitting quality of the nonlinear relation. Therefore, the binding capacity of the concrete based on nonlinear binding relationship will be valid for a wider range of free chloride concentration.

7.3.4 Binding Isotherm Coefficients

Table 7.4 summarizes the binding isotherm coefficients, also known as binding constants, which result from applying the regression analysis to the experimental data

Table 7.4 Binding isotherm coefficients

Curing temperature	Langmuir		Freundlich		Linear
	α	β	α	β	α
6.9	0.360	0.082	0.631	0.480	0.124
22.4	0.356	0.087	0.619	0.469	0.116
40	0.401	0.096	0.703	0.444	0.122

According to the literature review, these coefficients are solely dependent on the binder composition and have no physical meaning [34,86,95]. Therefore, they are unique for each cementitious system. It should be noted that these coefficients could have different numerical values depending on the units used to express the free chloride concentration and the bound chlorides. Sergi et al. [162] tested OPC paste made with w/c = 0.5 (C_f and C_b were expressed in mole/l and mole/g of cement, respectively) and obtained the values for α and β for Langmuir binding isotherms as 1.67 and 4.08, respectively. Martin-Perez et al. [95] tested cement paste contained 40% slag with w/c = 0.3 (C_f and C_b were expressed by the authors as kg/m^3 of pore solution and kg/m^3 of concrete, respectively) over two ranges of free chloride concentrations, 0.5 mole/l and 2.5 mole/l. They reported the following values for the binding isotherm parameters: α = 0.19 and 0.07 for linear isotherms at low and high concentrations, respectively; α = 1.03, β = 0 .36 and α = 1.05, β = 0.36 for Freundlich isotherms at low and high concentrations, respectively; and α = 0.98, β = 0 .29 and α = 0.39, β = 0.07 for Langmuir binding isotherms at low and high concentrations, respectively. It can be noted that from these results that the Freundlich isotherm parameters remained unchanged over the limit of the two concentrations, whereas the parameters of the linear as well as the Langmuir binding isotherms were influenced by the increased limit of the free chloride concentration range [34,95].

7.3.5 Influence of Curing Temperature on the Determined Chloride Binding Coefficients

Figure 7.11 shows the influence of curing temperature on the resulting binding coefficients. As can be seen, the curing temperature has no influence on the linear isotherm coefficient (α). However, it does seem to have a slight influence on the nonlinear coefficients.

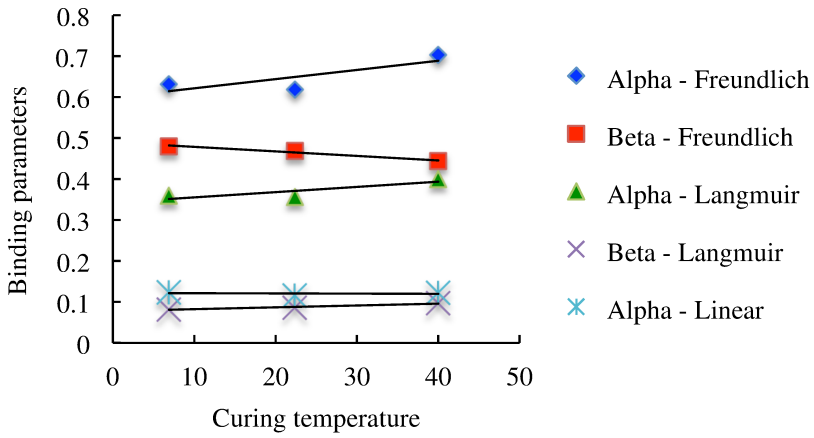

Figure 7.11 Influence of curing temperature on binding isotherm coefficients

For Freundlich isotherms, the value of α tends to slightly increase with increased curing temperatures, whereas the value of β tends to slightly decrease as the curing temperature increases. However, the values of α and β for Langmuir isotherms both tend to slightly increase with increased curing temperature. Also, it can be noted that the differences between Freundlich coefficients are much smaller than those between Langmuir coefficients. A larger range of curing temperatures and more data points may be required to confirm the above observations. It should be remembered that chloride binding, in the equilibrium test, is controlled by the isotherm condition at which the test was conducted. In other words, different exposure conditions could influence the relationship between bound and free chlorides, which may lead to different values of binding coefficients.

7.4 Bulk Diffusion Results

In this section, the results of the bulk diffusion test are presented and discussed. Water-soluble and acid-soluble chloride profiles after different exposure conditions are established.

7.4.1 Water-soluble Chloride Concentration Profiles

Figure 7.12 shows the average water-soluble chloride profiles obtained from concrete samples after 56, 90 and 180 days of exposure at 6.9^{o} C, 22.4^{o} C and 40^{o} C. These profiles were obtained by plotting the chloride concentration of the pulverized layers against their corresponding depths. Each data point in each chloride profile presents the average of three chloride concentration measurements. The chloride concentration of the first layer was disregarded, as suggested by the test standard ASTM C1556. The 56-day chloride profiles were obtained up to a depth of 10 mm from the exposed surface, while the 90- and 180-day profiles were obtained up to a depth of 20 mm from the exposed surface. The chloride profiles of individual samples can be found in Appendix (B).

As Figure 7.12 shows, the amount of chloride concentrations for all exposure conditions increased as the time of exposure increased. It can also be seen that the amount of intruded chlorides increased with an increase in the exposure temperature. Some discrepancies have been observed in the chloride concentrations at depths close to the surface. This could be due to the influence of coarse aggregates of unequal size at the exposed surface or the influence of the cut, which might have induced some macro and micro-cracks, leading to such discrepancies.

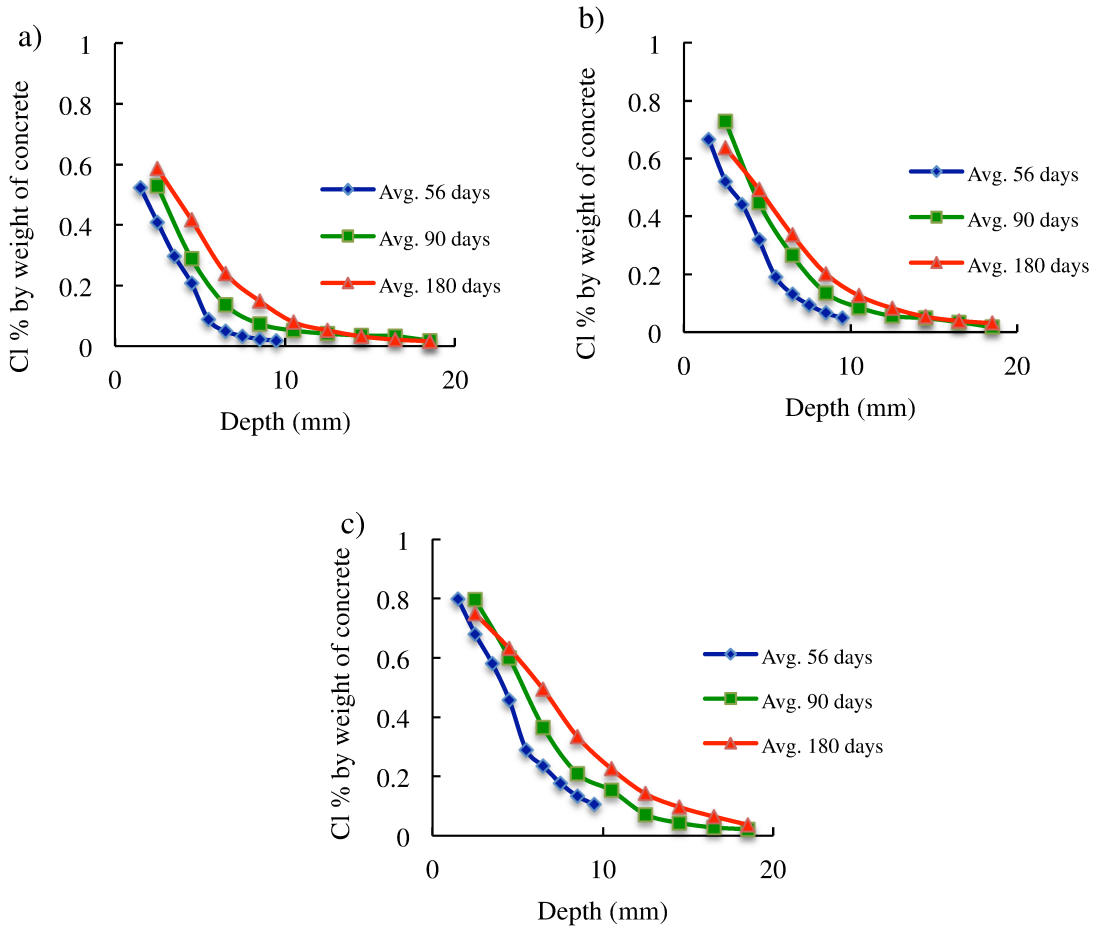

Figure 7.12 Average water-soluble chloride profiles at: a) 6.9° C, b) 22.4° C and c) 40° C

7.4.2 Acid-soluble Chloride Concentration Profiles

Figure 7.13 shows the experimental acid-soluble chloride profiles measured after 56, 90 and 180 days of exposure to 6.9° C and 22.4° C, and those measured after 56 and 90 days of exposure to 40° C. Each profile represents the average of three profiles measured from three concrete specimens. A full description of the individual profiles is provided in Appendix (B).

As in the case of water-soluble profiles, the chloride concentration of different depths increases with time and temperature. However, it can be noted that the chloride concentration of acid-soluble chloride is higher than that of water-soluble chlorides,

especially at the exposed surface. This was expected, as the acid soluble chlorides represent the total chloride content extracted by the nitric acid, whereas the water-soluble chlorides represent only the water-extracted chlorides.

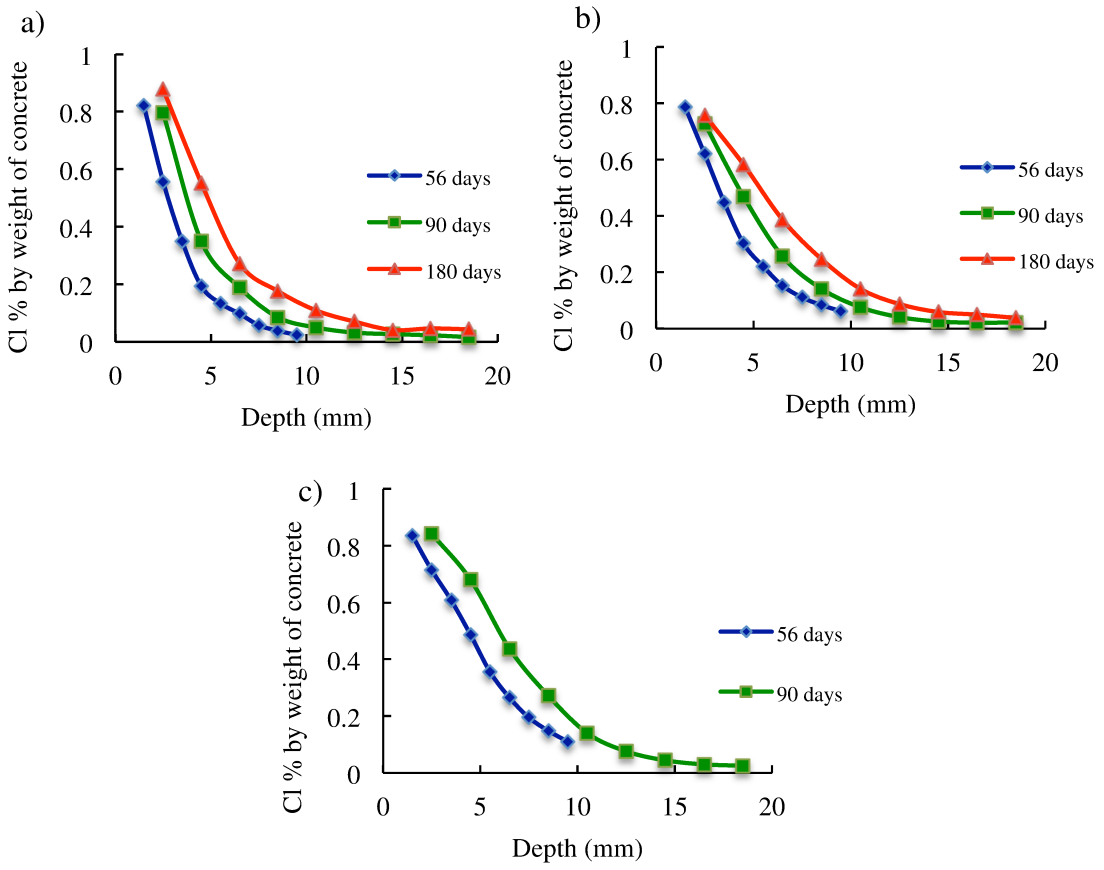

Figure 7.13 Averaged acid-soluble chloride profiles at: a) 6.9^{o} C, b) 22.4^{o} C and c) 40^{o} C

The acid-soluble chlorides represent both free and bound chlorides in the concrete, and the water-soluble chlorides are believed to represent the free chloride ions in the pore solution[81,83]. Although some researchers argued that the water-soluble chloride concentration in many cases overestimates the amount of free chloride concentrations in the pore solution[116,163], the reason is that a large amount of physically bound chlorides are loose and can be easy dissolved in water during the extraction process. Also, the heat generated during the grinding process can cause some chemically bound chlorides to be liberated in the pore solution, thus increasing the free chloride concentration.

7.5 Determination of Chloride Parameters

In this section, chloride parameters, including diffusion coefficients, surface concentrations, and values of m derived from the bulk diffusion test results, are analyzed and presented. The influence of temperature and time on chloride diffusion parameters is highlighted and discussed. Finally, the chloride parameters of acid-soluble and water-soluble chlorides obtained from both the error function solution and the linear finite difference models are summarized and compared.

7.5.1 Error Function Solution Approach

Concrete chloride parameters, mainly the average diffusion coefficients and the surface concentrations for both water-soluble and acid-soluble chlorides, were determined directly by the bulk diffusion test for the three exposure conditions. The instantaneous diffusion coefficients at age 28 days, D_{28}, and the values of m for both types of chloride profiles were determined using the three methods outlined in Chapter 4.

7.5.1.1 Water-soluble Chlorides

The chloride parameters resulting from fitting the error function solution to the experimental data of water-soluble chlorides, which includes the surface concentrations, C_s, and average diffusion coefficients, D_{AVG}, along with the obtained values of the instantaneous D_{28} and the value of m as determined by the different methods, are summarized in Table 7.5. Figures showing the error function solution-modeled profiles along with the experimental data of the water-soluble chloride profiles for all exposure conditions can be found in Appendix (B)

The various values of m are obtained by plotting the average diffusion coefficients obtained at different concrete ages for the three exposure conditions against the total time (age of the sample at the end of exposure), average time (the average age of the sample) and the effective time (affective age of the sample as calculated by Eq. (4.10)) on a log-

log scale. Linear regression analysis of the data is used to determine the values of m, as shown in Figure 7.14.

Table 7.5 Error function solution model- water-soluble chloride parameters

Temperature condition (T °C)	Exposure period (days)	C_s (%)	D_{AVG} *10^{-12} (m^2/s)	D_{28} *10^{-12} (m^2/s)	$m_{tot.}$	D_{28} *10^{-12} (m^2/s)	$m_{avg.}$	D_{28} *10^{-12} (m^2/s)	$m_{eff.}$
6.9	56	0.818	1.35	1.66	0.162	1.60	0.198	1.61	0.228
	90	0.876	1.38						
	180	0.866	1.18						
22.4	56	0.932	2.08	2.81	0.267	2.63	0.324	2.68	0.381
	90	1.102	1.95						
	180	0.89	1.64						
40	56	1.066	3.00	3.89	0.234	3.66	0.283	3.70	0.331
	90	1.143	2.79						
	180	1.001	2.43						

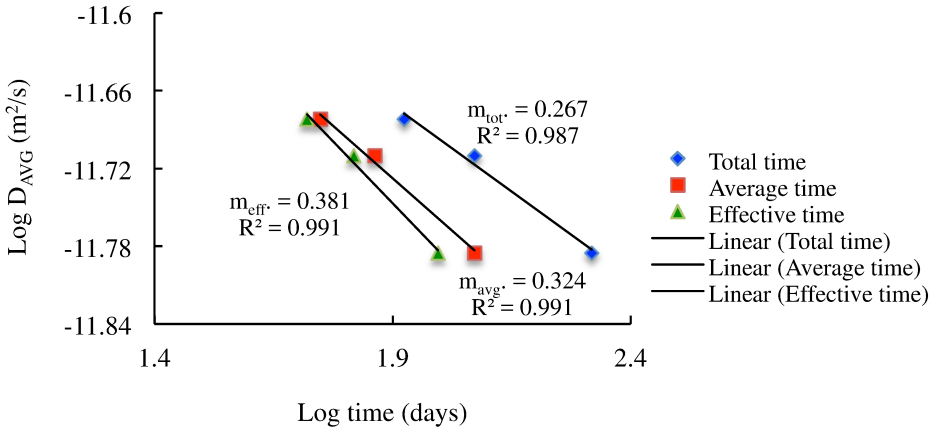

Figure 7.14 Determination of age parameter based on water-soluble chloride at 22.4° C

7.5.1.2 Acid-soluble Chlorides

Table 7.6 summarizes the results of the bulk diffusion test for the case of acid-soluble chlorides, along with the determined values of the instantaneous apparent diffusion coefficient, D_{a28}, and the age parameter, m. Figures showing the error function solution-modeled profiles and the experimental data of the acid-soluble chloride profiles for all exposure conditions can be found in Appendix (B).

As in the case of water-soluble chloride results, the different values of m were determined for each exposure condition by plotting the average apparent diffusion coefficients obtained at different concrete ages against the corresponding samples representative ages on log-log scale, as shown in Figure 7.15.

Table 7.6 Error function solution chloride parameters - acid-soluble measurements

Temperature condition (T °C)	Exposure period (days)	C_s (%)	D_{AVG} *10^{-12} (m^2/s)	D_{a28} *10^{-12} (m^2/s)	$m_{tot.}$	D_{a28} *10^{-12} (m^2/s)	$m_{avg.}$	D_{a28} *10^{-12} (m^2/s)	$m_{eff.}$
6.9	56	1.251	1.06	1.28	0.161	1.22	0.196	1.23	0.225
	90	1.457	1.03						
	180	1.352	0.92						
22.4	56	1.076	1.89	2.41	0.205	2.28	0.25	2.31	0.29
	90	1.131	1.84						
	180	1.063	1.58						
40	56	1.118	3.1	3.48	0.106	3.41	0.136	3.42	0.154
	90	1.222	2.99						

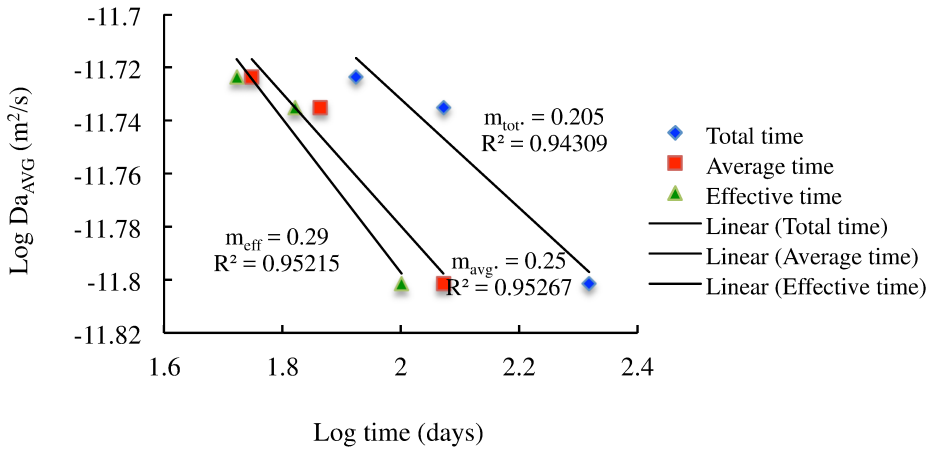

Figure 7.15 Determination of age parameter based on acid-soluble chloride at 22.4° C

Figures 7.14 and 7.15 also show the reduction in the value of the average diffusion coefficient over time. As can be seen, the time basis plotted for each method changes the slope of the relationship, thus leading to different values of m.

7.5.2 Linear Finite Difference Method

The chloride parameters of the tested concrete samples for the three exposure conditions were also determined using the linear finite difference model (L.F.D.M.). The L.D.F.M. was fitted to the experimental data of water-soluble and acid-soluble chlorides for the three exposure conditions to determine the related instantaneous diffusion values, D_{28}, the value of m, and the surface concentration, C_s.

7.5.2.1 Water-soluble Chloride Parameters

Table 7.7 summarizes the results of fitting the L.D.F.M. to the experimental data of water-soluble chloride at different exposure conditions. The predicted chloride profiles of the L.F.D.M. and those determined experimentally for the 22.4° C exposure condition are graphically illustrated in Figure 7.16. The chloride profiles obtained for the other two exposure conditions can be found in Appendix (B).

Table 7.7 Linear finite difference model - water-soluble chloride parameters

Temperature condition (T °C)	C_s (%)	D_{28} *10^{-12} (m^2/s)	m
6.9	0.855	1.54	0.20
22.4	0.967	2.67	0.38
40	1.088	3.47	0.30

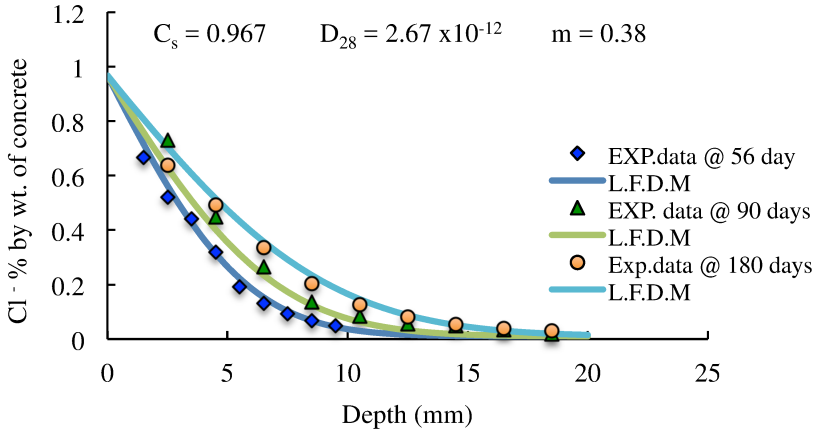

Figure 7.16 Experimentally water-soluble and linear finite difference chloride profiles at 22.4° C

It should be noted that the C_s values represent the average value of the three surface concentrations obtained for the three periods of exposure under each temperature condition. D_{28} and m are generated by the model to best fit the experimental profiles obtained at exposure periods of 56, 90 and 180 days while maintaining the surface concentration at a constant average value for each temperature condition. The Arrhenius equation was used in the model to shift the D_{28} to meet the temperature exposure conditions of the experimental profiles.

7.5.2.2 Acid-soluble Chloride Parameters

Table 7.8 summarizes the results of fitting the linear finite difference model to the acid-soluble experimental data at various exposure conditions. The modeled chloride profiles of the linear finite difference model and those determined experimentally at 22.4^{o} C are graphically illustrated in Figure 7.17. Chloride profiles obtained for the other two exposure conditions can be found in Appendix (B).

Table 7.8 Linear finite difference chloride parameters - acid-soluble chlorides

Temperature condition (T ^{o}C)	**C_s (%)**	**D_{a28} *10^{-12} (m^2/s)**	**m**
6.9	1.317	1.24	0.203
22.4	1.09	2.32	0.31
40	1.180	3.37	0.157

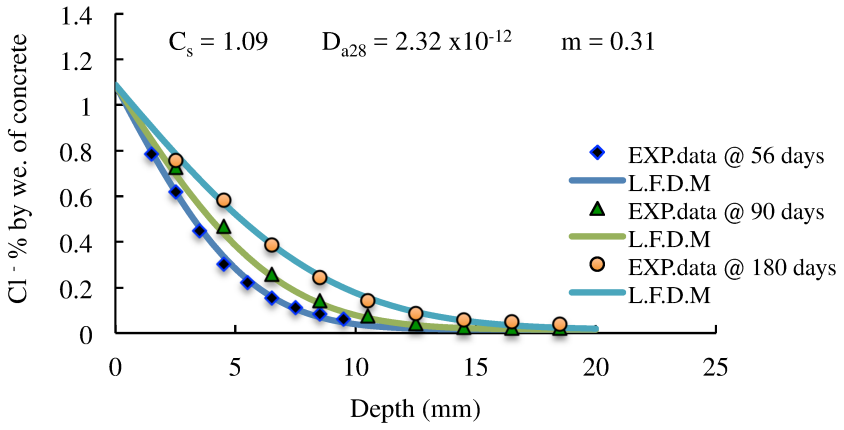

Figure 7.17 Experimentally acid-soluble and linear finite difference chloride profiles at 22.4o C

7.5.3 Discussion of Results

7.5.3.1 Surface Concentration (C_s)

The results of the error function solution (bulk diffusion test) for the water-soluble chloride presented in Table 7.5 show that the C_s value slightly increased as the exposure time increased to 90 days and then tended to decrease as the exposure time extended to 180 days. This was observed for all exposure temperature conditions. The results presented in Table 7.5 also show that the surface concentration slightly increased as the exposure temperature increased. This was also observed from the results of the linear finite difference model, as shown in Table 7.7. This could be due to variability in the binder content and the solubility of the bound chlorides at the surface, which increases as the temperature increases.

For the acid-soluble chlorides, similar behavior is observed for the influence of the exposure time on the C_s value, as shown in Table 7.6. Ninety days of exposure exhibited the highest C_s value. However, temperature has the opposite effect on the C_s values of acid-soluble chlorides than on those of water-soluble chlorides. As shown in Tables 7.6 and 7.8, the exposure condition of 6.9^{o} C resulted in the highest value of C_s, while, unexpectedly, the exposure condition of 22.4^{o} C exhibited the lowest. The variability in the values of C_s could also be attributed to variability in the binder content and the amount of coarse aggregate at the surface of the concrete samples.

7.5.3.2 Diffusion Coefficients

The results presented in Tables 7.5 and 7.6 show that the diffusion coefficient decreases as the exposure time increases. This confirms the findings of other research and studies reported in the literature. The results also show that the temperature has a significant influence on the value of the diffusion coefficient. The results of both the error function solution and the linear finite difference model demonstrate that the diffusion coefficient increases as the temperature increases. As reported by Ridding et al. [58], the temperature accelerates the rate at which the chloride ions diffuse, leading to higher chloride

concentrations in the concrete pore structure. The temperature can also change the rate of chloride diffusion by altering the rate of concrete densification from continued hydration.

7.5.3.3 Effect of Determination Method on Value of m

From the results presented above, it is clear that the effective time approach as proposed by Stanish and Thomas [85] provides the most accurate estimation of the value of m. As can be noted from Tables 7.7 and 7.8, the linear finite difference model resulted in values of m almost identical to those determined from the effective time approach shown in Tables 7.5 and 7.6 for the three exposure conditions. It can also be seen that the effective time method resulted in the highest value of m, while the total time method yielded the lowest value of m for all cases of exposure. The average time method resulted in a value of m close to that of the effective time. These results are in line with those presented in Nokken et al. [8] and suggest that if the value of m as projected from the effective time approach was used in the service life prediction model, it would result in the least conservative service life expectancy, while that of the total time would lead to an overly conservative estimation of the service life.

Furthermore, the value of m for the acid-soluble chloride as determined at 22.4^{o} C of exposure was found to be in very good agreement to that estimated in Life-365, based on the mix design mixture. Life-365 yields a value of m equal to 0.34 for the concrete mix design tested in this research. Since the service life is highly sensitive to the used value of m, large discrepancies can result if different methods are used to calculate it. Similarities in the values of m between the effective time approach and the linear finite difference method have resulted in similarities in the values of the instantaneous diffusion coefficients for the three exposure conditions.

7.5.3.4 Effect of Temperature on Value of m

Figure 7.18 shows the relationship between the exposure temperature and the values of m calculated from the effective time approach and those resulting from the linear finite difference model for both water-soluble and acid-soluble chlorides. As can be seen, the

exposure temperature has a significant influence on the values of the age parameter at early concrete ages. The value of m increased as the exposure temperature increased from 6.9^{o} C to 22.4^{o} C, but decreased as the temperature further increased to 40^{o} C. The low values of m at the high temperature of 40^{o} C could be attributed to the instability of the binding products, in particular Friedel's salt, which may have modified the pore size distribution and led to higher porosities, as explained earlier in section 7.2.2. Friedel's salt compounds can become unstable at higher temperatures and dissolve in the pore solution, leaving the pores unfilled, which would increase concrete porosity and reduce the value of m. This action will offset the influence of the hydration process in reducing the capillary pore size over time, thus eliminating the influence of time (ongoing hydration) on the rate of diffusion. Although the raised temperature is known to accelerate the rate of hydration, which would reduce the volume of the capillary pores at a faster rate, it could also induce microscopic cracking network, causing the capillary porosity to increase [164]. As a consequence, the value of m could have been modified and reduced by thermal treatment as well. Binding could also be responsible for the higher value of m at 22.4^{o} C, as suggested by the results of the MIP test presented earlier in this chapter. Compared to the results of water-soluble chlorides at 40^{o} C, it seems that the raised temperature has a greater influence on the value of m of the acid-soluble profiles.

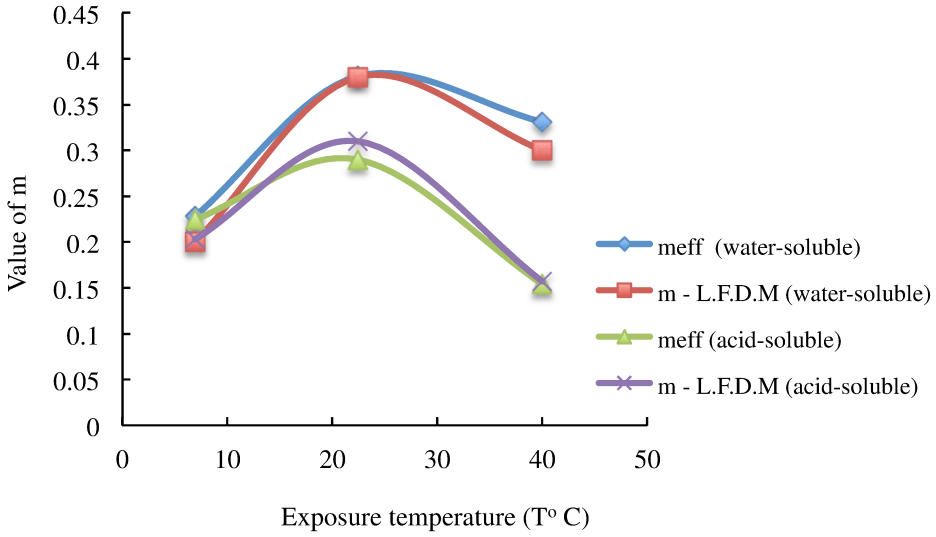

Figure 7.18 Influence of exposure temperature on value of age parameter

It is very interesting to note that the values of m at 6.9^{o} C for the two types of chlorides are almost the same. However, as the temperature increased to 22.4^{o} C and 40^{o}, the water-soluble chloride exhibited higher values of m. This shows the sensitivity of the calculated value of m to the type of chloride at elevated temperatures for the same type of concrete. Moreover, these results suggested that both temperature and binding can greatly influence the value of m, and that such an influence should be included in the calculation of m. Further work and long-term data are needed to investigate the influence of binding and temperature on the value of m to better understand and properly predict chloride behavior in concrete.

7.5.4 Chloride Parameters: Water-soluble Chloride vs. Acid-soluble

By comparing the results of water-soluble chlorides to those of acid-soluble chlorides as presented in this chapter, a few observations can be made: 1) The surface chloride concentrations projected from the water-soluble chlorides are lower than those of acid-soluble chlorides for all exposure conditions considered in this thesis. This was expected, as the surface concentration is controlled by the amount of bound chlorides, which was not accounted for in the case of water-soluble results. 2) The diffusion coefficients of the water-soluble chloride are higher than those of acid-soluble chlorides. 3) Both water-soluble and acid-soluble chloride profiles exhibited similar values of m at 6.9^{o} C. However, at 22.4^{o} C and 40^{o} C, the values of m for the water-soluble chlorides are higher than for those of acid-soluble chlorides.

As can be seen from the above results, the chloride parameters obtained based on acid-soluble chlorides are different from those obtained from water-soluble chlorides. The common practice is that the acid-soluble chloride data are often used in modeling chloride ingress into concrete. However, if water-soluble chloride is used instead, care must be paid to the parameters used.

Furthermore, it should be kept in mind that the above results were derived using the current practice models. These models assume that chloride binding is linear and that the

simplified Fick's second law as given in Eq. (2.5) is valid for describing chloride ingress into saturated concrete for cases of constant diffusion coefficient and cases of time-dependent diffusion coefficient. Therefore, if nonlinear binding is considered, different results for the chloride parameters of the concrete should be expected, in particular for the apparent diffusion coefficient, which will in this case be concentration-dependent in addition to the temperature and time dependencies. In the following chapter, the results of the nonlinear model developed in this thesis are presented and discussed.

8 NONLINEAR FINITE DIFFERENCE MODEL – ANALYSIS RESULTS

This chapter presents the results of the nonlinear finite deference model (N.L.F.D.M.) that was developed in this thesis. To fully understand the influence of binding type on key chloride transport properties and on the shape of the modeled chloride profiles, key chloride parameters – in particular, the instantaneous effective diffusion coefficient at age 28 days, D_{e28}, and the age parameters, m_e – are determined by fitting the nonlinear model to the experimental data of the acid-soluble chloride (total chloride profiles). This is one of two major contributions presented in this work. The researcher is unaware of any previous attempts aimed at using acid-soluble chloride profiles to determine the instantaneous effective diffusion coefficient of concrete. The other major contribution of this thesis is the use of time and temperature dependencies of the effective diffusion coefficient along with the nonlinear binding. The effective diffusion coefficient is usually determined experimentally using independent lengthy test methods such as those mentioned in Chapter 2 and often assumed to be constant in chloride prediction models.

The chloride parameters were obtained for the case of no binding, linear binding, and nonlinear binding. The determination of the chloride parameters of corresponding chloride binding isotherms is presented and discussed in section 8.1. The influence of binding relationships on the apparent diffusion coefficient is outlined in section 8.2. The change in the shape of calculated chloride profiles as a result of different binding isotherms is discussed in section 8.3. The influence of different chloride exposure environments on the shape of chloride profiles resulting from linear and nonlinear binding isotherms is discussed in section 8.4. The binding capacity of linear and nonlinear binding relationships is discussed in section 8.5. The service life prediction is discussed and outlined in section 8.6. Finally, a parametric study and sensitivity analysis, which was carried out using the nonlinear model, is provided in section 8.7.

8.1 Determination of Chloride Parameters

The key chloride parameters for the nonlinear model are obtained by fitting the nonlinear model to the experimental profiles of acid-soluble chloride. In the literature, the common practice is that chloride data are often obtained at laboratory room temperature. Only the

experimental acid-soluble chloride profiles, obtained at 22.4^{o} C, were used to determine the chloride transport parameters of the high performance mix design considered in this thesis. Note that in the nonlinear model, the age parameter, m_e, is determined for the effective diffusion coefficient, D_{e28}, for the three binding cases.

The chloride binding coefficients, as determined experimentally using the equilibrium test for both linear and nonlinear binding (Freundlich), are presented in Table 8.1. These values were used in the nonlinear model to describe the binding capacity behavior of nonlinear and linear binding isotherms. Note that the value of the linear binding coefficient, α, changes if the limit of the free chloride concentration of the external solution is changed. Therefore, the nonlinear isotherm function was used to estimate the value of this coefficient for higher levels of free chloride concentration such as that of the bulk diffusion test (see Appendix (I)).

Table 8.1 Binding coefficients for linear and nonlinear binding isotherms

Nonlinear (Freundlich)		**Linear**
α	β	α
0.62	0.47	0.055

Since the binding data were obtained from saturated concrete samples, the value of the ω_e, which is assumed herein to present the amount of evaporable water content, was determined experimentally and found to be equal to 10.4%. The chloride binding parameters which resulted from fitting the nonlinear model to the experimental acid-soluble chloride profiles for each binding case are presented in Table 8.2. The free chloride concentration at the concrete surface that gave a very reasonable fit to the experimental data was found to be equal to 165 kg/m^3 pore solution. This value is higher than that of the estimated free chloride concentration used in the exposure solution. Note that the total chloride concentration in the nonlinear model is calculated from Eq. (5.4).

Table 8.2 Chloride parameters as obtained from nonlinear model for each binding case

Condition	**Binding case**	**C_s % by weight of concrete**	**D_{e28} *10^{-12} (m^2/s)**	**D_{e28} *10^{-12} (m^2/s) @20^{o} C**	**m_e**	**Min_MSE *10^{-6}**
22.4^{o} C	No binding	0.746	4.8	4.29	0.39	16760.958
	Linear binding	1.14	3.62	3.24	0.34	1549.663
	Nonlinear	1.043	2.56	2.29	0.37	1136.649

Different values of total chloride at the surface, C_s, result for different binding isotherms, although the concentration of the external solution is the same for the three cases. The variation in the C_s values are related to the difference in the amount of bound chlorides, C_b, estimated from each binding relationship.

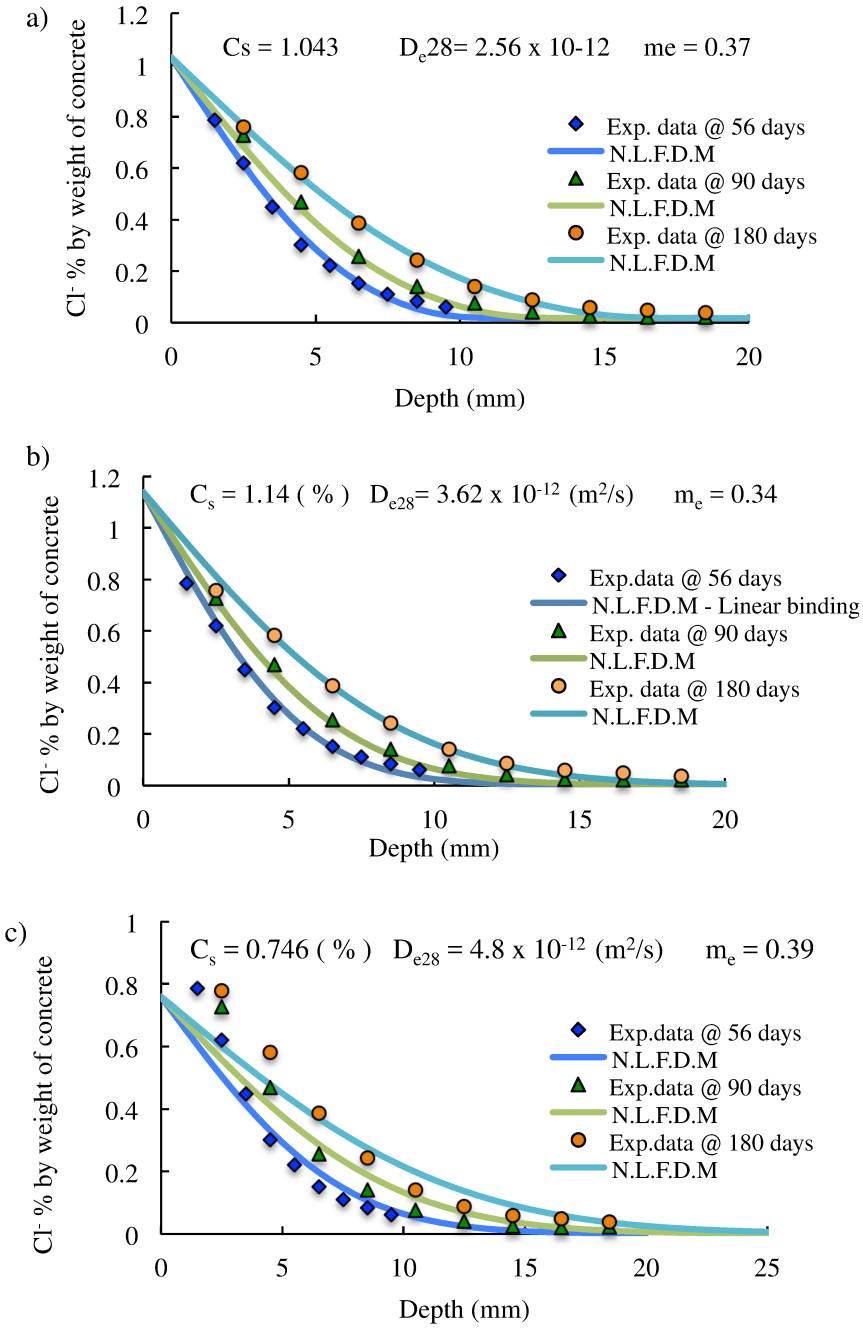

Figure 8.1 Experimental acid-soluble chloride profiles and nonlinear model chloride profiles for a) nonlinear binding, b) linear binding and c) no binding

Figure 8.1 shows the acid-soluble experimental chloride profiles along with the modeled total chloride profiles as obtained from the nonlinear model for all binding cases. As can be seen from Table 8.2 and Figure 8.1, when nonlinear binding was considered the model provides the best fit curves overall to the experimental data, followed by the case with linear binding. When the binding is completely ignored, however, the model results in poorer fit to the experimental data. This shows that the chloride binding is a vital part of the chloride penetration and must be included in chloride prediction models.

Furthermore, from Table 8.2, it can be seen that the effective diffusion coefficient, D_{e28}, varies with the type of binding used in the model. The nonlinear binding resulted in the lowest value of D_{e28} and when no binding at all is assumed, the value of D_{e28} was the highest. This implies that a strong relationship does exist between the type of assumed binding and the effective diffusion coefficient. This was expected, as different binding isotherms will result in different relationships between the bound and free chloride concentrations in a concrete pore system. Therefore, the diffusion rate of free chloride in pore solution will be different. This may also indicate that the D_e is a concentration-dependent.

Unlike its influence on the value of D_{e28}, the binding relation has only a slight influence on the value of m_e. Small variations in the value of m_e result from the model when different binding cases are considered. This could be due the fact that the value of m_e is a material property and more related to the type of cementitious material used in the concrete mix. It is worth noting that the linear binding has resulted in a value of m_e that is identical to the value of m estimated by Life-365; it is also in very good agreement with the other values projected from the linear finite difference model and the effective time method. This further confirms the validity of the nonlinear model presented in this research.

8.2 Influence of Binding on the Apparent Diffusion Coefficient

Figure 8.2 shows the influence of different binding isotherms on the apparent diffusion coefficient calculated using Eq. (5.7). This equation indicates that the reduction in the apparent diffusion coefficient, D_a^*, will be dependent on the type of binding capacity used

in the denominator. Different binding isotherms lead to different binding capacities. If binding is ignored the D_a^* will be equal to D_e and the ratio of D_a^*/D_e will equal to the unity. Therefore it remains constant over the range of the free chloride concentration, as shown in Figure 8.2. If linear binding is considered the ratio of D_a^*/D_e will depend on the binding capacity of the linear isotherm, α.

Note that the binding capacity of the linear binding for a particular concrete in any given exposure condition is constant and independent from the level of free chloride concentration in the pore solution. However, if the nonlinear binding is considered, the D_a^*/D_e ratio becomes concentration dependent. This is because the binding capacity of the nonlinear relation is a function of the level of the free chloride concentration; it becomes high at low concentrations and low at high chloride concentrations. Thus, the nonlinear binding relation will allow the D_a^* to vary through the concrete depth.

It can also be observed that the D_a^* for a nonlinear relation is lower than that of a linear one only when the chloride concentration in the pore solution is lower than 25 kg/m^3. For higher levels of free chloride concentration, the D_a^* of the nonlinear relation is always higher than that of the linear binding. This reflects the dependency of the binding capacity of the nonlinear relationship on the level of free chloride concentration in the pore solution. Also, note that when no binding is considered at all, the D_a^* value is the highest as there is no binding influencing its value. As for the case of the effective diffusion coefficient, the apparent diffusion coefficient is also binding-dependent.

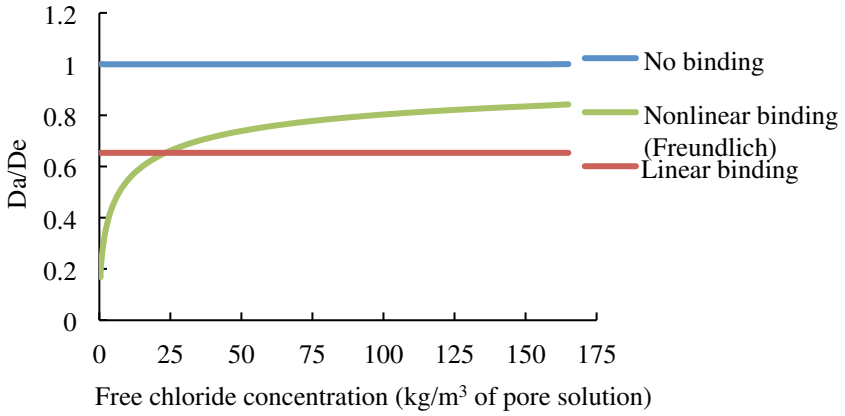

Figure 8.2 The influence of chloride binding on the apparent diffusion coefficient

From this it can be concluded that the apparent diffusion coefficient in the case of nonlinear binding is highly sensitive to changes in the free chloride concentration of pore solution at greater concrete depths where the binding capacity of the concrete becomes very high. Therefore, a large drop in the value of the apparent diffusion can be expected when the free chloride concentration in the pore solution is approaching zero. The reduction in the apparent diffusion coefficient value at depths close to the level of the reinforcement would have an impact on the time to corrosion initiation and life expectancy. It will reduce the penetration depth of total chlorides and increase the time required to initiate corrosion. This impact is neglected when linear binding is considered. Linear binding assumes that the apparent diffusion coefficient remains constant and does not change with free chloride concentration or concrete depth. Therefore, it tends to overestimate the amount of total chlorides at the level of reinforcement, which will underestimate the time to corrosion initiation.

8.3 Influence of Binding Type on the Shape of Free, Bound and Total Chloride Concentration Profiles

Free chloride profiles as estimated by the nonlinear model for the corresponding binding isotherms considered in this model are shown in Figure 8.3. These profiles are calculated after an exposure period of 180 days. The exposure conditions used were those of the bulk diffusion test. Note that the free chloride concentration is expressed in (kg/m^3 of pore solution).

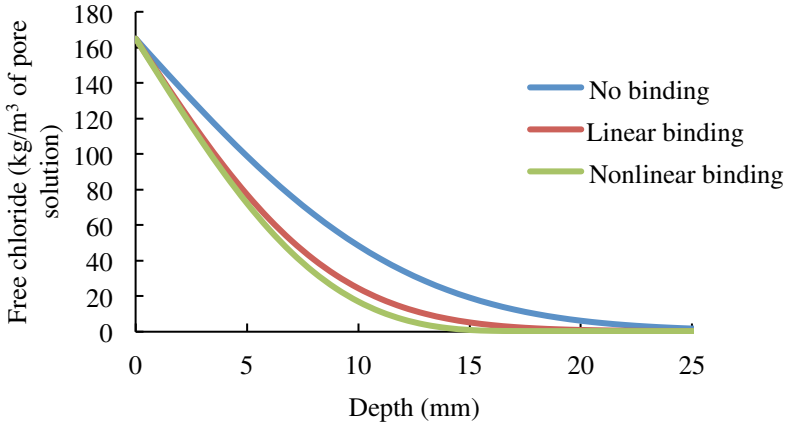

Figure 8.3 Calculated free chloride profiles after 180 days of exposure

Figure 8.3 shows that both nonlinear and linear binding resulted in lower free chloride concentrations at all concrete depths and that when no binding is considered, a considerable increase in the penetration depth of free chloride concentration results. If nonlinear binding is considered, the level of free chloride at any given depth is lower than that when no binding or linear binding is accounted for. The difference grows larger at greater depths. This is attributed to the different rates of effective diffusion coefficients resulting from the corresponding binding relations. Nonlinear binding resulted in the lowest value for the effective diffusion coefficient, and its free chloride profiles exhibited the least penetration depth. The increased difference in the depth of free chloride concentration resulting from different binding relationships at greater concrete depths is attributed to the influence of the concrete binding capacity of nonlinear relation. This capacity becomes very high at greater concrete depths, where the amount of bound chlorides becomes much higher than that of free chloride in the concrete pores. This can be further explained by examining the calculated bound chloride profiles.

Figure 8.4 shows the calculated bound chloride profiles for linear and nonlinear binding relationships over a range of concrete depths. The bound chlorides for linear and nonlinear binding were calculated up to a depth of 25 mm from Eq. (5.12) and Eq. (5.18), respectively.

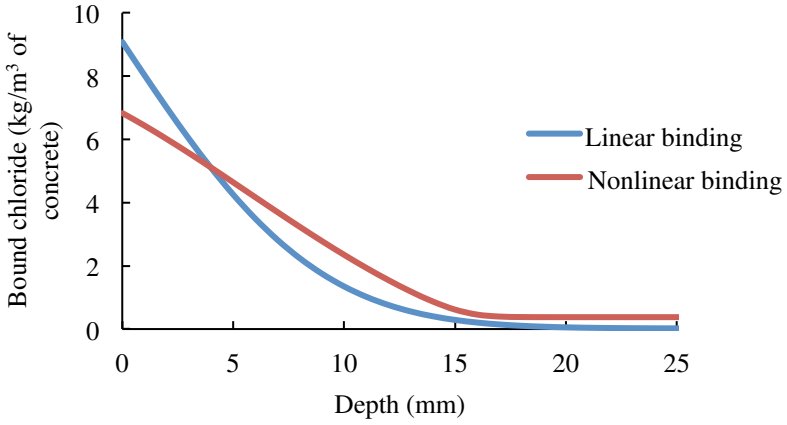

Figure 8.4 Calculated bound chloride profiles after 180 days of exposure

The difference in the shape of the bound chloride profiles between the linear and nonlinear binding results from the difference in the amount of bound chlorides estimated by the corresponding binding capacity of each binding relation at all concrete depths. The linear binding assumes constant binding capacity and the nonlinear binding results in a binding capacity that is a function of the free chloride concentration level in the pore solution. Therefore, different shapes of bound chloride profiles result.

It can be observed that the linear binding resulted in a higher amount of bound chloride at the exposed surface. As the chlorides ions diffuse in and the depth of the concrete increases, the bound chloride profiles of linear binding decreasing at a constant rate equal to its binding capacity, α, regardless of the level of the chloride concentration in the pore solution. However, in the case of nonlinear binding, the bound chloride profile follows the behavior of the corresponding binding capacity, which increases as the level of the free chloride concentration decreases in the pore solution. Thus, more chlorides are bound as they travel deeper in the concrete and become less free. That is why, after a certain depth from the surface, the amount of bound chloride estimated by the nonlinear binding is higher than that estimated by the linear binding relation.

Figure 8.5 shows the total chloride profiles along with the experimental data after an exposure period of 180 days. The total chloride profiles were calculated using Eq. (5.4) as the sum of free and bound chlorides. As can be seen, if the nonlinear binding is accounted for, the calculated total chloride profile gives a perfect fit to the experimental data and shows that the linear relation still provides a very good fit. The higher amount of total chloride at the surface of the linear binding is attributed to the higher amount of bound chlorides estimated by linear binding, as explained previously. When no binding is considered, the total chloride profile becomes flatter and significantly shifts from the normal distribution of the experimental data with concrete depth. This further confirms the significance of binding on the produced chloride profiles.

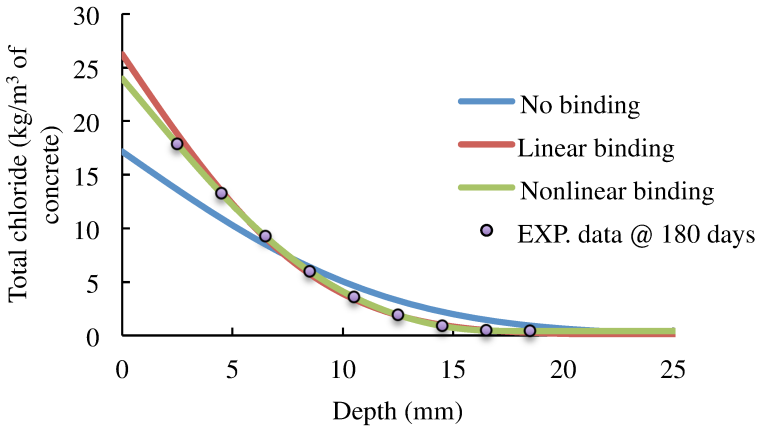

Figure 8.5 Experimental and calculated total chloride profiles after 180 days of exposure

It can also be observed that at high chloride concentrations, such as those in the bulk diffusion test, no difference can be noted in the total chloride content at concrete depths away from the surface between the linear and nonlinear binding. This could be due to the fact that the ratio of bound-to-free chlorides becomes very small at high levels of chloride concentrations, as suggested by Martin Perez et al. [95]. Note that the difference between the two types of total chloride profiles, in particular at the depth of the reinforcement, becomes more noticeable as the time of exposure increased to several years.

8.4 Shape of Chloride Profiles at Low and High Chloride Surface Concentrations

To highlight the influence of different chloride environments on the shape of the calculated chloride profiles, the free, bound, and total chloride profiles were simulated for more realistic chloride concentrations. Two surface chloride concentrations were used: 17.727 kg/m^3 of pore solution (low concentration) and 70.91 kg/m^3 of pore solution (high concentration). The former simulates the exposure conditions of submerged structures in seawater, and the latter simulates the exposure conditions of more aggressive environments such as a marine splash zone or a de-icing salt area (e.g., bridge deck). The calculated profiles were obtained for both linear and nonlinear binding relationships. These profiles were calculated after an exposure period of 50 years. The resulting profiles

for the low and high surface chloride concentrations are shown in Figures 8.6 and 8.7, respectively.

As can be seen from these figures, the shapes of the free and bound chloride profiles and their relationship to the linear binding remain the same and unaffected by the level of the surface concentration, despite the fact that the chloride concentration at any given depth is greater for higher surface chloride concentrations. However, the shapes of the nonlinear binding chloride profiles and their relationship are not the same at the two concentrations.

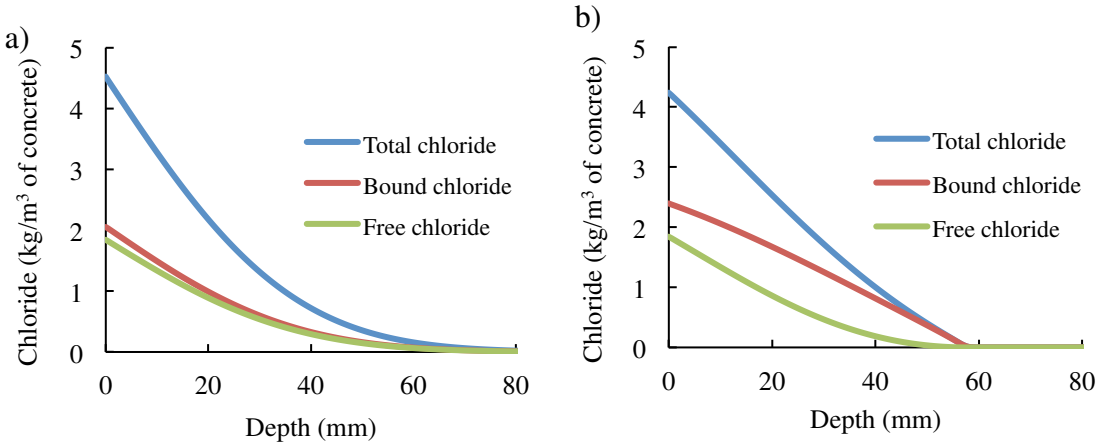

Figure 8.6 Calculated free, bound and total chloride profiles at low concentration: a) linear binding, b) nonlinear binding after 50 years

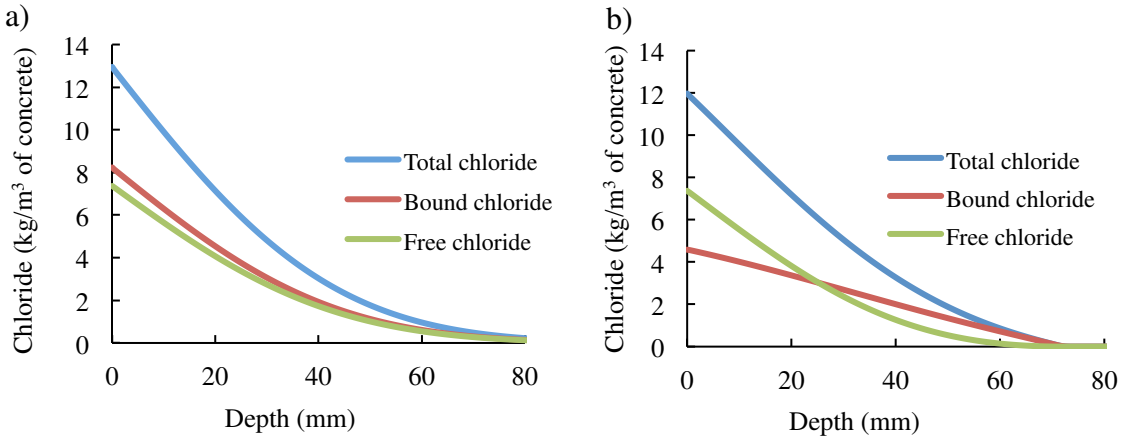

Figure 8.7 Calculated free, bound and total chloride profiles at high chloride concentration: a) linear binding, b) nonlinear binding after 50 years

The chloride profiles, when linear binding is assumed, tend to have a convex shape as the chlorides diffuse in. Also, it can be noted that for the two exposure conditions, the linear binding results in approximately 50% bound chloride and 50% free chlorides over the entire concrete depth except at the surface where the amount of bound chlorides is slightly higher than that of free chlorides. For the nonlinear binding relation, the shape of the calculated chloride profiles is different at the two surface concentration levels and also different from that of the linear binding. For the low surface concentration, the bound chloride profile is always higher than that of the free chloride at all concrete depths.

Furthermore, it can be seen that at low surface concentrations, the bound chloride profile of nonlinear binding tends to have a concave shape whereas the free chloride profile tends to have a convex curve. The concave shape of the bound chloride profile seems to have a significant influence on the shape of the total chloride profile, in particular at low surface chloride exposure conditions. The total chloride profile tends to decline in a linear trend and does not bend inward as in the case of that of the linear binding, as shown in Figure 8.8.

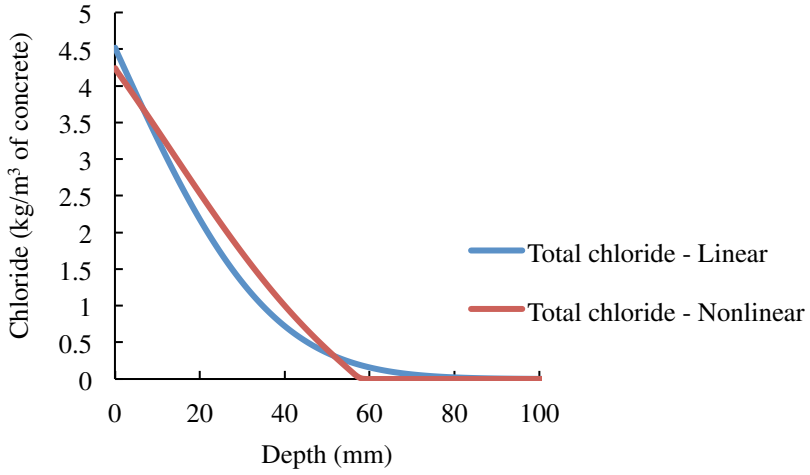

Figure 8.8 Total chloride profiles of linear and nonlinear binding at low surface concentration after 50 years of exposure

At high surface concentrations, the behavior of bound and free chlorides of nonlinear binding is somewhat different from that at low surface concentrations. At higher surface concentrations, the bound chloride profile tends to change its shape and become more linear than curved, as can be seen in Figure 8.7b. At the exposure surface, the binding capacity of the concrete is low where the concrete surface becomes saturated with chlorides as a result of high surface chloride concentration; thus, a higher free chloride concentration than that of bound chlorides results at the surface.

However, at greater depths, away from the surface, the binding capacity becomes higher, so more chlorides are bound and fewer chloride ions are free. Furthermore, it can be observed that the penetration depth of chloride ions estimated by the nonlinear relation for all cases is always less than that estimated by the linear relation. This has occurred because the nonlinear binding capacity becomes high and more sensitive to the change in concentration of free chlorides at greater concrete depths.

As stated above, the change in the shape of the calculated chloride profiles of nonlinear binding is attributed to the role of the concrete binding capacity of the nonlinear binding relation at low and high exposure chloride concentrations. The increased binding capacity at low chloride concentrations can be explained by the availability of numerous sites along the pore walls that are capable of physically and chemically binding chloride ions in large amounts. However, once these sites become saturated with chlorides, as is the case of high surface concentration, the binding capacity of concrete drops and the amount of free chlorides increases over that of bound chlorides.

8.5 Chloride Binding Capacity of High Performance Concrete

Figure 8.9 characterizes the behavior of the linear and nonlinear binding capacities of the high performance concrete mix design evaluated in this thesis at different levels of free chloride concentrations. As can be seen, the concrete binding capacity of the linear binding stays constant at a value of 1.115, regardless of the level of the free chloride concentration in the pore solution. However, the binding capacity of the nonlinear binding changes with the level of the free chloride concentration and is adversely proportional to

the increased chloride concentration in the pore solution. It tends to increase indefinitely at very low concentrations and gradually decreases as the chloride concentration increases.

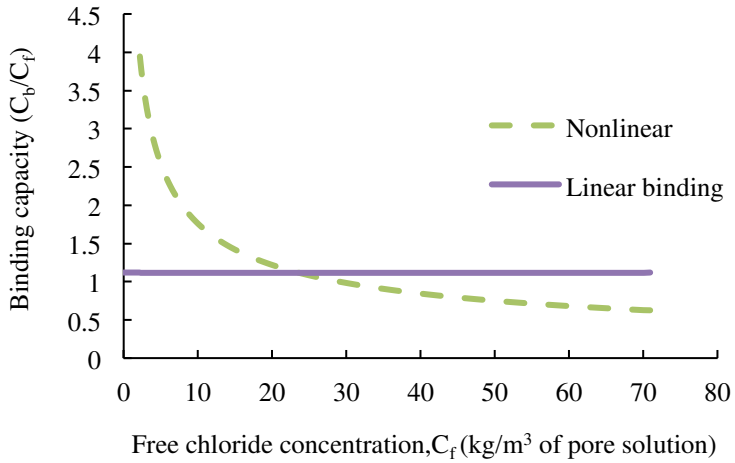

Figure 8.9 Linear and nonlinear binding capacities of high performance concrete

These results are in line with those reported by Akita and Fujiwara[165]and Massat et al. [166] Akita and Fujiwara suggested that the binding capacity is infinite or extremely high at very low chloride concentrations. Their data also show that the chloride binding capacities are still larger than zero at very high chloride concentrations. The behavior of nonlinear binding capacity at low and high chloride concentrations will have a significant influence on the calculated time to corrosion initiation and service life predictions of reinforced concrete structures' exposure to different exposure environments, as will be seen later in this chapter.

From Figure 8.9, it can also be observed that there is a point at a certain level of free chloride concentration where the binding capacities of both relationships become equal. For the concrete mix design considered in this thesis, the two binding capacities cross at a free chloride concentration of 25 kg/m^3 of pore solution (0.7 M). After this point, the binding capacity of the nonlinear binding becomes lower than that of the linear relation and continues to decrease at a lower slope as the free chloride concentration increases.

8.6 Service Life Predictions

In this thesis, the service life of the concrete was estimated as the time to corrosion initiation. Two cases for service life predictions were considered. In the first case, the time to corrosion initiation was estimated using the critical chloride content of the total chloride (acid-soluble chloride). For this case, the bulk diffusion test conditions were simulated to calculate the service life. The purpose in using the laboratory exposure conditions of the bulk diffusion test is to verify and validate the results of the developed model against those obtained from other models, such as the error function solution and Life-365 under the same exposure conditions. Therefore, the total chloride content was considered for the potential corrosion initiation of the reinforcement. In the second case, the time to corrosion initiation was estimated using the critical chloride content of free chloride for more realistic exposure conditions.

In the first case, where the total chloride was considered for the corrosion initiation potential, the critical chloride content, C_{crit}, used was 0.05%, as specified in Life-365. The temperature was held constant at 20^{o} C throughout the stimulated exposure period. Therefore, all instantaneous diffusion coefficients used in the service life calculations were normalized at 20^{o} C using the Arrhenius equation and referenced at age 28 days. The surface concentration, C_s, for the error function solution, Life-365, and linear finite difference model used was the averaged value as determined experimentally based on the results of the linear finite difference method (1.09 % by weight of concrete). For the nonlinear model, the free chloride concentration used at the surface, C_{se}, was 165 kg/m^3 of the solution. The surface concentration was kept constant throughout the exposure period. The chloride parameters, as determined in this thesis by each model at room temperature, were used to estimate the time to corrosion initiation. The background chloride was assumed to be equal to zero. The time to corrosion initiation was calculated assuming a 50 mm concrete cover thickness.

For the error function solution, the service life was calculated using the results of acid-soluble chloride profiles obtained at a 22.4^{o} C exposure condition for both average diffusion coefficients and time-dependent diffusion coefficients. Equation (2.6) was used

to estimate the time to corrosion initiation for the case of the average apparent diffusion coefficient. Equations (4.2) and (4.5) were used to estimate the time to corrosion initiation for the case of a time-dependent diffusion coefficient. Table 8.3 summarizes the chloride parameters used to estimate the time to corrosion initiation for the error function solution model.

Table 8.3 Error function solution chloride parameters at 22.4° C

Constant diffusion coefficient			**Time-dependent diffusion coefficient**					
D_{aAVG} *10^{-12} (m^2/s)			**D_{a28} *10^{-12} (m^2/s)**	**$m_{tot.}$**	**D_{a28} *10^{-12} (m^2/s)**	**$m_{avg.}$**	**D_{a28} *10^{-12} (m^2/s)**	**$m_{eff.}$**
56	90	180						
1.89	1.84	1.58	2.41	0.205	2.28	0.25	2.31	0.29

For Life-365, the time to corrosion initiation was calculated using the chloride parameters estimated from the concrete mix design (5% silica fume and 25% slag) and based on the experimental results as obtained from the linear finite difference model. Table 8.4 summarizes the chloride parameters used in Life-365 to estimate the time to corrosion initiation.

Table 8.4 Life-365 chloride parameters at 20° C

Based on mix design proportions		**Based on experimental results**	
D_{a28} *10^{-12} (m^2/s)	**m**	**D_{a28} *10^{-12} (m^2/s)**	**m**
2.24	0.34	2.08	0.31

For the nonlinear model, the time to corrosion initiation was estimated using the chloride parameters obtained from fitting the nonlinear model with different binding isotherms to the acid-soluble profiles chloride. Table 8.5 summarizes the chloride parameters for the different binding isotherms considered in this thesis.

Table 8.5 Nonlinear model chloride parameters for the different binding relations at 20° C

No binding		**Linear binding**		**Nonlinear binding**	
D_{e28} *10^{-12} (m^2/s)	**m_e**	**D_{e28} *10^{-12} (m^2/s)**	**m_e**	**D_{e28} *10^{-12} (m^2/s)**	**m_e**
4.29	0.39	3.24	0.34	2.29	0.37

The resulting service life estimates as projected from the error function solution for different status of the diffusion coefficients are graphically illustrated in Figure 8.9.

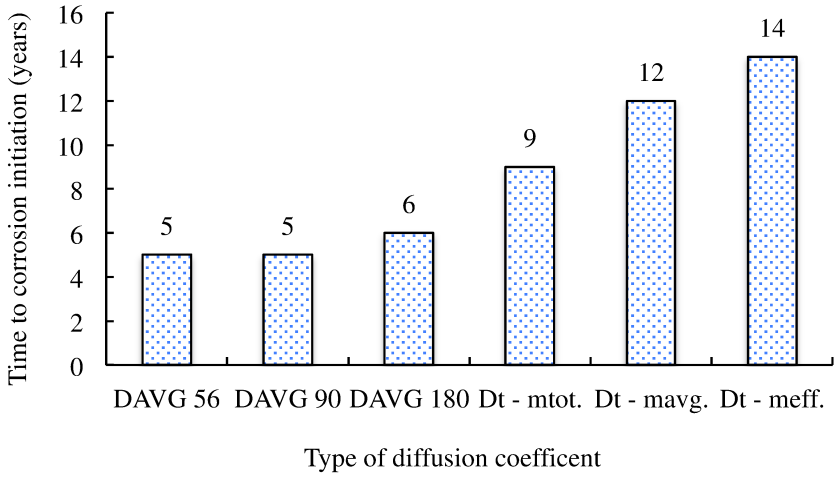

Figure 8.10 Service life estimations as resulting from the error function solution using different status of diffusion coefficient

Figure 8.10 shows that the concrete structure can have significantly different service life estimations when the error function solution is used, depending on the type of diffusion coefficient and the method used to calculate the value of m. The average diffusion coefficients resulted in very conservative estimation while that of time-dependent with effective time resulted in least conservative estimation. The difference is quite significant. The time-dependent diffusion coefficient of the effective time shows an increase up to 180% in the time to corrosion initiation compared to that resulting from the average diffusion coefficient. Compared to the total time, the effective time resulted in a 60% increase in the time to corrosion initiation.

It can also be observed that the average diffusion coefficients obtained at different ages of concrete have a minor influence on the predicted time to corrosion initiation. However, this influence tends to increase as the exposure time increases. Another drawback of the application of error function solution in estimating the service life is that the obtained results are test condition dependent. As pointed out by Stanish and Thomas [85], if the average diffusion coefficients are used to estimate the service life, the exposure

conditions in the field are assumed to be identical to the conditions during testing. If this is not the case (and in reality it is not), then the resulting service life estimated from using the average diffusion coefficients will be incorrect.

Figure 8.11 shows the resulting service life estimates as projected from different models. Note that for the purpose of comparison, the normalized value of D_{28} obtained from the effective time approach was used to estimate the time to corrosion initiation. It can clearly be seen that the time to corrosion initiation estimated by other models matches very well the time to corrosion initiation estimated by linear and nonlinear finite difference model (with linear binding). This confirms that the developed model produces very consistent results with other models. As expected, the nonlinear binding resulted in the longest time to corrosion initiation overall.

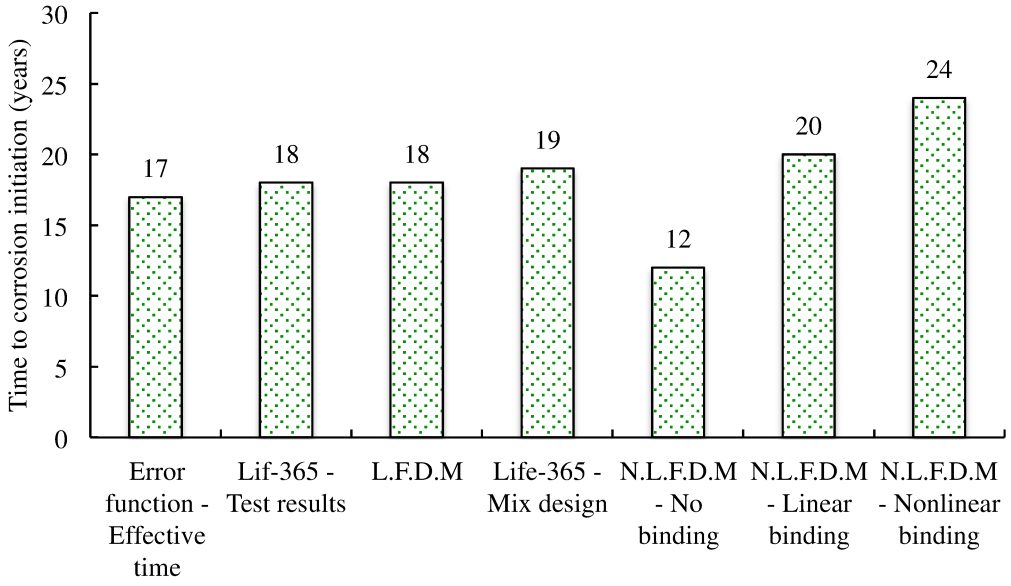

Figure 8.11 Service life estimates from different models for concrete cover of 50 mm

It can be also seen that for the nonlinear model when no binding is considered at all, the time to corrosion initiation is the lowest and exactly half of that estimated by the nonlinear binding for the given concrete mix design. This shows the beneficial influence of concrete binding with respect to reinforcement corrosion. These results also demonstrate that the effective time approach provides the most accurate estimation of the

service life for the error function solution. The discrepancies in the results of linear models are attributed to minor inconsistencies in the calculated value of m.

To further emphasize the importance of including the nonlinear behavior of binding in estimating the service life of reinforced concrete along with the consideration of some other decisive factors such as time and temperature dependencies of the effective diffusion coefficient, the nonlinear model was used to estimate the time to corrosion initiation for two cases of real exposure conditions. The first case is to stimulate the exposure condition of a marine structure submerged in seawater. In this case a surface chloride concentration of 17.727 kg/m^3 of pore solution (0.5 mole/l) was used. This value represents the typical value of the chloride concentration in the seawater. In the second case, the time to corrosion initiation was estimated by simulating a reinforced concrete structures such as a bridge deck exposed to de-icing salt condition. The surface chloride concentration used was 70.91 kg/m^3 of pore solution (2 mole/l). These two exposure conditions are referred to as low and high chloride exposure conditions, respectively. One assumption made here is that the exposure to high chloride concentrations (i.e. de-icing salts) is assumed constant during the simulation. In real conditions, the exposure to de-icing salts is concentrated in the winter period, i.e. a discontinuous exposure. Therefore, the surface concentration will increase with time during the winter. However, during the summer period, the surface concentration will decrease or be constant.

The time to corrosion initiation was calculated with respect to the critical content of the free chloride concentration at the depth of the reinforcement. The free chloride critical content used was 0.09% by weight of binder. This value represents a conservative value reported by Angst et al. and Glass et al. [20,148]. Martine et al. [95] also used this value in their study to calculate the time to corrosion initiation caused by free chloride concentration. This value is corresponds to 3.76 kg/m^3 of pore solution based on a 435 kg/m^3 binder content and a capillary porosity of a 10.4 % determined for this concrete. A typical temperature profile (monthly averaged temperatures) for Halifax, Nova Scotia was used in the model, as shown in Table 8.6.

Table 8.6 Typical average temperatures profile for Halifax, Nova Scotia [167]

Jan	Feb	Mar	Apr	May	Jun	Jul	Aug	Sep	Oct	Nov	Dec
-3.5	-3	0	5	9.5	14.5	18.5	18.5	16	10.5	5.5	-0.5

The service life was calculated for the three binding cases considered in the nonlinear model. A concrete cover thickness of 50 mm was assumed. The resulting service life predictions for the three binding cases are graphically shown in Figure 8.12.

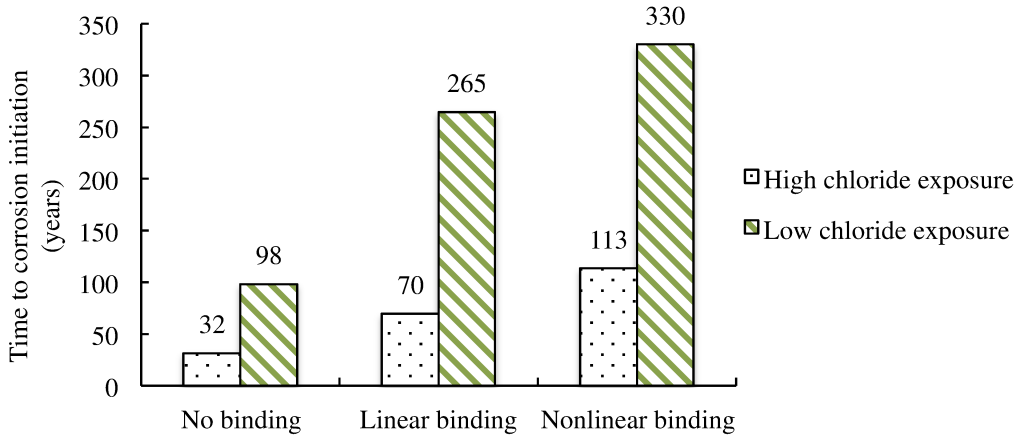

Figure 8.12 Nonlinear model service life estimations considering two exposure chloride conditions and concrete cover of 50 mm

As can be seen, the nonlinear nature behavior of chloride binding has a great influence on the results for both low and high chloride exposure conditions. For low chloride surface exposure, the nonlinear binding resulted in a 235% and 24.5% increase in time to corrosion initiation compared to no binding and linear binding, respectively, and a 259% and 63% increase for high surface chloride exposure, respectively. The longer surface life expectancy estimated by the nonlinear model is attributed to the behavior of the nonlinear binding capacity at the depth of the reinforcement, where a significant amount of chloride ions become bound chlorides and do not participate in the corrosion process.

The increased service life that resulted from modeling the nonlinear binding is quite significant for both of the above delineated exposure conditions and can have a great impact on the cycle cost and future repair and maintenance plans of reinforced concrete structures. Unfortunately, no real chloride profiles were made available to verify these

results. However, by including the nonlinear nature of the binding along with the time and temperature dependencies of the effective diffusion coefficient, the model should yield better estimation for the service life predictions of reinforced concrete structures exposed to a chloride environment. Furthermore, the nonlinear model developed in this thesis can provide better judgment and serve as a guideline to compare the performance of different concrete mix designs subjected to similar chloride exposure conditions.

8.7 Parametric Study and Sensitivity Analysis of the Nonlinear Model

A parametric study was carried out to determine the sensitivity of the service life predicted by the nonlinear model to changes in the values of some key parameters of interest. The predicted service life was calculated with respect to the critical content of free chloride concentration in the pore solution. In this study, the parameters of interest were varied over a likely range of values anticipated in real conditions, while the other parameters were maintained at their specific base case values for comparative purposes. The analysis of the parametric study was applied to the following selected model parameters:

- D_{e28}, instantaneous effective diffusion coefficient, which controls the rate at which free chloride ions travels through the pore pathways of the concrete cover,
- m_e, age parameter controls the reduction of the diffusivity over time as a result of binding and ongoing hydration of concrete,
- C_{se}, surface chloride concentration, which is in equilibrium with the chloride concentration in the surrounding environment,
- C_i, background chloride (the amount of chloride in concrete prior to exposure),
- Concrete cover thickness,
- T^o C, exposure temperature, and
- C_{crit}, chloride threshold required to initiate corrosion of reinforcement.

The values used for the base case and those of relevant range of the study for each input parameter are summarized in Table 8.7.

Table 8.7 Base case input parameters and their values

Input parameter	Base case values	Range of parameters
D_{e28} (m^2/s)	2.29×10^{-12}	$(3 - 4) \times 10^{-12}$
m_e	0.37	0.4 - 0.6
C_{se} (kg/m^3 od pose solution)	35.453	17.7 – 88.63
C_i (kg/m^3 od pose solution)	0.00	1 – 3
T^o C (Celsius)	20	5 - 35
Cover thickness (mm)	50	40 - 70
C_{crit} (% by weight of binder)	0.09 %	0.07% - 0.16%

The higher effective diffusion coefficients used in this study for the given concrete mix design could have resulted from poor compaction or inadequate curing regime or other construction factors reported in Chapter 2. The higher values of m are the typical values for concrete containing higher levels of slag cement or fly ash. The low and high surface exposures represent the range of surface chloride concentrations in two typical exposure conditions, as mentioned earlier in this chapter. The background chloride can be the result of chloride-contaminated ingredients from the concrete materials, such as fine and coarse aggregates or the use of chemical admixtures containing chlorides. The exposure temperatures represent the average values of low and high temperatures that are expected in real-life exposure conditions in cold and warm climates, respectively. For the cover thickness, in the current design practice, a typical 70 mm cover thickness is often used in highway bridge decks. From the inspection of existing structures, a 40 mm cover thickness or even lower is frequently reported. Finally, the values of the critical chloride content used represent the lower and upper limits of C_{crit} for free chloride concentrations, as reported by Angst et al. [20]

In addition, the following parameters were kept constant and were considered in this study: the activation energy is kept at 33,500 J/mole. The value of R (gas constant) was kept at 8.3144 J/mole. The amount of evaporable water used, ω_e, was 10.4%. The results of the parametric study are graphically shown in Figure 8.13. The predicted service life is shown as a percentage change of the base case estimation.

The sensitivity study was also evaluated from the numerical chloride profiles produced after 30 years of exposure. Relationships between the predicted service life and the concrete cover as well as the critical chloride content were established. In the following

paragraphs, the influence and sensitivity of the predicted service life and calculated chloride profiles to the change in each parameter investigated in this study are addressed.

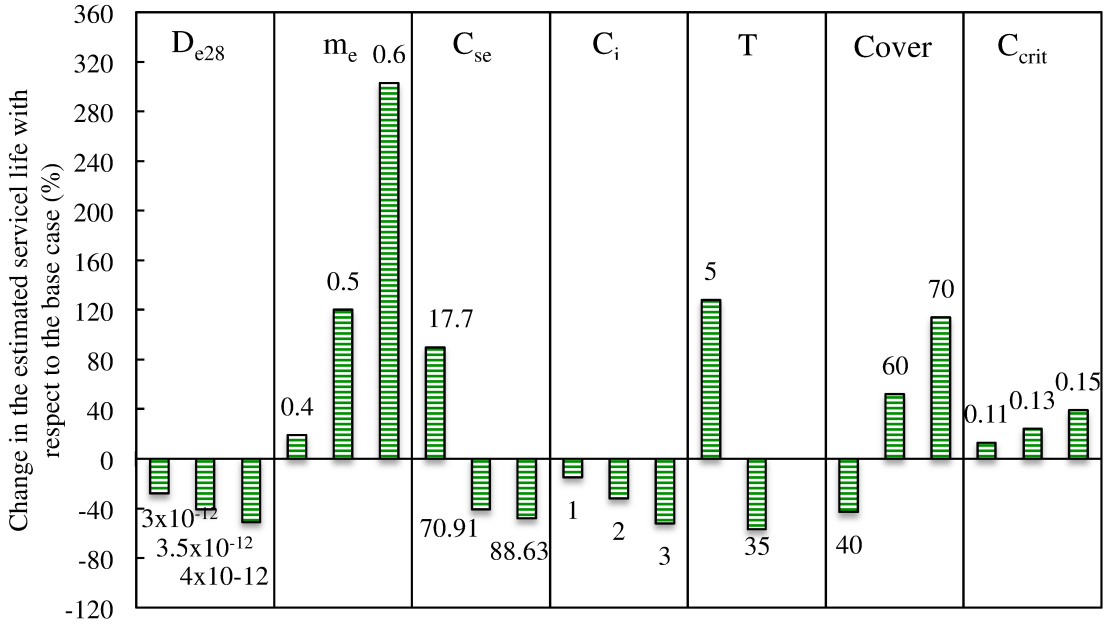

Figure 8.13 Change in estimated service life as a result of model sensitivity to different input parameters

As can be seen from Figures 8.13 and 8.14, the increase in the value of D_{e28} by a factor of 2 decreased the predicted service life by about 50% and increased the amount of chloride concentration at the 40 mm depth by 75%. The results show that the lower the D_{e28} value is, the higher the life expectancy of the structure will be. Therefore, for the sake of durability, it is desirable to design a concrete mix with low values of D_{e28}. The low diffusivity of concrete at age 28 days is achievable if the proper content of silica fume is added to the concrete mixture and adequate construction practice is applied. The value of D_{e28}, with respect to saline environments, can also be taken as a good indicator of the concrete quality and durability. Namely, low values of D_{e28} indicate durable concrete with good quality, and high values indicate lack of durability and poor concrete quality.

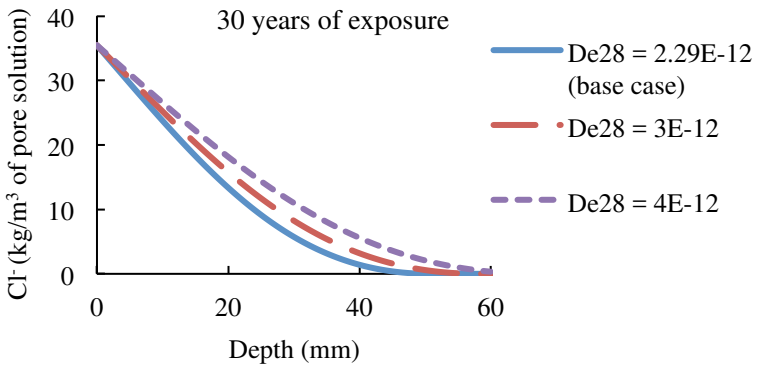

Figure 8.14 Influence of D_{e28} on predicted chloride profiles after 30 year of exposure

As expected, the estimated service life was found to be extremely sensitive to the change in the value of m_e. The results show that the value of m_e has the most significant impact overall on the predicted service life and that the service life is found to be proportional to the value of m_e: It increases as m_e increases. The significant increase in the predicted service life for higher values of m_e results from the greater reduction in the level of free chloride concentrations at the depth of the reinforcement, as shown in Figure 8.15. Therefore, care must be taken in choosing the proper value of this parameter when it comes to service life predictions and estimations. The results also emphasize that proper techniques to adequately quantify this parameter are crucial. From the results of this thesis, it was shown that both the effective time approach and the use of the finite difference model can provide adequate estimation for the value of m. Therefore, they are recommended to be used for obtaining the value of m from laboratory and field data.

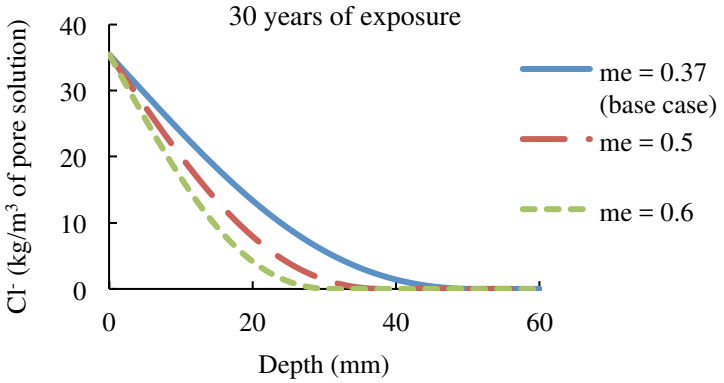

Figure 8.15 Influence of m_e on predicted chloride profiles after 30 years of exposure

The predicted service life is also found to be sensitive to changes in the surface concentration, C_{se}. As can be observed from Figure 8.13, changing the surface concentration from seawater exposure to that of de-icing salt resulted is a significant decrease in the predicted service life. The service life increased by about 90% for the seawater exposure and decreased by almost 50% for de-icing salt exposure compared to the service life predicted for the base case. This was due to the fact that, at lower surface concentrations, more time is required for chloride ions to penetrate in sufficient amounts to the depth of the reinforcement to initiate corrosion. The sensitivity of the predicted service life to changes in the C_{se} value can also be observed from Figure 8.16. The higher surface concentrations resulted in higher amounts of chloride concentration at the depth of the reinforcement.

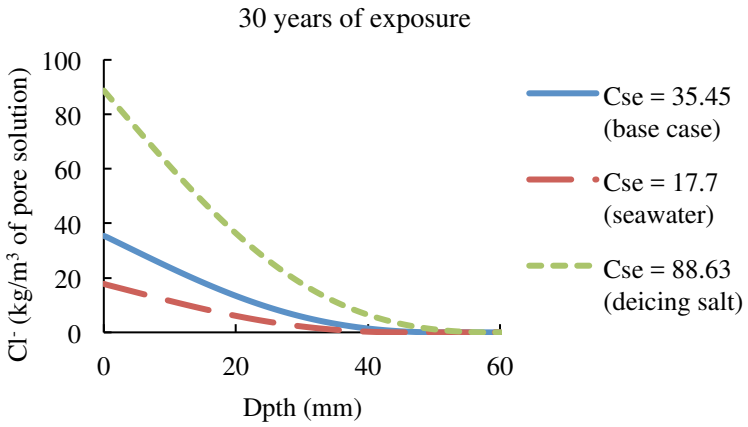

Figure 8.16 Influence of C_{se} on predicted chloride profiles after 30 years of exposure

For background chloride concentration in the pore solution, C_i, the predicted service life was found also to be sensitive to changes in the value of C_i. The current concrete codes and practices prohibit the use of any chloride-contaminated products in concrete to ensure that a long service life is maintained for the structure. The presence of chloride in concrete prior to exposure would increase the risk of reinforcement corrosion and thus shorten the time to corrosion initiation. As can be observed in Figure 8.17, the presence of chloride in the pore solution prior to exposure can significantly increase the level of free chloride concentration at the depth of the reinforcement.

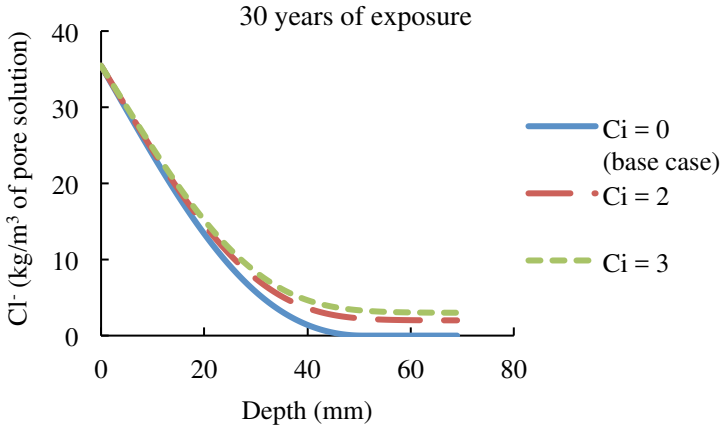

Figure 8.17 Influence of C_i on predicted chloride profiles after 30 years of exposure

Figure 8.18 shows the influence of different exposure temperature values on predicted chloride profiles after 30 years of exposure. As can be seen, the elevated temperature significantly influences the level of chloride concentration at the depth of reinforcement. Higher temperatures result in a significant increase in the penetration depth of the free chloride concentration. This is because the increased temperature accelerates the rate of diffusion, which in turn increases the depth of chloride penetration and reduces the time to corrosion initiation, as shown in Figure 8.13 for 35^{o} C. This implies that the deterioration of concrete structures built in warm climates will be faster than those built in relatively cold regions, given the same concrete properties. Adding the effect of elevated temperature on binding products, as explained in Chapter 7, will make the situation even worse.

Accordingly, precautions should be taken for concrete structures built in warm climates to mitigate such a detrimental effect. One way to do this is to use a high performance concrete with a low w/b ratio and high amount of cementitious materials while maintaining adequate construction practices, as recommended by some concrete codes and practices. This will help to produce a durable concrete with a high resistance to the ingress of chlorides, which can slow the movement of chlorides, reduce the amount of dissolved bound chlorides, and prevent premature deterioration and degradation of concrete structures.

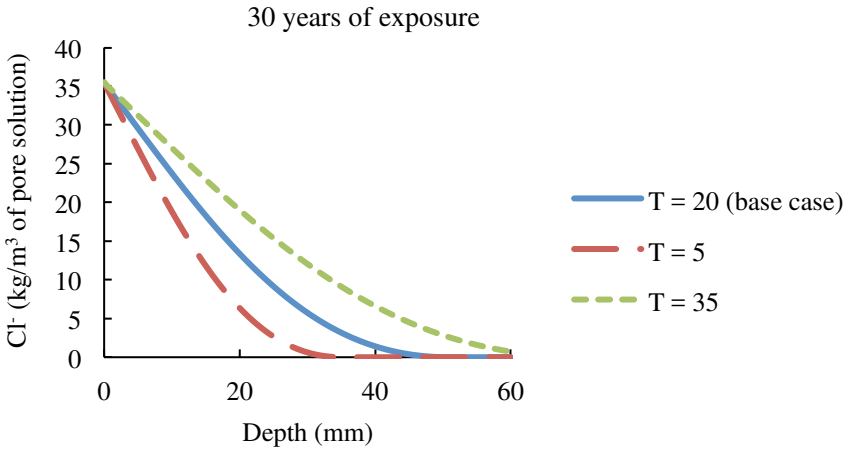

Figure 8.18 Influence of T on predicted chloride profiles after 30 years of exposure

In Chapter 2, it was mentioned that the concrete cover thickness is the first line of defense for reinforced concrete against chloride penetration and attacks. Therefore, the cover thickness is a key parameter in the durability design and redesign of concrete structures exposed to chloride environments. It is clear from the results of this study that inadequate concrete cover thickness would promote corrosion, even if a good quality concrete were provided. When adequate cover thickness is used, carbonation and leaching of alkali hydroxides at the depth of the reinforcement can be prevented, thus, stabilizing the highly alkaline environment at the steel surfaces. In practice, providing a consistent cover thickness over the reinforcement is difficult and in many cases not achievable. Variation in slab cover thickness during construction is a common problem in structures such as bridge decks, parking garages, and marine structures, but inadequate concrete cover can significantly reduce the time to corrosion initiation, which will result in short lifetime expectancy. Figure 8.13 shows that the predicted service life increases as the cover thickness increases. A good correlation has been found between the predicted service life and the concrete cover thickness, as shown in Figure 8.19. Boddy et al. [141] have reported a similar relationship.

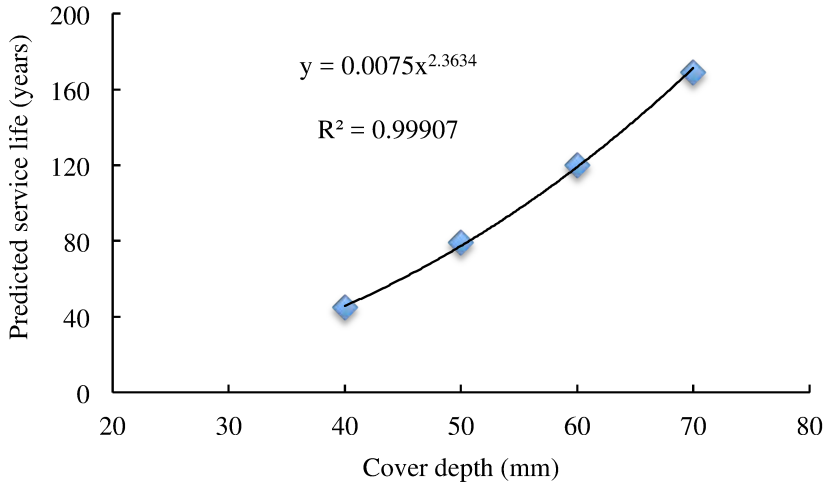

Figure 8.19 Correlation between predicted service life and concrete cover depth

As previously mentioned, the service life of reinforced concrete structures with respect to corrosion is often determined as the time required for chloride ions to reached a critical chloride content at the level of the reinforcement. Therefore, defining a value for the critical amount of chlorides is crucial for service life predictions. However, results reported in the literature with regard to critical chloride content are scattered over a large range. Angst et al. [20]conducted an intensive review study for the critical chloride content in reinforced concrete. They found that the critical chloride content is highly dependent on the technique used to calculate this value. They also found that the chloride threshold is influenced by a number of factors including binder type and content, steel and environmental factors.

Accordingly, they found that the reported critical chloride values for free chloride concentrations vary by an order of magnitude and span from 0.07 to 1.16% by weight of binder. This is quite scattered and can lead to a large discrepancy in the predicted service life. The results of this study showed that the difference between the lower and upper limits of the critical free chloride content, as reported by Angst et al., has led to a 47-year difference in predicted service life. It also has been found that, when other parameters are equal, predicted service life increases linearly as the critical chloride increases, as shown in Figure 8.20. Despite the importance of the C_{crit} parameter and its quantifications, it is

very obvious that its influence on the predicted service life is less pronounced compared to that of m value, temperature and concrete cover, as shown in Figure 8.13.

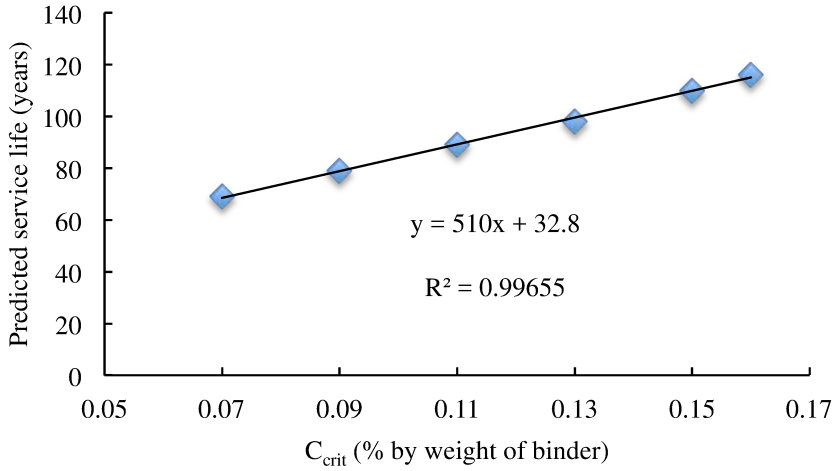

Figure 8.20 Relationship between predicted service life and critical content of free chloride concentration

The results of the parametric study clearly demonstrate that the predicted service life is almost sensitive to all investigated parameters, although the degree of sensitivity varies from one parameter to another. In this study, the sensitivity of the predicted service life to each parameter with respect to the base case is found in the following order (from extreme to least): m_e, T, cover thickness, C_{se}, D_{e28} , C_i and C_{crit}. It must be stressed that the results of this study consider the predicted service life to assume fully saturated concrete, with the chloride transport in concrete taking place due to diffusion process alone. This means that if other transport mechanisms (e.g., convection) are involved, the results might be affected. However, since the diffusion is often considered as the predominating process overall and the convection process is strictly limited to dry surfaces, the results of this study should be reasonably accurate.

9 CONCLUSIONS AND FURTHER RESEARCH

9.1 Summary of the Developed Model

Chloride ingress into concrete is a complicated process and involves numerous material and environmental factors. Chloride binding presents one of the most decisive material factors influencing the ingress of chloride ions into the concrete. Binding removes chloride ions from the pore solution and thus increases the time to corrosion initiation of reinforcement. In many service life prediction models, chloride binding is often assumed to be linear to facilitate and simplify the solution of Fick's second law. However, many researchers have proven that the chloride binding in concrete is nonlinear due to the dependency of the apparent diffusion coefficient on the binding capacity of the concrete, which in turn is influenced by the level of free chloride concentration in the pore solution. In addition, the diffusion coefficient is reported to be dependent on time and temperature. Therefore, for proper service life predictions, the nonlinearity of chloride binding as well as the time and temperature dependency of the effective diffusion coefficient should be taken into account in the modeling process.

In this research, the modified Fick's second law given by Eq. (5.6) was used to account for the nonlinear binding, and Eq. (5.33) was employed to account for the influence of time and temperature on the effective diffusion coefficient. The Freundlich isotherm given by Eq. (5.20) was used to model the nonlinear chloride binding behavior of the concrete. Although the solution of the modified Fick's second law is more complicated and can only be solved numerically due to the dependency of the apparent diffusion coefficient on the level of the free chloride concentration, it provides a more accurate estimation of the service life than that of the simplified Fick's second law form.

The modified Fick's second law was solved in this thesis using a finite difference method, as described in Chapter 5. The nonlinear model developed here allows for the influence of other binding types on the predicted service life to be evaluated. Therefore, the nonlinear model and the nonlinear binding were used to evaluate the influence of the linear binding and where no binding is accounted for at all. The effective diffusion coefficient, chloride

surface concentration, and value of m for the concrete were determined using the experimental data of acid-soluble chloride. The predicted chloride profiles were fit to the experimental acid-soluble profiles using the least-squared method. The results of the nonlinear model were compared to that of the current practice model, such as the error function solution and Life-365, which use the linear binding assumption. The above modeling approach summarizes the main contributions of this thesis.

9.2 General Conclusions

The following general conclusions have been drawn from the results of the nonlinear model:

- Different effective diffusion coefficients resulted when different binding relationships were considered in the nonlinear model. This shows that nonlinear binding resulted in the lowest value of D_{e28} and no binding resulted in the highest.

- The validation results show that the predicted service life of the developed model in the case of linear binding matches very well with those predicted by other linear models of the current practice considered in this thesis.

- The nonlinear model with nonlinear binding relation provided an excellent fit to the experimental data of acid-soluble (total) chloride overall. The linear binding still provides a reasonable estimation of the service life, if the total chloride content is considered to be responsible for the corrosion initiation of the reinforcement. However, if free chloride concentration is used to estimate service life, the linear binding can significantly underestimate the service life of the structure.

- The binding capacity of the concrete is found to be concentration-dependent. It is high at low chloride concentrations and low at high chloride concentrations. The high binding capacity of the nonlinear relation at low chloride concentrations was

found to be responsible for the increased time to corrosion initiation caused by free chloride concentrations in the pore solution.

- Chloride binding has been found to have a significant influence on the shape of the predicted chloride profiles, in particular those of free and bound chlorides.

- The results of the error function solution showed that the time-dependent diffusion coefficient obtained from the effective time method has a significant influence on the predicted service life. It increased the service life by 180% compared to that of the average diffusion coefficient.

- The results of the parametric study demonstrated that the predicted service life is extremely sensitive to the value of the age parameter (m), suggesting that the use of a high volume of cementitious materials such as slag and fly ash in concrete mixture would provide long service life expectancy.

- The predicted service life was found also to be sensitive to changes in other parameters, such as temperature, concrete cover thickness, chloride concentration in the surrounding environment, background chloride, and critical chloride content. Overall, the parametric study suggested that careful determination and proper estimation of the values of these parameters are of great importance for realistic predictions of service life.

Following are some other conclusions drawn from the work presented in this thesis:

- The results of the migration test show that curing conditions have a significant influence on the value of the age parameter. It was found that the value of m increases if the curing temperature and time increased. Therefore, a lengthy curing process at a warm temperature is beneficial for enhancing concrete durability against the ingress of chloride ions.

- Although higher curing temperatures prior to chloride exposure provide a positive influence, elevated temperatures during exposure to chlorides tend to have a negative influence on the concrete's durability. Elevated exposure temperature has been found to increase the concrete's porosity due to its effect on binding products that tend to decompose at higher temperatures.

- The influence of chloride binding on concrete porosity and pore volume was found to be temperature-dependent. The results of a chloride-contaminated concrete sample showed that the elevated temperature ($\geq 40^{o}$ C) resulted in high concrete porosity and pore volume. This was attributed to the instability of binding products at raised temperatures, where chemical binding products tend to dissolve in the pore solution, leaving the pores unfilled. This increases the overall porosity.

- The dependency of binding on the exposure temperature was found to impact the value of the age parameter. The highest value of m was recorded for concrete samples exposed to 22.4^{o} C, followed by those exposed to 6.9^{o} C. However, samples exposed to 40^{o} C revealed the lowest values of m. This would suggest that the chloride binding can only be beneficial to concrete structures built in cold climates where daily average temperatures are cold to moderate and do not exceed 25^{o} C in the summer. However, for structures built in warm climates where the average temperature is 40^{o} C or higher (such as in the Arabian Gulf area), the chloride binding could be detrimental.

- The results of the error function solution showed that the effective time approach yields a reasonable accurate estimation for the value of m, which was in very good agreement with that projected from other models. Therefore, these two methods are recommended for estimating the value of m using the bulk diffusion test.

- The main advantage of using the finite difference method over the error function solution in modeling and predicting concrete structure service life is that the finite difference method can accommodate the influence of temperature on the diffusion coefficient. Furthermore, the resulting instantaneous diffusion coefficient is independent of the testing condition that influences the outcomes when the error function solution approach is used.

9.3 Future Work

From the work presented in this thesis, there are some influencing factors requiring further research and investigations. These investigations may be needed to minimize or reduce the uncertainties in service life predictions for better design and more optimal plans for future inspections and maintenance. The influencing factors that require further investigations include:

- Concrete capillary porosity: Concrete porosity and pore volume evolve over time due to the ongoing hydration of cement paste. The amount of water in these pores is not constant but decreases as the volume of the capillary pores decreases with time. This can have an influence on the projected instantaneous effective chloride diffusion coefficient. In this thesis, the amount of evaporable water present, which is represented in the nonlinear model by the term porosity, was assumed to be constant and unchanging over time. Therefore, including a time-dependent porosity model in the developed model will provide more accurate results for the effective diffusion coefficient and consequently for the predicted service life.

- Binding and temperature dependencies of the value of m: Based on the results of this thesis, it has been found that binding has a significant effect on the value of m due to its impact on the pore structures of the concrete, and that this impact is temperature-dependent. The information obtained from the short-term tests was not sufficient to develop a model or relationship that can describe such an influence in long-term model predictions. Further research and long-term data are

needed before any attempt is made to include this influence in the proposed model.

- Temperature dependency of binding isotherm coefficients: Chloride binding coefficients were obtained for the concrete binder used in this thesis at a constant temperature of 20^{o} C, as suggested by the equilibrium test. However, recent studies have shown that the binding equilibrium is temperature-dependent. Therefore, the binding coefficients, which describe the binding characteristics of a specific cementitious system, can be temperature-dependent. Further research and investigations are needed to identify and establish the relationship between temperature and corresponding binding coefficients.

REFERENCES

[1] Mehta, P., Monteiro, J. M., (2006). Concrete: Microstructure, Properties, and Materials, Third Edition, McGraw-Hill Professional.

[2] Long, A. E., Henderson, G. D. and Montgomery, F. R. (2001). Why assess the properties of near-surface concrete? *Construction and Building Materials,* 15, pp. 65-79.

[3] Status of the Nations Highways and Bridges, (1991). Conditions, performance, and capital Investment requirements. Federal Highway Admisntration.

[4] Stanish, K.D., Hooton, R.D., and Thomas, M.D.A., (1997). Testing the chloride penetration resistance of concrete: A literature review. FHWA Contract DTFH61-97-R-00022 "Prediction of Chloride Penetration in Concrete".

[5] Nilsson, L. (2009). Models for chloride ingress into concrete - From Collepardi to today. *International Journal of Modelling, Identification and Control,* 7, pp. 129-134.

[6] Luping, T. and Gulikers, J. (2007). On the mathematics of time-dependent apparent chloride diffusion coefficient in concrete. *Cement and Concrete Research,* 37, pp. 589-595.

[7] Luping, T. and Nilsson, L. (1993). Chloride binding capacity and binding isotherms of OPC pastes and mortars. *Cement and Concrete Research,* 23, pp. 247-253.

[8] Nokken, M., Boddy, A., Hooton, R. D. and Thomas, M. D. A. (2006). Time dependent diffusion in concrete-three laboratory studies. *Cement and Concrete Research,* 36, pp. 200-207.

[9] Talero, R. and Trusilewicz, L. (2012). Morphological differentiation and crystal growth form of Friedel's salt originated from pozzolan and Portland cement. *Industrial and Engineering Chemistry Research,* 51, pp. 12517-12529.

[10] Larsson, J. (1995). The enrichment of chlorides in expressed concrete pore solution submerged in Saline solution.*Nordic seminar on field studies of chloride initiated reinforcement corrosion in concrete*, pp.171-176.

[11] Hussain, S. E., Rasheeduzzafar, X., Al-Musallam, A. and Al-Gahtani, A. (1995). Factors affecting threshold chloride for reinforcement corrosion in concrete. *Cement and Concrete Research,* 25, pp. 1543-1555.

[12] Mehta, P. K., (1991). Concrete in the marine environment, ELSEVIER SCIENCE PUBLISHERS LTD.

[13] Aït Mokhtar, K., Loche, J-M. Friedmann, H. Amiri, O. Ammar A., (2007). Concrete in marine environment - Steel corrosion in reinforced concrete . MEDACHS - Interreg IIIB Atlantic Space. Report n°2-2, pp. 18-20.

[14] Tuutti, K., (1982). Corrosion of steel in concrete. Swedish Cement Concrete Research Institute,Stockholm, ISSN 0346-6906. 0346-6906.

[15] Carino, N. J. (1999). Nondestructive techniques to investigate corrosion status in concrete structures. *Journal of Performance of Constructed Facilities,* 13, pp. 96-106.

[16] Bentur, A., Diamond, S., & Berke, (1997). Steel corrosion in concrete: Fundamentals and civil engineering practice.

[17] Kropp, J. and Hilsdorf, H.K., (1995). RILEM report 12 - Performance criteria for concrete durability
 . E & FN SPON. No 12.

[18] Hausman D.A.,. (1967). Steel corrosion in concrete. *Material Protection,* 6(11), pp. 19-22.

[19] Bamforth, P. (1996). Predicting the risk of reinforcement corrosion in marine structures. *Corrosion Prevention and Control,* 43, pp. 91-100.

[20] Angst, U., Elsener, B., Larsen, C. K. and Vennesland, O. (2009). Critical chloride content in reinforced concrete - A review. *Cement and Concrete Research,* 39, pp. 1122-1138.

[21] Alkailani, O., (2006). Development of fiber reinforced self-consolidating concrete for marine structures in hot environments. M.A.Sc Thesis, Dalhousie University.

[22] Fidjestöl, P. and Tuutti, K. (1995). The importance of chloirde diffusion.*RILEM International workshop on Chloride Pen€tration into Concret*.

[23] Karlsson, M. and Poulsen, E. (1995). Design of rebar concrete covers in marine concrete structures – probabilistic approach.*RILEM Workshop, StRemy-les-Chevreuse*.

[24] Poulsen, Ervin.,Mejlbro, Leif., (2006). Diffusion of chloride in concrete : theory and application.

[25] Kamal Hossain and Liping Fu, (2014). Optimal snow and ice control of parking lots and sidewalks. 2014.

[26] Tang, L. (1999). Concentration dependence of diffusion and migration of chloride ions Part 1. Theoretical considerations. *Cement and Concrete Research,* 29, pp. 1463-1468.

[27] Nilsson, L.O. Massat, M. and Tang, L. (1994). The effect of non-linear chloride binding on the prediction of chloride penetration into concrete structures. *ACI SP 145 - 24,* 145, pp. 469 - 486.

[28] Nilsson, L.O., Poulsen, E., Sandberg, P., Sorenesen, Klinghoffer, O., (1996). HETEK, chloride penetration into concrete, state-of-the-Art, transportation processes, corrosion initiation, test methods and prediction models. Road Directorate. No.53.

[29] Thomas, M. D. A., Hooton, R. D., Scott, A. and Zibara, H. (2012). The effect of supplementary cementitious materials on chloride binding in hardened cement paste. *Cement and Concrete Research,* 42, pp. 1-7.

[30] Ann, K. Y., Ahn, J. H. and Ryou, J. S. (2009). The importance of chloride content at the concrete surface in assessing the time to corrosion of steel in concrete structures. *Construction and Building Materials,* 23, pp. 239-245.

[31] Sandberg, P. (1999). Studies of chloride binding in concrete exposed in a marine environment. *Cement and Concrete Research,* 29, pp. 473-477.

[32] Suryavanshi, A. K., Scantlebury, J. D. and Lyon, S. B. (1996). Mechanism of Friedel's salt formation in cements rich in tri-calcium aluminate. *Cement and Concrete Research,* 26, pp. 717-727.

[33] Arya, C., Buenfeld, N. R. and Newman, J. B. (1990). Factors influencing chloride-binding in concrete. *Cement and Concrete Research,* 20, 291-300.

[34] Zibara, H., (2001). Binding of External Chlorides by Cement Pastes, Ph.D. dissertation, Univ. of Toronto, Toronto, Ontario, Canada.

[35] Murthi, P. and Sivakumar, V. (2008). Strength-porosity relationship for ternary blended concrete. *Indian Concrete Journal,* 82, pp. 35-41.

[36] Jones, M. R., Dhir, R. K. and Magee, B. J. (1997). Concrete containing ternary blended binders: Resistance to chloride ingress and carbonation. *Cement and Concrete Research,* 27, pp. 825-831.

[37] Byfors, K. (1986). Chloride binding in cement paste. *Nordic concrete research,* pp. 27-38.

[38] Byfors, K. (1987). Influence of silica fume and fly ash on chloride diffusion and pH values in cement paste. *Cement and Concrete Research,* 17, pp. 115-130.

[39] Song, L., Sun, W. and Gao, J. (2012). Effect of W/B to the time dependent chloride diffusion in concrete with GGBS.*2nd International Conference on Civil Engineering, Architecture and Building Materials, CEABM 2012, May 25, 2012 - May 27*, pp. 144-147.

[40] Page, C. L., Short, N. R. and El Tarras, A. (1981). Diffusion of chloride ions in hardened cement pastes. *Cement and Concrete Research,* 11, pp. 395-406.

[41] Chalee, W. and Jaturapitakkul, C. (2009). Effects of W/B ratios and fly ash finenesses on chloride diffusion coefficient of concrete in marine environment. *Materials and Structures/Materiaux et Constructions,* 42, pp. 505-514.

[42] Audenaert, K., Yuan, Q. and De Schutter, G. (2010). On the time dependency of the chloride migration coefficient in concrete. *Construction and Building Materials,* 24, pp. 396-402.

[43] Cheng, Y., Karmiadji, I. W. Z. and Huang, W. (2011). The effect of time dependent chloride diffusion coefficient on the chloride ingress in concrete.*2011 International Conference on Electric Technology and Civil Engineering, ICETCE 2011, April 22, 2011 - April 24*, pp.7098-7101.

[44] L. Tang, H. E. Sørensen. (2001). Precision of the Nordic test methods for measuring the chloride diffusion/migration coefficients of concrete. *Materials and Structures, RILEM Publications SARL,* 34, pp. 479 - 485.

[45] Shi, X., Xie, N., Fortune, K. and Gong, J. (2012). Durability of steel reinforced concrete in chloride environments: An overview. *Construction and Building Materials,* 30, pp. 125-138.

[46] Thomas, M. D. A., Shehata, M. H., Shashiprakash, S. G., Hopkins, D. S. and Cail, K. (1999). Use of ternary cementitious systems containing silica fume and fly ash in concrete. *Cement and Concrete Research,* 29, pp. 1207-1214.

[47] Mangat, P. S., Khatib, J. M. and Molloy, B. T. (1994). Microstructure, chloride diffusion and reinforcement corrosion in blended cement paste and concrete. *Cement and Concrete Composites,* 16, pp. 73-81.

[48] Chung, C., Shon, C. and Kim, Y. (2010). Chloride ion diffusivity of fly ash and silica fume concretes exposed to freeze-thaw cycles. *Construction and Building Materials,* 24, pp. 1739-1745.

[49] Yu, Z. and Ye, G. (2013). The pore structure of cement paste blended with fly ash. *Construction and Building Materials,* 45, pp. 30-35.

[50] Shekarchi, M., Rafiee, A. and Layssi, H. (2009). Long-term chloride diffusion in silica fume concrete in harsh marine climates. *Cement and Concrete Composites,* 31, pp. 769-775.

[51] Pavlik, Z., Pavlikova, M., Fiala, L., Beneova, H., Mihulka, J. and Cerny, R. (2010). Effect of slag on chloride transport and storage properties of HPC.*6th International Conference on Concrete under Severe Conditions-Environment and Loading, CONSEC'10*, pp.1497-1504.

[52] Dhir, R. K. and Jones, M. R. (1999). Development of chloride-resisting concrete using fly ash. *Fuel,* 78, pp. 137-142.

[53] Dhir, R. K., El-Mohr, M. and Dyer, T. D. (1996). Chloride binding in GGBS concrete. *Cement and Concrete Research,* 26, pp. 1767-1773.

[54] Hossain, K. M. A. (2005). Correlations between porosity, chloride diffusivity and electrical resistivity in volcanic pumice-based blended cement pastes. *Advances in Cement Research,* 17, pp. 29-37.

[55] Burris, L. E. and Riding, K. A. (2014). Diffusivity of binary and ternary concrete mixture blends. *ACI Materials Journal,* 111, pp. 373-382.

[56] Daube, J., and Bakker, R. (1986). Portland blast-furnace slag cement: A review in blended , Cements. *Ed. G. Frohnsdorff, ASTM Sp. Tech,* 897, pp. 5 - 15.

[57] Hossain, A. B., Shrestha, S. and Summers, J. (2009). Properties of concrete incorporating ultrafine fly ash and silica fume. *Transportation Research Record,* pp. 41-46.

[58] Riding, K. A., Thomas, M. D. A. and Folliard, K. J. (2013). Apparent diffusivity model for concrete containing supplementary cementitious materials. *ACI Materials Journal,* 110, 705-713.

[59] Hoshino, M. (1989). Relationship between bleeding, coarse aggregate, and specimen height of concrete. *ACI Materials Journal,* 86, pp. 185-190.

[60] Aldred, J. M., (1988). Hydrophobic poreblocking ingredient in concrete. Concrete International. 52-57.

[61] Griffiths, D., Marosszeky, M. and Sade, D. (1987). Site study of Ffactors leading to a reduction in durability of reinforced concrete. *ACI Special Publication,* 100, pp. 1703-1726.

[62] Mangat, P. S. and Molloy, B. T. (1994). Prediction of long term chloride concentration in concrete. *Materials and Structures,* 27, pp. 338 - 346.

[63] ACI Committee 308, (2001). Guide to Curing Concrete.

[64] Song, H., Lee, C. and Ann, K. Y. (2008). Factors influencing chloride transport in concrete structures exposed to marine environments. *Cement and Concrete Composites,* 30, pp. 113-121.

[65] Song, H., Shim, H., Petcherdchoo, A. and Park, S. (2009). Service life prediction of repaired concrete structures under chloride environment using finite difference method. *Cement and Concrete Composites,* 31, pp. 120-127.

[66] Song, L., Sun, W. and Gao, J. (2013). Time dependent chloride diffusion coefficient in concrete. *Journal Wuhan University of Technology, Materials Science Edition,* 28, pp. 314-319.

[67] Ann, K. Y., Song, H., Lee, C. and Lee, K. C. (2006). Build-up of surface chloride and its influence on corrosion initiation time of steel in concrete.*10th East Asia-Pacific Conference on Structural Engineering and Construction, EASEC 2010*, pp.767-772.

[68] Pack, S., Jung, M., Song, H., Kim, S. and Ann, K. Y. (2010). Prediction of time dependent chloride transport in concrete structures exposed to a marine environment. *Cement and Concrete Research,* 40, pp. 302-312.

[69] Costa, A. and Appleton, J. (1999). Chloride penetration into concrete in marine environment - Part I: Main parameters affecting chloride penetration. *Materials and Structures/Materiaux et Constructions,* 32, pp. 252-259.

[70] Thomas, M. D. A. and Bamforth, P. B. (1999). Modelling chloride diffusion in concrete effect of fly ash and slag. *Cement and Concrete Research,* 29, pp. 487-495.

[71] Song, L., Sun, W., Gao, J. and Zhang, Y. (2011). Influence on GGBS to time dependent chloride diffusion coefficient of HPC.*1st International Conference on Civil Engineering, Architecture and Building Materials, CEABM 2011*, pp.5703-5710.

[72] Song, L., Sun, W. and Gao, J. (2013). Time dependent chloride diffusion coefficient in concrete. *Journal Wuhan University of Technology, Materials Science Edition,* 28, pp. 314-319.

[73] Takewaka, K. and Mastumoto, S. (1988). Quality and cover thickness of concrete based on the estimation of chloride penetration in marine environments. *ACI SP 109-17,* 109, pp. 381-400.

[74] Uji, K., Matsuaka, Y., and Maruya, T. (1990). Fourmulation of an equation for surface chloride content due to permeation of chloride.*Proceeding of the Tird Inernational Symposion on Corrosion of Reinforcement in Concrete Construction*, pp.258 - 267.

[75] Dhir, R. K., Jones, M. R. and Elghaly, A. E. (1993). PFA concrete: exposure temperature effects on chloride diffusion. *Cement and Concrete Research,* 23, pp. 1105-1114.

[76] Yuan, Q., Shi, C., De Schutter, G. and Audenaert, K. (2009). Effect of temperature on transport of chloride ions in concrete.*2nd International Conference on Concrete Repair, Rehabilitation and Retrofitting, ICCRRR 2008*, pp.159-160.

[77] Yuan,Q., Schutter, G., Shi, C., Audenaert, K.,. (2008). The relationship between chloride diffusion and migration coefficients in concrete.*1st International Conference on Microstructure Related Durability of Cementitious Composities*, pp.553 - 563.

[78] Luping, T. (1996). Chloride transport in concrete - measurement and prediction. *Doktorsavhandlingar vid Chalmers Tekniska Hogskola, .*

[79] Truc, O., (2000). Prediction of Chloride Penetration into Saturated Concrete – Multi-species Approach.

[80] Hauck, C., (1993). The effect of curing temperature and silica fume on chloride migration and pore structure of high performance concrete. Department of Structural Technology, NTH, Trondheim, Norway.

[81] Mohammed, T. U. and Hamada, H. (2003). Relationship between free chloride and total chloride contents in concrete. *Cement and Concrete Research,* 33, pp. 1487-1490.

[82] Lu, X., Li, C. and Zhang, H. (2002). Relationship between the free and total chloride diffusivity in concrete. *Cement and Concrete Research,* 32, pp. 323-326.

[83] Lu, X., Mohammed, T. U. and Hamada, H. (2003). A discussion of the paper "Relationship between the free and total chloride diffusivity in concrete" by Xinying Lu, Cuiling Li, and Haixia Zhang 1] (multiple letters). *Cement and Concrete Research,* 33, pp. 451-453.

[84] Luping, T. and Nilsson, L. (1992). Rapid determination of the chloride diffusivity in concrete by applying an electrical field. *ACI Materials Journal,* 89, pp. 40-53.

[85] Stanish, K. and Thomas, M. (2003). The use of bulk diffusion tests to establish time-dependent concrete chloride diffusion coefficients. *Cement and Concrete Research,* 33, pp. 55-62.

[86] Yuan, Q., Shi, C., De Schutter, G., Audenaert, K. and Deng, D. (2009). Chloride binding of cement-based materials subjected to external chloride environment - A review. *Construction and Building Materials,* 23, pp. 1-13.

[87] Yuan, Q., Deng, D., Shi, C. and De Schutter, G. (2013). Chloride binding isotherm from migration and diffusion tests. *Journal Wuhan University of Technology, Materials Science Edition,* 28, pp. 548-556.

[88] Florea, M. V. A. and Brouwers, H. J. H. (2012). Chloride binding related to hydration products: Part I: Ordinary Portland Cement. *Cement and Concrete Research,* 42, pp. 282-290.

[89] Li, Q. (2015). Chemical composition and microstructure of hydration products of hardened white portland cement pastes containing admixtures. *Journal Wuhan University of Technology, Materials Science Edition,* 30, pp. 758-767.

[90] Glass, G. K., Reddy, B. and Buenfeld, N. R. (2000). The participation of bound chloride in passive film breakdown on steel in concrete. *Corrosion Science,* 42, pp. 2013-2021.

[91] Birnin-Yauri, U. and Glasser, F. P. (1998). Friedel's salt, Ca2Al(OH)6(Cl,OH)&middot2H2O: Its solid solutions and their role in chloride binding. *Cement and Concrete Research,* 28, pp. 1713-1723.

[92] Neville, A. M., (1996). Properties of Concrete, Forth Edition, PEARSON Prentice Hall.

[93] Suryavanshi, A. K., Scantlebury, J. D. and Lyon, S. B. (1998). Corrosion of reinforcement steel embedded in high water-cement ratio concrete contaminated with chloride. *Cement and Concrete Composites,* 20, pp. 263-281.

[94] Kayyali, O. A. and Haque, M. N. (1995). Cl-/OH- ratio in chloride-contaminated concrete - a most important criterion. *Magazine of Concrete Research,* 47, pp. 235-242.

[95] Martin-Perez, B., Zibara, H., Hooton, R. D. and Thomas, M. D. A. (2000). Study of the effect of chloride binding on service life predictions. *Cement and Concrete Research,* 30, pp. 1215-1223.

[96] Nilsson, L. O., Poulson, E., Sandberg, P., Sorensen, H. E., Klinghoffer, O., Fredriksen, J. M., (1996). HETEK Chloride penetration into concrete, state-of- the-Art, transport processes, corrosion initiation, test methods and prediction models. vol. 53, pp. 151.

[97] Reddy, B., (2001). Influence of the Steel-Concrete Interface on the Chloride Threshold Level. University of London.

[98] Jin, Z., Sun, W., Zhao, T. and Li, Q. (2009). Chloride binding in concrete exposed to corrosive solutions. *Kuei Suan Jen Hsueh Pao/ Journal of the Chinese Ceramic Society,* 37, pp. 1068-1078.

[99] Rasheeduzzafar, S., Hussain, E. and Al-Saadoun, S. (1991). Effect of cement composition on chloride binding and corrosion of reinforcing steel in concrete. *Cement and Concrete Research,* 21, pp. 777-794.

[100] Arya, C., Buenfeld, N. R. and Newman, J. B. (1990). Factors influencing chloride-binding in concrete. *Cement and Concrete Research,* 20, pp. 291-300.

[101] Rasheeduzzafar, Ehtesham Hussain, S. and Al-Saadoun, S. (1992). Effect of tricalcium aluminate content of cement on chloride binding and corrosion of reinforcing steel in concrete. *ACI Materials Journal,* 89, pp. 3-12.

[102] Beaudoin, J. J., Ramachandran, V. S. and Feldman, R. F. (1990). Interaction of chloride and C-S-H. *Cement and Concrete Research,* 20, pp. 875-883.

[103] Ramachandran, V. S. (1971). Possible states of chloride in the hydration of tricalcium silicate in the presence of calcium chloride. 4, pp. 3-12.

[104] Zibara, H., Hooton, R. D., Thomas, M. D. A. and Stanish, K. (2008). Influence of the C/S and C/A Ratios of Hydration Products on the Chloride Ion Binding Capacity of Lime-SF and Lime-MK Mixtures. *Cement and Concrete Research,* 38, pp. 422-426.

[105] Ishida, T., Miyahara, S. and Maruya, T. (2008). Chloride binding capacity of mortars made with various Portland cements and mineral admixtures. *Journal of Advanced Concrete Technology,* 6, pp. 287-301.

[106] Tan, K. and Cao, Q. (2011). Chloride binding of cementitious pastes. *International Conference on Advances in Materials and Manufacturing Processes, ICAMMP 2010*, pp.363-367.

[107] Bleszynski, R., Hooton, R. D., Thomas, M. D. A. and Rogers, C. A. (2002). Durability of ternary blend concrete with silica fume and blast-furnace slag: Laboratory and outdoor exposure site studies. *ACI Materials Journal,* 99, pp. 499-508.

[108] Hussain, E. S., Rasheeduzzafar and Al-Gahtani, A. (1994). Influence of sulfates on chloride binding in cements. *Cement and Concrete Research,* 24, pp. 8-24.

[109] Xu, Y. (1997). Influence of sulphates on chloride binding and pore solution chemistry. *Cement and Concrete Research,* 27, pp. 1841-1850.

[110] Hussain, S. E. (1993). Effect of temperature on pore solution composition in plain cements. *Cement and Concrete Research,* 23, pp. 1357-1368.

[111] Roberts MH, (1962). Effect of calcium chloride on the durability of pretensioned wire in prestressed concrete. Mag Concr Res. 14(42), pp. 143 -1 54.

[112] Nguyen, T. S., Lorente, S. and Carcasses, M. (2009). Effect of the environment temperature on the chloride diffusion through CEM-I and CEM-V mortars: An experimental study. *Construction and Building Materials,* 23, pp. 795-803.

[113] Dousti, A. and Shekarchi, M. (2015). Effect of exposure temperature on chloride-binding capacity of cementing materials. *Magazine of Concrete Research,* 67, 821-832.

[114] Wan, X., Wittmann, F. H., Zhao, T. and Fan, H. (2013). Chloride content and pH value in the pore solution of concrete under carbonation. *Journal of Zhejiang University: Science A,* 14, pp. 71-78.

[115] Suryavanshi, A. K. and Narayan Swamy, R. (1996). Stability of Friedel's salt in carbonated concrete structural elements. *Cement and Concrete Research,* 26, pp. 729-741.

[116] Sandberg, P., (1995). Critical Evaluation of Factors Affecting Chloride-Initiated Reinforcement Corrosion in Concrete. TVBM-7088.

[117] Page, C. L. and Lambert, P. and Vassie, P. R. W. (1991). Investigations of reinforcement corrosion 1. The pore electrolyte phase in chloride-contaminated concrete. *Materials and Structures,* 24, pp. 243-252.

[118] Tritthart, J. (1989). Chloride binding in cement. II. The influence of the hydroxide concentration in the pore solution of hardened cement paste on chloride binding. *Cement and Concrete Research,* 19, pp. 683-691.

[119] Blunk G, Gunkel P, Smolczyk HG. (1986). On the distribution of chloride between the hardening cement paste and its pore solution.*Proceedings of the 8th international congress on the chemistry of cement*, pp.85 - 90.

[120] Rasheeduzzafar. (1992). Influence of cement composition on concrete durability. *ACI Materials Journal,* 89, pp. 574-586.

[121] Kumar, R. and Bhattacharjee, B. (2003). Porosity, pore size distribution and in situ strength of concrete. *Cement and Concrete Research,* 33, pp. 155-164.

[122] Hope, B. B., Page, J. A. and Poland, J. S. (1985). Determination of the Chloride Content of Concrete. *Cement and Concrete Research,* 15, pp. 863-870.

[123] Delagrave, A., Marchand, J., Ollivier, J., Julien, S. and Hazrati, K. (1997). Chloride binding capacity of various hydrated cement paste systems. *Advanced Cement Based Materials,* 6, 28-35.

[124] Akita, H. and Fujiwara, T. (1995). Water and salt movement within mortar partially submerged in salty water.*Proceeding of the international conference on concrete under sever conditions*London.

[125] Pereira, C. J. and Hagedus, L. L. (1984). Diffusion and reaction of chloride ions in porous concrete.*ISCRE 8*, pp.427-438.

[126] Xu, A. (1990). The structure and some physical and properties of cement mortar with fly ash. Department of Building Materials Chalmers University of Technology, Goteborg, Sweden.

[127] Glass, G. K., Stevenson, G. M. and Buenfeld, N. R. (1998). Chloride-binding isotherms from the diffusion cell test. *Cement and Concrete Research,* 28, pp. 939-945.

[128] Andrade, C., Bettencourt-Ribeiro, A., Buenfeld, N. R., et al. (1999). Concrete durability - an approach towards performance testing. *Materials and Structures/Materiaux et Constructions,* 32, pp. 163-173.

[129] Castellote, M., Andrade, C. and Alonso, C. (1999). Chloride-binding isotherms in concrete submitted to non-steady-state migration experiments. *Cement and Concrete Research,* 29, pp. 1799-1806.

[130] Ollivier JP, Arsenault J, Truc O, Marchand J. (1997). Determination of chloride binding isotherms from migration tests. *Mario Collepardi symposium on advances in concrete science and technology,* pp. 198 - 217.

[131] Masi, M., Colella, D., Radaelli, G. and Bertolini, L. (1997). Simulation of chloride penetration in cement-based materials. *Cement and Concrete Research,* 27, pp. 1591-1601.

[132] Henchi, K., Samson, E., Chapdelaine, F. and Marchand, J. (2007). Advanced finite-element predictive model for the service life prediction of concrete infrastructures in support of asset management and decision-making.*2007 ASCE International Workshop on Computing in Civil Engineering,* pp.870-880.

[133] Fredriksen, J. M., Mejlbro, L. and Poulson, E. (2000). The HETEK model of chloride ingress into concrete made simpler by approximations.*Testing and Modelling the Chloride Ingress into Concrete, Proceedings of the 2nd International RILEM Workshop*, pp.317 - 336.

[134] Maage, M., Helland, S., Poulsen, E., Vennesland, O. and Carlsen, J. E. (1996). Service life prediction of existing concrete structures exposed to marine environment. *ACI Materials Journal,* 93, pp. 602-608.

[135] Collepardi, M., Marcialis, A. and Turriziani, R. (1972). Penetration of chloride ions into cement pastes and concretes. *Journal of the American Ceramic Society,* 55, pp. 524 - 535.

[136] Poulsen, E. (1993). On a model of chloride ingress into concrete having time dependent diffusion coefficient.*Nordic Miniseminar on Chloride Penetration into Concrete*(pp.1 - 12).

[137] Hooton, R. D., Geiker, M. R. and Bentz, E. C. (2002). Effects of curing on chloride ingress and implications on service life. *ACI Materials Journal,* 99, pp. 201-206.

[138] Andrade, C., Castellote, M. and D'Andrea, R. (2011). Measurement of ageing effect on chloride diffusion coefficients in cementitious matrices. *Journal of Nuclear Materials,* 412, pp. 209-216.

[139] Luping, T. and Nilsson, L. (1992). Chloride diffusivity in high strength concrete at different ages. *Nordic Concrete Research,* pp. 162-162.

[140] Bamforth, P. B. (1998). Spreadsheet model for reinforcement corrosion in structures exposed to chlorides.*Concrete Under Severe Conditions 2,* pp.64-75

[141] Boddy, A., Bentz, E., Thomas, M. D. A. and Hooton, R. D. (1999). Overview and sensitivity study of a multimechanistic chloride transport model. *Cement and Concrete Research,* 29, pp. 827-837.

[142] Nilsson, L. -. (2006). Present limitations of models for predicting chloride ingress into reinforced concrete structures.*International Workshop NUCPERF 2006: Corrosion and Long Term Performance of Concrete in NPP and Waste Facilities,* pp.123-130.

[143] Yuan, Q., Shi, C., De Schutter, G. and Audenaert, K. (2009). Effect of temperature on transport of chloride ions in concrete.*2nd International Conference on Concrete Repair, Rehabilitation and Retrofitting, ICCRRR 2008,* pp.159-160.

[144] Delagrave, A., Marchand, J., Ollivier, J., Julien, S. and Hazrati, K. (1997). Chloride Binding Capacity of Carious Hydrated Cement Paste Systems. *Advanced Cement Based Materials,* 6, pp. 28-35.

[145] Smith, G. D., (1965). Numerical solution of partial differential equations. Oxford University Press, Amen House, London E.C.4.

[146] John. Crank, (1975). The mathematics of diffusion.

[147] Schindler, A. K. (2004). Effect of temperature on hydration of cementitious materials. *ACI Materials Journal,* 101, pp. 72-81.

[148] Glass, GK and Buenfeld, NR. (1997). Chloride threshold levels for corrosion induced deterioration of steel in concrete.*RILEM*, pp.429-440.

[149] Das, B. B. and Kondraivendhan, B. (2012). Implication of pore size distribution parameters on compressive strength, permeability and hydraulic diffusivity of concrete. *Construction and Building Materials,* 28, pp. 382-386.

[150] Chan, S. Y. N., Luo, X. and Sun, W. (2000). Effect of high temperature and cooling regimes on the compressive strength and pore properties of high performance concrete. *Construction and Building Materials,* 14, pp. 261-266.

[151] Verbeck, G. J. and Helmuth, R. A. (1968). Structure and physical properties of cement paste. *Chemistry of Cement,* 3, pp. 132-137.

[152] Bouikni, A., Swamy, R. N. and Bali, A. (2009). Durability properties of concrete containing 50% and 65% slag. *Construction and Building Materials,* 23, pp. 2836-2845.

[153] Rapin, J. -., Renaudin, G., Elkaim, E. and Francois, M. (2002). Structural transition of Friedel's salt 3CaO&middotAl2O3&middotCaCl2&middot10H2 O studied by synchrotron powder diffraction. *Cement and Concrete Research,* 32, pp. 513-519.

[154] Panesar, D. K. and Chidiac, S. E. (2012). Effect of cold temperature on the chloride-binding capacity of cement. *Journal of Cold Regions Engineering,* 25, 133-144.

[155] Tuutti, K. (1982). Analysis of pore solution squeezed out of cement paste and mortar. *Nordic Concrete Research,* 25. pp.1-25.

[156] Ramachandran, V. S., Seeley, R. C. and Polomark, G. M. (1984). Free and combined chloride in hydrating cement and cement components. *Materiaux et constructions,* 17, pp. 285-289.

[157] Song, H. W., Lee, C. H., Jung, M. S. and Ann, K. Y. (2008). Development of Chloride Binding Capacity in Cement Pastes and Influence of the pH of Hydration Products. *Canadian Journal of Civil Engineering,* 35, pp. 1427-1434.

[158] Ipavec, A., Vuk, T., Gabrovek, R. and Kaucic, V. (2013). Chloride binding into hydrated blended cements: The influence of limestone and alkalinity. *Cement and Concrete Research,* 48, pp. 74-85.

[159] Hirao, H., Yamada, K., Takahashi, H. and Zibara, H. (2005). Chloride binding of cement estimated by binding isotherms of hydrates. *Journal of Advanced Concrete Technology,* 3, pp. 77-84.

[160] Nguyen, T. S., Lorente, S. and Carcasses, M. (2006). Influence of the temperature on the chloride transport through cementitious materials.*International Workshop NUCPERF 2006: Corrosion and Long Term Performance of Concrete in NPP and Waste Facilities,* pp.63-70.

[161] Dousti, A., Rashetnia, R., Ahmadi, B. and Shekarchi, M. (2013). Influence of exposure temperature on chloride diffusion in concretes incorporating silica fume or natural zeolite. *Construction and Building Materials,* 49, pp. 393-399.

[162] Yu, S. W., Sergi, G. and Page, C. L. (1993). Ionic diffusion across an interface between chloride-free and chloride-containing cementitious materials. *Magazine of Concrete Research,* 45, pp. 257-261.

[163] Glass, G. K., Wang, Y. and Buenfeld, N. R. (1996). Investigation of experimental methods used to determine free and total chloride contents. *Cement and Concrete Research,* 26, pp. 1443-1449.

[164] Care, S. (2008). Effect of temperature on porosity and on chloride diffusion in cement pastes. *Construction and Building Materials,* 22, pp. 1560-1573.

[165] Akita, H. and Fujiwara, T. (1995). Water and salt movement within mortar partially submerged in salty water.*Concrete under sever Conditions*, pp.645 - 654.

[166] Massata, M., Nilsson, L. O. and and Ollivier, J. P. (1992). Clarification of the fundamental relationships concerning ion diffusion in porous materials.*Third International Colloquium on Materials Science and Restoration*, pp.15-17.

[167] Clima Temps, Halifax, Nova Scptia climate and temperature. http://www. halifax. climatemps. com/temperatures. php. 2016.

APPENDIX (A) Rapid Migration Test Result

Chloride migration test results – 6.9^{o} C

Age of Concrete (days)	w/c	Curring T (^{o}C)	Sample No.	U (v)	T (^{o}C)	L (mm)	X_d (mm)	t (hrs)	D_{nssm} x10^{-12} m^2/s	Average D_{nssm} x10^{-12} m^2/s
84	0.32	6.9	1	29.5	18.5	49.1	5.21	24	2.1	2.08
			2	29.5	19.5	50	5.23	24	2.1	
			3	29.5	19.5	49.1	5.26	24	2.1	
118	0.32	6.9	1	40	21	48.8	5.99	24	1.8	1.88
			2	40	20.9	47.8	6.33	24	1.9	
			3	40	20.9	48	6.31	24	1.9	
208	0.32	6.9	1	50	21	48.5	6.61	24	1.6	1.57
			2	50	20.5	50.6	6.26	24	1.6	
			3	50	21.5	48.9	5.86	24	1.5	

Chloride migration test results – 22.4^{o} C

Age of Concrete (days)	w/c	Curring T (^{o}C)	Sample No.	U (v)	T (^{o}C)	L (mm)	X_d (mm)	t (hrs)	D_{nssm} x10^{-12} m^2/s	Average D_{nssm} x10^{-12} m^2/s
28	0.32	21	1	30.04	19.5	46	6.09	24	2.3	2.59
			2	30.04	20.5	47	7.32	24	2.9	
			3	30.04	20	47	6.68	24	2.6	
84	0.32	22.4	1	30.04	18.5	49.4	3.79	24	1.4	1.42
			2	30.04	18.5	50.5	4.06	24	1.5	
			3	30.04	18.5	49.5	3.55	24	1.3	
118	0.32	22.4	1	60	18.5	49	5.53	24	1.1	1.25
			2	60	18.5	47.8	6.37	24	1.3	
			3	60	19	47.8	6.36	24	1.3	
208	0.32	22.4	1	60	18.5	48.1	4.94	24	1.0	1.014
			2	60	18	49.8	5.01	24	1.0	
			3	60	19.5	49	4.96	24	1.0	

Chloride migration test results – 40^{o} C

Age of Concrete (days)	w/c	Curring T (^{o}C)	Sample No.	U (v)	T (^{o}C)	L (mm)	Xd (mm)	t (hrs)	D_{nssm} x10^{-12} m^2/s	Average D_{nssm} x10^{-12} m^2/s
84	0.32	40	1	29.96	18.5	49.9	3.23	24	1.2	1.34
			2	29.96	18.5	49.9	3.37	24	1.2	
			3	29.96	18.5	49.8	4.26	24	1.6	
118	0.32	40	1	60	19	49.1	5.59	24	1.2	1.14
			2	60	18	48.7	5.5	24	1.1	
			-	-	-	-	-	-	-	
208	0.32	40	1	60	18.75	48.6	3.82	24	0.8	0.88
			2	60	19	48.7	3.75	24	0.7	
			3	50	22	48.4	4.77	24	1.1	

APPENDIX (B) Bulk Diffusion Test Results

Water-soluble Test Results: solution temperature 6.9° C

56 days of exposure

Depth (mm)	Chloride concentration per sample (% by weight of concrete)			
	A	B	C	Avg.
0.5	1.182	0.985	1.014	1.060
1.5	0.523	0.53	0.514	0.522
2.5	0.407	0.424	0.396	0.409
3.5	0.331	0.378	0.184	0.298
4.5	0.24	0.229	0.154	0.208
5.5	0.159	0.053	0.05	0.087
6.5	0.055	0.046	0.046	0.049
7.5	0.038	0.026	0.036	0.033
8.5	0.021	0.026	0.022	0.023
9.5	0.019	0.018	0.018	0.018

Water-soluble experimental data: 6.9 °C - 56 days

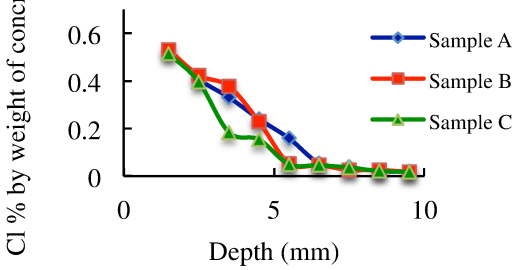

Water-soluble experimental data: 6.9 °C - 90 days

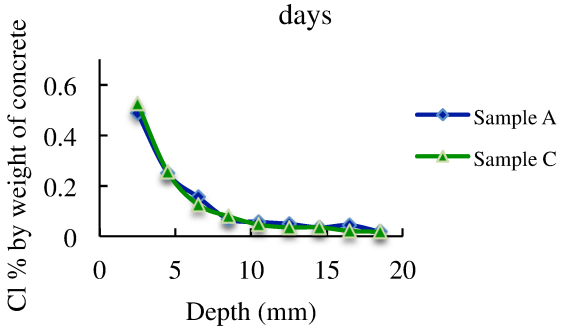

90 days of exposure

Depth (mm)	Chloride concentration per sample (% by weight of concrete)			
	A	B	C	Avg.
0.5	0.797	0.912	0.883	0.864
2.5	0.488	0.574	0.525	0.529
4.5	0.25	0.364	0.254	0.289
6.5	0.155	0.129	0.125	0.136
8.5	0.068	NaN	0.079	0.074
10.5	0.057	NaN	0.046	0.052
12.5	0.049	0.039	0.035	0.041
14.5	0.035	NaN	0.035	0.035
16.5	0.044	NaN	0.021	0.033
18.5	0.018	NaN	0.018	0.018

180 days of exposure

Depth (mm)	Chloride concentration per sample (% by weight of concrete)			
	A	B	C	Avg.
0.5	0.924	1.227	1.339	1.163
2.5	0.653	0.5	0.604	0.586
4.5	0.481	0.363	0.407	0.417
6.5	0.317	0.164	0.242	0.241
8.5	0.18	0.121	0.146	0.149
10.5	0.076	0.076	0.085	0.079
12.5	0.05	0.05	0.056	0.052
14.5	0.03	0.031	0.035	0.032
16.5	0.018	0.019	0.027	0.021
18.5	0.014	0.015	0.02	0.016

Water-soluble experimental data: 6.9 °C - 180 days

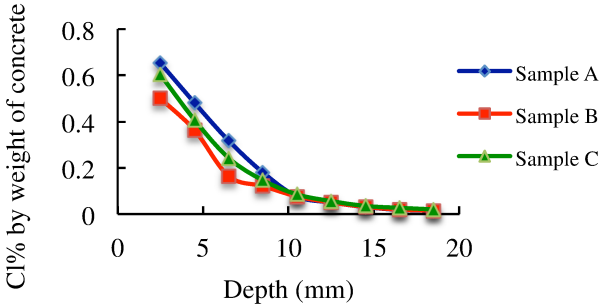

Water-soluble Test Results: solution temperature 22.4° C

56 days of exposure

Depth (mm)	Chloride concentration per sample (% by weight of concrete)			
	A	B	C	Avg.
0.5	0.954	1.051	1.008	1.004
1.5	0.667	0.658	0.676	0.667
2.5	0.521	0.518	0.525	0.521
3.5	0.441	0.392	0.492	0.442
4.5	0.317	0.308	0.332	0.319
5.5	0.195	0.181	0.196	0.191
6.5	0.125	0.133	0.136	0.131
7.5	0.061	0.093	0.098	0.094
8.5	0.061	0.068	0.07	0.066
9.5	0.045	0.051	0.05	0.049

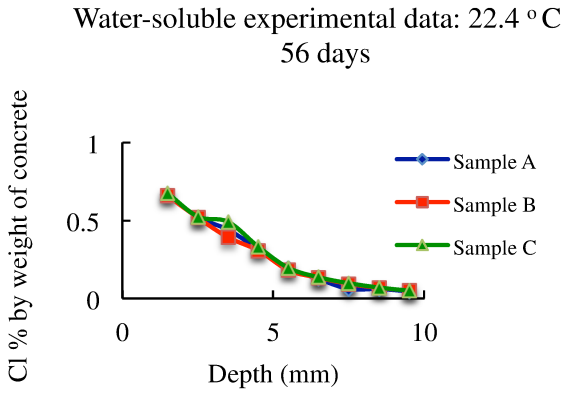

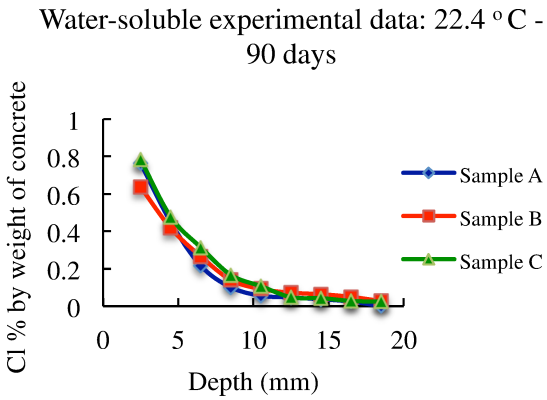

90 days of exposure

Depth (mm)	Chloride concentration per sample (% by weight of concrete)			
	A	B	C	Avg.
0.5	1.109	1.124	0.976	1.070
2.5	0.765	0.638	0.784	0.729
4.5	0.449	0.417	0.478	0.448
6.5	0.216	0.266	0.314	0.265
8.5	0.101	0.14	0.167	0.136
10.5	0.056	0.092	0.107	0.085
12.5	0.047	0.072	0.048	0.056
14.5	0.037	0.064	0.043	0.048
16.5	0.025	0.05	0.028	0.034
18.5	0	0.027	0.024	0.017

180 days of exposure

Depth (mm)	Chloride concentration per sample (% by weight of concrete)			
	A	B	C	Avg.
0.5	0.925	1.188	0.767	0.960
2.5	0.668	0.663	0.581	0.637
4.5	0.531	0.51	0.44	0.494
6.5	0.331	0.339	0.339	0.336
8.5	0.208	0.184	0.216	0.203
10.5	0.12	0.112	0.146	0.126
12.5	0.083	0.069	0.096	0.083
14.5	0.059	0.039	0.061	0.053
16.5	0.045	0.027	0.044	0.039
18.5	0.036	0.017	0.039	0.031

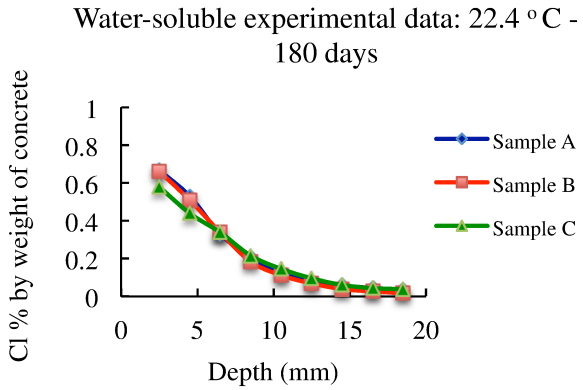

Water-soluble Test Results: solution temperature 40° C

56 days of exposure

Depth (mm)	Chloride concentration per sample (% by weight of concrete)			
	A	B	C	Avg.
0.5	1.319	0.976	1.176	1.157
1.5	0.769	0.86	0.768	0.799
2.5	0.644	0.756	0.642	0.681
3.5	0.545	0.626	0.573	0.581
4.5	0.441	0.492	0.442	0.458
5.5	0.246	0.332	0.29	0.289
6.5	0.244	0.246	0.214	0.235
7.5	0.182	0.171	0.179	0.177
8.5	0.113	0.15	0.136	0.133
9.5	0.102	0.106	0.109	0.106

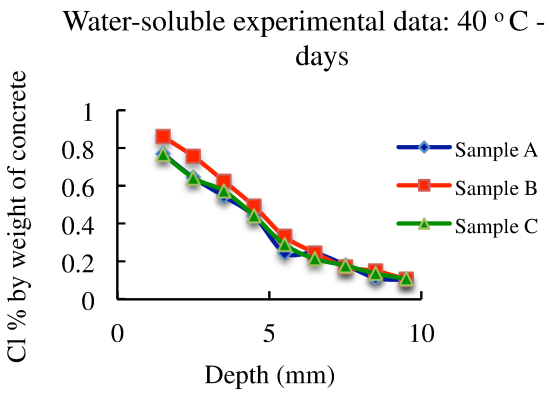

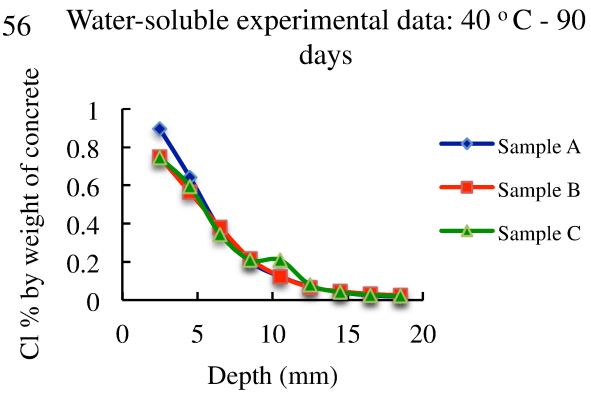

90 days of exposure

Depth (mm)	Chloride concentration per sample (% by weight of concrete)			
	A	B	C	Avg.
0.5	1.304	1.012	1.129	1.148
2.5	0.896	0.749	0.745	0.797
4.5	0.642	0.563	0.596	0.600
6.5	0.369	0.382	0.345	0.365
8.5	0.202	0.216	0.21	0.209
10.5	0.123	0.124	0.21	0.152
12.5	0.07	0.067	0.078	0.072
14.5	0.041	0.046	0.042	0.043
16.5	0.024	0.032	0.027	0.028
18.5	0.019	0.025	0.021	0.022

180 days of exposure

Depth (mm)	Chloride concentration per sample (% by weight of concrete)			
	A	B	C	Avg.
0.5	1.128	0.979	0.854	0.987
2.5	0.854	0.718	0.673	0.748
4.5	0.729	0.619	0.546	0.631
6.5	0.564	0.487	0.429	0.493
8.5	0.343	0.328	0.331	0.334
10.5	0.223	0.262	0.192	0.226
12.5	0.148	0.139	0.137	0.141
14.5	0.095	0.097	0.097	0.096
16.5	0.064	0.07	0.06	0.065
18.5	0.036	0.044	0.031	0.037

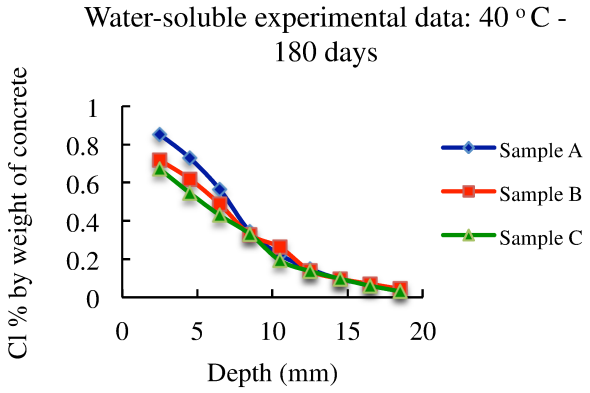

Acid-soluble Test Results: solution temperature 6.9° C

56 days of exposure

Depth (mm)	Chloride concentration per sample (% by weight of concrete)			
	D	E	F	Avg.
0.5	0.96	0.964	1.127	1.017
1.5	0.821	0.765	0.878	0.821
2.5	0.554	0.508	0.609	0.557
3.5	0.358	0.311	0.378	0.349
4.5	0.164	0.185	0.231	0.193
5.5	0.12	0.113	0.167	0.133
6.5	0.104	0.086	0.103	0.098
7.5	0.031	0.055	0.087	0.058
8.5	0.022	0.038	0.055	0.038
9.5	0	0.03	0.041	0.024

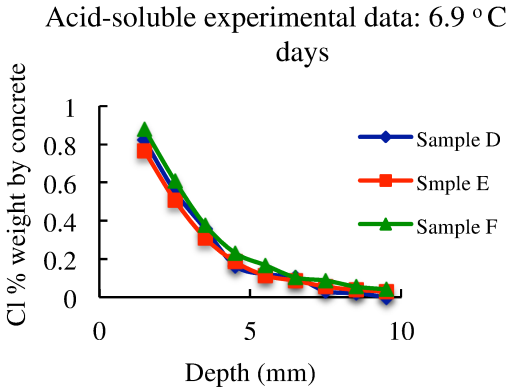

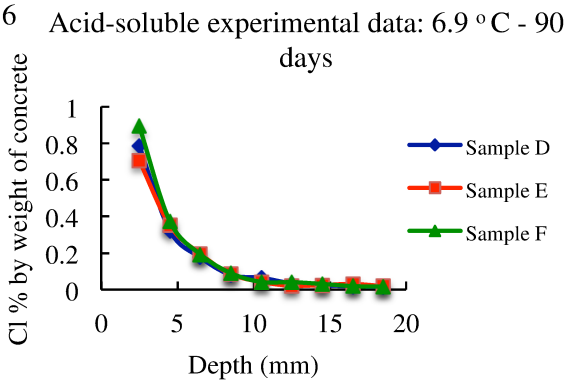

90 days of exposure

Depth (mm)	Chloride concentration per sample (% by weight of concrete)			
	D	E	F	Avg.
0.5	1.07	0.93	1.357	1.119
2.5	0.788	0.707	0.895	0.797
4.5	0.322	0.351	0.374	0.349
6.5	0.176	0.196	0.193	0.188
8.5	0.08	0.085	0.09	0.085
10.5	0.065	0.042	0.042	0.050
12.5	0.034	0.021	0.041	0.032
14.5	0.024	0.025	0.031	0.027
16.5	0.018	0.031	0.019	0.023
18.5	0.014	0.019	0.016	0.016

180 days of exposure

Depth (mm)	Chloride concentration per sample (% by weight of concrete)			
	D	E	F	Avg.
0.5	1.302	1.339	1.297	1.313
2.5	0.893	0.857	0.89	0.880
4.5	0.603	0.521	0.531	0.552
6.5	0.285	0.279	0.252	0.272
8.5	0.236	0.142	0.151	0.176
10.5	0.16	0.072	0.095	0.109
12.5	0.104	0.033	0.074	0.070
14.5	0.086	0.031	0.006	0.041
16.5	0.063	0.029	0.047	0.046
18.5	0.07	0.024	0.036	0.043

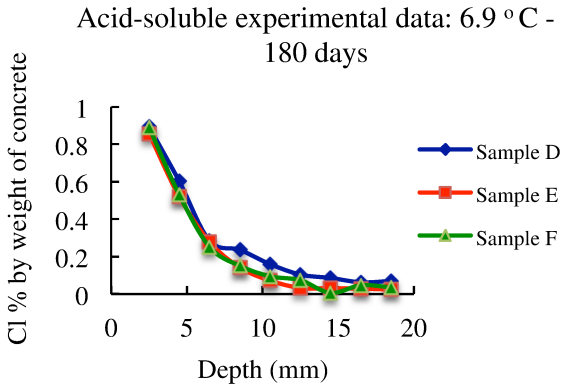

Acid-soluble Test Results: solution temperature 22.4° C

56 days of exposure

Depth (mm)	Chloride concentration per sample (% by weight of concrete)			
	D	E	F	Avg.
0.5	0.901	0.976	0.956	0.944
1.5	0.786	0.783	0.789	0.786
2.5	0.637	0.596	0.627	0.620
3.5	0.459	0.443	0.446	0.449
4.5	0.316	0.307	0.283	0.302
5.5	-	0.24	0.203	0.222
6.5	-	0.172	0.133	0.153
7.5	-	0.126	0.096	0.111
8.5	-	0.092	0.075	0.084
9.5	-	0.069	0.055	0.062

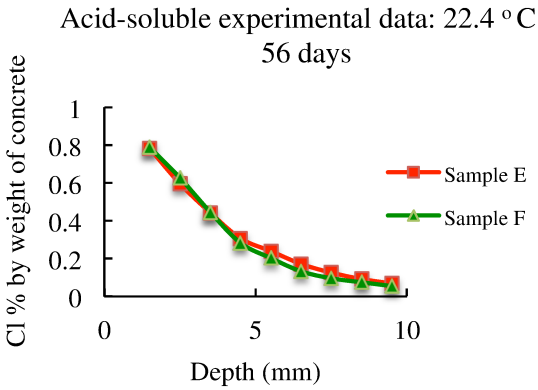

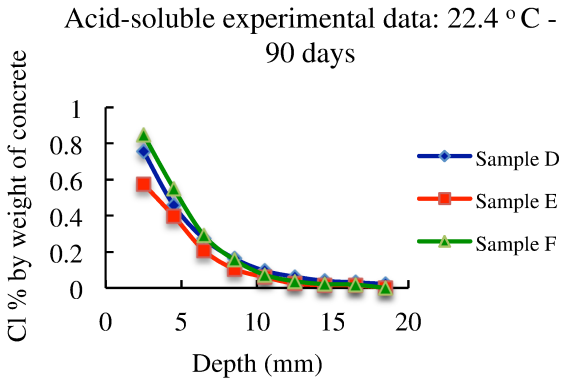

90 days of exposure

Depth (mm)	Chloride concentration per sample (% by weight of concrete)			
	D	E	F	Avg.
0.5	1.242	0.829	1.408	1.160
2.5	0.756	0.576	0.849	0.727
4.5	0.458	0.398	0.551	0.469
6.5	0.272	0.207	0.291	0.257
8.5	0.163	0.105	0.156	0.141
10.5	0.095	0.06	0.073	0.076
12.5	0.062	0.024	0.037	0.041
14.5	0.039	0.016	0.021	0.025
16.5	0.031	0.014	0.018	0.021
18.5	0.022	0	0	0.022

180 days of exposure

Depth (mm)	Chloride concentration per sample (% by weight of concrete)			
	D	E	F	Avg.
0.5	0.852	1.124	1.046	1.007
2.5	0.726	0.742	0.806	0.758
4.5	0.479	0.618	0.651	0.583
6.5	0.345	0.401	0.415	0.387
8.5	0.235	0.254	0.252	0.247
10.5	0.132	0.157	0.135	0.141
12.5	0.091	0.098	0.073	0.087
14.5	0.068	0.071	0.038	0.059
16.5	0.061	0.063	0.025	0.050
18.5	0.043	0.049	0.022	0.038

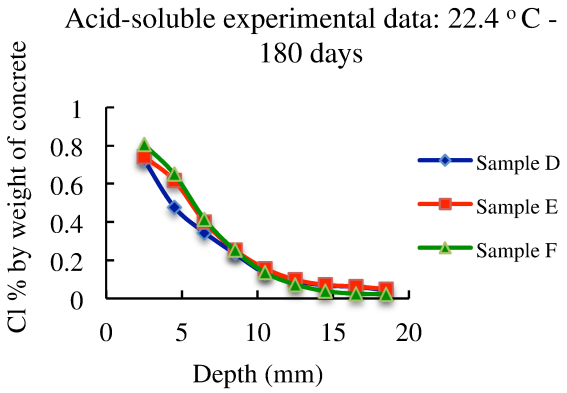

Acid-soluble Test Results: solution temperature 40º C

56 days of exposure

Depth (mm)	Chloride concentration per sample (% by weight of concrete)			
	D	E	F	Avg.
0.5	0.968	1.005	1.025	0.999
1.5	0.915	0.806	0.786	0.836
2.5	0.82	0.643	0.68	0.714
3.5	0.681	0.536	0.608	0.608
4.5	0.558	0.443	0.458	0.486
5.5	0.375	0.345	0.347	0.356
6.5	0.276	0.248	0.271	0.265
7.5	0.202	0.175	0.208	0.195
8.5	0.145	0.14	0.159	0.148
9.5	0.108	0.102	0.12	0.110

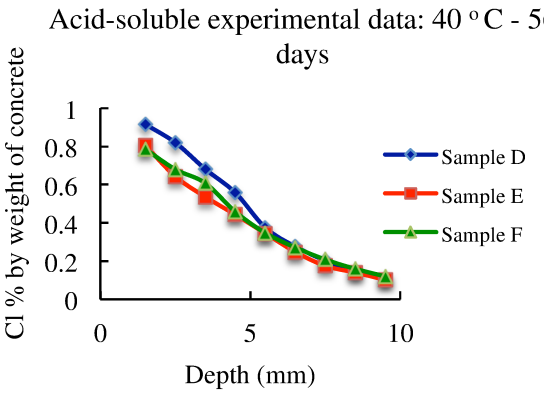

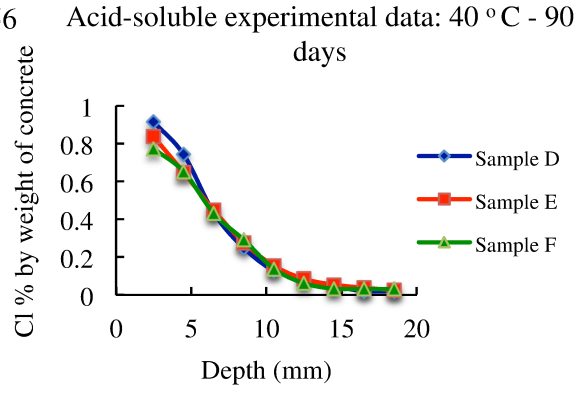

90 days of exposure

Depth (mm)	Chloride concentration per sample (% by weight of concrete)			
	D	E	F	Avg.
0.5	1.246	1.254	1.234	1.245
2.5	0.915	0.838	0.773	0.842
4.5	0.742	0.647	0.652	0.680
6.5	0.434	0.448	0.431	0.438
8.5	0.248	0.276	0.291	0.272
10.5	0.128	0.154	0.138	0.140
12.5	0.081	0.085	0.062	0.076
14.5	0.046	0.054	0.033	0.044
16.5	0.02	0.038	0.032	0.030
18.5	0.02	0.025	0.031	0.025

Experimentally water-soluble and Error Function Solution chloride profiles: a) @ 6.9^{o} C, b) @ 22.4^{o} C and c) @ 40^{o} C

a)

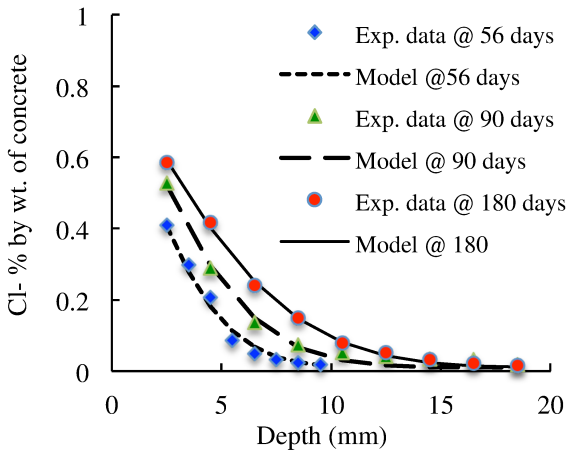

b)

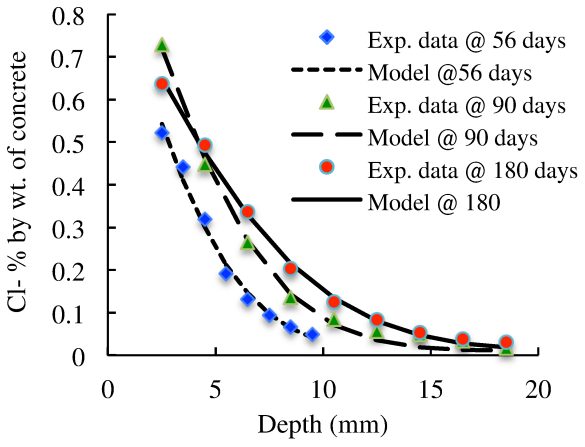

c)

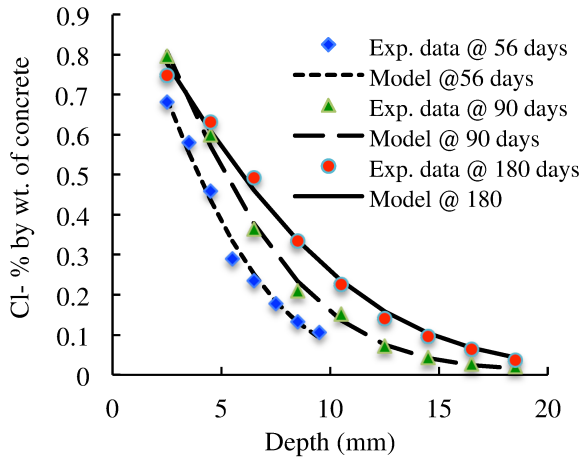

Determination of values of m based on three different methods – water-soluble results @: a) 6.9° C and b) 40° C

a)

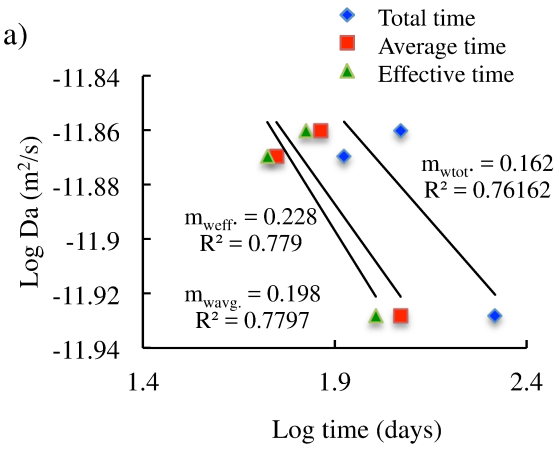

c)

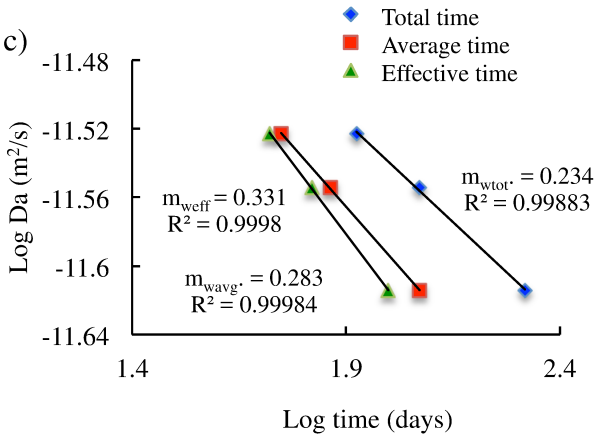

Experimentally acid-soluble and Error Function Solution chloride profiles: a) @6.9^{o} C, b) @ 22.4^{o} C and c) @ 40^{o} C

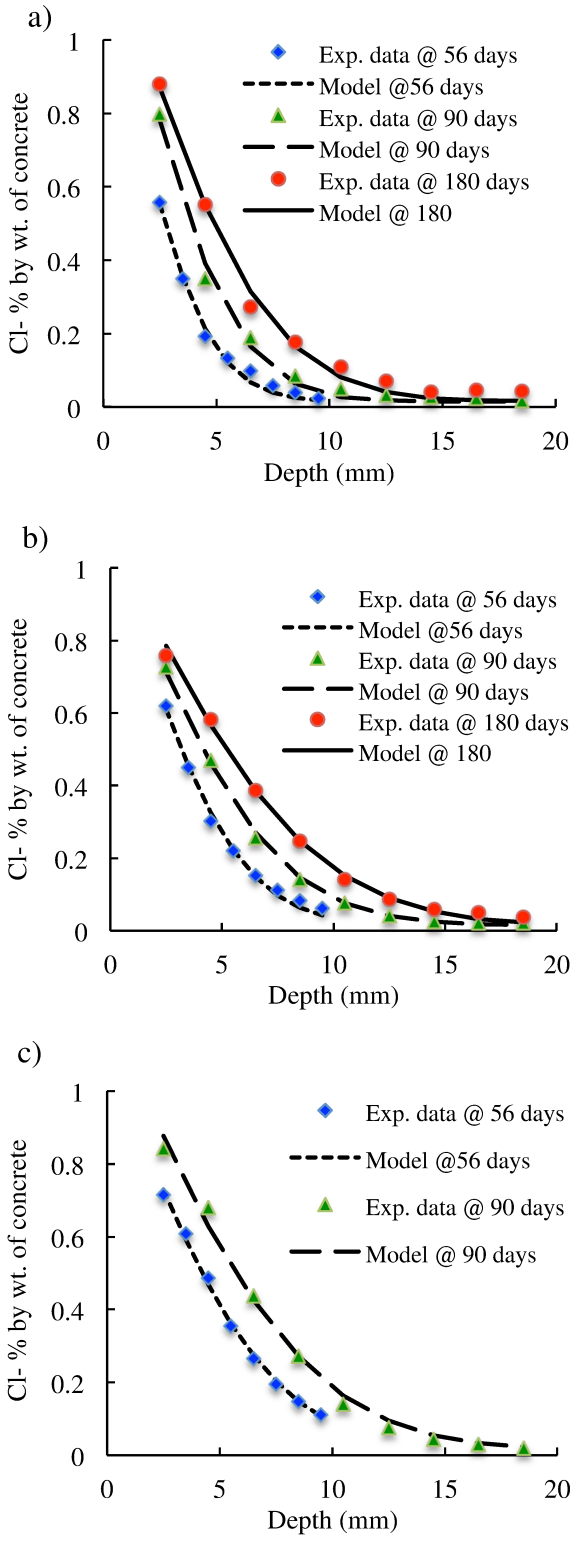

Determination of values of m based on three different methods – acid-soluble results @: a) 6.9° C and b) 40° C

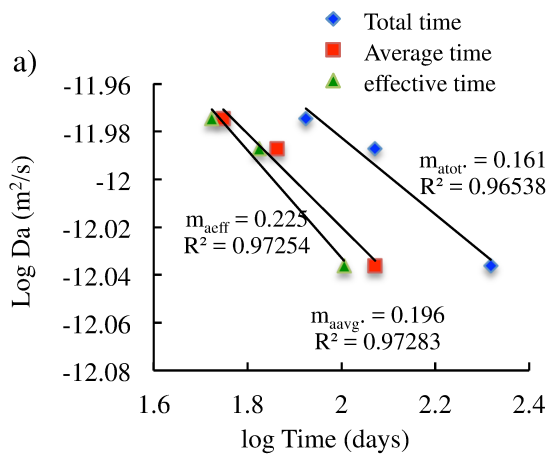

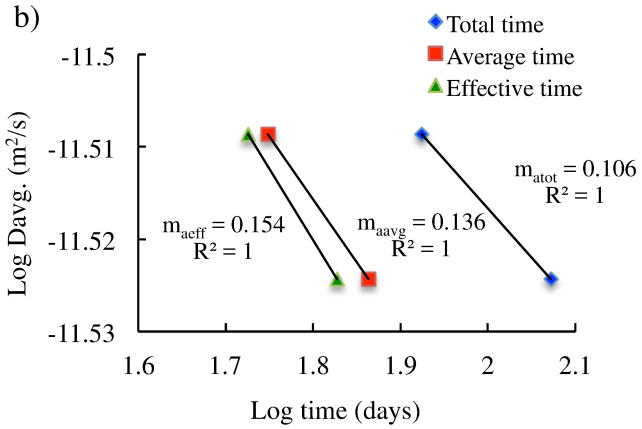

Experimentally water-soluble and linear finite difference chloride profiles @ a) 6.9° C and b) 40° C

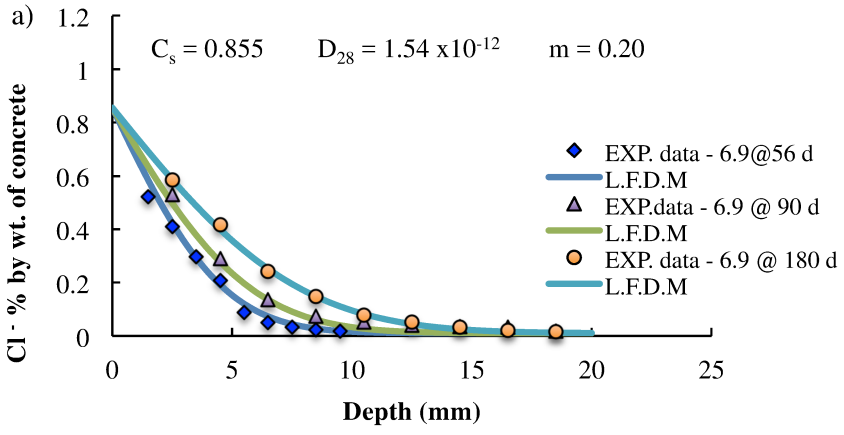

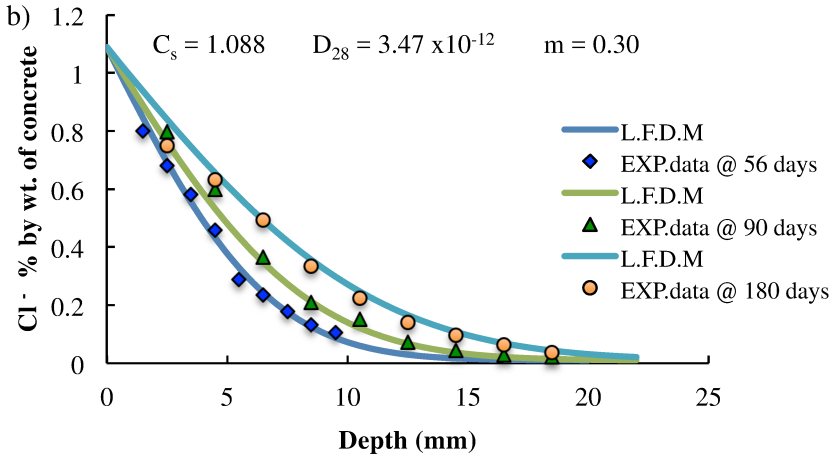

Experimentally acid-soluble and linear finite difference chloride profiles @: a) 6.9^{o} C and b) 40^{o} C.

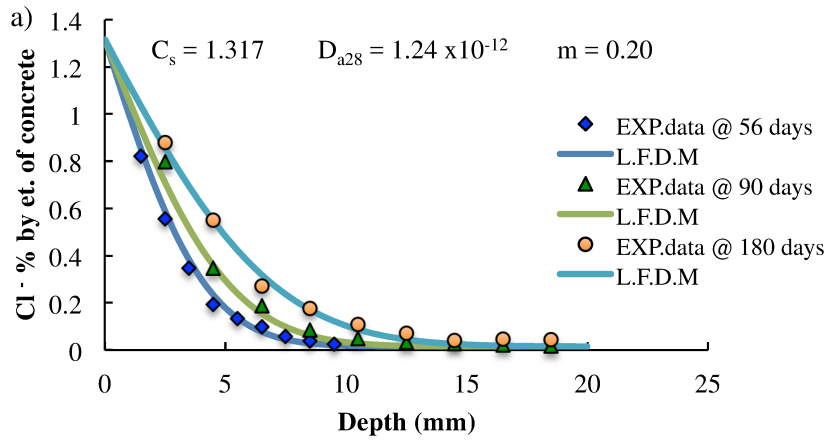

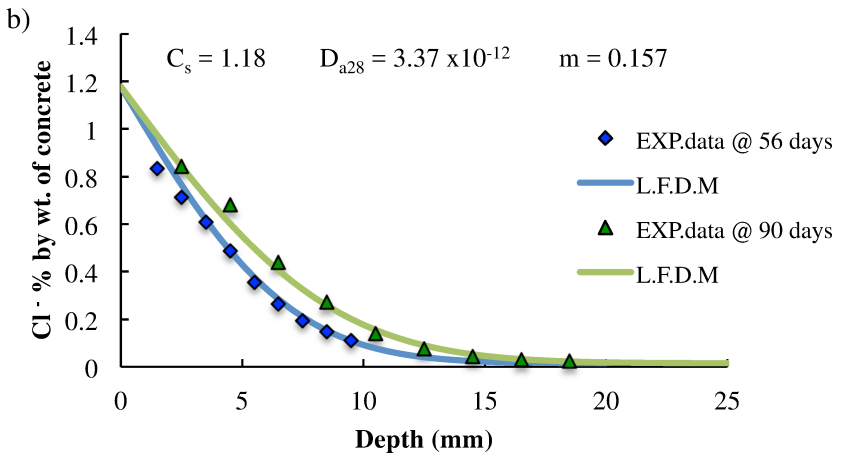

APPENDIX (C) Equilibrium Test Results

Binding isotherm test results

Curing temperature: 6.9° C

Curing condition	C_i (mol/L)	C_e (mol/L)	V (ml)	W (g)	C_b (mg Cl/g – sample)	C_b (Kg/m^3) of concrete
6.9° C	0	0	0	0	0	0
	0.1	0.0836	110	24.48	2.61	1.14
	0.3	0.248	55	24.54	4.13	1.80
	0.5	0.43	50	24.36	5.09	2.22
	0.7	0.612	50	24.6	6.34	2.76
	0.97	0.864	50	24.6	7.64	3.32

Curing temperature: 22.4° C

Curing condition	C_i (mol/L)	C_e (mol/L)	V (ml)	W (g)	C_b (mg Cl/g – sample)	C_b (Kg/m^3) of concrete
22.4° C	0	0	0	0	0	0
	0.1	0.089	120	19.55	2.37	1.03
	0.3	0.260	55	19.64 5	3.97	1.73
	0.5	0.438	50	19.89	5.54	2.41
	0.7	0.637	50	19.35	5.77	2.51
	0.97	0.889	50	19.69	7.26	3.16

Curing temperature: 40° C

Curing condition	C_i (mol/L)	C_e (mol/L)	V (ml)	W (g)	C_b (mg Cl/g – sample)	C_b (Kg/m^3) of concrete
40° C	0	0	0	0	0	0
	0.1	0.0849	100	19.65	2.72	1.19
	0.3	0.2593	55	19.63 5	4.04	1.76
	0.5	0.4433	55	19.72	5.61	2.44
	0.7	0.6257	50	19.89	6.62	2.88
	0.97	0.8891	50	19.58	7.32	3.19

APPENDIX (D) Mercury Intrusion Porosimetry Test Results

56 days - 6.9^{o} C

Plain concrete (Average)

Applied pressure (psi)	Cumulative volume (cm^3/g - sample)	Pore radius (Å)
51.3221435	0.01454975	17625.67519
101.9044553	0.01810825	8875.545924
201.2852895	0.02428225	4493.604628
303.934326	0.02907925	2975.42494
401.1072465	0.031997	2254.688866
503.4070433	0.03413575	1796.497197
599.207779	0.03560875	1509.238973
702.592819	0.036935	1287.126564
802.060974	0.0377505	1127.563191
901.1923675	0.0382445	1003.500561
994.8849793	0.038614	908.9762041
2005.296295	0.0421325	450.9741526
2998.518433	0.04567975	301.5897493
4001.033508	0.04819075	226.0223505
5001.041626	0.049825	180.826778
5991.544189	0.05145275	150.9338465
7043.86853	0.052384	128.400531
8083.419434	0.05307025	111.9049106
9003.867676	0.05371325	100.4371725
10225.4895	0.05427475	88.57644121
15012.57788	0.05616975	60.23806488
20025.72314	0.0569615	45.15800581
24998.89404	0.05754525	36.17444895
30260.45215	0.05808975	29.89337186
32810.000	0.05863375	27.56311521

Chloride contaminated (Average)

Applied pressure (psi)	Cumulative volume (cm^3/g - sample)	Pore radius (Å)
52.669342	0.013599	17175.60452
102.029192	0.0156025	8873.190956
201.285286	0.01841575	4493.844605
301.6141588	0.01948525	2999.6135
401.518921	0.020033	2252.245224
500.4631503	0.020597	1807.468056
602.900116	0.0210095	1499.971108
705.8859255	0.0212465	1281.112227
803.8447265	0.02141275	1125.106801
899.8077085	0.021517	1005.067955
998.277908	0.0215905	906.6544933
2079.579376	0.02241475	438.0597801
3004.531006	0.023063	300.9868117
3945.885742	0.0233935	232.8311393
5107.757447	0.0236645	177.7100228
6003.793701	0.023904	150.6256967
6998.912232	0.024195	129.2126237
8006.629028	0.02445425	112.9474848
9004.553711	0.0245925	100.4290894
10012.09619	0.0246715	90.32346335
14988.84644	0.02543075	60.33339085
19985.01953	0.025676	45.24985118
25025.35156	0.026246	36.13628238
29980.40918	0.0266075	30.16370655
32658.39453	0.0269065	27.69171461

90 days - 6.9° C

Plain concrete (Average)

Applied pressure (psi)	Cumulative volume (cm^3/g - sample)	Pore radius (Å)
50.224434	0.01735	18005.67133
98.873268	0.0201495	9147.53089
203.056618	0.0253465	4453.870558
305.044525	0.0279315	2964.560183
401.269455	0.0296135	2253.646298
504.4797975	0.0307305	1792.602037
598.658966	0.0314815	1510.595923
700.297577	0.0319555	1291.390919
798.8177185	0.032187	1132.089129
900.855499	0.03239	1003.940705
1003.192719	0.032554	901.5554428
1998.971985	0.0341735	452.3944289
3005.154663	0.0351385	300.9243594
4020.143555	0.036126	224.946974
4999.058106	0.036978	180.8979102
6013.249756	0.037853	150.3877863
6979.938965	0.0382565	129.7920579
8014.113281	0.0386175	112.8533069
9005.053223	0.0391565	100.4235145
10036.60767	0.03924975	90.36775441
15001.49512	0.040421	60.28240824
20004.85352	0.0409005	45.20543234
25064.38281	0.041363	36.07984617
30030.71631	0.041555	30.15259795
32819.52246	0.041685	27.55447275

Chloride contaminated (Average)

Applied pressure (psi)	Cumulative volume (cm^3/g - sample)	Pore radius (Å)
52.669342	0.013599	17175.60452
102.029192	0.0156025	8873.190956
201.285286	0.01841575	4493.844605
301.6141588	0.01948525	2999.6135
401.518921	0.020033	2252.245224
500.4631503	0.020597	1807.468056
602.900116	0.0210095	1499.971108
705.8859255	0.0212465	1281.112227
803.8447265	0.02141275	1125.106801
899.8077085	0.021517	1005.067955
998.277908	0.0215905	906.6544933
2079.579376	0.02241475	438.0597801
3004.531006	0.023063	300.9868117
3945.885742	0.0233935	232.8311393
5107.757447	0.0236645	177.7100228
6003.793701	0.023904	150.6256967
6998.912232	0.024195	129.2126237
8006.629028	0.02445425	112.9474848
9004.553711	0.0245925	100.4290894
10012.09619	0.0246715	90.32346335
14988.84644	0.02543075	60.33339085
19985.01953	0.025676	45.24985118
25025.35156	0.026246	36.13628238
29980.40918	0.0266075	30.16370655
32658.39453	0.0269065	27.69171461

90 days – 22.4° C

Plain concrete (Average)

Applied pressure (psi)	Cumulative volume (cm^3/g - sample)	Pore radius (Å)
50.9480685	0.0085475	17784.35758
102.59053	0.012487	8814.839656
201.1855015	0.020032	4496.766235
297.884399	0.024293	3035.805417
402.566711	0.027092	2246.38314
502.009888	0.028774	1801.396932
597.910522	0.02953	1512.465559
701.245544	0.030083	1289.589759
795.349976	0.030715	1137.007732
901.7286985	0.0312345	1002.954265
997.579468	0.031494	906.5133167
2005.483521	0.0333	450.9232126
2988.638916	0.03444	302.5855908
3992.101807	0.036325	226.5270566
4989.328613	0.037194	181.2506536
5977.972168	0.037826	151.2752229
7001.344238	0.038334	129.1636351
7995.626465	0.039666	113.1017158
9013.459961	0.041133	100.3298485
9984.69043	0.04145	90.57056686
14964.73438	0.043052	60.43001162
19982.25	0.043797	45.25611841
25003.73242	0.044418	36.16765793
30066.63086	0.044836	30.07716682
33065.59766	0.045186	27.34924321

Chloride contaminated (Average)

Applied pressure (psi)	Cumulative volume (cm^3/g - sample)	Pore radius (Å)
51.2168125	0.00698675	17681.61489
101.5302393	0.00913975	8917.019095
199.913147	0.0148225	4523.565491
298.258621	0.01743	3032.035648
401.7808763	0.018401	2251.364567
499.9891205	0.0188695	1808.700201
603.985382	0.0191485	1497.433312
700.0107115	0.0193065	1292.042386
802.4602055	0.0194675	1126.991357
901.7412108	0.01964825	1002.984939
994.785156	0.019812	909.0623204
1990.402313	0.02057075	457.9050946
2999.765808	0.0207855	301.5342978
4002.081665	0.021324	225.9656147
4997.860962	0.02192825	180.9449829
5996.07251	0.02240475	150.8234084
7003.689453	0.022628	129.1209858
8029.045411	0.022817	112.64477
8930.458008	0.0231135	101.2662522
10011.06055	0.0233785	90.33226606
14936.56836	0.0240725	60.54567678
19971.97266	0.0245805	45.27941075
24986.71875	0.0247445	36.1920322
30010.59863	0.024891	30.13333401
32535.76074	0.024926	27.79962315

56 days – 40° C

Plain concrete (Average)

Applied pressure (psi)	Cumulative volume (cm^3/g - sample)	Pore radius (Å)
55.29705358	0.01306575	16584.20585
100.2578843	0.015290333	9026.106437
200.4994291	0.02219875	4510.814299
302.1214371	0.02656775	2993.63608
402.5916696	0.029549583	2246.435526
501.1658504	0.031745	1804.607452
601.5071615	0.0333335	1503.539504
701.923355	0.034357833	1288.428535
798.767827	0.035039083	1132.17799
903.2754923	0.035564667	1001.179538
999.7332558	0.035900167	904.5774598
2012.926351	0.0374205	449.2685396
2994.42279	0.038795417	302.0448488
4010.746663	0.040702167	225.4797438
5007.906657	0.042019	180.5820754
5957.082764	0.042894833	151.8446462
6964.662761	0.043357667	130.4057606
8019.60197	0.04376375	112.7666531
8925.285482	0.044211833	101.3560494
10198.23779	0.044614167	88.77243006
15024.65967	0.045885667	60.18928052
20033.28548	0.046546167	45.14095627
25015.8584	0.047166833	36.14994958
30019.03776	0.048004083	30.12529054
32691.71094	0.0484195	27.66222539

Chloride contaminated (Average)

Applied pressure (psi)	Cumulative volume (cm^3/g - sample)	Pore radius (Å)
52.611135	0.008876	17227.124
101.2599743	0.011141	8931.676456
202.8487247	0.017687333	4458.6325
298.9488727	0.021525	3025.207754
401.3692217	0.024085667	2253.464581
501.8602397	0.025573667	1801.999499
603.132975	0.026404667	1499.393679
701.661438	0.026914833	1288.903373
802.1191813	0.027327	1127.412634
902.4771323	0.027624	1002.044467
999.5087283	0.027793333	904.796357
1994.996948	0.028781	453.3097291
3023.574626	0.029142167	303.4254383
4000.052572	0.029945333	226.0786477
5005.527832	0.031098667	180.6658033
6007.386393	0.032026333	150.5362264
7000.504557	0.033207333	129.1804591
8061.223633	0.033933667	112.1940703
9001.352214	0.034487	100.4648615
10017.15641	0.034868333	90.27755889
15009.84863	0.035946667	60.24895367
20018.64128	0.036796667	45.17401326
25029.97135	0.037538	36.12953093
30261.09408	0.0384805	29.89530675
32197.07552	0.038826667	28.09746478

90 days – 40° C

Plain concrete (Average)

Applied pressure (psi)	Cumulative volume (cm^3/g - sample)	Pore radius (Å)
57.81697717	0.0150155	16051.16537
101.5593493	0.018170333	8904.436193
200.145996	0.024175	4519.207694
301.4603167	0.027783333	2999.868583
399.9554853	0.030390667	2261.062429
499.8144833	0.032177667	1809.345377
602.9001365	0.033579333	1500.025334
697.2206623	0.034307333	1297.099674
801.6368613	0.035022	1128.096163
896.1237387	0.035413333	1009.179367
1004.032583	0.0357935	900.7280337
2007.845093	0.037140333	450.3966312
3025.645426	0.037599	298.9328275
4010.597005	0.038096	225.482564
4979.133138	0.038712833	181.8513167
6089.083578	0.039397833	148.8664602
6999.049317	0.040466167	129.2090633
7992.550293	0.041181333	113.1462725
9034.48291	0.041707833	100.098111
9985.538249	0.042439833	90.56375417
15009.64128	0.043867333	60.24924771
19996.30404	0.044800333	45.2243896
25021.98633	0.045586667	36.14098569
29769.87956	0.046500667	30.38137727
32901.60742	0.046985	27.48582359

Chloride contaminated (Average)

Applied pressure (psi)	Cumulative volume (cm^3/g - sample)	Pore radius (Å)
51.0422861	0.0198008	19806.98268
100.0757628	0.0214236	9041.066025
200.7863251	0.0264781	4504.919162
300.0648833	0.0302998	3014.101625
401.3392823	0.0326929	2253.587277
500.3982821	0.0341183	1807.343164
593.310083	0.0351286	1524.476268
701.5799136	0.0358364	1289.01603
803.7824098	0.036235	1125.131016
900.6808838	0.0365946	1004.106276
1015.112934	0.0368634	892.5014232
1994.171948	0.0381636	461.4201342
3017.064832	0.0384493	307.2513613
4001.951758	0.0387402	225.9703591
5023.876856	0.0390879	180.1951121
6021.317285	0.0397065	150.2806776
6955.809229	0.0405238	130.0415483
7912.78916	0.0411537	114.6719926
9011.419629	0.0415691	100.3531746
10007.23418	0.0422607	90.36741368
15012.75479	0.043481	60.2370682
20010.91582	0.044104	45.19150121
25012.78398	0.0447565	36.15442296
30141.56504	0.0455456	30.01261889
32775.95273	0.0461016	27.59216675

APPENDIX (E) Linear Finite Difference Model (Fitting Process)

Contents

Linear Finite Difference model (Crank-Nicolson)

```
% Created by Alkailani Omer / PhD. Candidate / Civil & Resource Eng. / Dalhousie University
  clear all;
% close all
  format long;
%--------------------------------------------------------------------------%
```

Import data (experimental chloride profiles)

```
%Acid-Soluble Profiles
%--------------------------------------------------------------------------%
Chlorides = xlsread('coldfirst_mV.xlsx');
% q=size(Chlorides);
% ExpChlors=Chlorides(:,2);

% Chlorides = xlsread('coldsecond_mV.xlsx');
% q=size(Chlorides);
% ExpChlors=Chlorides(:,2);

% Chlorides = xlsread('coldthird_mV.xlsx');
% q=size(Chlorides);
% ExpChlors=Chlorides(:,2);
%--------------------------------------------------------------------------%
% Chlorides = xlsread('roomfirst_mV.xlsx');
% q=size(Chlorides);
% ExpChlors = Chlorides(:,2);

% Chlorides = xlsread('roomsecond_mV.xlsx');
% q=size(Chlorides);
% ExpChlors = Chlorides(:,2);

% Chlorides= xlsread('roomthird_mV.xlsx');
% q=size(Chlorides);
% ExpChlors=Chlorides(:,2);
%--------------------------------------------------------------------------%
% Chlorides = xlsread('hotfirst_mV.xlsx');
% q = size(Chlorides);
% ExpChlors = Chlorides(:,2);

% Chlorides = xlsread('hotsecond_mV.xlsx');
% q=size(Chlorides);
```

```
% ExpChlors = Chlorides(:,2);

% Chlorides= xlsread('hotthird_mV.xlsx');
% q=size(Chlorides);
% ExpChlors=Chlorides(:,2);
%-------------------------------------------------------------------------%
```

Input parameters

```
%-------------------------------------------------------------------------%
Ci = 0.015;             % initial chloride content percent by weight of concrete
Dt = 24*3600;           % time step (one hour) per seconds
thickness = 0.200;      % mm
slices = 200; Dx = thickness/slices;
Cs = 1.137;
m = .35;
% Exposure Conditions
%-------------------------------------------------------------------------%
t_exposure = 180*24*3600;           % exposure period per seconds
t_28 = 28*24*3600;                  % age of concrete at 28 days per seconds
t = t_28; t_limit_maturity=25*365*24*3600;
T_ref=20+273; % Refernce Temperature
nT = 12; % number of months per year
% T = ([6.9 6.9 6.9 6.9 6.9 6.9 6.9 6.9 6.9 6.9 6.9 6.9]);
% T = ([22.4 22.4 22.4 22.4 22.4 22.4 22.4 22.4 22.4 22.4 22.4 22.4]); % Room Temperature (R.T)
T = ([40 40 40 40 40 40 40 40 40 40 40 40]);
%Start of Exposure Time
%-------------------------------------------------------------------------%
init_month=6;
init_day=15;
E=33500;
R=8.314472;
%-------------------------------------------------------------------------%
% Initializing temperature shifted 28-day diffusion coefficients for each time   period per year as zero.
dift1_28(1:nT)=0;
%-------------------------------------------------------------------------%
% cover initiation
for n = 1:slices+1
x(n) = 1000*(n-1)*Dx;
end;

%-------------------------------------------------------------------------%
% Establish parameters of the structure analysis model:
Dmin=100;             %Minimum of search range for optimal Dvalue.
Dmax=1000;            %Maximum of search range for optimal Dvalue.
Dres=100;             %Resolution by which Dvalue is divided to determine MSE.
P = 0;
PP = 0;
PPP = 0;
%-------------------------------------------------------------------------%
```

Modeling Process: (Determination of D28 & m for MSE)

```
for m = 0.05:.01:1
% for Cs = 1.129:0.001:1.129
for run=4:-1:2            %Each run for optimizing the diffusion coefficient by its 100, 10, 1, .1, 0.01and 0.001
decimal place.
u((slices+1),1)=0;      % chloride concentration in all slices is equal to zero (empty array)
Min_MSE=[0 10^10];              % initial values for D28 and MSE
y=0;
for yy=Dmin:Dres:Dmax
y=y+1;         % initial & boundary conditions
for i = 1:slices+1
   u(i,1) = Ci;
   u(1,1) = Cs;
end;

D_value=yy/100*10^-12; % D_28 from the best fitting
%-------------------------------------------------------------------------%
% temperature & time effect on diffusivity
for n=1:nT        %Compute the temperature shifted 28-day diffusion coefficient.
dift1_28(n)=(D_value*exp(E/R*((1/T_ref)-(1/(T(n)+273)))))*((28/(28))^m);
end;
%-------------------------------------------------------------------------%
t=t_28;
month=init_month;
day=init_day;
hour=0; minute=0;
year=0;
%-------------------------------------------------------------------------%
%Exposure cerculation
for t_step =Dt/Dt:(t_exposure)/Dt
   t = t + Dt;
%-------------------------------------------------------------------------%
% To compute the correct diffusivity keeping tracking the reduction in the diffusivity on daily bases (what
day and month it is).

%minute=minute+1;
hour=hour+1;
if minute==61 hour=hour+1;minute=1;end
if hour>24;day=day+1;hour=hour-24;end;day=day+1;
if (month==1)&&(day==32), month=2;day=1;end;
if month==2&&(day==29), month=3;day=1;end;
if month==3&&(day==32), month=4;day=1;end;
if month==4&&(day==31), month=5;day=1;end;
if month==5&&(day==32), month=6;day=1;end;
if month==6&&(day==31), month=7;day=1;end;
if month==7&&(day==32), month=8;day=1;end;
if month==8&&(day==32), month=9;day=1;end;
if month==9&&(day==31), month=10;day=1;end;
if month==10&&(day==32), month=11;day=1;end;
```

```
if month==11&&(day==31), month=12;day=1;end;
if month==12&&(day==32), year=year+1;month=1;day=1;end;
%-------------------------------------------------------------------------%
%Determine what the diffusivity is for the current time and temperature.

   dift=dift1_28(month)*((28/(t/3600/24))^m);
   if t>t_limit_maturity  %Limiting maturity effect to t<t_limit_maturity
   dift=dift1_28(month)*((28/(t_limit_maturity/3600/24))^m);
   end;
%-------------------------------------------------------------------------%
% CRANK-NICHOLSON METHOD

r=dift*Dt/(Dx^2);
N = slices+1;
b = sparse(2:N-1,2:N-1,2+2*r,N,N);
c = sparse(2:N-1,3:N,-r,N,N);
a = sparse(2:N-1,1:N-2,-r,N,N);
A = a+b+c;
A(1,1) = 1;
A(N,N) = 1;
e = sparse(2:N-1,2:N-1,2-2*r,N,N);
f = sparse(2:N-1,3:N,r,N,N);
d = sparse(2:N-1,1:N-2,r,N,N);
B = d+e+f;
B(1,1) = 1;
B(N,N) = 1;
k = B*u;
u= A\k;
end;
%-------------------------------------------------------------------------%
%Linearly interpolate modelled chloride concentrations at the %experimentally sampled depths.
SSE(y)=0;
  for i=1:q(1);
   u_index(i,1)=floor(Chlorides(i,1)*1000)+1;  % cover depths (x-axis)
   u_index(i,2)=ceil(Chlorides(i,1)*1000)+1;
    if u_index(i,2)>u_index(i,1)
      ModelChlors(i)=u((u_index(i,1)),1)+(Chlorides(i,1)*1000-floor(Chlorides(i,1)*1000))/(u_index(i,2)-
u_index(i,1))*(u(u_index(i,2))-u(u_index(i,1)));
   else
     ModelChlors(i)=u((u_index(i,1)),1); % detemine the chloride concentration (model) at the same depth
as the experimental data
   end;
%-------------------------------------------------------------------------%
% fitting the model to the experimental data

ExpChlors(i)=Chlorides(i,2);
SE=10^6*(ExpChlors(i)-ModelChlors(i))^2; % square error at each concentration between the model and
the experimental data
SSE(y)=SSE(y)+SE;                    % accumulative value
depth(i)=Chlorides(i,1)*1000;
```

```
end;
%-------------------------------------------------------------------------%
% optimization of D_value

MSE(y)=SSE(y)/q(1);
P = P+1;
if MSE(y)<Min_MSE(2)
SSE_opt=SSE(y)';
Min_MSE(2)=MSE(y);
Min_MSE(1)=yy/100*10^-12;
u_opt=u;
ModelChlors_opt=ModelChlors';  % final model chloride concentrations
Dmin_new=yy-Dres/2;
Dmax_new=yy+Dres/2;
end;
end;
Dmin=Dmin_new;
Dmax=Dmax_new;
Dres=10^(run-2);
end;
% if Min_MSE(2)<lower_MSE(2)
% Cs that gives the lowest MSE %
lower_MSE=[Min_MSE,Cs];
%     Cs % end;
Min_f(P)=Min_MSE(2);
m   Min_D(P) = Min_MSE(1);
if Min_f(P)~= 0
PP = PP+1;
Min_ff(PP) = Min_f(P);
Min_DD(PP) = Min_D(P);
end
PPP = PPP+1;
AA(PPP,1) = m ;
AA(PPP,2)= Min_ff(PP);
AA(PPP,3) = Min_DD(PP);
end;
% end
%-------------------------------------------------------------------------%
```

Graphs & Plots

```
figure;
hold on;
plot(x,u_opt,'LineWidth',2);
title('Profile of Chloride Ion Content (kg/m^3) vs Cover Depth (mm)');
xlabel('Concrete Cover Depth (mm)'); ylabel('Chloride Ion Content (kg/m^3)');
%axis([0,1.3,-25,0]);
plot(depth,ExpChlors,'.r'); axis([0 20 0 1.5]);  hold off;  grid on;
```

APPENDIX (F) Linear Finite Difference Model (service life Predictions)

Contents

Linear Finite Difference model(Cranck-Nicolson)

```
% Created by Alkailani Omer/ PhD. candidate / Civil & Resource Eng. / % Dalhousie University
clear all;
%close all;
format long;
%-------------------------------------------------------------------------%
```

Input parameters

```
D_28 = 2.08e-12;         % m2/s
Cin = 1;                 % chloride surface concentration percent by weight of concrete
Ci = 0.015;              % initial chloride content percent by weight of concrete
m1 = 0.34; % Cs = 1;
Dt = 24*3600;            % time step (one hour) per seconds
thickness = .20;         % m
slices = 200;
Dx = thickness/slices;
t_limit = 25*365*24*3600;
%-------------------------------------------------------------------------% t_exposure = 5*365*24*3600;   % exposure
period per seconds
t_28 = 28*24*3600;           % age of concrete at 28 days per seconds
t = t_28; t_limit_maturity=25*365*24*3600;
Ccrt = 0.05; % % by weight of concrete
%-------------------------------------------------------------------------% T_ref=20+273;              % Refernce
Temperature
nT=12;                   % number of months per year
% T=([22.4 22.4 22.4 22.4 22.4 22.4 22.4 22.4 22.4 22.4 22.4 22.4]); % Room Temperature (R.T)
% T=([40 40 40 40 40 40 40 40 40 40 40 40]);
T=([6.9 6.9 6.9 6.9 6.9 6.9 6.9 6.9 6.9 6.9 6.9 6.9]);
init_month=6;
init_day=15;
E=35000;
R=8.314472;
%-------------------------------------------------------------------------%  difT_28(1:nT)=0;          %Initializing
temperature shifted 28-day diffusion coefficients for each time period per year as zero. %----------------------
-----------------------------------------------------%  % cover initiation
for n = 1:slices+1
  x(n) = 1000*(n-1)*Dx;
end;
% initial & boundary conditions
for i = 1:slices+1
```

```
u(i,1) = Ci;
end;
```

Modeling of Temperature & time effects

```
for n=1:nT%Compute the temperature shifted 28-day diffusion coefficient.
difT_28(n)=(D_28*exp(E/R*((1/T_ref)-(1/(T(n)+273)))))*((28/(28))^m1);  end;
month=init_month;
day=init_day;
hour=0; minute=0;
year=0; ii=0;

for h=1:slices;
  corroded(h)=0;
  CorrosionTime(h)=0;
end;
for t_step =Dt/Dt:(t_exposure)/Dt
   t = t + Dt;     ii=1+ii;     %to compute the correct diffusivity Keeping tracking the reduction in the
diffusivity on daily bases (what day and month it is).
minute=minute+1;
hour=hour+1;
if minute==61, hour=hour+1;minute=1;end
if hour>24;day=day+1;hour=hour-24;end;day=day+1;
if (month==1)&&(day==32), month=2;day=1;end;
if month==2&&(day==29), month=3;day=1;end;
if month==3&&(day==32), month=4;day=1;end;
if month==4&&(day==31), month=5;day=1;end;
if month==5&&(day==32), month=6;day=1;end;
if month==6&&(day==31), month=7;day=1;end;
if month==7&&(day==32), month=8;day=1;end;
if month==8&&(day==32), month=9;day=1;end;
if month==9&&(day==31), month=10;day=1;end;
if month==10&&(day==32), month=11;day=1;end;
if month==11&&(day==31), month=12;day=1;end;
if month==12&&(day==32), year=year+1;month=1;day=1;end;
%-------------------------------------------------------------------------% For time dependent Cs
% t1 = 365*24*3600;
% PC = 350;
% SL = 108; % SF = 10;
% W = 140;
% % Eqv = W/(PC +0.75*SL - 1.5*SF);
% % Kb_1 = 2.2;              % for ATM
% % Kb_2 = 3.67;             % for SPL
% Kb_3 = 5.13;             % for SUB
% C1 = (Kb_3 * Eqv)/5.5;    % by mass of concrete

% % K100_1 = 7;              % for ATM
% % K100_2 = 4.5;            % for SPL
% K100_3 = 1.5;            % for SUB
% C100 = K100_3 * C1;
```

```
% p = (log(C100 - Ci) - log(C1 - Ci))/(2*(1-m1));

% S1 = C1 - Ci; % % Cs = Ci + S1*(t/t1)^((1-m1)*p);

% if t > t_limit %
    Cs = Ci + S1*(t_limit/t1)^((1-m1)*p);
% end % l(ii)=Cs;
  u(1,1) = Cs;  %Determine what the diffusivity is for the current time and temperature.
%-------------------------------------------------------------------------%
dift=difT_28(month)*((28/(t/3600/24))^m1);
  if t>t_limit_maturity  %Limiting maturity effect to t<t_limit_maturity
    dift=difT_28(month)*((28/(t_limit_maturity/3600/24))^m1);
  end;
```

Modeling chloride ingress process in time steps (Crank-Nicolson Method)

```
r=dift*Dt/(Dx^2);
N = slices+1;
b = sparse(2:N-1,2:N-1,2+2*r,N,N);
c = sparse(2:N-1,3:N,-r,N,N);
a = sparse(2:N-1,1:N-2,-r,N,N);
A = a+b+c;
A(1,1) = 1;
A(N,N) = 1;
e = sparse(2:N-1,2:N-1,2-2*r,N,N);
f = sparse(2:N-1,3:N,r,N,N);
d = sparse(2:N-1,1:N-2,r,N,N);
B = d+e+f;
B(1,1) = 1;
B(N,N) = 1;
u=(A\B)*u;

for i=2:(slices+1);
  if (u(i,1)>Ccrt&&corroded(i)==0)        % zero is not corroded (false)
    CorrosionTime(i)=t/365/24/3600;
    corroded(i)=1;                    % one is corroded (true)
  end;
 end;
end;
```

plots of figures

```
figure;
% hold on;
plot(x,u, 'k-','LineWidth',2); grid;
title('Profile of Chloride Ion Content (%) vs Cover Depth (mm)'); xlabel('concrete Cover Depth (mm)');
ylabel('Chloride Ion Content (%)');
axis([0 200 0 1.2]);
```

APPENDIX (G) MATLAB Code - Nonlinear Finite Difference Model

Contents

Nonlinear Chloride Model

```
% Nonlinear Chloride Model
% A script for solving modified Fick's second law of diffusion (adding binding influence)
% Created by Alkailani Omer - PhD. Candidate, Civil & Resource Eng., Dalhousie University
    clear all;
%  close all;
%--------------------------------------------------------------------------%
```

Primary input data

```
De_28 = 2.29e-12;                   % diffusion coefficient m2/s
m = 0.37;
%   Csf = 17.727;   % kg/m3 of solution (0.5 M)
%   Csf = 35.453;   % kg/m3 of solution (1 M)
%   Csf = 70.91;    % kg/m3 of solution (2 M)
%   Csf = 88.63;    % kg/m3 of solution (2.5 M)
%   Csf = 106.36;   % kg/m3 of solution (3 M)
%   Csf = 165;      % kg/m3 of solution (4.6 M)
Ci = 0.00;              % (0.000%)kg/m3 of concrete
%Ci = 0.345;          % (0.015%)kg/m3 of concrete
Dt = 24*3600;       % time step (1 day)
t_28 = 28*24*3600;      % age of concrete at first exposure (sec)
Slab_thickness = 0.2;     % meter
N = 200;                    % number of slices or grid points
Dx = Slab_thickness/N;
xPosition=fix(0.050/Dx + 0.5);   % to determine the corrosion at specific depth based on the threshold value
% (+0.5 just to around the number)
t_exposure = 50*365*24*3600;     % exposure period per seconds
t_limit_maturity=25*365*24*3600;
w = 0.104;                          % amount of evaporable water = capillary porosity
Ccrt = 1.15;                            % kg/m3 of concrete
%--------------------------------------------------------------------------%
```

Initializing concrete cover with initial and boundary conditions

```
% Initializing concrete thickness from 0 to 200(mm)
```

```
x = zeros(N+1,1);
for i = 2:N+1
x(i) = 1000*(i-1)*Dx;
end
%-------------------------------------------------------------------------%
% Initial conditions
oldu = zeros(N+1,1);
for i = 1:N+1
oldu(i,1) = Ci;              % initial chloride content in all slices (kg/m3 of solution)
end
%-------------------------------------------------------------------------%
% Load the diffusion coefficient array for each binding case

% Set up D
D = ones(N+1,1);                % just 1 for now, (as start values)
%-------------------------------------------------------------------------%
% No binding
% for i=1:N+1 %
        D(i) = De_28;
% end
%-------------------------------------------------------------------------%
% Binding isotherm cases
%*****CHOOSE DIFFUSION COEFFICIENT: SEE BELOW NEAR LINE 237 ALSO*****
%*****CHOOSE DIFFUSION COEFFICIENT: SEE BELOW NEAR LINE 237 ALSO*****
%*****CHOOSE DIFFUSION COEFFICIENT: SEE BELOW NEAR LINE 237 ALSO*****
%-------------------------------------------------------------------------
% Linear  binding isotherm - constant
% alpha = 0.055; %
for i=1:N+1 %
     D(i) = De_28/(1+alpha/w);
% end
 %-------------------------------------------------------------------------%
 % Nonlinear binding isotherm- Langmuir
% alpha = 0.3 ;
% beta = 0.07 ;
% for i=1:N+1
%     D(i) = De_28/(1+alpha/(w*(1+beta*oldu(i)^2)));
% end
%-------------------------------------------------------------------------%
 % Nonlinear binding isotherm - Freundlich
% Binding parameters
alpha = 0.620;
beta = 0.470;
for i=1:N+1
     D(i) = De_28/(1+alpha*beta/w*oldu(i)^(beta-1.0));
end
%-------------------------------------------------------------------------%
 %*****END CHOOSE HOW DIFFUSION COEFFICIENT DEPENDS ON U*****
%*****END CHOOSE HOW DIFFUSION COEFFICIENT DEPENDS ON U*****
%*****END CHOOSE HOW DIFFUSION COEFFICIENT DEPENDS ON U*****
```

```
%-------------------------------------------------------------------------%
% How D depends upon u
% Load Dm with average values D(i-1/2) = (D(ui) + D(ui-1))/2 and Dp =
% D(i+1/2) = (D(ui) +D(ui+1))/2
Dm = zeros(N-1,1);              % initiation - i-1/2 column vector
Dp = zeros(N-1,1);              % initiation - i+1/2 column vector
for i=1:N-1
    Dm(i)=0.5*(D(i) + D(i+1));
    Dp(i)=0.5*(D(i+1) + D(i+2));
end
%-------------------------------------------------------------------------%
% Create the matrices A by loading them with zeros
A = zeros(N+1);
%-------------------------------------------------------------------------%
% Load matrix A r = Dt/Dx^2;          %factor - includes De from diffusion coefficient %set up A
A(1,1) = 1;                         % u(0) = 0:first eq. is left hand bc
for i = 2:N
   A(i,i-1) = -r*Dm(i-1);
   A(i,i) = 2 + r*(Dm(i-1) + Dp(i-1));
   A(i,i+1) = -r*Dp(i-1);
end
A(N+1,N+1) = 1;    % u(L) = 0:last eq. is right hand bc
 %-------------------------------------------------------------------------%
% Initialize right hand side as a column vector
b = zeros(N+1,1);  b(1) = Ci;           %left hand bc (boundary condition at the surface, top of the slab)

% Calculate the initial concentration at the internal points
for i=2:N
b(i) = r*Dm(i-1)*oldu(i-1)+(2-r*(Dp(i-1)+Dm(i-1)))*oldu(i) + r*Dp(i-1)*oldu(i+1);
end
b(N+1)= Ci;                         %right hand bc (boundary condition at the bottom of the slab)
%-------------------------------------------------------------------------%
```

Including temperature dependency

```
%Create yearly temperature profile (with monthly average values)

nT = 12; E=33500;
R = 8.314472;
T_ref = 20+273;
% T = [5 5 5 5 5 5 5 5 5 5 5 5];                                    % temperature profile
% T = [35 35 35 35 35 35 35 35 35 35 35 35];
   T = [20 20 20 20 20 20 20 20 20 20 20 20];
% T = ([6.9 6.9 6.9 6.9 6.9 6.9 6.9 6.9 6.9 6.9 6.9 6.9]);
% T = [22.4 22.4 22.4 22.4 22.4 22.4 22.4 22.4 22.4 22.4 22.4 22.4];
% T = [40 40 40 40 40 40 40 40 40 40 40 40];
```

```
% T = [-3.5 -3 0 5 9.5 14.5 18.5 18.5 16 10.5 5.5 -0.5];   % actual average of monthly temperature in
Halifax, NS
% T = [7.95 10.45 12.55 14.8 18.6 21.9 24.1 23.65 21.95 17.7 11.85 7.9]; % California
D_T = zeros(nT,1);
for i = 1:nT
    D_T(i) = De_28*exp((E/R)*((1/T_ref) - (1/(T(i)+273))));
end

init_month=1;
 init_day=1;
 month=init_month;
day=init_day;
hour=0; minute=0;
year=0;
%-------------------------------------------------------------------------%
```

Solving for free and total chloride concentrations in time steps

```
% Concentration vs. depth plot
% figure(1); hold on; grid on;

idump = 4000;
icount = 1;
ncount =1;

%corrosion plot
savetimes =1:t_exposure/Dt;
save_reinforcement_depth = zeros(1,length(savetimes));
%-------------------------------------------------------------------------%
for h=1:N;
    corroded(h)=0;
    CorrosionTime(h)=0;
end;
%-------------------------------------------------------------------------%
% Iteration process (calculating free chloride concentration increase with time)
t = t_28;
% Iteration process

for t_step = 1:t_exposure/Dt
ncount = ncount+1;
icount = icount + 1;
 t = t + Dt;              %increment time starts from concrete age of 28 days
newu = A\b;               % linear solve to update u
save_reinforcement_depth(ncount)=newu(xPosition);
if(icount == idump)    % plot(x,newu);           % plot several profiles at several time steps
icount = 1;
end
oldu = newu;
```

```
% Dump new concentration to old concentration
%-------------------------------------------------------------------------%
% To compute the correct diffusivity keeping tracking the reduction in the diffusivity on daily bases (what
day and month it is).
% minute=minute+1;
hour=hour+1;
if minute==61 hour=hour+1;minute=1;end
if hour>24;day=day+1;hour=hour-24;end;day=day+1;
if (month==1)&&(day==32), month=2;day=1;end;
if month==2&&(day==29), month=3;day=1;end;
if month==3&&(day==32), month=4;day=1;end;
if month==4&&(day==31), month=5;day=1;end;
if month==5&&(day==32), month=6;day=1;end;
if month==6&&(day==31), month=7;day=1;end;
if month==7&&(day==32), month=8;day=1;end;
if month==8&&(day==32), month=9;day=1;end;
if month==9&&(day==31), month=10;day=1;end;
if month==10&&(day==32), month=11;day=1;end;
if month==11&&(day==31), month=12;day=1;end;
 if month==12&&(day==32), year=year+1;month=1;day=1;
end;
% Determine what the diffusivity is for the current time and temperature.
%-------------------------------------------------------------------------%
dift=D_T(month)*((28/(t/3600/24))^m);
 if t>t_limit_maturity                                    % Limiting maturity effect to t < t_limit_maturity
dift=D_T(month)*((28/(t_limit_maturity/3600/24))^m);
end;
%-------------------------------------------------------------------------%
% To include just time influence on diffusion without temperature influence
%            dift=De_28*(28/(t/24/3600))^m;
%  if t>t_limit_maturity                          % Limiting maturity effect to t<t_limit_maturity

%           dift=De_28*((28/(t_limit_maturity/3600/24))^m);
% end
%-------------------------------------------------------------------------%
% Update D required for coefficient matrix A and right hand side b

% No binding
% for i=1:N+1
%     D(i) = dift;
% end
%-------------------------------------------------------------------------%
% Update D required for coefficient matrix A and right hand side b
% Update D
%*****START CHOOSE HOW DIFFUSION COEFFICIENT DEPENDS ON U*****
%*****START CHOOSE HOW DIFFUSION COEFFICIENT DEPENDS ON U*****
%*****START CHOOSE HOW DIFFUSION COEFFICIENT DEPENDS ON U*****
%-------------------------------------------------------------------------%
%Linear binding - constant
%     alpha = 0.03; %
```

```
for i=1:N+1
%       D(i) = dift/(1+alpha/w);
%    end
%-------------------------------------------------------------------------%
% Nonlinear - Langmuir
% binding parameters
%    alpha = 0.3 ; %
beta = 0.07 ; %
for i=1:N+1
%       D(i) = dift/(1+alpha/(w*(1+beta*oldu(i)^2)));
%    end
%-------------------------------------------------------------------------%
% Nonlinear - Freundlich binding parameters
alpha = 0.620;
beta = 0.470;
for i=1:N+1
    D(i) = dift/(1+alpha*beta/w*oldu(i)^(beta-1.0));
end %-------------------------------------------------------------------------%
%*****END CHOOSE HOW DIFFUSION COEFFICIENT DEPENDS ON U*****
%*****END CHOOSE HOW DIFFUSION COEFFICIENT DEPENDS ON U*****
%*****END CHOOSE HOW DIFFUSION COEFFICIENT DEPENDS ON U*****
%-------------------------------------------------------------------------%
% Update half step values
for i=1:N-1
% Update D i-1/2
      Dm(i)=0.5*(D(i) + D(i+1));
% Update D i+1/2
       Dp(i)=0.5*(D(i+1) + D(i+2));
end
%-------------------------------------------------------------------------%
% Update coefficient matrix A
r = Dt/Dx^2;
for i = 2:N
       A(i,i-1) = -r*Dm(i-1);
       A(i,i) = 2 + r*(Dm(i-1) + Dp(i-1));
       A(i,i+1) = -r*Dp(i-1);
end
%-------------------------------------------------------------------------%
% Update right hand side
b(1) = Csf;
for i=2:N
       b(i) = r*Dm(i-1)*oldu(i-1)+(2-r*(Dp(i-1)+Dm(i-1)))*oldu(i) + r*Dp(i-1)*oldu(i+1);
end
%-------------------------------------------------------------------------%
% Calculating total chloride content, Ct = bound chlorides + free chlorides
for i = 1:N+1
%  c(i) = w*newu(i);                                        % No binding
%  c(i) = alpha*newu(i) + w*newu(i);                        % assuming linear binding
%  c(i) = alpha*newu(i)/(1+beta*newu(i)) + w*newu(i);       % non-linear binding (Langmuir)
c(i) = alpha*newu(i)^beta + w*newu(i);                      % non-linear binding (Freundlich)
```

```
end
c = c';
%-------------------------------------------------------------------------%
% calculating the time to corrosion initiation based on total chloride content
for i=2:N+1;
    if (c(i)>Ccrt&&corroded(i)==0)        % zero is not corroded (false)
       CorrosionTime(i)=t/365/24/3600;
       corroded(i)=1;                      % one is corroded (true)
    end;
 end;
end
%-------------------------------------------------------------------------%
```

Acid-soluble chloride profiles (Total) - Experimental Profiles

```
% Acid-soluble chloride profiles (Total) - Experimental data @ 6.9
%-------------------------------------------------------------------------%
% ExpCl_RT56 = [0.821 0.557 0.349 0.193 0.133 0.098 0.058 0.038 0.024]*23;
% ExpCl_RT90 = [0.797 0.349 0.188 0.085 0.050 0.032 0.027 0.023 0.016]*23;
% ExpCl_RT180 = [0.880 0.552 0.272 0.176 0.109 0.070 0.041 0.046 0.043]*23;
% depth = 1.5:9.5;
% depth = 2.5:2:18.5;

% Acid-soluble chloride profiles (Total) - Experimental data @ 22.4
%-------------------------------------------------------------------------%
% ExpCl_RT56 = [0.786 0.620 0.449 0.302 0.222 0.153 0.111 0.084 0.062]*23;
% ExpCl_RT90 = [0.727 0.469 0.257 0.141 0.076 0.041 0.025 0.021 0.022]*23;
% ExpCl_RT180 = [0.758 0.583 0.387 0.247 0.141 0.087 0.059 0.050 0.038]*23;
 % depth = 1.5:9.5;
% depth = 2.5:2:18.5;

% Acid-soluble chloride profiles (Total) - Experimental data @ 40
%-------------------------------------------------------------------------%
% ExpCl_RT56 = [0.836 0.714 0.608 0.486 0.356 0.265 0.195 0.148 0.110]*23;
% ExpCl_RT90 = [0.842 0.680 0.438 0.272 0.140 0.076 0.044 0.030 0.025]*23;
% ExpCl_RT180 = [0.862 0.739 0.568 0.470 0.300 0.214 0.161 0.099 0.089]*23;
% depth = 1.5:9.5;
% depth = 2.5:2:18.5;
%-------------------------------------------------------------------------%
```

Producing free and total chloride profiles

```
figure(1);

hold on;
plot(x,newu,'k-','LineWidth',1);      % fit to free chloride profiles
% plot(x,c,'k-','LineWidth',1);      % fit to total chloride profiles
title('Profile of Total Chloride Ion Content at 500 years (kg/m^3 of Solution) vs Cover Depth (mm)');
xlabel('Concrete Cover Depth (mm)');
ylabel('Cf (kg/m^3 of Solution)');
```

```
axis([0 100 0 40]);
%axis([0 80 0 10]);
hold on; %
plot(depth,ExpCl_RT180, 'r.'); %
axis([0 20 0 30]); grid on;
%-------------------------------------------------------------------------%
```

Prediction of service life based on free chloride content

```
figure; plot(savetimes*Dt/(365*24*3600),save_reinforcement_depth(1:length(savetimes)));
[ChlorideThreshold,NChlorideThreshold]=min((save_reinforcement_depth-3.76).^2);
title(['Corrosion plot ',num2str(savetimes(NChlorideThreshold)*Dt/(365*24*3600))]);
grid on;

%  plot(newu,D/De_28,'g-','LineWidth',1.5); grid on;       % fit to free chloride profiles
% title('Influence of binding on the apparent diffusion coefficient');
% xlabel('Free chloride concentration (kg/m3 of pore solution');
% ylabel('D/De_28'); % axis([0 20 0 .06]);
% hold off;
```

APPENDIX (H) Nonlinear Fitting Results and Chloride Profiles Data Points

Nonlinear mode fitting results

Binding isotherm	Parameter - variables		56	90	180	Total
	m	D_{e28} *10^{-12} @ 20° C	Min_MSE *10^{-6}	Min_MSE *10^{-6}	Min_MSE *10^{-6}	Min_MSE *10^{-6}
No binding	0.35	4.14	6629.012	4669.029	5468.969	16767.011
	0.36	4.18	6632.938	4666.556	5465.166	16764.660
	0.37	4.22	6637.300	4664.283	5461.583	16763.166
	0.38	4.26	6642.064	4662.198	5458.244	16762.506
	0.39	4.29	6643.344	4664.752	5452.862	16760.958
	0.4	4.33	6648.499	4662.893	5450.387	16761.779
	0.41	4.37	6653.970	4661.196	5448.224	16763.391
	0.42	4.40	6655.234	4663.976	5445.232	16764.443
	0.43	4.44	6660.976	4662.481	5444.059	16767.517
Linear binding	0.31	3.15	568.839	336.668	650.114	1555.621
	0.32	3.18	578.802	332.207	641.376	1552.384
	0.33	3.21	589.287	328.109	633.011	1550.408
	0.34	3.24	600.245	324.358	625.059	1549.663
	0.35	3.27	611.627	320.937	617.556	1550.121
	0.36	3.3	623.389	317.831	610.537	1551.757
	0.37	3.33	635.485	315.027	604.037	1554.550
	0.38	3.36	647.877	312.512	598.089	1558.479
	0.39	3.39	660.526	310.274	592.727	1563.527
	0.4	3.42	673.393	308.302	587.983	1569.678
	0.41	3.45	686.446	306.886	583.886	1577.218
Nonlinear binding (Freundlich)	0.35	2.26	517.285	288.835	343.156	1149.276
	0.36	2.27	511.540	303.847	322.767	1138.155
	0.37	2.29	519.083	302.582	314.984	1136.649
	0.38	2.32	541.914	285.650	316.693	1144.257
	0.39	2.34	550.503	285.024	309.240	1144.767
	0.41	2.38	568.077	284.390	296.570	1149.037

Determination of linear binding coefficient at different limits of free chloride concentrations

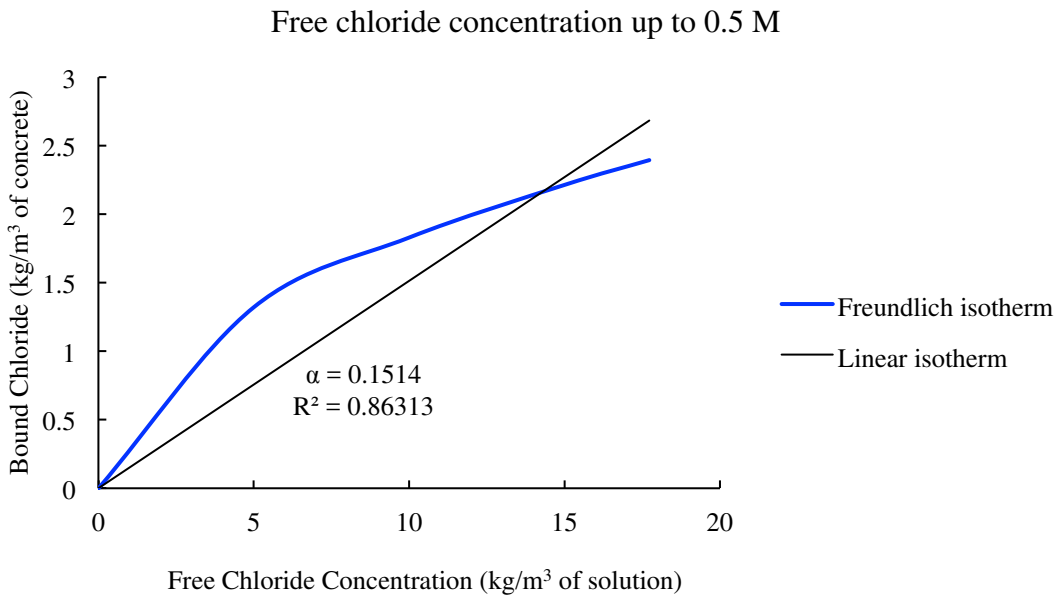

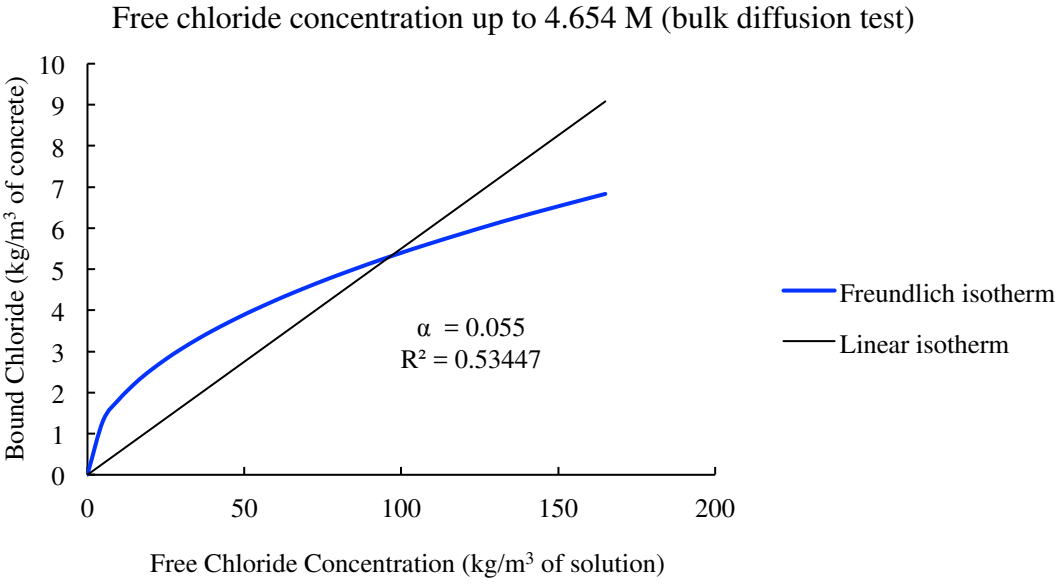

Data points – Figure 8.2

No bindin C_f (kg/m^3 of solution)	Da/D_{e28}	Linear binding C_f (kg/m^3 of solution)	$Da/_{De28}$ (dift)	Nonlinear binding C_f (kg/m^3 of solution)	Da/D_{e28} (dift)
165	1	165	6.54E-01	165	8.42E-01
151.1893	1	145.9642	6.54E-01	145.1590	8.33E-01
137.5313	1	127.3280	6.54E-01	125.5643	8.22E-01
124.1734	1	109.4660	6.54E-01	106.6493	8.09E-01
111.2535	1	92.7048	6.54E-01	88.8083	7.94E-01
98.8950	1	77.3059	6.54E-01	72.3727	7.75E-01
87.2042	1	63.4543	6.54E-01	57.5946	7.54E-01
76.2669	1	51.2543	6.54E-01	44.6369	7.28E-01
66.1473	1	40.7324	6.54E-01	33.5719	6.97E-01
56.8875	1	31.8459	6.54E-01	24.3872	6.60E-01
48.5075	1	24.4957	6.54E-01	16.9976	6.16E-01
41.0071	1	18.5413	6.54E-01	11.2608	5.63E-01
34.3678	1	13.8165	6.54E-01	6.9952	5.00E-01
28.5550	1	10.1437	6.54E-01	3.9983	4.27E-01
23.5216	1	7.3467	6.54E-01	2.0629	3.44E-01
19.2106	1	5.2596	6.54E-01	0.9839	2.61E-01
15.5588	1	3.7334	6.54E-01	0.5228	2.02E-01
12.4989	1	2.6397	6.54E-01	0.3841	1.77E-01
9.9629	1	1.8714	6.54E-01	0.3526	1.70E-01
7.8840	1	1.3423	6.54E-01	0.3464	1.69E-01
6.1981	1	0.9850	6.54E-01	0.3452	1.69E-01
4.8457	1	0.7485	6.54E-01	0.3450	1.69E-01
3.7726	1	0.5949	6.54E-01	0.3450	1.69E-01
2.9302	1	0.4970	6.54E-01	0.3450	1.69E-01
2.2760	1	0.4359	6.54E-01	0.3450	1.69E-01
1.7734	1	0.3984	6.54E-01	0.3450	1.69E-01
1.3913	1	0.3758	6.54E-01	0.3450	1.69E-01
1.1040	1	0.3625	6.54E-01	0.3450	1.69E-01
0.8903	1	0.3547	6.54E-01	0.3450	1.69E-01
0.7329	1	0.3503	6.54E-01	0.3450	1.69E-01
0.6183	1	0.3479	6.54E-01	0.3450	1.69E-01
0.5356	1	0.3465	6.54E-01	0.3450	1.69E-01
0.4767	1	0.3458	6.54E-01	0.3450	1.69E-01
0.4351	1	0.3454	6.54E-01	0.3450	1.69E-01
0.4060	1	0.3452	6.54E-01	0.3450	1.69E-01
0.3860	1	0.3451	6.54E-01	0.3450	1.69E-01
0.3722	1	0.3450	6.54E-01	0.3450	1.69E-01

No bindin C_f (kg/m^3 of solution)	Da/D_{e28}	Linear binding C_f (kg/m^3 of solution)	Da/D_{e28} (dift)	Nonlinear binding C_f (kg/m^3 of solution)	Da/D_{e28} (dift)
0.3629	1	0.3450	6.54E-01	0.3450	1.69E-01
0.3567	1	0.3450	6.54E-01	0.3450	1.69E-01
0.3525	1	0.3450	6.54E-01	0.3450	1.69E-01
0.3498	1	0.3450	6.54E-01	0.3450	1.69E-01
0.3480	1	0.3450	6.54E-01	0.3450	1.69E-01
0.3469	1	0.3450	6.54E-01	0.3450	1.69E-01
0.3462	1	0.3450	6.54E-01	0.3450	1.69E-01
0.3457	1	0.3450	6.54E-01	0.3450	1.69E-01
0.3454	1	0.3450	6.54E-01	0.3450	1.69E-01
0.3453	1	0.3450	6.54E-01	0.3450	1.69E-01
0.3452	1	0.3450	6.54E-01	0.3450	1.69E-01
0.3451	1	0.3450	6.54E-01	0.3450	1.69E-01
0.3451	1	0.3450	6.54E-01	0.3450	1.69E-01
0.3450	1	0.3450	6.54E-01	0.3450	1.69E-01
0.3450	1	0.3450	6.54E-01	0.3450	1.69E-01
0.3450	1	0.3450	6.54E-01	0.3450	1.69E-01
0.3450	1	0.3450	6.54E-01	0.3450	1.69E-01
0.3450	1	0.3450	6.54E-01	0.3450	1.69E-01
0.3450	1	0.3450	6.54E-01	0.3450	1.69E-01
0.3450	1	0.3450	6.54E-01	0.3450	1.69E-01
0.3450	1	0.3450	6.54E-01	0.3450	1.69E-01
0.3450	1	0.3450	6.54E-01	0.3450	1.69E-01
0.3450	1	0.3450	6.54E-01	0.3450	1.69E-01
0.3450	1	0.3450	6.54E-01	0.3450	1.69E-01
0.3450	1	0.3450	6.54E-01	0.3450	1.69E-01
0.3450	1	0.3450	6.54E-01	0.3450	1.69E-01
0.3450	1	0.3450	6.54E-01	0.3450	1.69E-01
0.3450	1	0.3450	6.54E-01	0.3450	1.69E-01
0.3450	1	0.3450	6.54E-01	0.3450	1.69E-01
0.3450	1	0.3450	6.54E-01	0.3450	1.69E-01
0.3450	1	0.3450	6.54E-01	0.3450	1.69E-01
0.3450	1	0.3450	6.54E-01	0.3450	1.69E-01
0.3450	1	0.3450	6.54E-01	0.3450	1.69E-01
0.3450	1	0.3450	6.54E-01	0.3450	1.69E-01
0.3450	1	0.3450	6.54E-01	0.3450	1.69E-01
0.3450	1	0.3450	6.54E-01	0.3450	1.69E-01
0.3450	1	0.3450	6.54E-01	0.3450	1.69E-01
0.3450	1	0.3450	6.54E-01	0.3450	1.69E-01
0.3450	1	0.3450	6.54E-01	0.3450	1.69E-01
0.3450	1	0.3450	6.54E-01	0.3450	1.69E-01
0.3450	1	0.3450	6.54E-01	0.3450	1.69E-01

No bindin C_f (kg/m^3 of solution)	**Da/D$_{e28}$**	**Linear binding C_f (kg/m^3 of solution)**	**Da/$_{De28}$ (dift)**	**Nonlinear binding C_f (kg/m^3 of solution)**	**Da/D$_{e28}$ (dift)**
0.3450	1	0.3450	6.54E-01	0.3450	1.69E-01
0.3450	1	0.3450	6.54E-01	0.3450	1.69E-01
0.3450	1	0.3450	6.54E-01	0.3450	1.69E-01
0.3450	1	0.3450	6.54E-01	0.3450	1.69E-01
0.3450	1	0.3450	6.54E-01	0.3450	1.69E-01
0.3450	1	0.3450	6.54E-01	0.3450	1.69E-01
0.3450	1	0.3450	6.54E-01	0.3450	1.69E-01
0.3450	1	0.3450	6.54E-01	0.3450	1.69E-01
0.3450	1	0.3450	6.54E-01	0.3450	1.69E-01
0.3450	1	0.3450	6.54E-01	0.3450	1.69E-01
0.3450	1	0.3450	6.54E-01	0.3450	1.69E-01
0.3450	1	0.3450	6.54E-01	0.3450	1.69E-01
0.3450	1	0.3450	6.54E-01	0.3450	1.69E-01
0.3450	1	0.3450	6.54E-01	0.3450	1.69E-01
0.3450	1	0.3450	6.54E-01	0.3450	1.69E-01
0.3450	1	0.3450	6.54E-01	0.3450	1.69E-01
0.3450	1	0.3450	6.54E-01	0.3450	1.69E-01
0.3450	1	0.3450	6.54E-01	0.3450	1.69E-01
0.3450	1	0.3450	6.54E-01	0.3450	1.69E-01
0.3450	1	0.3450	6.54E-01	0.3450	1.69E-01
0.3450	1	0.3450	6.54E-01	0.3450	1.69E-01
0.3450	1	0.3450	6.54E-01	0.3450	1.69E-01
0.3450	1	0.3450	6.54E-01	0.3450	1.69E-01
0.3450	1	0.3450	6.54E-01	0.3450	1.69E-01
0.3450	1	0.3450	6.54E-01	0.3450	1.69E-01
0.3450	1	0.3450	6.54E-01	0.3450	1.69E-01
0.3450	1	0.3450	6.54E-01	0.3450	1.69E-01
0.3450	1	0.3450	6.54E-01	0.3450	1.69E-01
0.3450	1	0.3450	6.54E-01	0.3450	1.69E-01
0.3450	1	0.3450	6.54E-01	0.3450	1.69E-01
0.3450	1	0.3450	6.54E-01	0.3450	1.69E-01
0.3450	1	0.3450	6.54E-01	0.3450	1.69E-01
0.3450	1	0.3450	6.54E-01	0.3450	1.69E-01
0.3450	1	0.3450	6.54E-01	0.3450	1.69E-01
0.3450	1	0.3450	6.54E-01	0.3450	1.69E-01
0.3450	1	0.3450	6.54E-01	0.3450	1.69E-01
0.3450	1	0.3450	6.54E-01	0.3450	1.69E-01
0.3450	1	0.3450	6.54E-01	0.3450	1.69E-01

No bindin C_f (kg/m^3 of solution)	**Da/D_{e28}**	**Linear binding C_f (kg/m^3 of solution)**	**Da/$_{De28}$ (dift)**	**Nonlinear binding C_f (kg/m^3 of solution)**	**Da/D_{e28} (dift)**
0.3450	1	0.3450	6.54E-01	0.3450	1.69E-01
0.3450	1	0.3450	6.54E-01	0.3450	1.69E-01
0.3450	1	0.3450	6.54E-01	0.3450	1.69E-01
0.3450	1	0.3450	6.54E-01	0.3450	1.69E-01
0.3450	1	0.3450	6.54E-01	0.3450	1.69E-01
0.3450	1	0.3450	6.54E-01	0.3450	1.69E-01
0.3450	1	0.3450	6.54E-01	0.3450	1.69E-01
0.3450	1	0.3450	6.54E-01	0.3450	1.69E-01
0.3450	1	0.3450	6.54E-01	0.3450	1.69E-01
0.3450	1	0.3450	6.54E-01	0.3450	1.69E-01
0.3450	1	0.3450	6.54E-01	0.3450	1.69E-01
0.3450	1	0.3450	6.54E-01	0.3450	1.69E-01
0.3450	1	0.3450	6.54E-01	0.3450	1.69E-01
0.3450	1	0.3450	6.54E-01	0.3450	1.69E-01
0.3450	1	0.3450	6.54E-01	0.3450	1.69E-01
0.3450	1	0.3450	6.54E-01	0.3450	1.69E-01
0.3450	1	0.3450	6.54E-01	0.3450	1.69E-01
0.3450	1	0.3450	6.54E-01	0.3450	1.69E-01
0.3450	1	0.3450	6.54E-01	0.3450	1.69E-01
0.3450	1	0.3450	6.54E-01	0.3450	1.69E-01
0.3450	1	0.3450	6.54E-01	0.3450	1.69E-01
0.3450	1	0.3450	6.54E-01	0.3450	1.69E-01
0.3450	1	0.3450	6.54E-01	0.3450	1.69E-01
0.3450	1	0.3450	6.54E-01	0.3450	1.69E-01
0.3450	1	0.3450	6.54E-01	0.3450	1.69E-01
0.3450	1	0.3450	6.54E-01	0.3450	1.69E-01
0.3450	1	0.3450	6.54E-01	0.3450	1.69E-01
0.3450	1	0.3450	6.54E-01	0.3450	1.69E-01
0.3450	1	0.3450	6.54E-01	0.3450	1.69E-01
0.3450	1	0.3450	6.54E-01	0.3450	1.69E-01
0.3450	1	0.3450	6.54E-01	0.3450	1.69E-01
0.3450	1	0.3450	6.54E-01	0.3450	1.69E-01
0.3450	1	0.3450	6.54E-01	0.3450	1.69E-01
0.3450	1	0.3450	6.54E-01	0.3450	1.69E-01
0.3450	1	0.3450	6.54E-01	0.3450	1.69E-01
0.3450	1	0.3450	6.54E-01	0.3450	1.69E-01
0.3450	1	0.3450	6.54E-01	0.3450	1.69E-01
0.3450	1	0.3450	6.54E-01	0.3450	1.69E-01

No bindin C_f (kg/m^3 of solution)	**Da/D_{e28}**	**Linear binding C_f (kg/m^3 of solution)**	**Da/$_{De28}$ (dift)**	**Nonlinear binding C_f (kg/m^3 of solution)**	**Da/D_{e28} (dift)**
0.3450	1	0.3450	6.54E-01	0.3450	1.69E-01
0.3450	1	0.3450	6.54E-01	0.3450	1.69E-01
0.3450	1	0.3450	6.54E-01	0.3450	1.69E-01
0.3450	1	0.3450	6.54E-01	0.3450	1.69E-01
0.3450	1	0.3450	6.54E-01	0.3450	1.69E-01
0.3450	1	0.3450	6.54E-01	0.3450	1.69E-01
0.3450	1	0.3450	6.54E-01	0.3450	1.69E-01
0.3450	1	0.3450	6.54E-01	0.3450	1.69E-01
0.3450	1	0.3450	6.54E-01	0.3450	1.69E-01
0.3450	1	0.3450	6.54E-01	0.3450	1.69E-01
0.3450	1	0.3450	6.54E-01	0.3450	1.69E-01
0.3450	1	0.3450	6.54E-01	0.3450	1.69E-01
0.3450	1	0.3450	6.54E-01	0.3450	1.69E-01
0.3450	1	0.3450	6.54E-01	0.3450	1.69E-01
0.3450	1	0.3450	6.54E-01	0.3450	1.69E-01
0.3450	1	0.3450	6.54E-01	0.3450	1.69E-01
0.3450	1	0.3450	6.54E-01	0.3450	1.69E-01
0.3450	1	0.3450	6.54E-01	0.3450	1.69E-01
0.3450	1	0.3450	6.54E-01	0.3450	1.69E-01
0.3450	1	0.3450	6.54E-01	0.3450	1.69E-01
0.3450	1	0.3450	6.54E-01	0.3450	1.69E-01
0.3450	1	0.3450	6.54E-01	0.3450	1.69E-01
0.3450	1	0.3450	6.54E-01	0.3450	1.69E-01
0.3450	1	0.3450	6.54E-01	0.3450	1.69E-01
0.3450	1	0.3450	6.54E-01	0.3450	1.69E-01
0.3450	1	0.3450	6.54E-01	0.3450	1.69E-01
0.3450	1	0.3450	6.54E-01	0.3450	1.69E-01
0.3450	1	0.3450	6.54E-01	0.3450	1.69E-01
0.3450	1	0.3450	6.54E-01	0.3450	1.69E-01
0.3450	1	0.3450	6.54E-01	0.3450	1.69E-01
0.3450	1	0.3450	6.54E-01	0.3450	1.69E-01
0.3450	1	0.3450	6.54E-01	0.3450	1.69E-01
0.3450	1	0.3450	6.54E-01	0.3450	1.69E-01
0.3450	1	0.3450	6.54E-01	0.3450	1.69E-01
0.3450	1	0.3450	6.54E-01	0.3450	1.69E-01
0.3450	1	0.3450	6.54E-01	0.3450	1.69E-01
0.3450	1	0.3450	6.54E-01	0.3450	1.69E-01
0.3450	1	0.3450	6.54E-01	0.3450	1.69E-01

No bindin C_f (kg/m^3 of solution)	Da/D_{e28}	Linear binding C_f (kg/m^3 of solution)	Da/$_{De28}$ (dift)	Nonlinear binding C_f (kg/m^3 of solution)	Da/D_{e28} (dift)
0.3450	1	0.3450	6.54E-01	0.3450	1.69E-01
0.3450	1	0.3450	6.54E-01	0.3450	1.69E-01
0.3450	1	0.3450	6.54E-01	0.3450	1.69E-01
0.3450	1	0.3450	6.54E-01	0.3450	1.69E-01
0.3450	1	0.3450	6.54E-01	0.3450	1.69E-01
0.3450	1	0.3450	6.54E-01	0.3450	1.69E-01
0.3450	1	0.3450	6.54E-01	0.3450	1.69E-01
0.3450	1	0.3450	6.54E-01	0.3450	1.69E-01
0.3450	1	0.3450	6.54E-01	0.3450	1.69E-01
0.3450	1	0.3450	6.54E-01	0.3450	1.69E-01
0.3450	1	0.3450	6.54E-01	0.3450	1.69E-01
0.3450	1	0.3450	6.54E-01	0.3450	1.69E-01

Figure 8.3 - data points (Free chloride profiles)

Depth (mm)	No binding, C_f (kg/m^3 of solution)	Linear binding, C_f (kg/m^3 of solution)	Nonlinear binding, C_f (kg/m^3 of solution)
0	165	165	165
1	151.1893	145.9642	145.1590
2	137.5313	127.3280	125.5643
3	124.1734	109.4660	106.6493
4	111.2535	92.7048	88.8083
5	98.8950	77.3059	72.3727
6	87.2042	63.4543	57.5946
7	76.2669	51.2543	44.6369
8	66.1473	40.7324	33.5719
9	56.8875	31.8459	24.3872
10	48.5075	24.4957	16.9976
11	41.0071	18.5413	11.2608
12	34.3678	13.8165	6.9952
13	28.5550	10.1437	3.9983
14	23.5216	7.3467	2.0629
15	19.2106	5.2596	0.9839
16	15.5588	3.7334	0.5228
17	12.4989	2.6397	0.3841
18	9.9629	1.8714	0.3526
19	7.8840	1.3423	0.3464
20	6.1981	0.9850	0.3452
21	4.8457	0.7485	0.3450

Depth (mm)	No binding, C_f (kg/m^3 of solution)	Linear binding, C_f (kg/m^3 of solution)	Nonlinear binding, C_f (kg/m^3 of solution)
22	3.7726	0.5949	0.3450
23	2.9302	0.4970	0.3450
24	2.2760	0.4359	0.3450
25	1.7734	0.3984	0.3450
26	1.3913	0.3758	0.3450
27	1.1040	0.3625	0.3450
28	0.8903	0.3547	0.3450
29	0.7329	0.3503	0.3450
30	0.6183	0.3479	0.3450

Figure 8.4 data points (Bound chloride profiles)

Depth (mm)	Linear binding, C_b (kg/m^3 of concrete)	Nonlinear binding, C_b (kg/m^3 of concrete)
0	9.0750	6.8330
1	8.0280	6.4337
2	7.0030	6.0098
3	6.0206	5.5659
4	5.0988	5.1070
5	4.2518	4.6387
6	3.4900	4.1665
7	2.8190	3.6961
8	2.2403	3.2330
9	1.7515	2.7820
10	1.3473	2.3479
11	1.0198	1.9348
12	0.7599	1.5468
13	0.5579	1.1893
14	0.4041	0.8714
15	0.2893	0.6153
16	0.2053	0.4571
17	0.1452	0.3954
18	0.1029	0.3798
19	0.0738	0.3767
20	0.0542	0.3761
21	0.0412	0.3760
22	0.0327	0.3760
23	0.0273	0.3760
24	0.0240	0.3760
25	0.0219	0.3760
26	0.0207	0.3760

Depth (mm)	Linear binding, C_b (kg/m^3 of concrete)	Nonlinear binding, C_b (kg/m^3 of concrete)
27	0.0199	0.3760
28	0.0195	0.3760
29	0.0193	0.3760
30	0.0191	0.3760

Figure 8.5 data points (Total chloride profiles)

Depth (mm)	No binding, Ct (kg/m^3 of concrete)	Linear binding, Ct (kg/m^3 of concrete)	Nonlinear binding, Ct (kg/m^3 of concrete)
0	17.1600	26.2350	23.9930
1	15.7237	23.2083	21.5302
2	14.3033	20.2452	19.0685
3	12.9140	17.4051	16.6574
4	11.5704	14.7401	14.3430
5	10.2851	12.2916	12.1654
6	9.0692	10.0892	10.1563
7	7.9318	8.1494	8.3384
8	6.8793	6.4764	6.7244
9	5.9163	5.0635	5.3183
10	5.0448	3.8948	4.1156
11	4.2647	2.9481	3.1059
12	3.5742	2.1968	2.2743
13	2.9697	1.6129	1.6051
14	2.4462	1.1681	1.0859
15	1.9979	0.8363	0.7176
16	1.6181	0.5936	0.5115
17	1.2999	0.4197	0.4354
18	1.0361	0.2975	0.4165
19	0.8199	0.2134	0.4127
20	0.6446	0.1566	0.4120
21	0.5040	0.1190	0.4119
22	0.3924	0.0946	0.4119
23	0.3047	0.0790	0.4119
24	0.2367	0.0693	0.4119
25	0.1844	0.0633	0.4119
26	0.1447	0.0598	0.4119
27	0.1148	0.0576	0.4119
28	0.0926	0.0564	0.4119
29	0.0762	0.0557	0.4119
30	0.0643	0.0553	0.4119

Figure 8.6 data points (Low surface chloride concentration)

Depth (mm)	Linear binding C_t (kg/m^3 of concrete)	Linear binding C_b (kg/m^3 of concrete)	Linear binding C_f (kg/m^3 of concrete)
0	4.5204	2.0563	1.8436
1	4.3936	1.9987	1.7919
2	4.2670	1.9411	1.7403
3	4.1407	1.8836	1.6888
4	4.0149	1.8264	1.6374
5	3.8897	1.7694	1.5864
6	3.7652	1.7128	1.5356
7	3.6417	1.6566	1.4852
8	3.5192	1.6009	1.4353
9	3.3980	1.5457	1.3858
10	3.2781	1.4912	1.3369
11	3.1596	1.4373	1.2886
12	3.0428	1.3842	1.2410
13	2.9277	1.3318	1.1940
14	2.8144	1.2803	1.1478
15	2.7031	1.2296	1.1024
16	2.5938	1.1799	1.0578
17	2.4866	1.1312	1.0141
18	2.3817	1.0834	0.9714
19	2.2791	1.0368	0.9295
20	2.1788	0.9912	0.8886
21	2.0810	0.9467	0.8487
22	1.9858	0.9033	0.8099
23	1.8930	0.8611	0.7721
24	1.8029	0.8201	0.7353
25	1.7154	0.7803	0.6996
26	1.6306	0.7418	0.6650
27	1.5484	0.7044	0.6315
28	1.4690	0.6682	0.5991
29	1.3922	0.6333	0.5678
30	1.3182	0.5996	0.5376
31	1.2468	0.5672	0.5085
32	1.1782	0.5360	0.4805
33	1.1122	0.5059	0.4536
34	1.0488	0.4771	0.4277
35	0.9880	0.4495	0.4030

Depth (mm)	Nonlinear binding C_t (kg/m^3 of concrete)	Nonlinear binding C_b (kg/m^3 of concrete)	Nonlinear binding C_f (kg/m^3 of concrete)
0	4.2383	2.3947	1.8436
1	4.1571	2.3638	1.7933
2	4.0750	2.3322	1.7428
3	3.9922	2.3001	1.6921
4	3.9087	2.2674	1.6413
5	3.8246	2.2341	1.5905
6	3.7399	2.2003	1.5397
7	3.6548	2.1659	1.4889
8	3.5692	2.1309	1.4383
9	3.4832	2.0955	1.3878
10	3.3970	2.0595	1.3376
11	3.3106	2.0230	1.2876
12	3.2241	1.9860	1.2381
13	3.1374	1.9485	1.1889
14	3.0508	1.9106	1.1402
15	2.9643	1.8722	1.0921
16	2.8779	1.8334	1.0445
17	2.7917	1.7942	0.9975
18	2.7058	1.7546	0.9512
19	2.6203	1.7146	0.9057
20	2.5351	1.6742	0.8609
21	2.4505	1.6335	0.8170
22	2.3664	1.5925	0.7739
23	2.2828	1.5511	0.7317
24	2.2000	1.5094	0.6905
25	2.1178	1.4675	0.6503
26	2.0364	1.4252	0.6112
27	1.9558	1.3828	0.5731
28	1.8761	1.3400	0.5361
29	1.7973	1.2971	0.5002
30	1.7195	1.2540	0.4655
31	1.6426	1.2107	0.4319
32	1.5668	1.1672	0.3996
33	1.4920	1.1236	0.3685
34	1.4184	1.0798	0.3386
35	1.3458	1.0359	0.3100

Depth (mm)	Linear binding C_t (kg/m^3 of concrete)	Linear binding C_b (kg/m^3 of concrete)	Linear binding C_f (kg/m^3 of concrete)
36	0.9298	0.4230	0.3792
37	0.8742	0.3977	0.3565
38	0.8210	0.3735	0.3348
39	0.7703	0.3504	0.3142
40	0.7219	0.3284	0.2944
41	0.6759	0.3075	0.2757
42	0.6322	0.2876	0.2578
43	0.5906	0.2687	0.2409
44	0.5513	0.2508	0.2248
45	0.5140	0.2338	0.2096
46	0.4787	0.2178	0.1952
47	0.4454	0.2026	0.1816
48	0.4139	0.1883	0.1688
49	0.3843	0.1748	0.1567
50	0.3564	0.1621	0.1453
51	0.3301	0.1502	0.1346
52	0.3055	0.1390	0.1246
53	0.2824	0.1285	0.1152
54	0.2608	0.1186	0.1064
55	0.2406	0.1094	0.0981
56	0.2217	0.1008	0.0904
57	0.2040	0.0928	0.0832
58	0.1876	0.0853	0.0765
59	0.1723	0.0784	0.0703
60	0.1580	0.0719	0.0645
61	0.1448	0.0659	0.0591
62	0.1326	0.0603	0.0541
63	0.1212	0.0551	0.0494
64	0.1107	0.0504	0.0452
65	0.1010	0.0459	0.0412
66	0.0920	0.0419	0.0375
67	0.0838	0.0381	0.0342
68	0.0762	0.0347	0.0311
69	0.0692	0.0315	0.0282
70	0.0628	0.0286	0.0256
71	0.0569	0.0259	0.0232
72	0.0515	0.0234	0.0210

Depth (mm)	Nonlinear binding C_t (kg/m^3 of concrete)	Nonlinear binding C_b (kg/m^3 of concrete)	Nonlinear binding C_f (kg/m^3 of concrete)
36	1.2744	0.9918	0.2826
37	1.2042	0.9477	0.2565
38	1.1352	0.9035	0.2317
39	1.0674	0.8592	0.2082
40	1.0008	0.8148	0.1860
41	0.9354	0.7703	0.1651
42	0.8713	0.7258	0.1454
43	0.8083	0.6812	0.1271
44	0.7466	0.6366	0.1100
45	0.6861	0.5919	0.0942
46	0.6268	0.5471	0.0797
47	0.5687	0.5022	0.0664
48	0.5117	0.4573	0.0544
49	0.4558	0.4121	0.0436
50	0.4009	0.3668	0.0340
51	0.3470	0.3213	0.0257
52	0.2939	0.2754	0.0185
53	0.2417	0.2292	0.0125
54	0.1900	0.1823	0.0077
55	0.1386	0.1346	0.0040
56	0.0872	0.0857	0.0015
57	0.0392	0.0389	0.0003
58	0.0092	0.0091	0.0000
59	0.0008	0.0008	0.0000
60	0.0000	0.0000	0.0000
61	0.0000	0.0000	0.0000
62	0.0000	0.0000	0.0000
63	0.0000	0.0000	0.0000
64	0.0000	0.0000	0.0000
65	0.0000	0.0000	0.0000
66	0.0000	0.0000	0.0000
67	0.0000	0.0000	0.0000
68	0.0000	0.0000	0.0000
69	0.0000	0.0000	0.0000
70	0.0000	0.0000	0.0000
71	0.0000	0.0000	0.0000
72	0.0000	0.0000	0.0000

Depth (mm)	Linear binding C_t (kg/m^3 of concrete)	Linear binding C_b (kg/m^3 of concrete)	Linear binding C_f (kg/m^3 of concrete)
73	0.0466	0.0212	0.0190
74	0.0421	0.0191	0.0172
75	0.0380	0.0173	0.0155
76	0.0342	0.0156	0.0140
77	0.0308	0.0140	0.0126
78	0.0277	0.0126	0.0113
79	0.0249	0.0113	0.0101
80	0.0223	0.0101	0.0091

Depth (mm)	Nonlinear binding C_t (kg/m^3 of concrete)	Nonlinear binding C_b (kg/m^3 of concrete)	Nonlinear binding C_f (kg/m^3 of concrete)
73	0.0000	0.0000	0.0000
74	0.0000	0.0000	0.0000
75	0.0000	0.0000	0.0000
76	0.0000	0.0000	0.0000
77	0.0000	0.0000	0.0000
78	0.0000	0.0000	0.0000
79	0.0000	0.0000	0.0000
80	0.0000	0.0000	0.0000

Figure 8.7 data points (High surface chloride concentration)

Depth (mm)	Linear binding C_t (kg/m^3 of concrete)	Linear binding C_b (kg/m^3 of concrete)	Linear binding C_f (kg/m^3 of concrete)
0	12.9411	8.2256	7.3746
1	12.6340	8.0304	7.1997
2	12.3273	7.8354	7.0249
3	12.0210	7.6408	6.8504
4	11.7156	7.4467	6.6763
5	11.4113	7.2532	6.5029
6	11.1083	7.0606	6.3302
7	10.8069	6.8691	6.1585
8	10.5074	6.6787	5.9878
9	10.2100	6.4896	5.8183
10	9.9149	6.3021	5.6502
11	9.6225	6.1162	5.4835
12	9.3329	5.9321	5.3184
13	9.0463	5.7500	5.1551
14	8.7630	5.5699	4.9937
15	8.4832	5.3921	4.8343
16	8.2071	5.2166	4.6769
17	7.9348	5.0435	4.5218
18	7.6667	4.8731	4.3690
19	7.4027	4.7053	4.2185
20	7.1432	4.5403	4.0706
21	6.8882	4.3783	3.9253

Depth (mm)	Nonlinear binding C_t (kg/m^3 of concrete)	Nonlinear binding C_b (kg/m^3 of concrete)	Nonlinear binding C_f (kg/m^3 of concrete)
0	11.9690	4.5944	7.3746
1	11.7304	4.5400	7.1904
2	11.4906	4.4849	7.0057
3	11.2497	4.4288	6.8208
4	11.0080	4.3720	6.6360
5	10.7656	4.3144	6.4512
6	10.5228	4.2560	6.2669
7	10.2798	4.1968	6.0830
8	10.0367	4.1369	5.8998
9	9.7938	4.0764	5.7175
10	9.5513	4.0151	5.5362
11	9.3093	3.9532	5.3561
12	9.0681	3.8906	5.1774
13	8.8278	3.8275	5.0003
14	8.5886	3.7638	4.8248
15	8.3508	3.6995	4.6513
16	8.1145	3.6347	4.4797
17	7.8798	3.5695	4.3103
18	7.6470	3.5038	4.1433
19	7.4163	3.4376	3.9786
20	7.1877	3.3711	3.8166
21	6.9615	3.3042	3.6573

Depth (mm)	Linear binding C_t (kg/m^3 of concrete)	Linear binding C_b (kg/m^3 of concrete)	Linear binding C_f (kg/m^3 of concrete)
22	6.6379	4.2192	3.7827
23	6.3925	4.0631	3.6428
24	6.1519	3.9103	3.5058
25	5.9165	3.7606	3.3716
26	5.6861	3.6142	3.2403
27	5.4610	3.4711	3.1120
28	5.2413	3.3314	2.9868
29	5.0269	3.1952	2.8646
30	4.8179	3.0623	2.7455
31	4.6144	2.9330	2.6296
32	4.4164	2.8071	2.5168
33	4.2239	2.6848	2.4071
34	4.0370	2.5660	2.3005
35	3.8556	2.4507	2.1972
36	3.6798	2.3389	2.0970
37	3.5094	2.2306	1.9999
38	3.3445	2.1258	1.9059
39	3.1851	2.0245	1.8151
40	3.0311	1.9266	1.7273
41	2.8824	1.8321	1.6426
42	2.7391	1.7410	1.5609
43	2.6009	1.6532	1.4822
44	2.4680	1.5687	1.4064
45	2.3401	1.4874	1.3335
46	2.2171	1.4092	1.2635
47	2.0991	1.3342	1.1962
48	1.9859	1.2623	1.1317
49	1.8774	1.1933	1.0699
50	1.7735	1.1273	1.0106
51	1.6741	1.0641	0.9540
52	1.5790	1.0037	0.8998
53	1.4883	0.9460	0.8481
54	1.4017	0.8909	0.7988
55	1.3191	0.8385	0.7517
56	1.2405	0.7885	0.7069
57	1.1656	0.7409	0.6643
58	1.0945	0.6957	0.6237

Depth (mm)	Nonlinear binding C_t (kg/m^3 of concrete)	Nonlinear binding C_b (kg/m^3 of concrete)	Nonlinear binding C_f (kg/m^3 of concrete)
22	6.7378	3.2370	3.5008
23	6.5168	3.1695	3.3473
24	6.2985	3.1017	3.1968
25	6.0831	3.0337	3.0495
26	5.8708	2.9655	2.9054
27	5.6617	2.8970	2.7646
28	5.4558	2.8285	2.6273
29	5.2533	2.7598	2.4935
30	5.0542	2.6911	2.3632
31	4.8588	2.6223	2.2365
32	4.6669	2.5535	2.1134
33	4.4788	2.4847	1.9941
34	4.2944	2.4159	1.8785
35	4.1139	2.3472	1.7667
36	3.9372	2.2786	1.6586
37	3.7644	2.2101	1.5543
38	3.5956	2.1418	1.4539
39	3.4308	2.0736	1.3572
40	3.2700	2.0057	1.2643
41	3.1131	1.9379	1.1752
42	2.9603	1.8705	1.0899
43	2.8115	1.8033	1.0082
44	2.6667	1.7364	0.9303
45	2.5258	1.6698	0.8560
46	2.3889	1.6035	0.7854
47	2.2560	1.5376	0.7183
48	2.1269	1.4721	0.6548
49	2.0016	1.4070	0.5947
50	1.8802	1.3423	0.5380
51	1.7626	1.2780	0.4846
52	1.6486	1.2141	0.4345
53	1.5382	1.1506	0.3876
54	1.4315	1.0876	0.3438
55	1.3282	1.0251	0.3031
56	1.2283	0.9629	0.2654
57	1.1318	0.9013	0.2305
58	1.0385	0.8401	0.1985

Depth (mm)	Linear binding C_t (kg/m^3 of concrete)	Linear binding C_b (kg/m^3 of concrete)	Linear binding C_f (kg/m^3 of concrete)
59	1.0269	0.6527	0.5852
60	0.9627	0.6119	0.5486
61	0.9018	0.5732	0.5139
62	0.8442	0.5366	0.4811
63	0.7896	0.5019	0.4500
64	0.7380	0.4691	0.4205
65	0.6892	0.4380	0.3927
66	0.6431	0.4088	0.3665
67	0.5997	0.3812	0.3417
68	0.5587	0.3551	0.3184
69	0.5201	0.3306	0.2964
70	0.4839	0.3075	0.2757
71	0.4498	0.2859	0.2563
72	0.4177	0.2655	0.2380
73	0.3877	0.2464	0.2209
74	0.3595	0.2285	0.2049
75	0.3331	0.2117	0.1898
76	0.3084	0.1960	0.1757
77	0.2853	0.1813	0.1626
78	0.2637	0.1676	0.1503
79	0.2436	0.1548	0.1388
80	0.2248	0.1429	0.1281

Depth (mm)	Nonlinear binding C_t (kg/m^3 of concrete)	Nonlinear binding C_b (kg/m^3 of concrete)	Nonlinear binding C_f (kg/m^3 of concrete)
59	0.9484	0.7793	0.1692
60	0.8614	0.7189	0.1425
61	0.7773	0.6589	0.1184
62	0.6961	0.5993	0.0968
63	0.6176	0.5401	0.0775
64	0.5417	0.4811	0.0606
65	0.4682	0.4223	0.0459
66	0.3970	0.3636	0.0334
67	0.3280	0.3050	0.0230
68	0.2607	0.2461	0.0146
69	0.1949	0.1868	0.0081
70	0.1303	0.1267	0.0035
71	0.0677	0.0668	0.0009
72	0.0207	0.0207	0.0001
73	0.0026	0.0026	0.0000
74	0.0001	0.0001	0.0000
75	0.0000	0.0000	0.0000
76	0.0000	0.0000	0.0000
77	0.0000	0.0000	0.0000
78	0.0000	0.0000	0.0000
79	0.0000	0.0000	0.0000
80	0.0000	0.0000	0.0000

APPENDIX (I) Nonlinear Model - Parametric Study Data

Data points for Figure (8.13)

Input parameter		Predicted service life	Change (%)
base case		79	0%
D_{e28}	3	57	-28
	3.5	47	-41
	4	39	-51
m_e	0.4	94	19
	0.5	174	120
	0.6	318	303
C_{se}	17.727	150	90
	88.632	41	-41
	106.36	36	-48
C_i	1	67	-15
	2	54	-32
	3	38	-52
To C	5	180	128
	35	34	-57
Cover (mm)	40	45	-43
	60	120	52
	70	169	114
C_{crit} (% bw of binder)	0.11	98	13
	0.13	110	24
	0.15	116	39

De28 (2.29, 3, 4)& me (0.37, 0.5, 06)

Figure 8.14 & 8.15

Depth (mm)	Free Cl^- (kg/m^3 of pore solution)	Free Cl^- (kg/m^3 of pore solution)	Free Cl^- (kg/m^3 of pore solution)
0	35.453	35.453	35.453
1	34.278	34.427	34.565
2	33.099	33.398	33.674
3	31.918	32.366	32.781
4	30.737	31.334	31.887
5	29.557	30.302	30.993
6	28.382	29.273	30.100
7	27.211	28.246	29.209
8	26.049	27.224	28.320
9	24.896	26.208	27.434
10	23.755	25.199	26.553
11	22.627	24.199	25.677
12	21.515	23.208	24.806
13	20.420	22.228	23.942
14	19.343	21.260	23.086
15	18.287	20.306	22.238
16	17.253	19.366	21.399
17	16.242	18.442	20.570
18	15.256	17.534	19.752
19	14.297	16.644	18.945
20	13.364	15.773	18.150
21	12.461	14.921	17.368
22	11.586	14.089	16.599
23	10.742	13.278	15.844
24	9.930	12.490	15.103
25	9.149	11.723	14.378
26	8.400	10.980	13.668
27	7.685	10.260	12.975
28	7.003	9.565	12.298
29	6.354	8.894	11.638
30	5.739	8.248	10.995
31	5.158	7.627	10.370
32	4.610	7.032	9.763
33	4.096	6.462	9.174

Depth (mm)	Free Cl^- (kg/m^3 of pore solution)	Free Cl^- (kg/m^3 of pore solution)	Free Cl^- (kg/m^3 of pore solution)
0	35.453	35.453	35.453
1	34.278	33.887	33.520
2	33.099	32.314	31.579
3	31.918	30.740	29.638
4	30.737	29.168	27.708
5	29.557	27.605	25.796
6	28.382	26.054	23.911
7	27.211	24.520	22.062
8	26.049	23.008	20.257
9	24.896	21.522	18.503
10	23.755	20.067	16.807
11	22.627	18.645	15.177
12	21.515	17.262	13.618
13	20.420	15.920	12.135
14	19.343	14.624	10.732
15	18.287	13.375	9.414
16	17.253	12.177	8.183
17	16.242	11.031	7.041
18	15.256	9.941	5.989
19	14.297	8.907	5.029
20	13.364	7.931	4.160
21	12.461	7.014	3.380
22	11.586	6.156	2.689
23	10.742	5.358	2.085
24	9.930	4.620	1.564
25	9.149	3.942	1.125
26	8.400	3.322	0.763
27	7.685	2.761	0.476
28	7.003	2.257	0.260
29	6.354	1.808	0.110
30	5.739	1.414	0.027
31	5.158	1.072	0.002
32	4.610	0.781	0.000
33	4.096	0.539	0.000

Depth (mm)	Free Cl^- (kg/m^3 of pore solution)	Free Cl^- (kg/m^3 of pore solution)	Free Cl^- (kg/m^3 of pore solution)
34	3.615	5.918	8.604
35	3.167	5.399	8.053
36	2.752	4.906	7.521
37	2.369	4.439	7.007
38	2.017	3.998	6.513
39	1.697	3.581	6.038
40	1.406	3.190	5.583
41	1.146	2.824	5.147
42	0.914	2.483	4.730
43	0.710	2.165	4.332
44	0.534	1.872	3.953
45	0.384	1.602	3.594
46	0.259	1.355	3.253
47	0.160	1.130	2.931
48	0.085	0.928	2.627
49	0.034	0.747	2.342
50	0.007	0.586	2.075
51	0.000	0.447	1.825
52	0.000	0.327	1.594
53	0.000	0.226	1.379
54	0.000	0.145	1.181
55	0.000	0.082	1.000
56	0.000	0.037	0.835
57	0.000	0.010	0.686
58	0.000	0.001	0.553
59	0.000	0.000	0.434
60	0.000	0.000	0.331

Depth (mm)	Free Cl^- (kg/m^3 of pore solution)	Free Cl^- (kg/m^3 of pore solution)	Free Cl^- (kg/m^3 of pore solution)
34	3.615	0.344	0.000
35	3.167	0.194	0.000
36	2.752	0.088	0.000
37	2.369	0.025	0.000
38	2.017	0.002	0.000
39	1.697	0.000	0.000
40	1.406	0.000	0.000
41	1.146	0.000	0.000
42	0.914	0.000	0.000
43	0.710	0.000	0.000
44	0.534	0.000	0.000
45	0.384	0.000	0.000
46	0.259	0.000	0.000
47	0.160	0.000	0.000
48	0.085	0.000	0.000
49	0.034	0.000	0.000
50	0.007	0.000	0.000
51	0.000	0.000	0.000
52	0.000	0.000	0.000
53	0.000	0.000	0.000
54	0.000	0.000	0.000
55	0.000	0.000	0.000
56	0.000	0.000	0.000
57	0.000	0.000	0.000
58	0.000	0.000	0.000
59	0.000	0.000	0.000
60	0.000	0.000	0.000

C_{se} (35.453, 17.727, 88.632) & Ci (0, 2, 3)

Figure 8.16 & 8.17

Depth (mm)	Free Cl^- (kg/m^3 of pore solution)	Free Cl^- (kg/m^3 of pore solution)	Free Cl^- (kg/m^3 of pore solution)
0	35.453	17.727	88.63
1	34.278	17.109	85.828
2	33.099	16.488	83.021
3	31.918	15.865	80.213
4	30.737	15.240	77.407
5	29.557	14.616	74.610
6	28.382	13.994	71.825
7	27.211	13.374	69.055
8	26.049	12.757	66.306
9	24.896	12.146	63.582
10	23.755	11.540	60.886
11	22.627	10.942	58.223
12	21.515	10.352	55.597
13	20.420	9.771	53.010
14	19.343	9.200	50.467
15	18.287	8.641	47.971
16	17.253	8.094	45.525
17	16.242	7.561	43.133
18	15.256	7.042	40.796
19	14.297	6.537	38.518
20	13.364	6.049	36.301
21	12.461	5.577	34.146
22	11.586	5.122	32.057
23	10.742	4.684	30.035
24	9.930	4.265	28.081
25	9.149	3.865	26.196
26	8.400	3.484	24.381
27	7.685	3.122	22.638
28	7.003	2.780	20.967
29	6.354	2.459	19.367
30	5.739	2.157	17.840
31	5.158	1.875	16.385
32	4.610	1.614	15.002
33	4.096	1.373	13.690

Depth (mm)	Free Cl^- (kg/m^3 of pore solution)	Free Cl^- (kg/m^3 of pore solution)	Free Cl^- (kg/m^3 of pore solution)
0	35.453	35.453	35.453
1	34.278	34.336	34.366
2	33.099	33.215	33.276
3	31.918	32.093	32.184
4	30.737	30.971	31.093
5	29.557	29.851	30.004
6	28.382	28.735	28.919
7	27.211	27.625	27.840
8	26.049	26.522	26.769
9	24.896	25.430	25.707
10	23.755	24.349	24.657
11	22.627	23.281	23.621
12	21.515	22.229	22.600
13	20.420	21.193	21.595
14	19.343	20.176	20.609
15	18.287	19.180	19.643
16	17.253	18.205	18.698
17	16.242	17.253	17.776
18	15.256	16.325	16.879
19	14.297	15.424	16.007
20	13.364	14.549	15.162
21	12.461	13.703	14.344
22	11.586	12.886	13.555
23	10.742	12.098	12.795
24	9.930	11.341	12.066
25	9.149	10.616	11.367
26	8.400	9.922	10.700
27	7.685	9.261	10.064
28	7.003	8.633	9.461
29	6.354	8.037	8.889
30	5.739	7.475	8.350
31	5.158	6.945	7.843
32	4.610	6.449	7.368
33	4.096	5.985	6.925

Depth (mm)	Free Cl^- (kg/m^3 of pore solution)	Free Cl^- (kg/m^3 of pore solution)	Free Cl^- (kg/m^3 of pore solution)
34	3.615	1.152	12.449
35	3.167	0.951	11.277
36	2.752	0.770	10.174
37	2.369	0.609	9.139
38	2.017	0.467	8.171
39	1.697	0.345	7.267
40	1.406	0.241	6.427
41	1.146	0.156	5.648
42	0.914	0.090	4.929
43	0.710	0.042	4.269
44	0.534	0.012	3.665
45	0.384	0.001	3.115
46	0.259	0.000	2.617
47	0.160	0.000	2.170
48	0.085	0.000	1.771
49	0.034	0.000	1.418
50	0.007	0.000	1.109
51	0.000	0.000	0.842
52	0.000	0.000	0.616
53	0.000	0.000	0.428
54	0.000	0.000	0.276
55	0.000	0.000	0.159
56	0.000	0.000	0.075
57	0.000	0.000	0.023
58	0.000	0.000	0.003
59	0.000	0.000	0.000
60	0.000	0.000	0.000

Depth (mm)	Free Cl^- (kg/m^3 of pore solution)	Free Cl^- (kg/m^3 of pore solution)	Free Cl^- (kg/m^3 of pore solution)
34	3.615	5.553	6.513
35	3.167	5.153	6.131
36	2.752	4.785	5.779
37	2.369	4.447	5.456
38	2.017	4.138	5.161
39	1.697	3.859	4.894
40	1.406	3.607	4.651
41	1.146	3.381	4.434
42	0.914	3.179	4.239
43	0.710	3.002	4.066
44	0.534	2.846	3.912
45	0.384	2.710	3.778
46	0.259	2.592	3.660
47	0.160	2.491	3.558
48	0.085	2.405	3.469
49	0.034	2.333	3.393
50	0.007	2.271	3.328
51	0.000	2.220	3.272
52	0.000	2.178	3.225
53	0.000	2.143	3.186
54	0.000	2.115	3.153
55	0.000	2.091	3.125
56	0.000	2.072	3.102
57	0.000	2.057	3.083
58	0.000	2.045	3.067
59	0.000	2.035	3.054
60	0.000	2.028	3.043

Temperature ^{o} C (20, 5, 35)

Figure 8.18

Depth (mm)	Free Cl^- (kg/m^3 of pore solution)	Free Cl^- (kg/m^3 of pore solution)	Free Cl^- (kg/m^3 of pore solution)
0	35.453	35.453	35.453
1	34.278	33.749	34.613
2	33.099	32.038	33.771
3	31.918	30.325	32.927
4	30.737	28.618	32.082
5	29.557	26.923	31.237
6	28.382	25.244	30.392
7	27.211	23.589	29.549
8	26.049	21.962	28.707
9	24.896	20.370	27.868
10	23.755	18.817	27.032
11	22.627	17.309	26.201
12	21.515	15.850	25.374
13	20.420	14.445	24.553
14	19.343	13.096	23.738
15	18.287	11.808	22.930
16	17.253	10.584	22.130
17	16.242	9.425	21.337
18	15.256	8.334	20.554
19	14.297	7.312	19.780
20	13.364	6.361	19.016
21	12.461	5.480	18.263
22	11.586	4.670	17.522
23	10.742	3.930	16.792
24	9.930	3.260	16.074
25	9.149	2.659	15.369
26	8.400	2.125	14.678
27	7.685	1.656	14.000
28	7.003	1.251	13.337
29	6.354	0.908	12.688
30	5.739	0.623	12.054
31	5.158	0.394	11.435
32	4.610	0.220	10.832

Depth (mm)	Free Cl^- (kg/m^3 of pore solution)	Free Cl^- (kg/m^3 of pore solution)	Free Cl^- (kg/m^3 of pore solution)
33	4.096	0.098	10.245
34	3.615	0.026	9.674
35	3.167	0.002	9.120
36	2.752	0.000	8.582
37	2.369	0.000	8.061
38	2.017	0.000	7.557
39	1.697	0.000	7.070
40	1.406	0.000	6.600
41	1.146	0.000	6.147
42	0.914	0.000	5.712
43	0.710	0.000	5.293
44	0.534	0.000	4.892
45	0.384	0.000	4.509
46	0.259	0.000	4.142
47	0.160	0.000	3.792
48	0.085	0.000	3.460
49	0.034	0.000	3.144
50	0.007	0.000	2.845
51	0.000	0.000	2.562
52	0.000	0.000	2.296
53	0.000	0.000	2.045
54	0.000	0.000	1.811
55	0.000	0.000	1.592
56	0.000	0.000	1.389
57	0.000	0.000	1.201
58	0.000	0.000	1.027
59	0.000	0.000	0.869
60	0.000	0.000	0.724